1975

# An application of the Mossbauer effect to the study of some magnetic properties of ilmenite

L. K.L.Joseph Lising
*University of Wollongong*

THE UNIVERSITY OF NEW SOUTH WALES

# AN APPLICATION OF THE MÖSSBAUER EFFECT TO THE STUDY OF SOME MAGNETIC PROPERTIES OF ILMENITE

A THESIS SUBMITTED FOR THE DEGREE OF MASTER OF SCIENCE

by

L.K.L.J. LISING,
B.Sc. (N.S.W.) Grad. A.I.P.,
Department of Physics,
University of Wollongong.



April, 1975

808052

## ABSTRACT

The investigations described in this thesis clarify and supplement, by means of Mössbauer spectroscopy, the magnetic properties and chemical composition of natural ilmenite and its oxidation products.

Natural ilmenite was found by some investigators, using a magnetic measurement method, to be weakly ferrimagnetic but was revealed to be in a paramagnetic state by others using Mössbauer spectroscopy. There was an uncertainty about the nature of the magnetic properties of an ilmenite sample which had been partially oxidised by heat treatment. The types of compounds existing in natural ilmenite and its oxidation products were not clearly determined.

A unique constant velocity pneumatic-hydraulic Mössbauer spectrometer was designed and built for these investigations. Despite an $^{57}Fe$ content of approximately 0.7 per cent by weight in the samples, well resolved spectra were obtained.

Analyses of the spectra obtained showed that the magnetic anomaly observed in natural ilmenite and its

partially oxidised products is the result of super-paramagnetism exhibited by these specimens at room temperature. Hence the ferrimagnetic characteristic of these specimens is not observable. The spectra also provide convincing evidence that the final oxidation product is pseudobrookite and that the partially oxidised specimens contain various types of iron compounds. Furthermore, they provide strong evidence that the ferric compound existing in natural ilmenite is hematite in ilmenite-hematite solid solution rather than pseudo-brookite previously suggested by other investigators.

## ACKNOWLEDGEMENTS

I wish to thank my supervisor, Dr. K.J. Ausburn, for his guidance and enlightening discussions. My thanks are also due to Professor L.G. Parry for providing the natural ilmenite samples for the present investigations. His helpful suggestions are greatly appreciated. To Professor P. Fisher and Dr. J.N. Stephens I offer my thanks for their stimulating discussions. The assistance of Dr. N. Kennon in the preparation of the X-ray diffraction spectra of the samples is also greatly appreciated. I am grateful to the engineering staff of Jeffries, Parker Hannifin Pty. Ltd., the technical staff of the Engineering Department and the Physics Department of the University of Wollongong, and Mr. H.J. Fraser of Australian Atomic Energy Commission for their assistance in the construction of the Mössbauer spectrometer.

My sincere thanks are due to Miss A.M. Akers for her clerical assistance in the preparation of this thesis. Finally, I wish to thank my wife, Elizabeth, for her moral support and patience during the entire period of my study.

CONTENTS

# CHAPTER 1

# INTRODUCTION

## (1.1.) The Ilmenite Problem and the Relevance of Mössbauer Spectroscopy

Natural ilmenite is a rock-forming mineral which consists of a ferrimagnetic ilmenite-hematite solid solution (Akimoto 1954, Uyeda 1956) and a small amount of impurities. Both ilmenite ($FeTiO_3$) and hematite ($\alpha Fe_2O_3$) have a rhombohedral crystal structure. Although the amount of ferrimagnetic ilmenite-hematite series mineral found in rocks is very small compared with the amounts of titano-magnetite and titano-maghemite minerals, it is considered important in geophysical studies involving rock magnetism (Nagata 1952, Nagata et al 1953 a,b, Uyeda 1956, 1958) because of its strong magnetic coupling and its capability of causing a self-reversal of thermal-remanent magnetization.

It is therefore important to understand the structural and chemical changes which may occur in ilmenite bearing rocks and the corresponding magnetic properties.

The magnetic characteristics of naturally occurring ilmenite have been investigated by many workers (Nagata 1950, 1952, Akimoto 1954, Curnow and Parry 1954, 1955, Uyeda 1956, Westcott 1966, Gibb et al 1969, Avrahami and Golding, 1969;

see also Chapter 4). In particular, investigations by Curnow and Parry (1954, 1955) and Westcott (1966) revealed some anomalies in the partially oxidised sample (see Chapter 5) which might be better studied by observing the Mössbauer spectra of the samples. Thus it arose that in the present study Mössbauer Spectroscopy is used to investigate further the magnetic properties and chemical composition of natural ilmenite and its oxidised forms. The extreme sensitivity of Mössbauer Spectroscopy enables the observation of any magnetic effect and the identification of the various types of iron compounds in the sample by the characteristics of their absorption lines in the Mössbauer spectrum, such as line position, isomer shift, quadrupole splitting and magnetic hyperfine splitting . The relative amounts of these compounds can also be estimated from their respective absorption intensities.

The present investigations are mainly concerned with the observation of the transition of ilmenite ($FeTiO_3$) to pseudobrookite ($Fe_2TiO_5$)by oxidation, the observation of magnetic hyperfine splitting, if possible, of the more strongly magnetic specimen which has been partially

oxidised, the identification of the chemical composition of specimens and the investigation of the dependence of the oxidation process on grain size, temperature and the time duration of oxidising reaction.

Although Mössbauer spectroscopy is in principle very sensitive in detecting nuclear energy changes, its practical usefulness is dependent on the sensitivity of the spectrometer and the number of absorption nuclei (in this case $^{57}Fe$ nuclei) present in the sample. Since the samples under investigation are naturally occurring ilmenite with a substantial amount of impurities and also the $^{57}Fe$ to total Fe ratio in a natural sample is approximately 2/100, the absorption intensity is expected to be small and the signal to noise ratio becomes the main concern in the analysis of the Mössbauer spectra. However, in most cases, the spectrum was well resolved and enabled a detailed analysis of the oxidation effect on samples.

In the remainder of this chapter a summary of the theory and application of Mössbauer spectroscopy will be given, followed in Chapter 2 by a review of general experimental considerations.

In Chapter 3 the spectrometer designed and constructed for the ilmenite investigations is described. Its novel constant velocity drive mechanism is described in detail. The results of experiments with "standard specimens" are given as a measure of the overall performance of the instrument.

In Chapter 4 a survey of the relevant literature on ilmenite and the ternary $FeO-Fe_2O_3-TiO_2$ system is given.

The reasons for the specific Mössbauer measurements on members of the $FeO-Fe_2O_3-TiO_2$ system herein described are discussed in Chapter 5. The spectra of important relevant compounds are also given in this chapter.

Chapter 6 contains a description of the series of experimental results that evolved as the investigation proceeded. Discussion of the experimental results and the model on the basis of which these and other workers' observations can be satisfactorily described is also given in this chapter.

Chapter 7 contains the summary and conclusions of the investigation.

## (1.2) The Theory of the Mössbauer Effect

The discovery of the Mössbauer Effect (Mössbauer, 1958) has greatly improved the resolving power of nuclear energy spectroscopy. The Mössbauer Effect is based on the concept that there is a finite probability for nuclei embedded in solids to emit or absorb, without recoil, the low energy gamma rays which possess the full transition energy. The natural linewidth of the gamma ray is extremely small compared to the transition energy and the ratio is of the order of $10^{-13}$ for the transition energy in the range of 10-100 keV. With such a narrow linewidth, the Doppler shift can be used to measure interaction energy shifts with an accuracy comparable to this linewidth. Since the application of the Mössbauer Effect to the measurement of gravitational red shift, (Pound and Rebka, 1960), there has been rapid growth in its application. The direct observation of the Zeeman splitting of excited energy levels, formerly thought to be impossible, by Craig et al (1960),

emphasizes the importance of the Mössbauer Effect. Recent applications of the Mössbauer Effect appear not only in nuclear physics, but also in solid state physics, bio-physics, chemistry, acoustics and other areas such as quality control and non-destructive testing of materials. It is particularly useful for the investigation of solid state properties where interaction energies are sensitive to a wide range of parameters.

## (a) Resonance Fluorescence

At the end of the last century Lord Rayleigh predicted the existence of resonance fluorescence, the resonance scattering and absorption of light in atomic systems. This prediction was first demonstrated by R.W. Wood in 1904. The explanation of resonance fluorescence was based purely on classical mechanics, though such a phenomenon is a quantum property which involved transitions between definite energy levels. Kuhn (1929) started to investigate the resonance fluorescence of nuclei. He deduced that, since nuclei, like atoms and molecules, also possess quantized energy levels, there is a possibility of observing

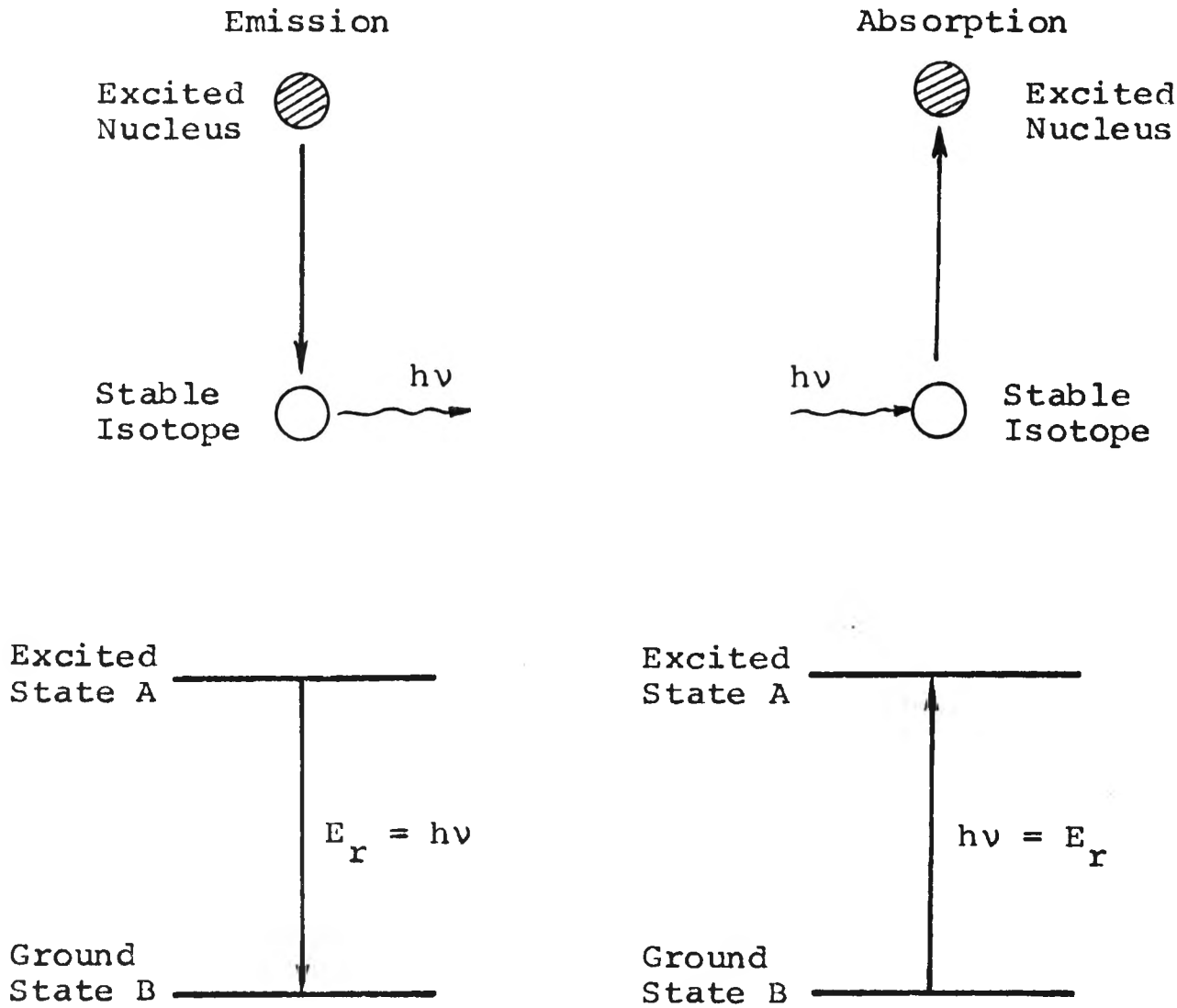


FIGURE 1.1. The resonance fluorescence process

the resonance fluorescence of gamma rays emitted or absorbed in transition between the energy levels.

A nucleus at excited state A will decay to ground state B by emitting a photon possessing the full transition energy $E_r$. This photon may encounter a stable nucleus of the same element and may be resonantly absorbed by it, transforming the absorbing nucleus to state A. This process is called resonance fluorescence, and is shown schematically in Figure 1.1. A more comprehensive description of the processes of emission, absorption and resonance fluorescence of gamma rays was given by Weisskopf and Heitler (1930), Weisskopf (1931), and Heitler (1949).

However, this resonance fluorescence was difficult to observe, because when a photon is emitted from a nuclear transition process, a fraction of the transition energy appears as nuclear recoil energy R, as required by the conservation of momentum. Similarly, in the absorption process, the nucleus requires excess kinetic energy to balance the absorbed photon momentum. The shift in the emission energy and absorption energy, which should equal 2R, therefore appears to prevent the resonant absorption of gamma rays.

Non-relativistically the recoil energy of the nucleus of mass M is given by

$$R = \frac{1}{2} Mv^2 = \frac{P^2}{2M} = \frac{p^2}{2M} = \frac{E_\gamma^2}{2Mc^2} \qquad (1.1)$$

where the momentum P of the nucleus is equal and opposite to the momentum p of the gamma photon and $E_\gamma$ is the photon energy. Since by energy conservation the transition energy is given by

$$E_r = E_\gamma + R \qquad (1.2)$$

and R is very small compared to $E_\gamma$, the recoil energy can be expressed as

$$R = \frac{E_r^2}{2Mc^2} \qquad (1.3)$$

According to the Heisenberg Uncertainty Principle the energy of the excited state of mean life $\tau$ cannot be measured

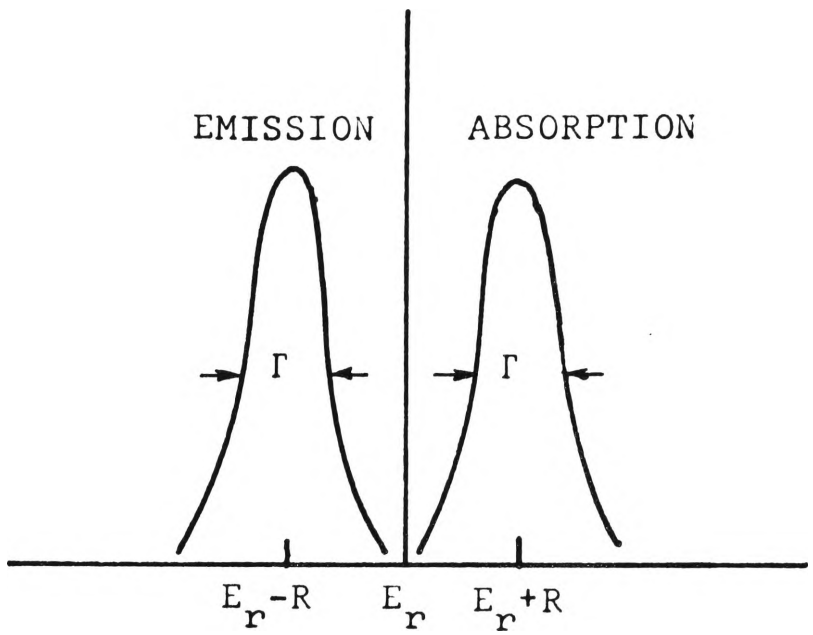


FIGURE 1.2(a). Non-resonance florescence condition.

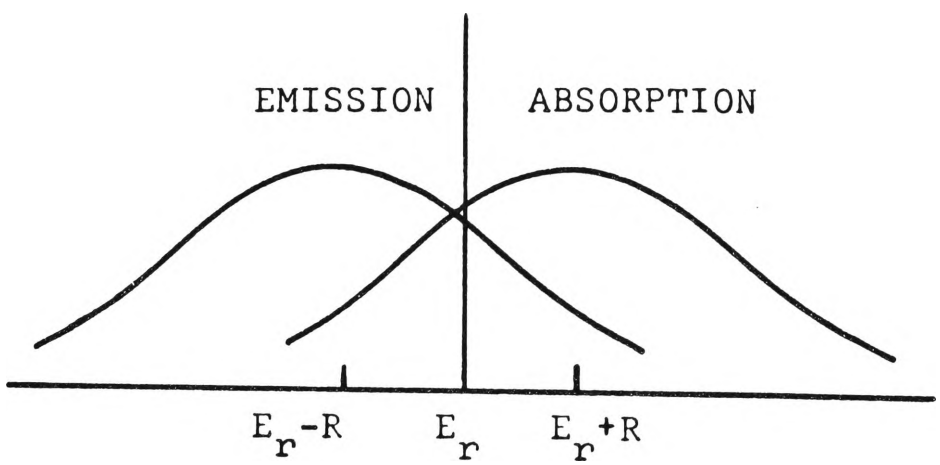


FIGURE 1.2(b). Resonance florescence condition, $2R \leq \Gamma$

sharply but within an uncertainty given by

$$\tau\Gamma = \hbar \qquad (1.4)$$

where $\Gamma$ is the linewidth of the energy and $2\pi\hbar$ is Plank's constant. The energy distribution for emission is therefore centred around $E_r - R$ and for absorption around $E_r + R$, as shown in Figure 1.2. The condition for resonance fluorescence to occur is when

$$2R \leq \Gamma \qquad (1.5)$$

that is when the emission and absorption spectra overlap each other.

A few methods were developed for the observation of resonance fluorescence, for example by:

(i) the Doppler broadening arising from thermal agitation, and

(ii) the Coincidence method, which makes use of recoil by former decay to compensate for the energy loss.

The results obtained by these methods were unsatisfactory and interest in nuclear resonance fluorescence faded away until the discovery of recoilless emission by Mössbauer.

(b) The Discovery of Mössbauer Effect

While investigating the nuclear resonance scattering of 119 keV γ-rays from $^{191}$Ir, Mössbauer discovered that contrary to the expectation from Doppler broadening as in (a) above, resonance scattering could be achieved by cooling both the source and absorber, which were bound separately in a host lattice. In his publication, (Mössbauer, 1958) he successfully explained this effect with the help of a paper by Lamb (1939) which discussed the effect of lattice binding on the capture cross section of slow neutrons.

In the beginning, the discovery of the Mössbauer Effect did not arouse much interest. The resonance effect in $^{191}$Ir is too small and requires low-temperature techniques to perform. However, after the discovery of the convenience of the resonance effect in $^{57}$Fe by groups of scientists at Argonne, Harvard, Harwell and the University of Illinois between 1959 and 1960, the new significance of

the Mössbauer Effect became evident. The resonance effect in $^{57}Fe$ is very large and can be obtained easily at room temperature or even up to 1000°C. The most valuable characteristic of $^{57}Fe$ is its narrow linewidth $\Gamma$ which is of the order of $4.7 \times 10^{-9}$ eV. The ratio of the linewidth compared to the transition energy $E_r$ (14.4 keV) is of order $10^{-13}$. The Mössbauer Effect has evolved into an extremely high resolving power form of spectroscopy.

(c) The Quantum Theory of the Mössbauer Effect

The recoil energy of the nucleus for most low energy gamma rays does not exceed a few tenths of an electron volt and, according to radiation damage investigation, is far less than the 15 - 30 electron volts required to dislodge an atom from its lattice site. The nucleus thus remains in its lattice site after the emission or absorption. But, if the recoil energy is higher than the lattice vibrational transition energy ($h\omega$) then it will be radiated in the form of excitation quanta or phonons and the resonance effect still cannot be observed. However, there is a finite probability that no excitation will occur, that the nucleus remains in the initial state after emission or absorption,

and a sharp resonance peak may occur at the transition energy level $E_r$. The Mössbauer Effect is, in fact, a zero phonon transmission or recoilless emission in which the gamma ray gets the entire transition energy.

Consider the emission or absorption of gamma rays by a nucleus bound in a crystal lattice. The probability that a gamma ray of momentum hk emitted by a nucleus whose centre of mass coordinate is $r_L$, while the lattice goes from initial state i to final state f, is proportional to the square of the matrix element of the interaction Hamiltonian H.

$$P(f,i) \propto |\langle f|\exp(i\underset{\sim}{k}.\underset{\sim}{r}_L)|i\rangle|^2 \qquad (1.7)$$

or

$$P(f,i) = \text{const.}\ |\langle f|\exp(i\underset{\sim}{k}.\underset{\sim}{r}_L)|i\rangle|^2 \qquad (1.8)$$

where the constant in the equation represents the factor depending only upon the initial structure of the nucleus. The probability thus is assumed to depend on the lattice's dynamic property. The constant will become unity if the total probability of a transition from state i to any

other state is unity,

i.e. $$\sum_f P(f,i) = 1 \qquad (1.9)$$

therefore

$$P(f,i) = |\langle f|\exp\ (i\underset{\sim}{k}.\underset{\sim}{r}_L)|i\rangle|^2 \qquad (1.10)$$

The average energy transfer, $\bar{R}$, to the lattice is defined by

$$\bar{R} = \sum_f P(f,i)\ (E_f - E_i) \qquad (1.11)$$

where $E_f$ and $E_i$ are the energy of the nucleus in the final state and the initial state respectively. Substituting the equation (1.10) gives

$$\bar{R} = \sum |\langle f|\exp\ (i\underset{\sim}{k}.\underset{\sim}{r}_L)|i\rangle|^2\ (E_f - E_i) \qquad (1.12)$$

If apply closure, $\sum |f\rangle\langle f| = 0$, equation (1.12) becomes

$$\bar{R} = \langle i|\exp(i\underset{\sim}{k}.\underset{\sim}{r}_L)\ H\ \exp(i\underset{\sim}{k}.\underset{\sim}{r}_L)|i\rangle - E_i \qquad (1.13)$$

It is known generally that

$$H|n\rangle = \sum_k \left(\frac{P_k}{2M_k} + V_k\right)|n\rangle = E_n|n\rangle \qquad (1.14)$$

and $\langle i|p_k|i\rangle = 0$ (1.15)

where $p_k$ is the momentum operator of the kth particle.

With the help of (equation 1.14) and (equation 1.15) it can be shown that (equation 1.13) becomes

$$\overline{R} = \frac{(hk)^2}{2M} \qquad (1.16)$$

or $$\overline{R} = \frac{p_\gamma^2}{2M} = \frac{E_r^2}{2Mc^2} \qquad (1.17)$$

which shows that the amount of energy transferred to the lattice is exactly equal to the recoil energy of a free nucleus given by (equation 1.3).

If the vibrational transition energy of the lattice is given by

$$h\omega = k\theta \qquad (1.18)$$

where $\omega$ is the upper frequency (in energy units) of the vibration and $\theta$ is the Debye temperature of the crystal lattice, then for

$$\bar{R} > > k\theta \qquad (1.19)$$

a phonon is radiated by the nucleus ("heating" the lattice). The probability of the Mössbauer Effect is then very small. However if

$$\bar{R} \simeq k\theta \qquad (1.20)$$

the Mössbauer Effect may occur if the temperature is sufficiently low.

Finally, if

$$\bar{R} < < k\theta \qquad (1.21)$$

then the Mössbauer Effect probability is very large and can be obtained at room temperature.

The fraction $f$ of gamma rays emitted without energy loss to the lattice is defined by

$$f = \frac{P(i,i)}{\sum_f P(f,i)} = \frac{|\langle i|\exp(i\underset{\sim}{k}.\underset{\sim}{r}_L)|i\rangle|^2}{\sum_f |\langle f|\exp(i\underset{\sim}{k}.\underset{\sim}{r}_L)|i\rangle|^2} \qquad (1.22)$$

where

$$\sum_f |\langle f|\exp(i\underset{\sim}{k}.\underset{\sim}{r}_L)|i\rangle|^2$$

$$= \sum_f \langle i|\exp(-i\underset{\sim}{k}.\underset{\sim}{r}_L)|f\rangle \langle f|\exp(i\underset{\sim}{k}.\underset{\sim}{r}_L)|i\rangle$$

$$= 1 \qquad (1.23)$$

therefore

$$f = P(i,i) = |\langle i|\exp(i\underset{\sim}{k}.\underset{\sim}{r}_L)|i\rangle|^2 \qquad (1.24)$$

For an Einstein solid, the ground state wave function of one dimension is given by

$$\Psi_0(x) = \sqrt[4]{M\omega/\pi\hbar}\ \exp(-M\omega x^2/2\hbar) \qquad (1.25)$$

where M is the mass of the oscillator

$\omega$ is its angular frequency.

The recoilless fraction $f$ can be shown to be

$$f = \exp(-\hbar^2 k^2 / 2M\hbar\omega) \tag{1.26}$$

or

$$f = \exp(-R/\hbar\omega) \tag{1.27}$$

For a Debye solid, the individual atoms in the crystal are assumed to have different vibration frequencies. The recoilless fraction $f$ in this case has been calculated by several investigators (Mössbauer, 1959; Lipkin, 1960; and Visscher, 1960) and is given by

$$f = \exp(-2w) \tag{1.28}$$

where

$$w = 3 \frac{R}{k\theta} \left[ \frac{1}{4} + \left( \frac{T}{\theta} \right)^2 \int_0^{\theta/T} \frac{x \, dx}{\exp(x) - 1} \right] \tag{1.29}$$

or approximately given by

$$f = \exp(-3R/2k\theta) \tag{1.30}$$

The occurrence of the Mössbauer Effect depends on three important factors:

i) the Debye temperature $\theta$ of the lattice,

ii) the recoil energy $\overline{R}$ of the nucleus, and

iii) the ambient temperature.

The lattice temperature (in energy units) should be no more than of the same order as the free recoil energy, but the ambient temperature should be relatively lower. The recoilless fraction $f$ is exponentially dependent on the Debye temperature and the recoil energy, which indicates that a small change in these parameters can produce large effects on the experimental results. It is preferable to choose nuclei having a low recoil energy and crystal lattices having a relatively high Debye temperature. For these reasons Mössbauer radioactive sources are restricted to those which have nuclear transition energy less than 150 keV.

## 1.3. Applications of the Mössbauer Effect

The linewidth of a nuclear transition is very narrow and therefore the resonant absorption is extremely

sensitive to energy changes of the gamma radiation due to change in nuclear environment. Any energy change which is more than the linewidth will destroy the resonance effect. The typical linewidth of resonant absorption is of order of $10^{-8}$ ev which is usually smaller than the characteristic energies of the magnetic dipole and electric quadrupole interactions of nuclei with their surrounding electrons. The interactions induce hyperfine splitting of the nuclear energy levels which can be scanned by Doppler shifting a suitable narrow single Mössbauer emission line. Since the peaks of the split and shifted resonant absorption lines can be recorded accurately by employing Mössbauer spectroscopy, these energy levels can therefore be determined accurately. The hyperfine splittings of nuclear energy levels, though larger than the linewidth, are extremely small ($\sim 10^{-8}$ ev to $10^{-7}$ ev) and direct observation was regarded as impossible before 1960. However, the discovery of resonant absorption by Mössbauer, together with the application of Doppler shift in energy, make these small energies readily observable.

The sample in which the hyperfine splittings are to be investigated can be made as a source or an

absorber. Generally it is made as an absorber because it is much easier and cheaper to prepare. A single emission line (unsplit energy) source is usually chosen for such experiments so as to reduce complications in interpretating the resonant absorption curve or the velocity spectra. A single line source can be prepared by imbedding substitutionally the radioactive nuclei into a diamagnetic material. For example, $^{57}Co$ imbedded in Cu, Pd or Stainless steel lattice.

In order to obtain a velocity spectrum, the source is mounted on the velocity drive which provides motion for the Doppler shift in energy. A stationary absorber is placed in between the source and a gamma ray detector. The countings recorded by the detector indicate the absorption of gamma ray by the absorber. The counting rate of gamma rays drops sharply whenever the Doppler shift in energy brings the emitted gamma ray into coincidence with one of the absorption energies in the absorber. A velocity spectrum of the sample can be obtained and energy levels can be accurately determined in terms of the velocities, thereby the properties of the sample can be revealed. The environment of the sample

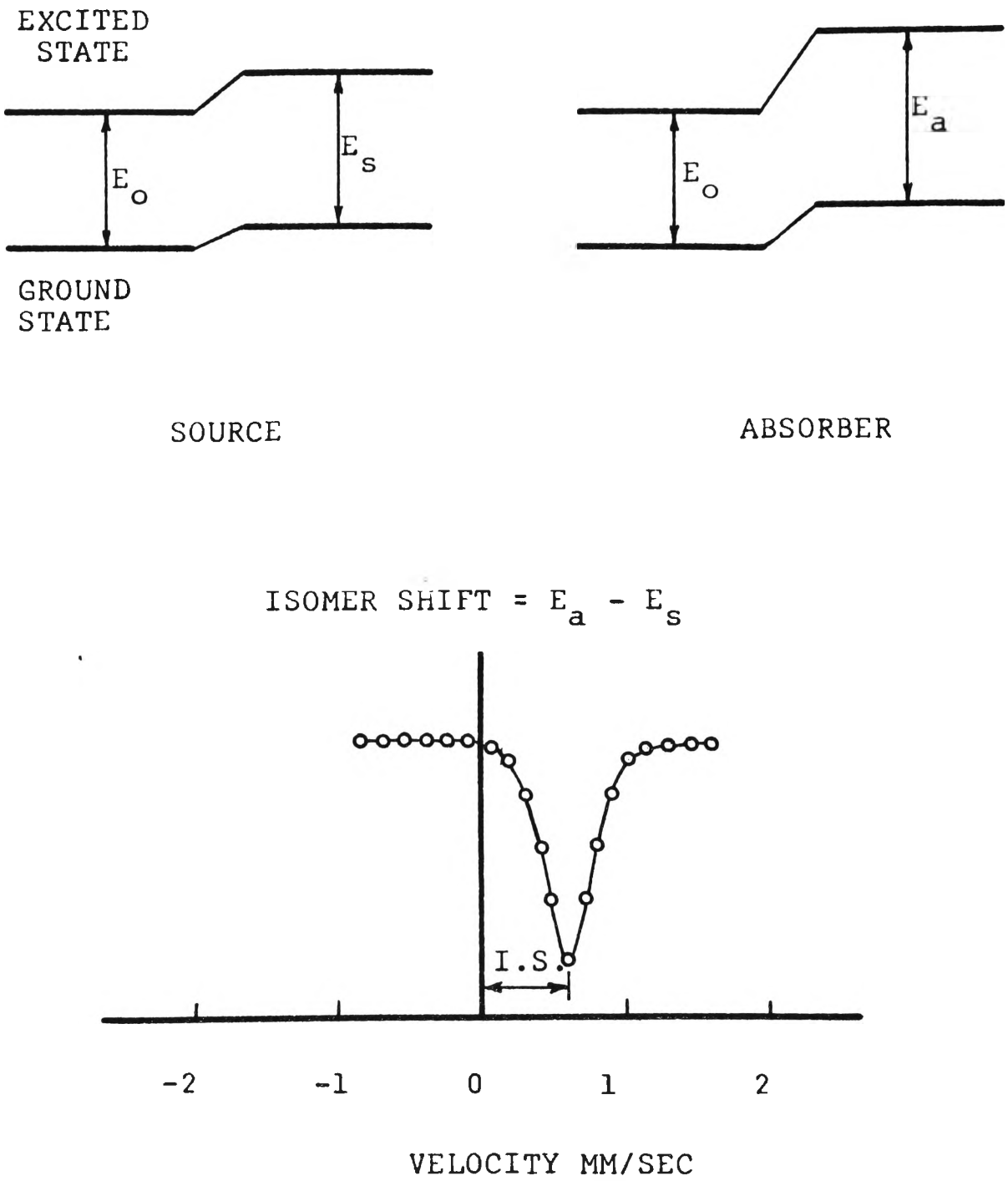


FIGURE 1.3. Mössbauer spectrum of isomer shift in nuclear energy.

can be varied by temperature or pressure changes, variation of impurities, or application of magnetic field or electric field, and thus a wide range of property investigations can be accomplished.

The three main interactions which are of interest in solid-state research and which can be measured from the Mössbauer spectra are

i) Isomer shift or chemical shift
ii) Quadrupole coupling
iii) Magnetic hyperfine splitting

## a. Isomer Shift

The nucleus is surrounded by electronic charges with which it interacts electrostatically. The interaction energy can be calculated theoretically. If there is a change in the S-electron density due to valency changes, the interaction will be affected and consequently the energy levels will be shifted. This effect is called electric monopole interaction, chemical shift or isomer shift. The electrostatic energy of the nucleus is different for each nuclear state. The difference can be observed by measuring the

gamma rays resulting from the transition. The expression for the change in gamma ray transition energy between excited state and ground state is given by

$$\delta E_{ex} - \delta E_{gd} = \frac{2\pi}{5} Ze^2 \, |\psi(o)|^2 \left[R_{ex}^2 - R_{gd}^2\right] \qquad (1.31)$$

where

$e|\psi(o)|^2$ is the electronic charge density,

$Z$ is the atomic number,

$e$ is the charge of an electron,

$R_{ex}$ is the radius of the nucleus in excited state,

$R_{gd}$ is the radius of the nucleus in ground state.

Because of difference in environment it is expected that the change in gamma ray transition energy of the source will be different to that of the absorber.

$$\delta E_s = E_s - E_o = \frac{2\pi}{5} Z_e^2 \, |\psi_s(o)|^2 \left[R_{ex}^2 - R_{gd}^2\right] \qquad (1.32)$$

$$\delta E_a = E_a - E_o = \frac{2\pi}{5} Z_e^2 |\psi_a(o)|^2 \left[R_{ex}^2 - R_{gd}^2\right] \qquad (1.33)$$

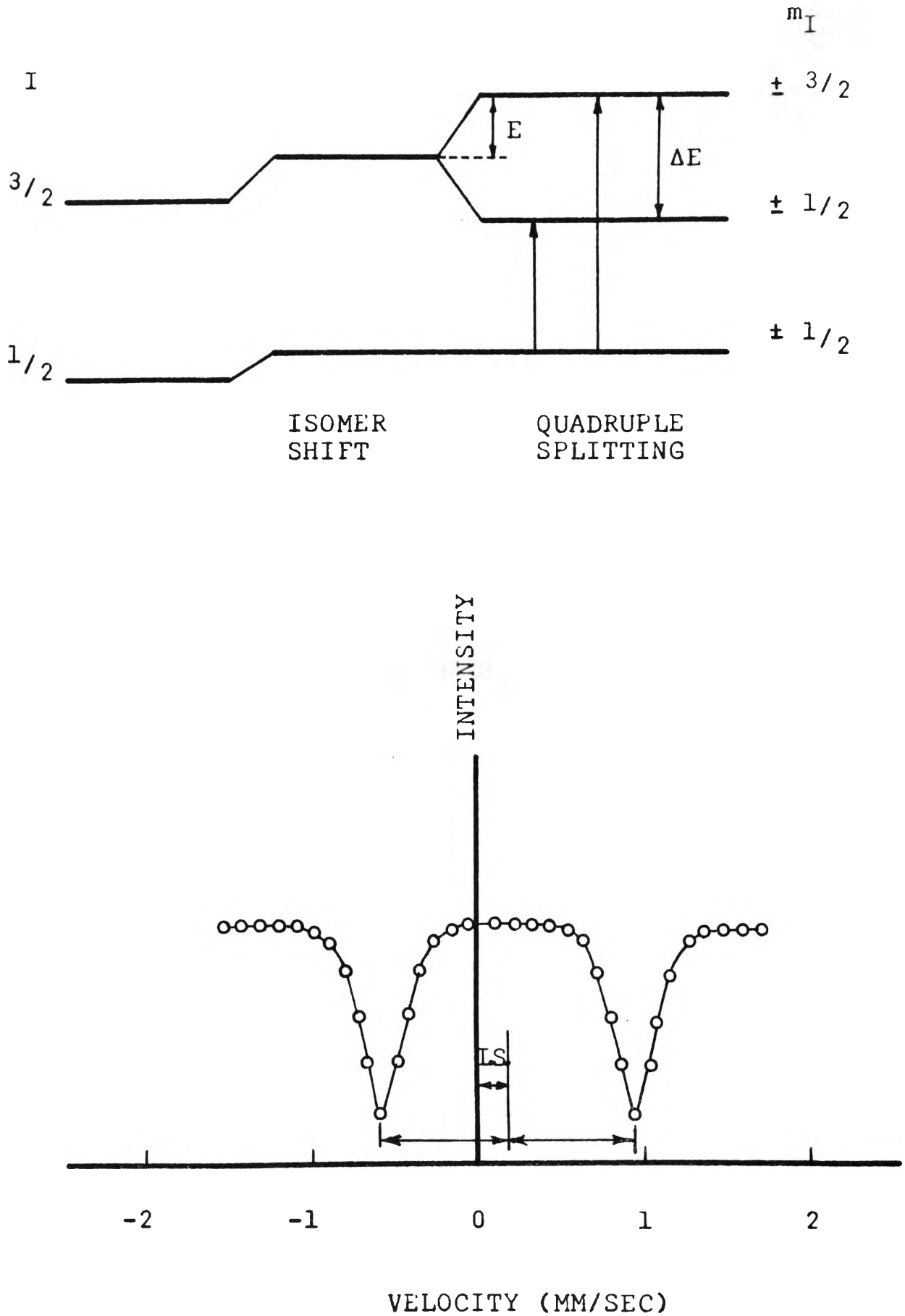


FIGURE 1.4. Mössbauer spectrum of nuclear energy splitting due to quadropole coupling.

where

$E_o$ is the transition energy without shift,

$E_s$ is the transition energy of the source,

$E_a$ is the transition energy of the absorber.

The isomer shift is given by

$$I.S. = E_a - E_s = \frac{2\pi}{5} Z_e^2 \left[ |\psi_a(o)|^2 - |\psi_s(o)|^2 \right] \left[ R_{ex}^2 - R_{gd}^2 \right] \tag{1.34}$$

The isomer shift is extremely small, but in the comparison of the nuclear transition energy in a source with that in an absorber it becomes readily observable. From the measurement of the isomer shift the nuclear radius and the total electron density at the radius can be determined.

b. Quadrupole coupling

The interaction of the nuclear quadrupole moment, Q, with the gradient of the electric field results in splitting the nuclear levels into 2I+1 fold degeneracy. (I is the nuclear spin of the energy state). The field

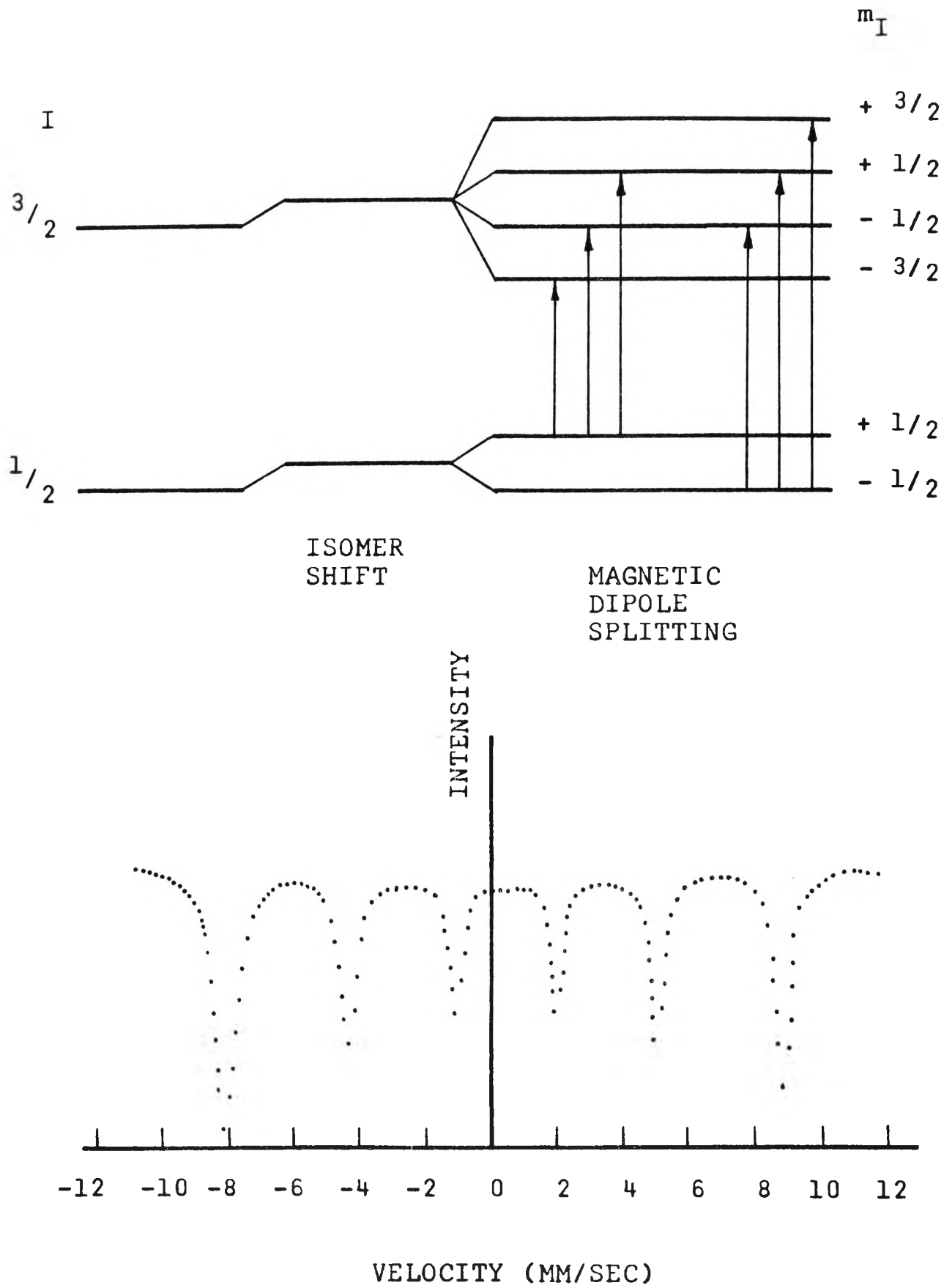


FIGURE 1.5. Mössbauer spectrum of nuclear energy splitting due to magnetic hyperfine interaction.

The polarization effect can be observed in a single crystal. The measured quadrupole changes in intensity as the angle of incidence of the gamma radiation is changed. For polycrystalline materials with isotropic distribution of the field gradients the two peaks of the quadrupole coupling are of the same intensity.

## c. Magnetic hyperfine interaction

The nuclear magnetic dipole moment can interact with the internal magnetic fields which arise from unpaired electrons of the atoms and its neighbours, and it can also interact with an externally applied field ($H$). The Hamiltonian for the interaction is

$$H_m = \mu H = -g\mu_n I H \qquad (1.38)$$

and the energy levels are

$$E_m = \mu H \; m_I/I = -g\mu_n H m_I \qquad (1.39)$$

where $\mu_n$ is the nuclear magneton, $5.05 \times 10^{-24}$ erg/gauss, and g the gyromagnetic ratio or nuclear g factor. For

paramagnetic atoms interaction occurs in free ions while for diamagnetic atoms the interaction only occurs if the atoms are embedded in a ferromagnetic or antiferromagnetic material. The energy level will be split into 2I+1 levels with equal spacing

$$\Delta E_m = g\mu_n H \qquad (1.40)$$

and the splitting between the lowest and the highest level is $2g\mu_n HI$.

The energy gaps due to splitting are very small but they are usually larger than the linewidth of the resonant absorption and are clearly observable in the velocity spectrum. In ferromagnetic and paramagnetic substances, strong internal magnetic fields are present and the velocity spectrum obtained will become more complicated and need more careful analysis.

More detailed discussions of the above mentioned interactions are given in the literature, for example, by Boyle and Hall (1962), Frauenfelder (1963) and Wertheim (1964).

From the velocity spectrum the quantities that can be directly measured are line shape, absorption intensity, isomer shift, quadrupole splitting and magnetic hyperfine splitting ; from it also the Lamb-Mössbauer factor can be calculated. These quantities, however, are not fixed in value but change in accordance with the environmental variation of the samples such as temperature, pressure, external magnetic field, external electric field, crystal structure, percentage of impurity and so on. Methods of sample preparation such as oxidation, annealing and straining also have their effect. With such vast variations in conditions and parameters possible, it is clear that extensive solid state and chemical property investigations can be carried out by Mössbauer spectroscopy.

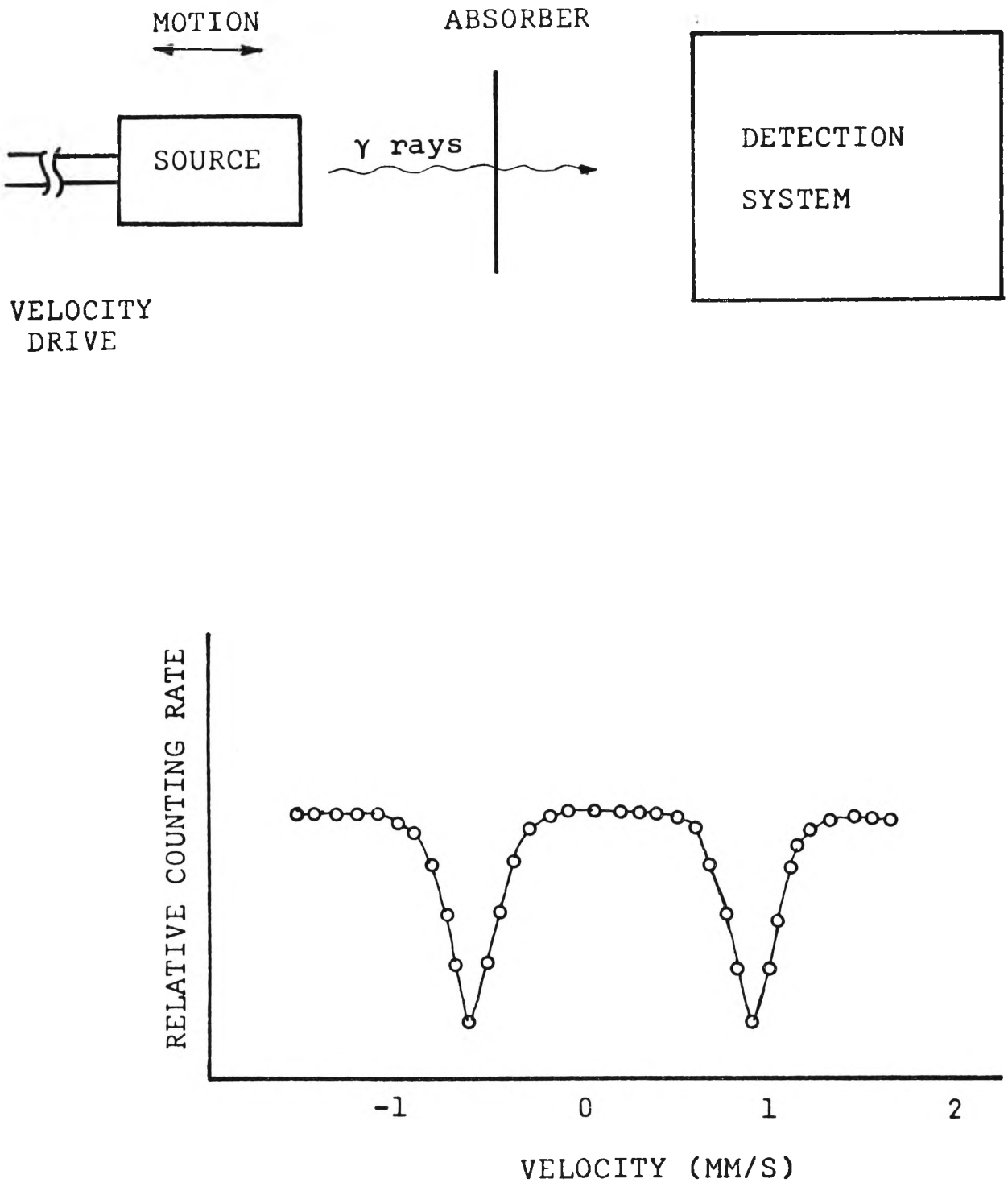


FIGURE 2.1. Detection of Mössbauer Effect

# CHAPTER 2

## GENERAL EXPERIMENTAL CONSIDERATIONS

In Mössbauer spectroscopy a sample under investigation is placed between a source which is mounted on the velocity drive and a gamma ray detector (Fig. 2.1). Mössbauer spectrum of this sample is represented by the change in gamma ray counting rate with respect to the change in relative velocity between the source and absorber. Information about the structure and interactions within solids may be obtained by analysis of relevant Mössbauer spectra as described in Chapter 1. The reliability of this information, however, depends on the precision of the velocity drive and the sensitivity and resolving power of the gamma ray detection system. Hence in designing a Mössbauer spectrometer, special attention is given to the quality of velocity drive and the detection system.

In this chapter a brief general discussion of experimental considerations leading to the choice of equipment used in the present investigation will be given. In the following chapter details of design and construction will be given for the particular equipment used.

## (2.1) Velocity Drives

A precisely controlled velocity is essential for obtaining a reliable spectrum. Since the discovery of the Mössbauer Effect, many devices have been developed to produce the suitable relative motion between the source and absorber. The following are a few examples:-

(i) lathe (Preston et al, 1962, Nussbaum et al, 1965)

(ii) Pendulum (Flinn, 1963)

(iii) Cam (Frauenfelder, 1963)

(iv) Rotational disc (Adler and Hane, 1966)

(v) Hydraulic drive (Pound and Rebka, 1960**a**, Kocher, 1965)

(vi) Electromechanical drive (Kandeleit, 1964; Lipkin et al, 1964; Ruegg et al, 1965)

Each of these drives has its advantages and disadvantages. More detailed discussions on driving systems are given in the literature, for example, by Boyle and Hall (1962), Frauenfelder (1963) and Gruverman (1965).

Generally these drives fall into two basic categories; constant velocity drive and velocity scanning

devices (constant acceleration). For the first type, the source is moved with a constant velocity relative to the absorber, or vice versa; and the gamma radiation transmitted through the absorber is recorded by a single channel analyzer. The counting rate of gamma rays at one velocity is recorded. The velocity is then changed to another value and the gamma radiation intensity is again recorded. The same procedure is repeated many times until the velocity spectrum is satisfactorily resolved. For the second type, the driving device sweeps through a range of velocities necessary for the completion of the spectrum. The gamma radiation intensities are recorded in individual channels of a multichannel analyzer calibrated to represent corresponding minimal velocity intervals. The velocity spectrum can be displayed directly on a Cathode Ray Oscilloscope. Since equal time durations must be spent on equal velocity increments, a velocity scanning device requires a constant acceleration motion or a parabolic motion in time.

The main advantage of constant velocity drives lies in the fact that they provide highly accurate velocities and enable detailed investigation of a particular section of the spectrum. They also require simple and less costly

electronic equipment for gamma ray detection. Generally they are sufficiently robust to carry a cryostat for temperature control for source and absorber. However, since the spectrum is recorded point by point, long term drifts in the detecting system may become significant. Moreover, for a source with a very short half-life, its decay must be taken into account. The velocity scanning devices, on the other hand, provide a compensation for drifts in the detecting system because counting of gamma rays at all velocities are recorded "simultaneously". They allow a quick observation of the general pattern of the spectrum.

A constant velocity drive is most useful when a source of relatively long half-life is used or when the recoilless fraction is sufficiently large for the drift in the counting system to be neglected. The relatively low cost of the electronic equipment for a constant velocity system was the main reason for its choice in this investigation. The pneumatic-hydraulic velocity drive built for the present investigations is described in Section 3.2., Chapter 3.

## (2.2) Radiation Detectors

The energy of gamma rays in Mössbauer Effect studies is in the range of a few KeV to about 150 KeV. Detectors used for recording energies at this range are proportional counters, scintillation counters and semiconductor detectors. Generally a source may emit more than one radiation energy, thus it is most desirable that the detector chosen for the detection of one of its radiation energies should provide the best resolution for that particular energy. For example, $^{57}Fe$ emits 14.4 KeV as well as 122 KeV and 136 KeV gamma rays and 6.5 KeV $K_{\alpha\beta}$. It is found that gas-filled proportional counters are most efficient for 14.4 KeV resonant energy detection. Proportional counters of this kind are insensitive to 122 KeV and 136 KeV energies. The 122 KeV gamma ray has an intensity more than ten times that of the 14.4 KeV and will certainly affect the resolving power of the detector if they are recorded simultaneously. Scintillation counters with a very thin sodium iodide crystal are quite efficient for low energies detection, but a fair fraction of high energies are still recorded and interfere with the 14.4 KeV resolution. This latter problem was encountered early in these investigations.

Semiconductor detectors are very efficient for low energy as well as for high energy detection but they are much more costly.

The efficiency of proportional counters drops sharply for gamma ray energies higher than 40 KeV. However, the resolving power of scintillation counters improves immensely and they are considered to be better detectors for energies in this range.

The detector chosen for the present investigation is RSG-61-M1 proportional counter. Its quality will be discussed in the following Chapter (Section 3.3b).

## (2.3) The Electronics

The gamma ray detection system used with a constant velocity drive is a single channel analyzer which is composed of standard electronic equipment readily available commercially. Its cost was comparatively much lower than of a multichannel analyzer used with a constant acceleration drive and for this reason a constant velocity drive was built.

Examinations of the quality of the gamma ray detecting equipment used in the present investigation will be given in Section 3.3, Chapter 3.

## (2.4) Mössbauer Source

There are many Mössbauer sources and those which are used extensively include $^{57}Fe$, $^{119}Sn$, $^{161}Dy$, $^{169}Tm$ and $^{197}Au$. The lattice environment of a source determines whether its recoilless emission is a single line or multiple lines. In order to avoid complication in the investigation of hyperfine splitting, a single line source is used. The sample in which hyperfine splitting is to be investigated is made the absorber because it is more convenient to prepare. Most of the sources are prepared by neutron irradiation but a few are prepared by charged particle bombardment. A source will emit single line energy if it is a diamagnetic material or paramagnetic material with the electron spin correlation time very short compared with the life time of the transition. For a source which is ferromagnetic or antiferromagnetic a single line can be obtained by embedding the source into a host lattice of diamagnetic material or suitable paramagnetic material. For example, $^{57}Fe$ ($^{57}Co$) single line source is prepared by embedding $^{57}Co$ in stainless steel, copper or palladium.

The linewidth of the gamma ray observed is always larger than the natural linewidth. The broadening is due

to the nuclear environment of the source being altered by non-uniformity, unresolved quadrupole splitting, presence of stable isotopes, and self-absorption; and these effects are impossible to eliminate. However, the broadening should be reduced as much as possible, because the reliability of the velocity spectrum depends on the sharpness of the linewidth recorded. Annealing the source is an effective method for reducing the line broadening.

Self-absorption of gamma radiation will occur if the source is made too thick, and for this reason the thickness of the source is kept to less than or about $\frac{1}{\mu}$ cm where $\mu(cm^{-1})$ is the linear atomic absorption coefficient. The strength of the source is therefore limited by its thickness. For example, $^{57}Co$ is limited to about 10 curies per $cm^2$.

The experiments in this thesis involve investigation of the magnetic properties of ilmenite-hematite series mineral. Since the sample consists of Fe atoms, and a fraction (2.19%) of these are $^{57}Fe$ atoms (in stable state), the obvious choice of source is $^{57}Fe$ decay from $^{57}Co$. For the convenience of investigation a single line

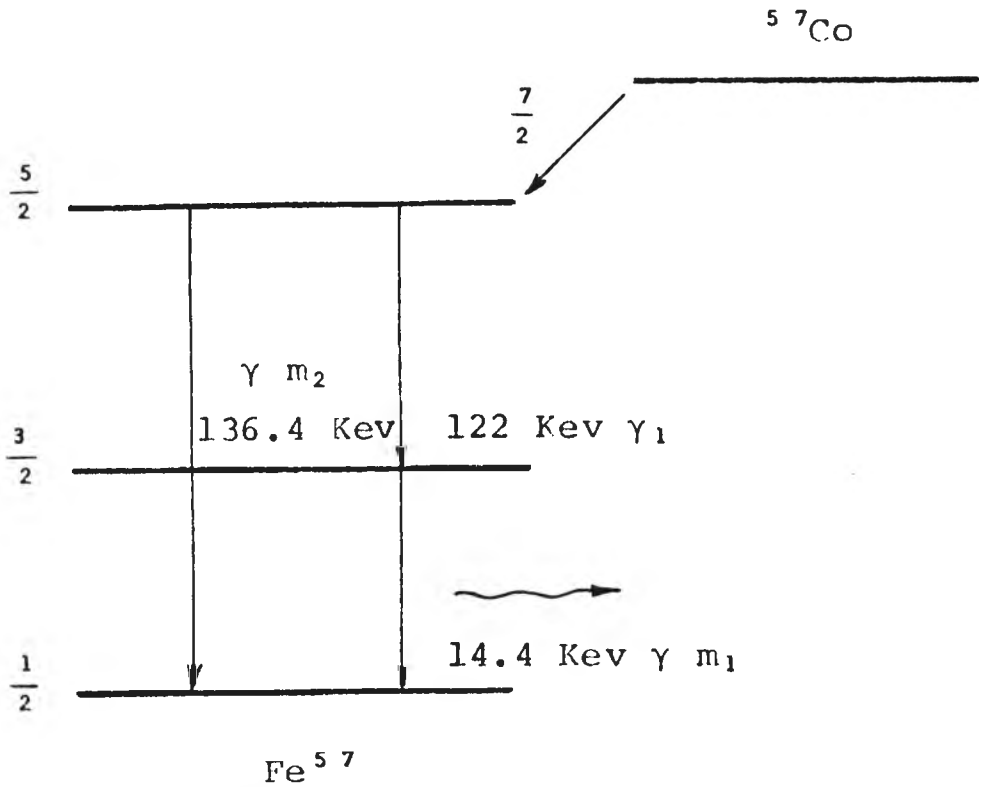


FIGURE 2.2. Decay scheme of $^{57}Co$

source, $^{57}Co$ embedded in a Cu host lattice, is chosen.

The $^{57}Co$ source is prepared by charged particle bombardment. Its decay is shown in Fig. (2.2). There are four simultaneous emissions with different energies and intensities, as shown in Table 2.1 (Muir 1967).

TABLE 2.1

Energy emitted from $^{57}Co$ source

| Emission | Energy ($E_\gamma$) | Intensity ($I_{co}$)% |
|---|---|---|
| $\gamma_{m1}$ | 14.4 KeV | 9.8 |
| $\gamma_{m2}$ | 136.6 KeV | 12.6 |
| $\gamma_1$ | 122.0 KeV | 100.0 |
| $\gamma_{\alpha\beta}$ | 6.5 KeV | 55.0 |

Since the source emits four energies and the lowest intensity 14.4 KeV is the only one required for Mössbauer Effect investigation, therefore a very sensitive detector is necessary for resolving the 14.4 KeV from the adjacent more intense 6.5 KeV and eliminating the interference (overlapping) from the very intense high energy 122 KeV.

TABLE 2.2

Properties of $Fe^{57}$

| | Ground State | First Excited State |
|---|---|---|
| Energy (keV) | 0 | 14.4 |
| Spin and parity | $\frac{1}{2}^-$ | $3/2^-$ |
| Magnetic moment (nm) | 0.0903 | -0.1547 |
| Quadrupole moment (barns) | 0 | 0.29±0.02 |
| Mean life (s) | stable | $1.4 \times 10^{-7}$ |
| Resonance cross section $\sigma_o$ | | $2.38 \times 10^{-18} cm^2$ |
| Resonance cross section, $\sigma_o$, calculated | | $2.2 \times 10^{-18} cm^2$ |
| $t_{\frac{1}{2}}$ ($\gamma_m$) | | $9.77 \times 10^{-8} s$ |
| Internal conversion coefficient, $\alpha_T(\gamma_m)$ | | 9.00 |
| IA | | 2.19% |
| Derived Parameters | | |
| $\Gamma$, Natural linewidth | | $4.6697 \times 10^{-12} keV$ |
| Wo Observable linewidth | | 0.19427 mm/s |
| $E_\gamma$ Recoil energy | | $1.9567 \times 10^{-13} ev$ |

The properties of $^{57}Fe$ are shown in Table 2.2. Some formulae for the calculations of its properties are given as follows:

Resonance cross-section:

$$\sigma_o = 2.446\ 36 \times 10^{-15} \frac{1}{E_\gamma (kev)2} \frac{1 + 2Ie}{1 + 2I_g} \frac{1}{1 + \alpha_t} cm^2 \qquad (2.2)$$

Natural linewidth

$$\Gamma = 4.56231 \times 10^{-19} \frac{1}{t_{\frac{1}{2}} (sec)} kev \qquad (2.3)$$

Observable linewidth (minimum)

$$W_o = 2.99793 \times \frac{2\Gamma\ (kev)}{E\ (kev)} mm/s \qquad (2.4)$$

Recoil energy

$$E_r = 5.36942 \times 10^{-4} \frac{E_\gamma\ (kev)^2}{m\ (amu)} eV \qquad (2.5)$$

## (2.5) Absorbers

In preparing the absorbers precautions must be taken to ensure the uniformity of lattice environment. To prevent the effect of self absorption the thickness of absorber is in general about $\frac{2}{\mu}$ cm, where $\mu$ ($cm^{-1}$) is

the atomic absorption coefficient. Absorbers made commercially include compounds and foils, and are fabricated using isotopically enriched materials or natural materials. For natural iron absorbers the content of $^{57}Fe$ stable isotope is 2.19% but the enriched absorbers can have greater than 90% of $^{57}Fe$.

Shirley et al (1961) proved that if the linewidth of the source is $\Gamma_s$ and the linewidth of the absorber is $\Gamma_a$, then the apparent linewidth $\Gamma_{app}$ of the absorption spectrum is given by

$$\Gamma_{app} \simeq 2\Gamma_s \simeq 2\Gamma_a \simeq 2\Gamma_\tau$$

where

$$\Gamma_s = \Gamma_a = \Gamma_\tau$$

and $\Gamma_\tau$ is the linewidth of nuclear transition. The experimental linewidth $\Gamma_{exp}$, however, is larger than $\Gamma_{app}$ because of the broadening effect mentioned in Section (2.4).

Absorbers used in the present investigations for calibration purposes include materials of known properties such as iron and $K_4Fe(CN)_6.3H_2O$ which have a

very narrow linewidth and well defined energy shift. Their velocity spectra are valuable for standardizing the unknown velocity spectrum and for evaluating the constancy and reproducability of the velocity of the drive. The iron foil contains 1.9 mg per $cm^2$ of enriched $^{57}Fe$ (90%) and the $K_4Fe(CN)_6.3H_20$ contains 0.05 mg per $cm^2$ of enriched $^{57}Fe$. Enriched absorbers will give a sharper absorption line. In Section 3.4, Chapter 3, the velocity spectra of $K_4Fe(CN)_6.3H_20$ and iron are obtained and analyzed to determine the constancy of the velocity drive.

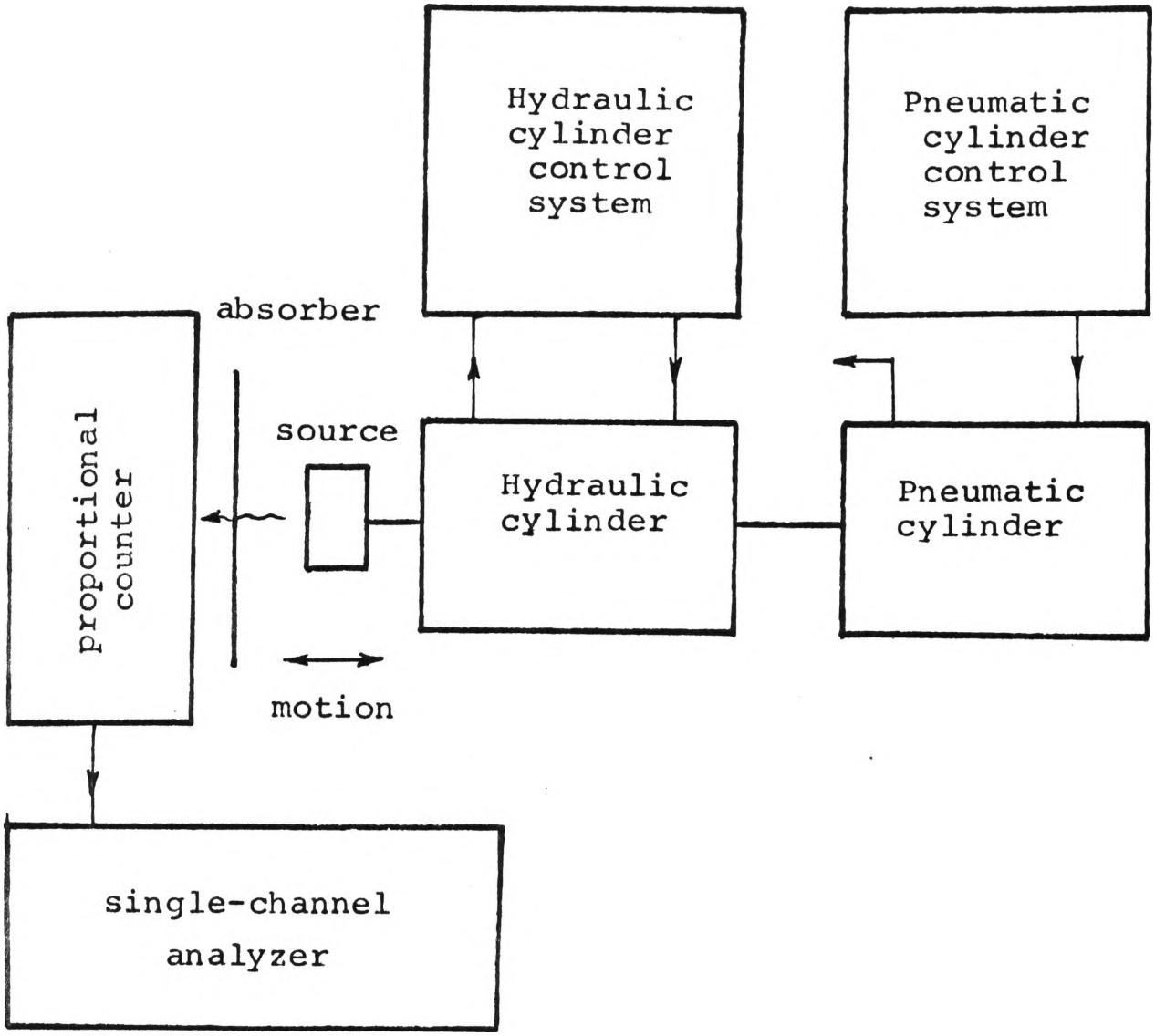


FIGURE 3.1. Schematic diagram of the Mössbauer Spectrometer

# CHAPTER 3

# THE DESIGN, CONSTRUCTION AND PERFORMANCE OF THE MÖSSBAUER SPECTROMETER

There are many Mössbauer Spectrometers available commercially. A study of their prices established that they were beyond the financial resources of the department. It was decided, therefore, to construct a spectrometer suitable for the present investigation, from the limited resources available. The constant velocity drive built for the present research is a pneumatic-hydraulic unit, composed of commercial industrial components readily and cheaply available. The electronic equipment of the gamma-ray detection system is also cheaply available commercially.

## (3.1) Schematic Diagram of Complete Spectrometer

A schematic diagram of the Mössbauer spectrometer built in this department is shown in Figure 3.1. The Doppler shift in the emission energy of the source is provided by the coupled cylinders which are controlled to give a constant velocity motion. The counting rate of $\gamma$-rays which pass through the sample (absorber) is recorded by the single channel analyzer. More detailed diagrams of the pneumatic-hydraulic drive and the detection system are

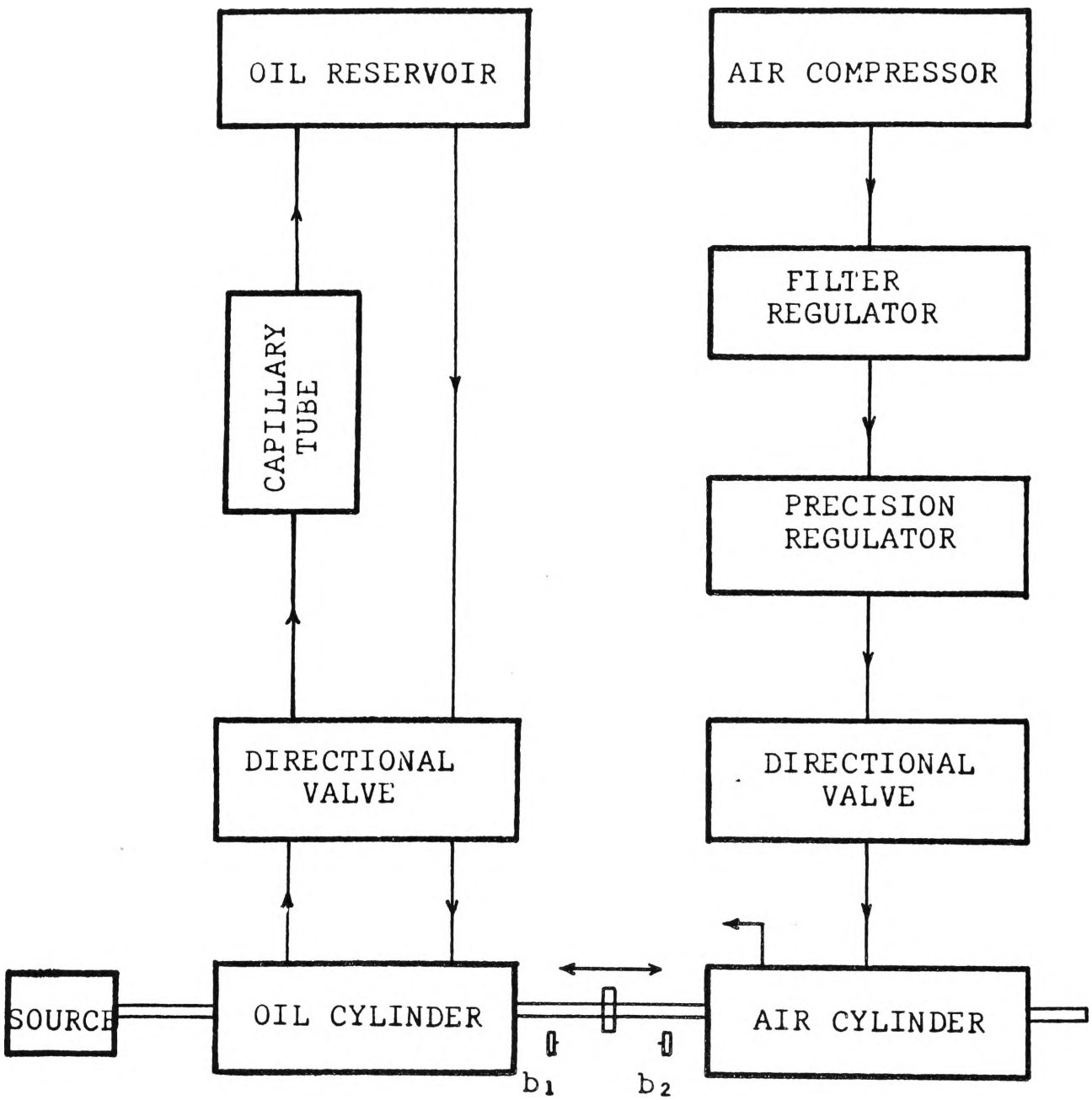


FIGURE 3.2. Pneumatic-hydraulic constant velocity drive.

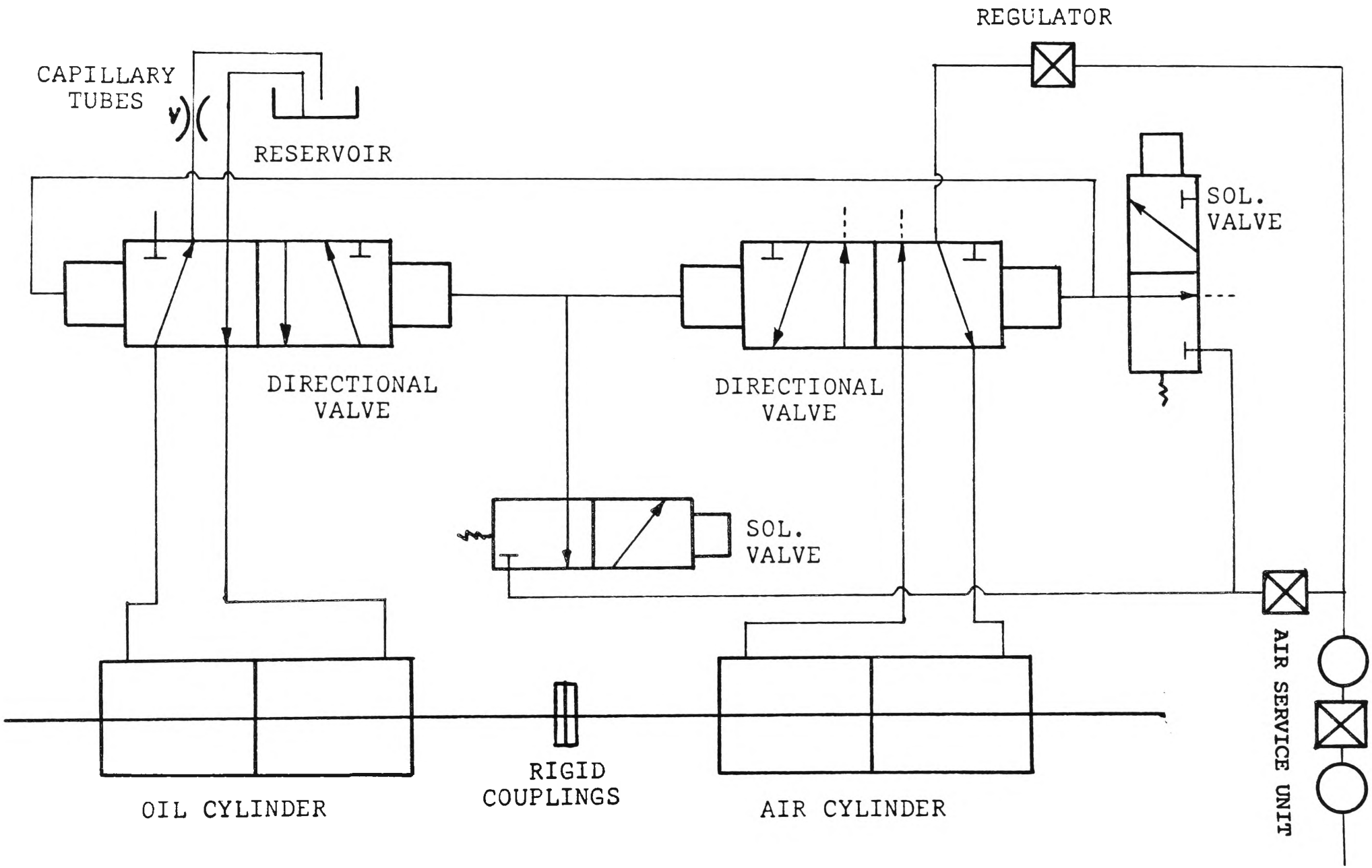


FIGURE 3.3. Pneumatic-hydraulic constant velocity drive

given in Figures 3.2, 3.3 and 3.15. The components of the drive and the detection system are listed in Appendixes 1 and 2 respectively.

A detailed discussion of the design and construction of the constant velocity drive is given in Section 3.2. The performance of the detection system is discussed in Section 3.3 followed by the testing of the overall performance of the spectrometer using absorbers with known spectra (Section 3.4).

## (3.2) The Constant Velocity Drive

A schematic diagram of the components of the constant velocity drive is shown in Figure 3.2, a pneumatic-hydraulic circuit diagram is shown in Figure 3.3 and a photograph of the drive is shown in Figure 3.15. The thrust of the drive is provided by the air cylinder which drives the hydraulic cylinder by direct axial coupling of their shafts. The controlled flow rate of oil at the exhaust of the hydraulic cylinder determines the velocity of the drive. This rate is controlled by the use of various lengths of capillary tube and an appropriate pneumatic pressure.

An air supply is provided by an air compressor unit which is adjusted automatically to maintain an air pressure of 100 to 125 p.s.i. The air passes through a service unit which provides filtration and lubrication and also regulates the pressure to a relatively constant value of 90.0 ± 0.5 p.s.i. A precision pressure regulator further regulates the pressure to any chosen value between 0.14 to 60 p.s.i. ± 0.05 p.s.i. for an input pressure fluctuation of ± 20 p.s.i. This constant pressure is then applied to one side of a double-acting air cylinder through a four-way directional valve. The other side of the air cylinder is opened to atmospheric pressure. The shaft of the air cylinder is coupled to that of the hydraulic cylinder and hence provides the driving force for the piston in the hydraulic cylinder. Because of the pressure applied on the hydraulic cylinder, the oil from the reservoir is drawn through another four-way directional valve into one side of the double-acting hydraulic cylinder. At the other end of the cylinder, the oil is driven back by the pressure to the reservoir via a series of capillary tubes of various bore sizes and tube lengths. These capillary tubes are submerged in a temperature controlled water bath so that the viscosity

of the oil can be kept constant. The speed of travel of the hydraulic piston is determined by the pneumatic pressure and capillary tubes which are chosen. The Poiseuille's flow formula for a capillary is

$$Q = \frac{\pi P R^4}{8\eta L} \tag{3.1}$$

where Q is the volume of oil flowing through a cross section per unit time,

P is the pressure difference between the ends of the tube.

R is the inside radius of the tube.

$\eta$ is the viscosity of the oil.

L is the length of the tube.

From this it can be seen that with fixed R and $\eta$ the flow rate is directly proportional to the length L of capillary and the pressure difference P between its ends. With the combination of pressure adjustment and capillary selection, the drive is capable of providing nearly continuous velocity variation with a precision of ± 0.005 mm/s and an accuracy of better than ±0.8% (see Section 3.3).

The fourth power dependence on R shows the dangers inherent in using a variable constriction (needle valve) as a control mechanism.

The required Doppler shift in gamma ray energy can be attained by mounting the source on the shaft of the hydraulic cylinder. At the end of a stroke a micro-switch is tripped, enabling a control circuit to activate a solenoid valve which in turn reverses the position of the four-way directional valves. The flow direction of both air and oil is then reversed simultaneously, hence the cylinder motion is also reversed. The same procedure is repeated at the end of the reversed stroke. Two micro-switches, in this way, produce a reciprocating motion of the drive.

It is unsatisfactory to use an air cylinder alone for the production of constant motion, due to the fact that air is compressible and elastic. Any friction arising during a working stroke of the cylinder will thus generate serious vibrations in motion. Hydraulic-mechanical systems give a better stability but a constant pressure control will be more difficult to achieve due to possible mechanical

vibration. However, the hydro-pneumatic system described in this chapter performs very well. The high pressure provided by the compressed air can be adjusted to maintain at one constant value throughout the experiment. The extremely large driving force (1130 lb) used and the dominating resistive effect of the capillaries makes all the frictional force negligible. The smaller diameter of the hydraulic piston compared with the pneumatic piston assures an amplification of pressure to the capillary inlets (see Section 3.2f).

As previously mentioned, this drive has the advantage over other types of pneumatic-hydraulic drives whose velocity is controlled by employing a needle valve, because the rate of flow is linearly proportional to the length of capillary but proportional to the fourth power of a capillary diameter. By the choice of capillaries with diameters very large compared with any particle suspensions in the oil, control is affected simply by the length of capillary and pressure difference between its ends.

The remaining of this Section describes the characteristics and function of components of the constant velocity drive.

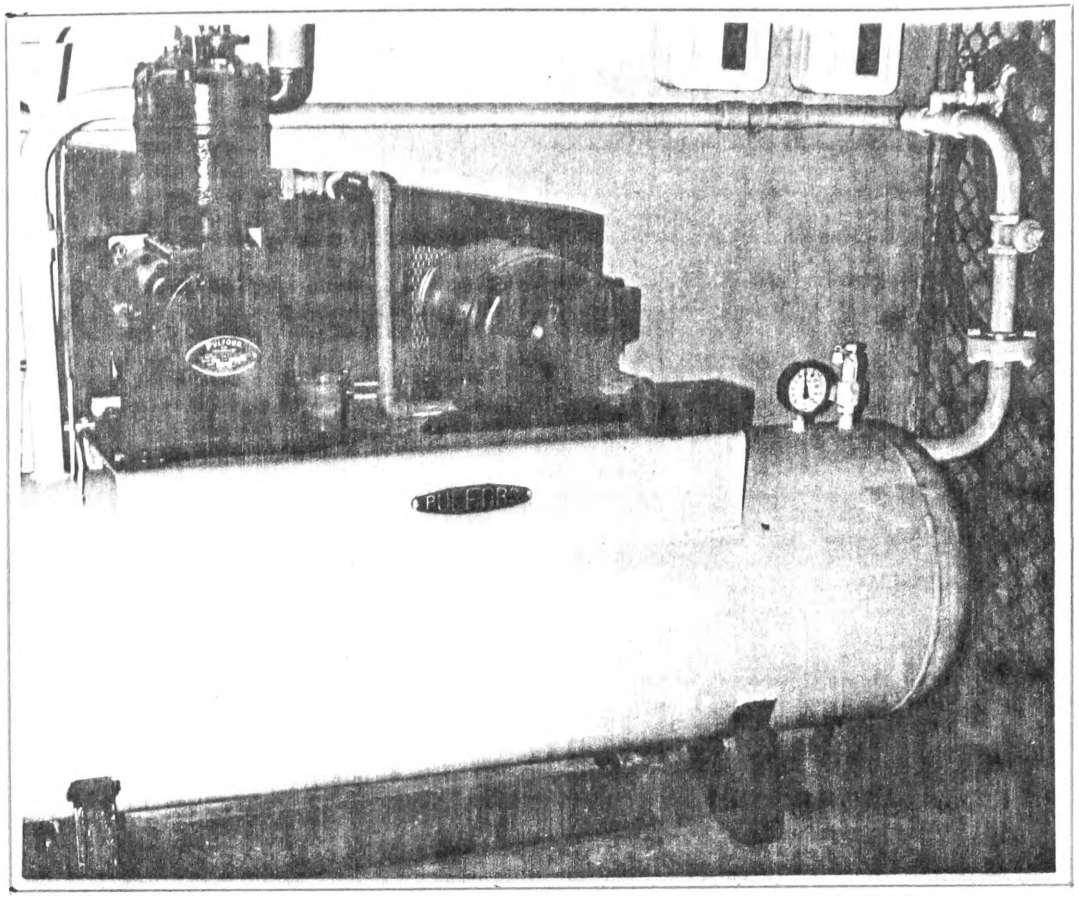

FIGURE 3. 4. Air Compressor Unit

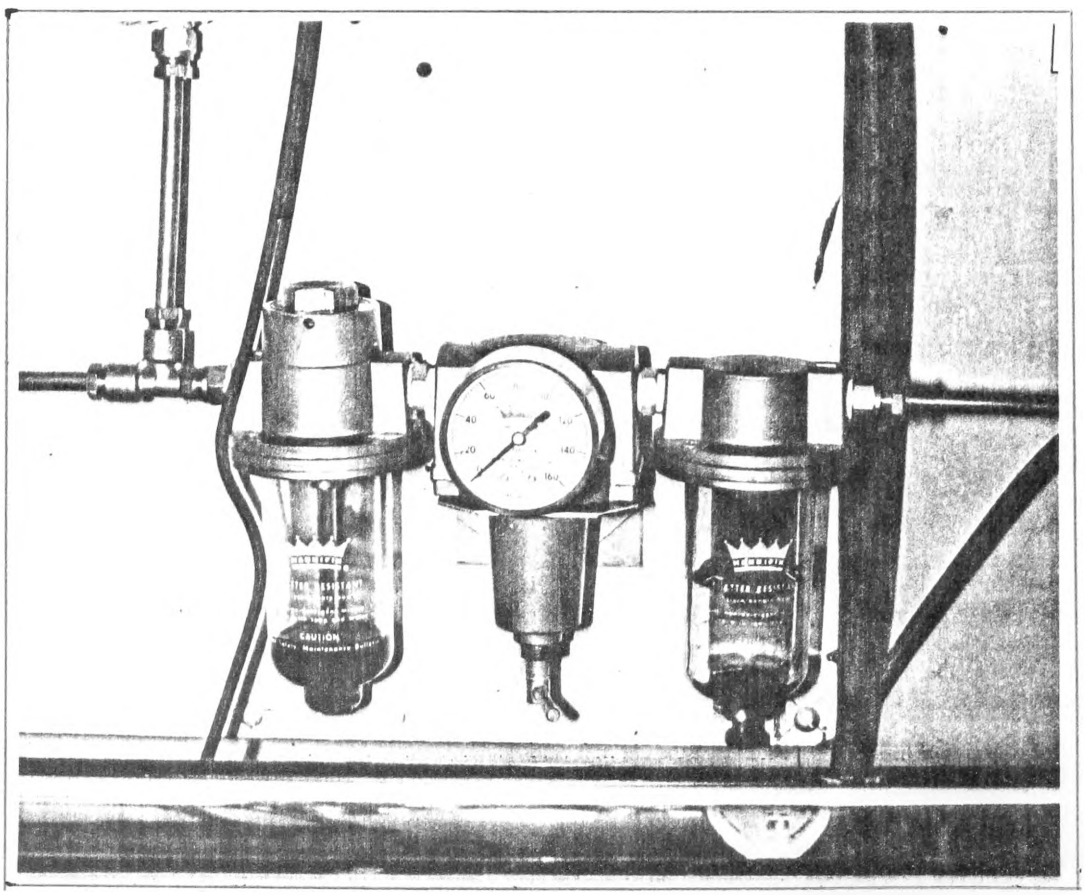

FIGURE 3.5. Air Service Unit

(a) Air Compressor

The main air supply is provided by an air compressor unit (Figure 3.4) consisting of a compressor and a large receiver tank of dimension two feet in diameter by six feet long. A large tank has the advantage of keeping the pressure free from rapid fluctuations during operation. The air pressure is regulated automatically to maintain a pressure between 100 and 125 p.s.i.

(b) Compressed Air Service Unit

A compressed-air-service unit (Figure 3.5) is used for purification of the air and control of pressure. It consists of an air filter, a regulator and a lubricator. This unit is essential for maximum protection of pneumatic equipment and is also responsible for the vibration free motion of the cylinders. Corrosive moisture, dust and other foreign particles in the air supply are first filtered, then the air pressure is regulated to a relatively constant value of 90.0 ± 0.05 p.s.i. The air is then lubricated by the oil filled lubricator where atomised oil enters the

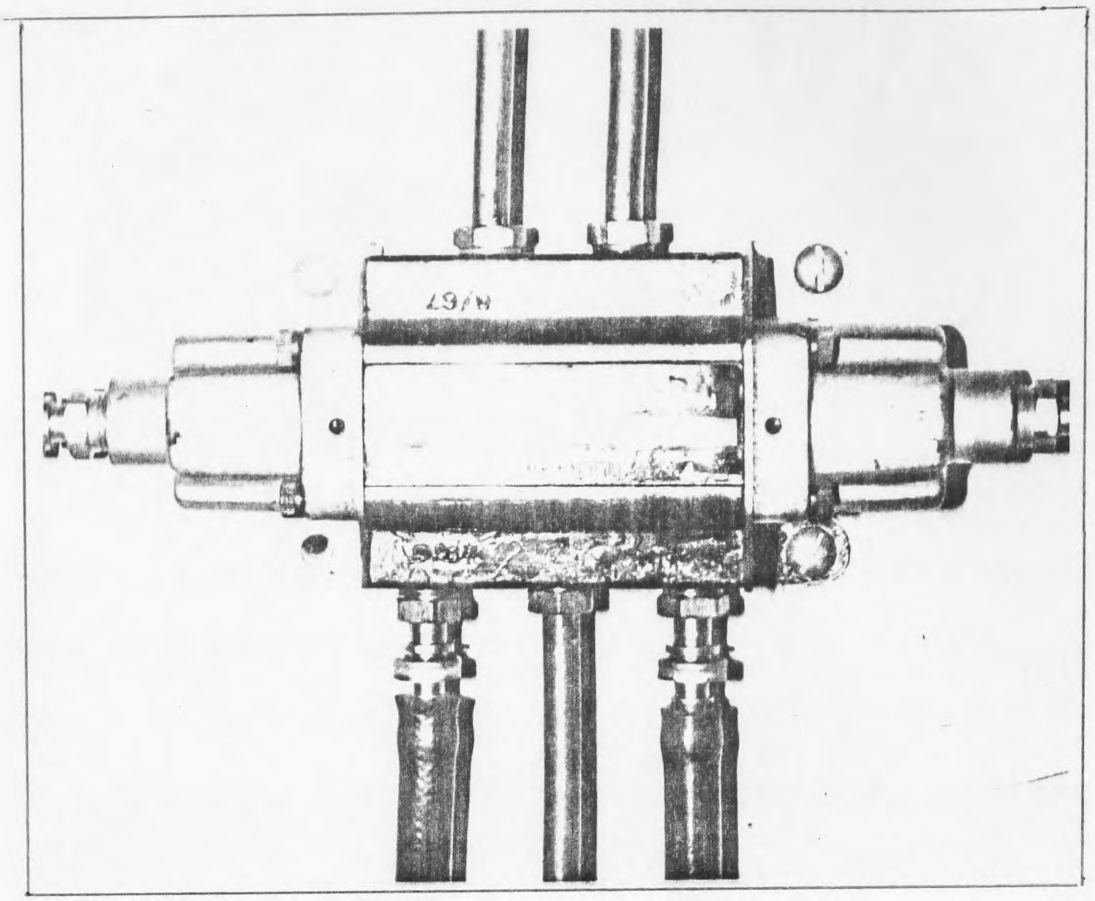

FIGURE 3.6. Four-way directional Valve

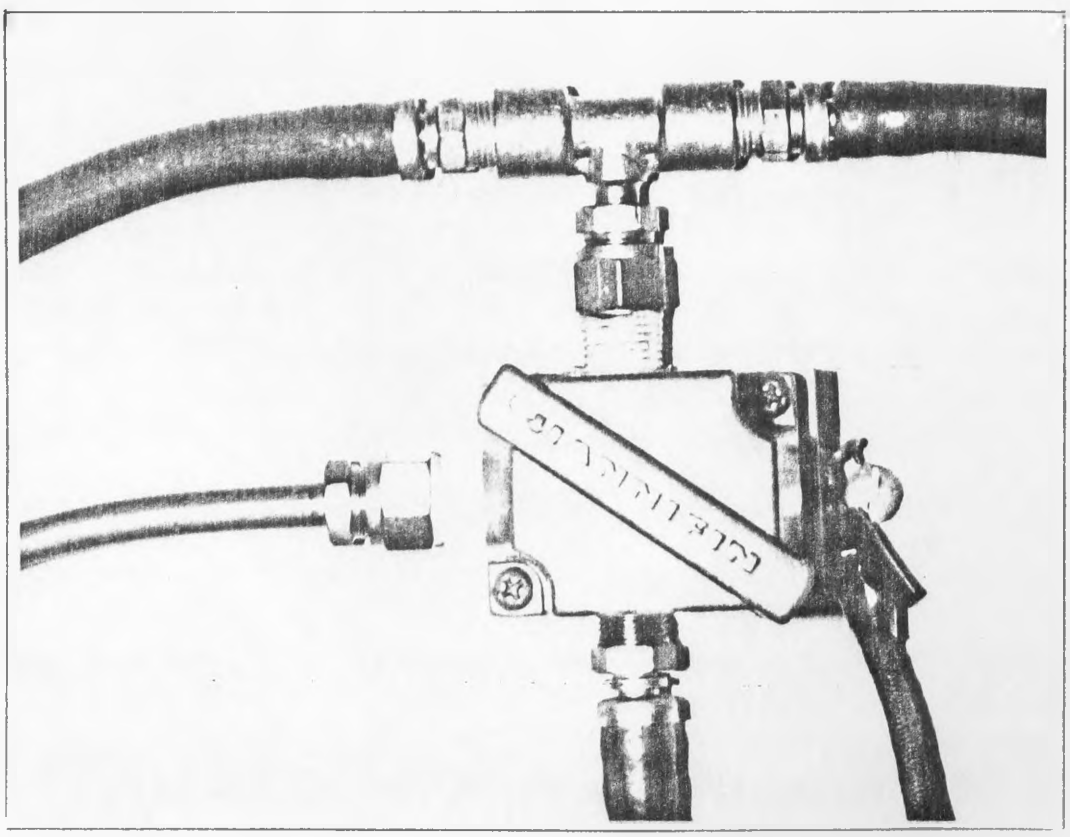

FIGURE 3.7. Three-way Solenoid Valve

flowing air in accurately controlled amounts. This protects the pneumatic equipment from unnecessary wear and corrosion.

(c) Precision Pressure Regulator

A precision regulator, Shoketsu Model No. 2302-202, is used to provide an extremely accurate pressure for the operation of the air cylinder. The pressure is continuously adjustable within the range of 0.14 to 60 p.s.i. It has the important characteristic of reducing to a negligible value any fluctuations in input pressure. For example, an input pressure fluctuation of 60 - 100 p.s.i. only causes a fluctuation of ± 0.05 p.s.i. in an output pressure of 30 p.s.i. Since the input pressure is relatively constant at 90.0 ± 0.05 p.s.i. a practically fluctuation free operational pressure is expected.

(d) Four-way Directional Valve

Two four-way directional valves (Figure 3.6) Hannifin Model V2/74, are used for directing the flow of oil and air to the cylinders because they can be operated

automatically by a double-acting air pressure impulse pilot system. They are capable of controlling compressed air and oil pressures at up to 200 p.s.i. and 300 p.s.i. respectively. An important characteristic of this valve is that all passages through the valve are closed when the spool is located at the mid-position or when passing by this position, a feature of great importance in controlling the motion of the cylinders, for oil and air are prevented from exhausting prematurely from their respective cylinders due to slight lack of synchronism in the movement of the valves.

(e) Three-way Solenoid Valve

Two three-way solenoid valves (Figure 3.7) together with a control circuit system are designed to operate the air pilots of the four-way directional valves. These solenoid valves are in the normally-closed position when they are not actuated; thus, the air supply of approximately 20 p.s.i. necessary for the operation of the pilots is normally shut off by the solenoid valves. When a solenoid valve is actuated by closing a microswitch of the control circuit system, the valve is opened and allows

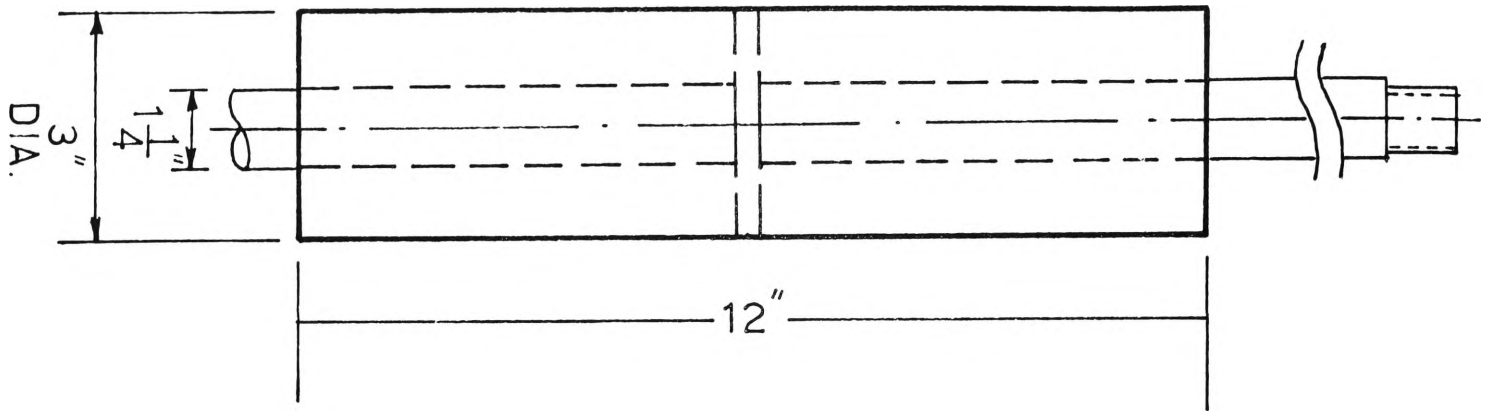


FIGURE 3.8.(a) Oil Cylinder

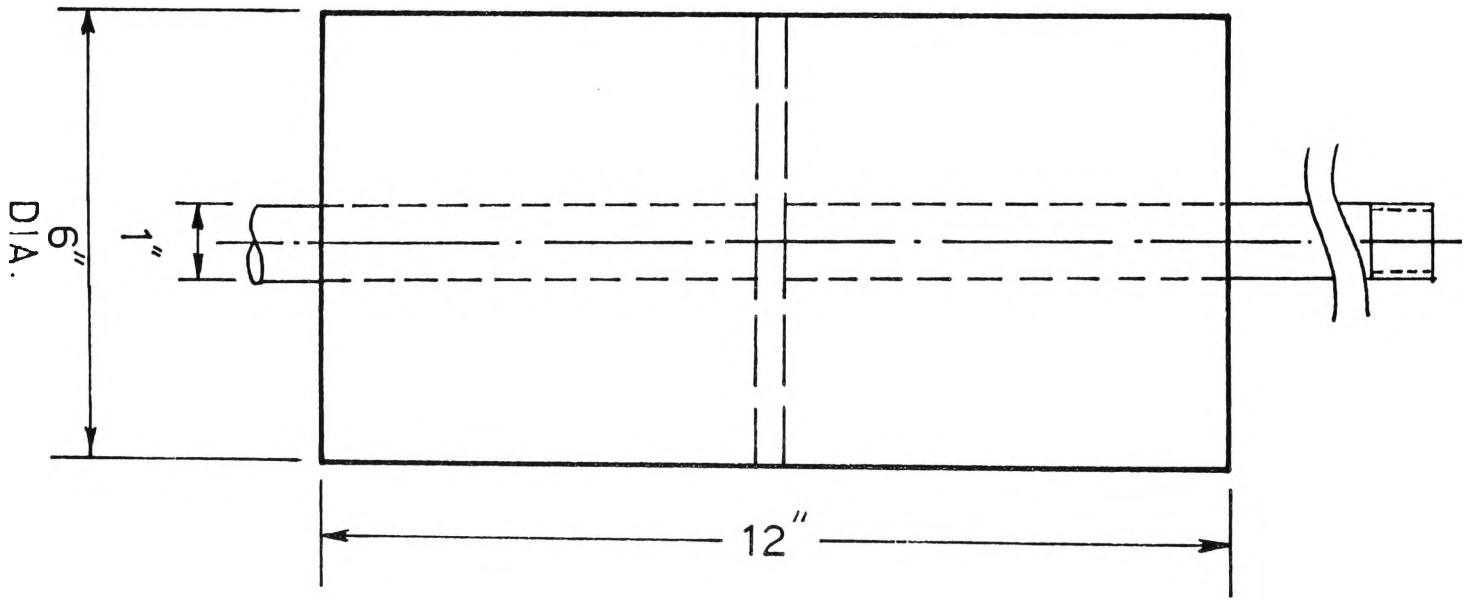


FIGURE 3.8.(b). Air Cylinder

air to operate the pilots of the four-way directional valves; hence reversing the direction of oil and air flow. The same procedure is repeated when the second solenoid valve is actuated by a second microswitch at the end of the reversed stroke. Two microswitches, in this way, produce a reciprocating motion of the cylinders. The control circuit, which will be discussed in more detail in Section 3.2 ($\ell$), is designed to prolong the duration of actuation of the solenoid valves, so that sufficient time is allowed for the complete operation of the pilots. After actuation is over the solenoid valve returns to its normally-closed position. The compressed air in the pilot housing now escapes to the atmosphere through a long rubber tube connected to the solenoid valve so that the exhaust air becomes a stream line flow and the loud exhaust noise is considerably reduced.

(f) Air Cylinder and Hydraulic Cylinder

The main components of the system are an air cylinder of 6 in. (15.2 cm) bore diameter and an hydraulic cylinder of 3 in. (7.6 cm) bore diameter (Figure 3.8). Both cylinders have a working stroke of 12 inches (30.48 cm). They are

coupled together in series by a pair of rigid couplings which are screwed and locked on the shafts of the cylinders and tightened together by bolts and nuts. The shaft (1¼" diameter) of the hydraulic cylinder is robust enough to carry the weight of the source or absorber housing, and also a cryostat or other necessary accessories. The air cylinder can stand a working pressure of up to 200 p.s.i. and the hydraulic cylinder up to 300 p.s.i. Double acting cylinders are chosen because the thrust, which depends on the annular area of the piston between piston rod and cylinder wall, will be the same in both directions of motion. It is preferable to have the magnitude of the velocity equal in both directions.

TABLE 3.1.

Dimensions of the air cylinder and the hydraulic cylinder

| Cylinder | Cylinder Area | Rod Diam. | Annular Area |
|---|---|---|---|
| Air | 28.27 $in^2$ | 1" | 27.49 $in^2$ |
| Hydraulic | 7.065 $in^2$ | 1¼" | 5.87 $in^2$ |

Since the annular area of the air cylinder is about 4.6 larger than that of the hydraulic cylinder, there is a

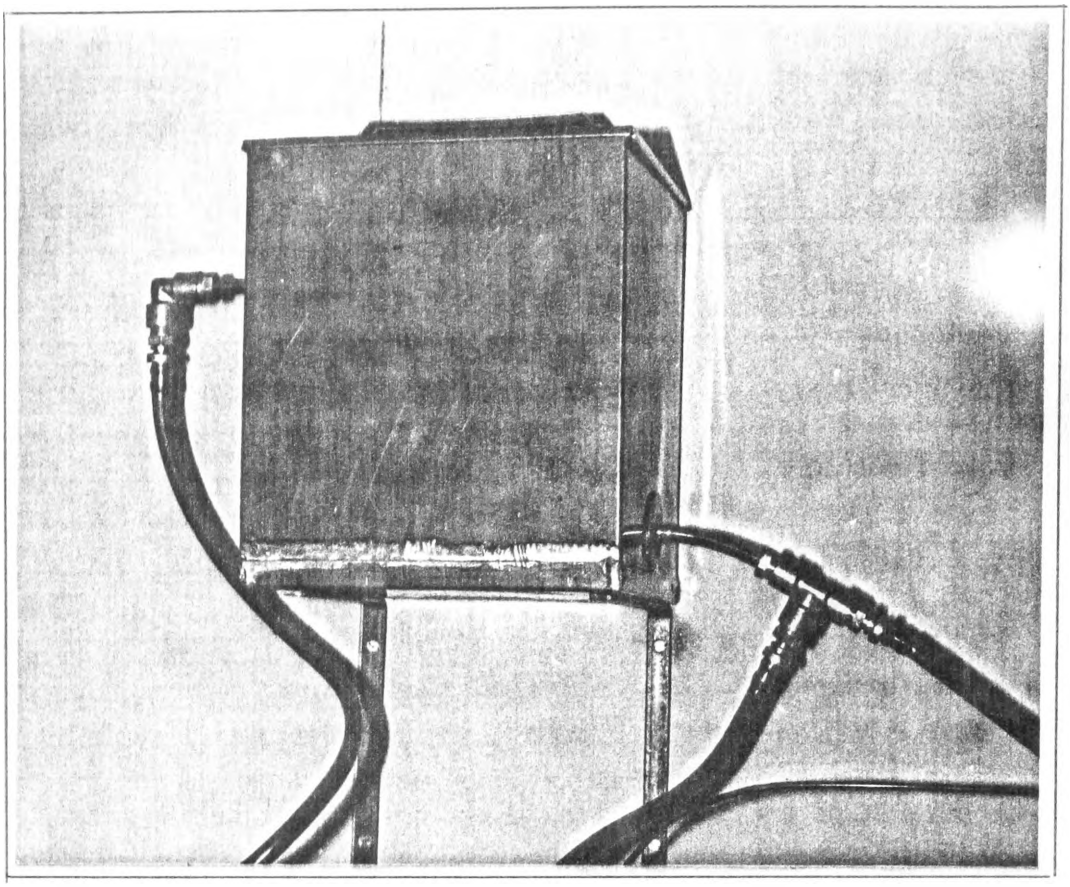

FIGURE 3.9. Oil Reservoir

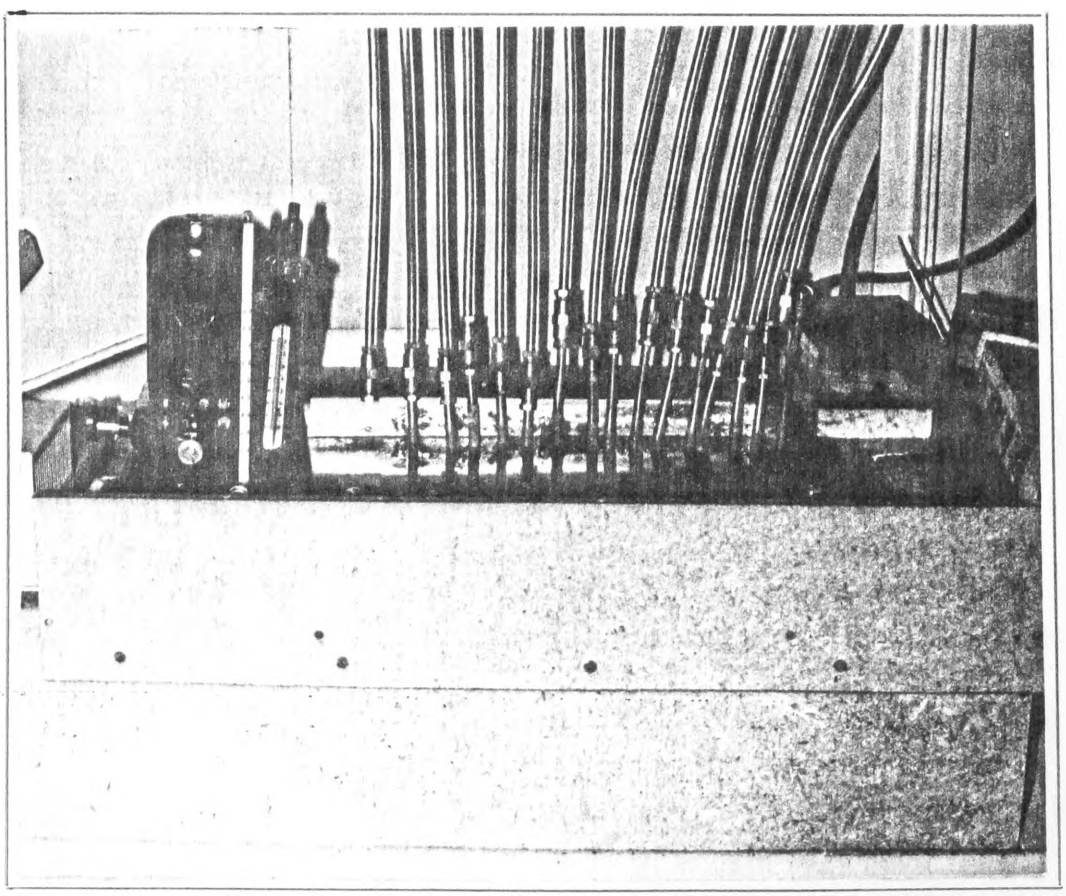

**FIGURE 3.10** **Water Bath** containing a set of capillary tubes

4.6 times amplification of hydraulic pressure. For example, a pneumatic pressure of 40 p.s.i. (or a driving force of 1130.80 lb) is amplified to give a hydraulic pressure of 184 p.s.i. (or a force of 5201.68 lb).

(g) Oil Reservoir and Hydraulic Fluid

A copper container of size 18 cm x 18 cm x 20 cm (Figure 3.9) is used as an oil reservoir. A lid is provided to keep the oil free from dust. The reservoir has a capacity of about one gallon, which is sufficient for providing oil for the small hydraulic system. A large reservoir is unnecessary since the oil flowing into the reservoir must equal the amount flowing out back into the system. The outlet is situated at 4 cm above the bottom of the tank so that no air bubbles or sediment will be picked up when the oil flows out of the reservoir. The inlet is situated on the opposite wall about 4 cm from the top so that the flow of oil into the reservoir will not disturb the sediments at the bottom of the reservoir. Two clear plastic tubes are used for outlet and inlet piping. The transparency of these tubes enables any air bubbles and impurities present in the oil to be readily

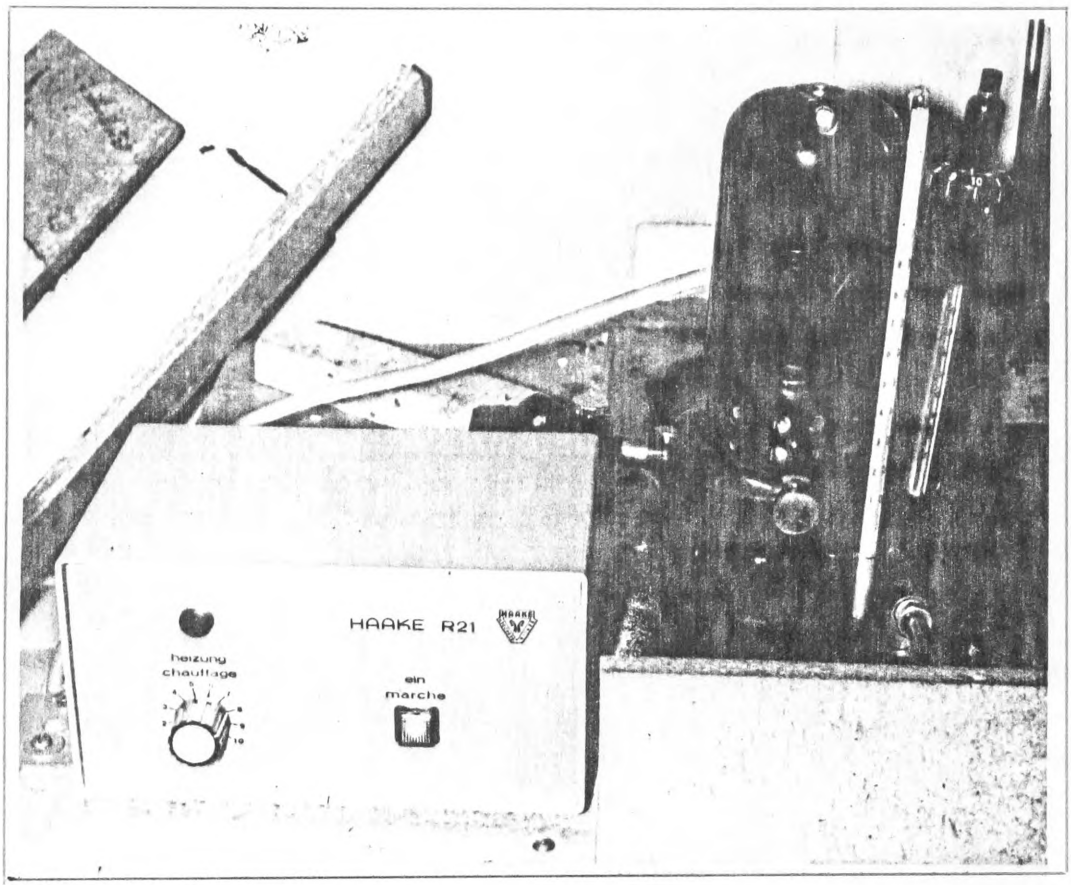


FIGURE 3.11. Temperature Control Unit

observed. This is particularly useful when bleeding the hydraulic cylinder.

The oil used for the hydraulic system is Caltex Rando-A hydraulic fluid. Its specific gravity (60/60°F) is 0.873, viscosity 33.1 centistoke at 100°F (37.8°C) and 5.48 centistoke at 210°F (99°C). It has a high viscosity index of 112 (ASTM D 2270). A high viscosity index signifies relative small change of viscosity with temperature. The temperature-viscosity relationship is discussed in Section 3.2 (i).

(h) Constant Temperature Bath

A stainless steel tub of dimension 43 cm x 60 cm x 25 cm which has a capacity of 60 litres of water is housed in an insulation box of dimension 60 cm x 75 cm x 30 cm (Figure 3.10). The space surrounding the tub is filled with vermiculite. A lid, also lined with an insulating sheet, is provided to prevent heat loss due to evaporation.

The temperature control unit (Figure 3.11) used is the Haake "Unitherm" constant temperature circulator

capable of providing temperature control up to 150°C. The heater output can be varied continuously from 0 to 1000 watt by employing a solid-state electronics Triac relay. The precision of temperature control is ±0.01°C.

The relationship between the viscosity and temperature of a hydraulic fluid (Blackburn et al, 1960) is given by

$$\eta = \eta_o e^{-\lambda (T-T_o)} \qquad (3.2)$$

where $\eta$ is the viscosity of hydraulic fluid at temperature T°C.

$\eta_o$ is the viscosity of hydraulic fluid at temperatures $T_o$°C.

$\lambda$ is the temperature coefficient of viscosity.

The typical value of $\lambda$ for a petroleum base hydraulic fluid is of order $10^{-2}$/°C. For a change in bath temperature, $T-T_o$, of order $\pm 10^{-2}$°C the corresponding variation in viscosity is about ± 0.01% and this would result in a speed variation of about ± 0.01%.

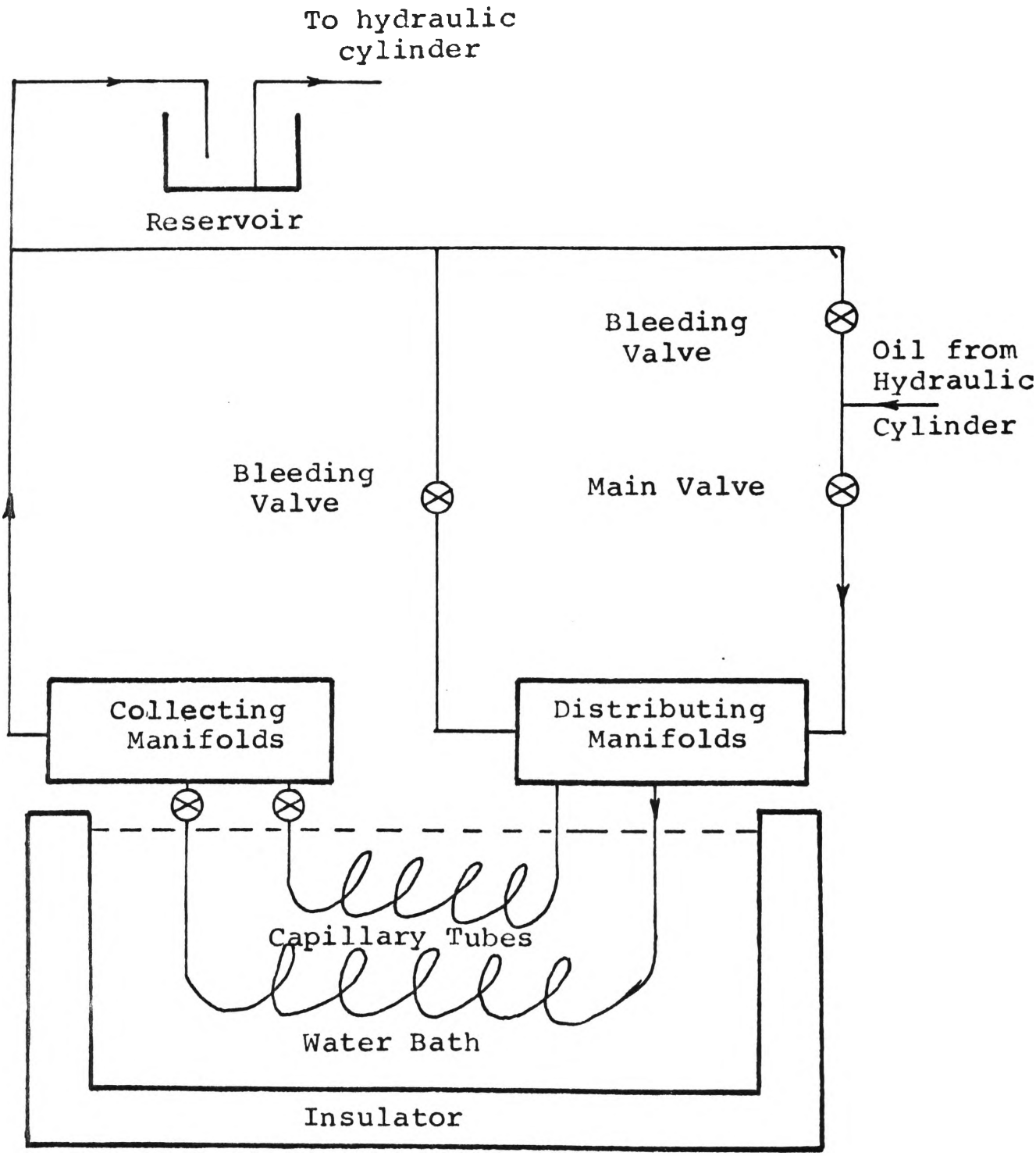


FIGURE 3.12. Velocity Control System

(i) Capillary Tube Assembly

The flow rate of oil which determines the velocity of the motion, is controlled by a series of copper capillary tubes of various bore sizes and different tube lengths. Copper tubes are used because they are more flexible and less corrosive when in the water bath. A simple capillary tube assembly is shown in Figure 3.12.

The oil from the hydraulic cylinder is diverted into two directions at a tee junction. One path leads to a bleeding valve where any air from the hydraulic cylinder can escape with the oil and flows directly back to the reservoir without flowing through the velocity control system. The other leads to a main valve which connects to a velocity control system. Oil is allowed to flow through the system only after the bleeding of the hydraulic cylinder is completed. During operation the bleeding valve is normally at a closed position. For convenience during operation the motion of the piston and therefore the oil flow, can be stopped immediately if necessary by simply closing the main valve.

Another bleeding valve is attached to the end of the second manifold. The air which is trapped in the dis-

tributing manifolds can be removed quickly by opening this valve and letting the air, together with the oil, flow directly back to the reservoir without flowing through the capillary tubes. This bleeding valve is particularly useful when replacement of capillary tubes is required.

Once the hydraulic cylinder and the velocity control system are bled free of air they should stay in that condition indefinitely. An occasional check can ensure that the operation is satisfactory.

The capillary tubes are of various diameters and therefore it is necessary that each capillary tube be connected by brazing onto a 12" long by 5/16" diameter copper tube which can fit the outlet port size of the distributing manifold. About 9" of the copper tube is submerged in the water bath to ensure that the oil will gradually be raised to operational temperature before it enters the capillary tube. Each of the capillary tubes is wound in coils before submerging in the water bath so that it can be removed easily when replacement is required. The other end of the capillary tube is also brazed onto

a 12" long by 5/16" diameter copper tube which is connected to a shut off valve. Again part of the copper tube is submerged in water to ensure that the oil is still at operational temperature before it leaves the capillary tube. The outlets of the shut off valves are connected to the two collecting manifolds which in turn are connected to the reservoir via a transparent plastic tube. The transparent tube is used so that any air bubbles coming out of the capillary tubes can be seen; thus indicating that the system needs bleeding. In the absence of accidents or system alteration this should not happen.

The choice of capillary tube size depends on the viscosity of oil and the hydraulic pressure. For example, it was found by experiment that for an air pressure of 40 p.s.i., corresponding to an induced hydraulic pressure of 184 p.s.i., and for an oil temperature of 30°C, a 3.5 feet tube of 0.026" diameter will give a very slow velocity of 0.01 mm/s. A series of capillary can be cut to appropriate length empirically so as to give a velocity range from 0.005 mm/s to 6.6 mm/s in convenient steps. A required velocity can be obtained by the opening

TABLE 3.2

Capillary Assembly System

| Tube No. | Velocity (mm/s) |
|---|---|
| 1 | 0.005 |
| 2 | 0.01 |
| 3 | 0.02 |
| 4 | 0.02 |
| 5 | 0.02 |
| 6 | 0.02 |
| 7 | 0.1 |
| 8 | 0.2 |
| 9 | 0.3 |
| 10 | 0.4 |
| 11 | 0.5 |
| 12 | 1.0 |
| 13 | 1.0 |
| 14 | 1.0 |
| 15 | 1.0 |
| 16 | 1.0 |

of valves of the appropriate capillaries. For example, the opening of valves Nos. 7 and 2 gives a velocity of 0.11 mm/s, Nos. 7 and 3 , 0.12 mm/s; Nos. 7,2 and 3 , 0.13 mm/s. and Nos. 11, 7, 2 and 3 , 0.63 mm/s, and so on. As many capillaries as necessary can be operated to obtain the desired velocity.

The velocity range can be changed if required by simply replacing or adding a few more capillaries or changing the driving pressure. However, for the investigation of natural ilmenite which has absorption lines lying mainly within the limits of ± 2 mm/s, the velocity range given above is more than adequate to scan the whole Mössbauer spectrum with a precision of ± 0.005 mm/s.

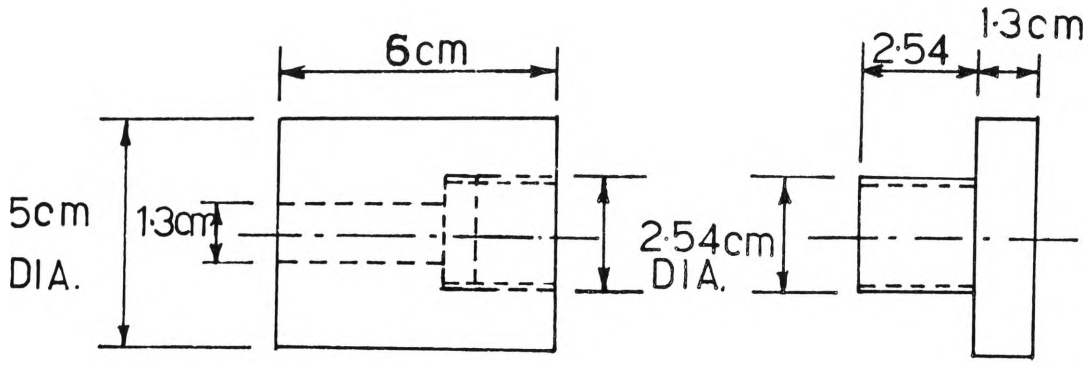


FIGURE 3.13 Source Holder

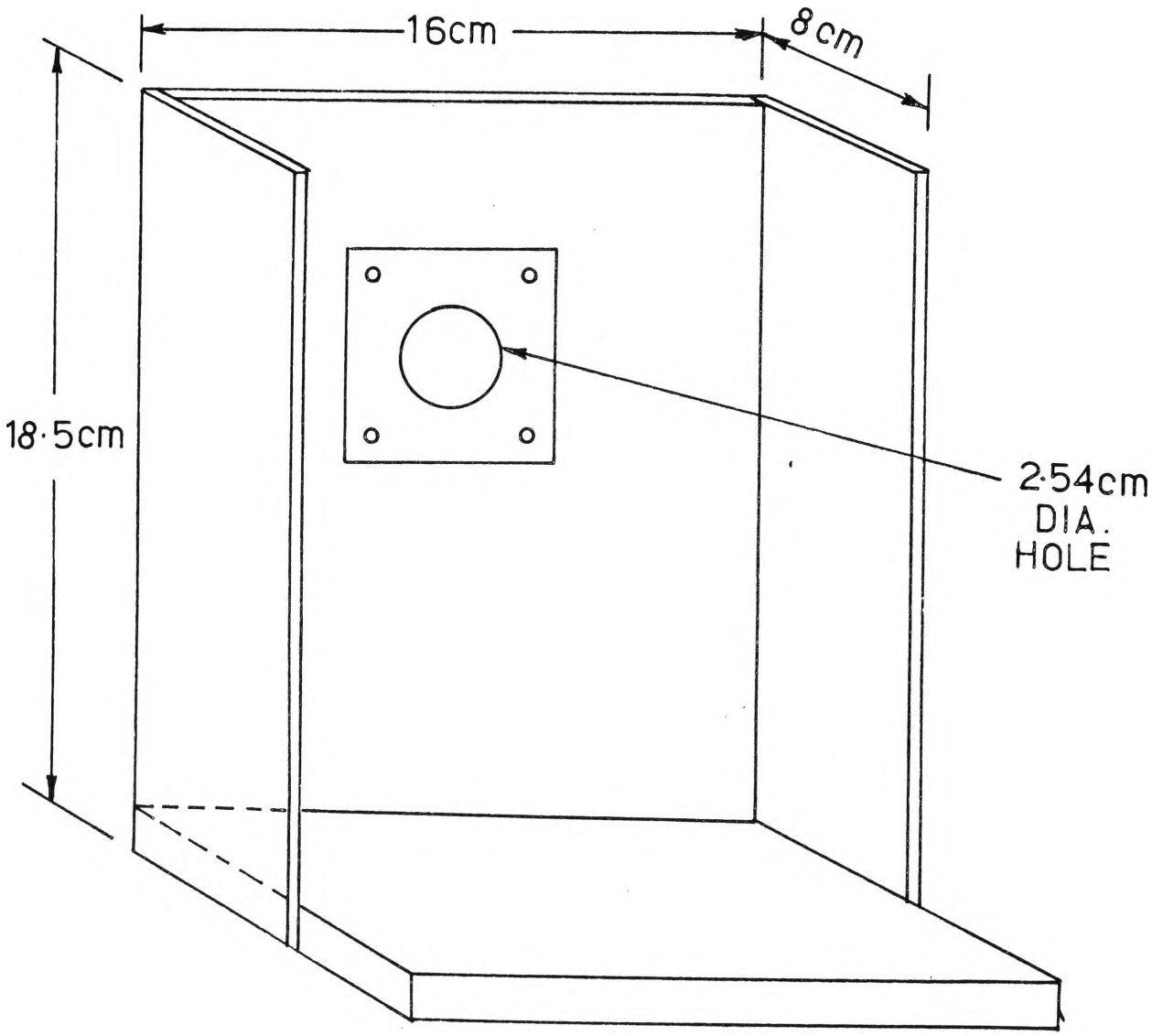


FIGURE 3.14 Absorber Holder

(j) Source Holder and Absorber Holder

A perspex tube shown in Figure 3.13 is designed to house the radioactive source. The screw top is rigidly glued onto the shaft of the velocity drive, and the section which houses the radioactive source can be screwed tightly onto it. Thus the source is pressed firmly inside the perspex housing so that no vibration will occur when the drive is in motion. An aluminium collimator is inserted in the perspex tube just in front of the source so that the gamma radiation is directed towards the absorber.

The absorber holder shown in Figure 3.14 is made of perspex plates of 0.64 cm thick. On the main plate a hole of 2.54 cm diameter is cut. The centre of the hole coincides with the axis of the source holder. A small piece of perspex of 7.5 cm x 7.5 cm also with a 2.54 cm hole can be bolted onto the main plate with the holes coincident. Holes are cut because the perspex is too thick and will absorb some of the 14.4 keV gamma rays. The sample absorber can be placed in between the plates so that the absorber covers the hole. To increase the stability of the holder, two reinforced perspex plates

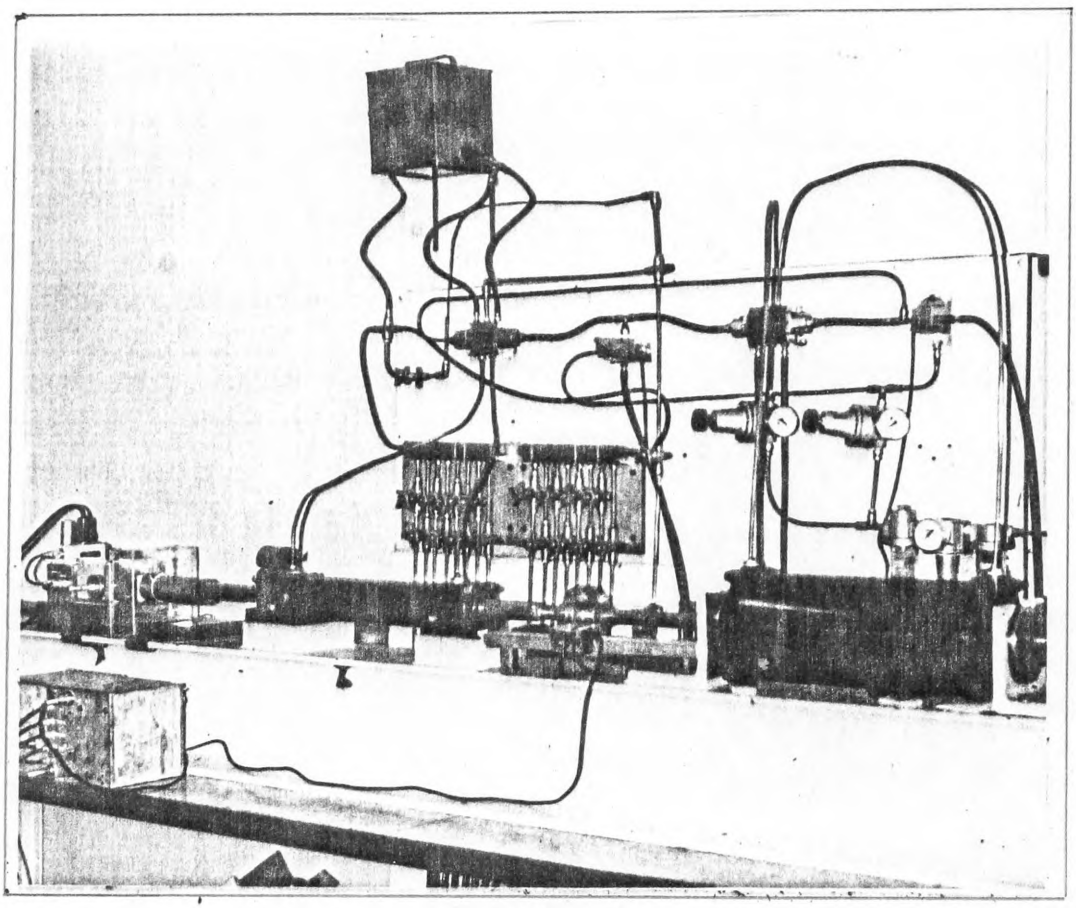

FIGURE 3.15. Pneumatic-hydraulic constant velocity drive.

are screwed onto the sides of the main plate. The base of the holder can be clamped firmly on the velocity drive platform, so that there will be no relative vibration between the source and the absorber.

(k) The Mounting of the Velocity Drive Components

The components of the velocity drive are divided into two main groups; the cylinders and the control units. The hydraulic cylinder and air cylinder are mounted on a rigid platform; and the control units are mounted on a vertical board above the platform. For convenience of operation, the oil reservoir is situated above the control board and the water bath which houses the capillary tube is put on the floor under the bench. The air compressor is situated at the other part of the building so that the engine vibration will not affect the motion of the velocity drive. The detailed arrangement of the mounting is shown in the photograph (Figure 3.15).

A steel beam, SAA No. ASB 111 of 3.35 meters long and 0.2 meters wide is used as a platform. It is placed on a bench 0.76 meters high. The rigidity of the beam is necessary to ensure complete elimination of any relative

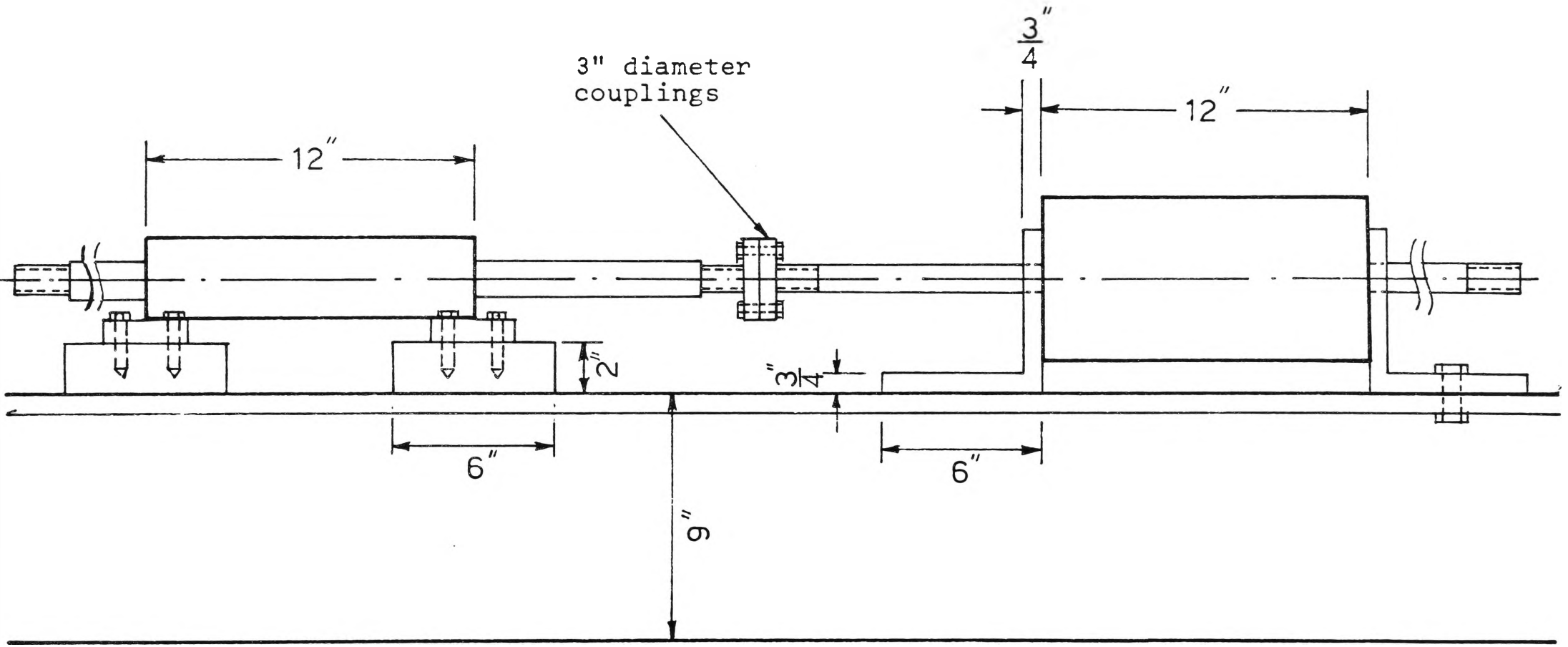


FIGURE 3.16 Mounting of Cylinders

vibration between the cylinders, or relative vibration between the source and absorber. Besides providing a baseplate for the cylinders, the steel beam also provides room at both ends for fitting the absorber holder and detector, so that two experiments can be performed at the same time if desired.

Great care was taken to ensure accurate and rigid alignment of the axes of the two cylinders. A right angle bracket of 0.152 m x 0.152 m, with its vertical surface machine polished, and a slot cut in it for the support of the air cylinder, is welded onto the platform. Another similar bracket, adjustable in position, can be bolted rigidly onto the platform about 0.47 m from the first bracket. The air cylinder can be mounted on these brackets and tightened by nuts on both ends. Two steel blocks of 0.15 m x 0.15 m, and 0.5 m thick are welded onto the platform 0.3 m apart. They are used to raise the axis of the hydraulic cylinder to the same level as that of the air cylinder. Finer adjustment of the height can be done by adding shims. The shafts of the cylinders are connected by rigid couplings (Figure 3.16).

On the vertical mounting board, the hydraulic control units and the air control units are mounted on the side close to their respective cylinders. The hydraulic and pneumatic circuit is shown in Figure 3.3 and the actual lay out is shown in the photograph. The water bath housing the capillary tubes is put under the bench. Holes are drilled on the bench to allow the passage of hydraulic pipes. For convenience of operation, the control valves of the capillary tubes are mounted on the board.

The source housing is glued onto a nut, screwed on the shaft of the hydraulic cylinder, and locked firmly. A sheet of lead is wrapped around the housing for radiation shielding. The absorber holder is clamped onto the platform and is situated between the source and the detector, which is also clamped tightly onto the platform.

Two microswitches used for limiting the travel distance of the shaft are also attached firmly to the platform. They are situated at positions where they can be actuated by the rigid couplings.

Two other microswitches of the gating circuit (Section 3.3a) for gamma ray counting control are also

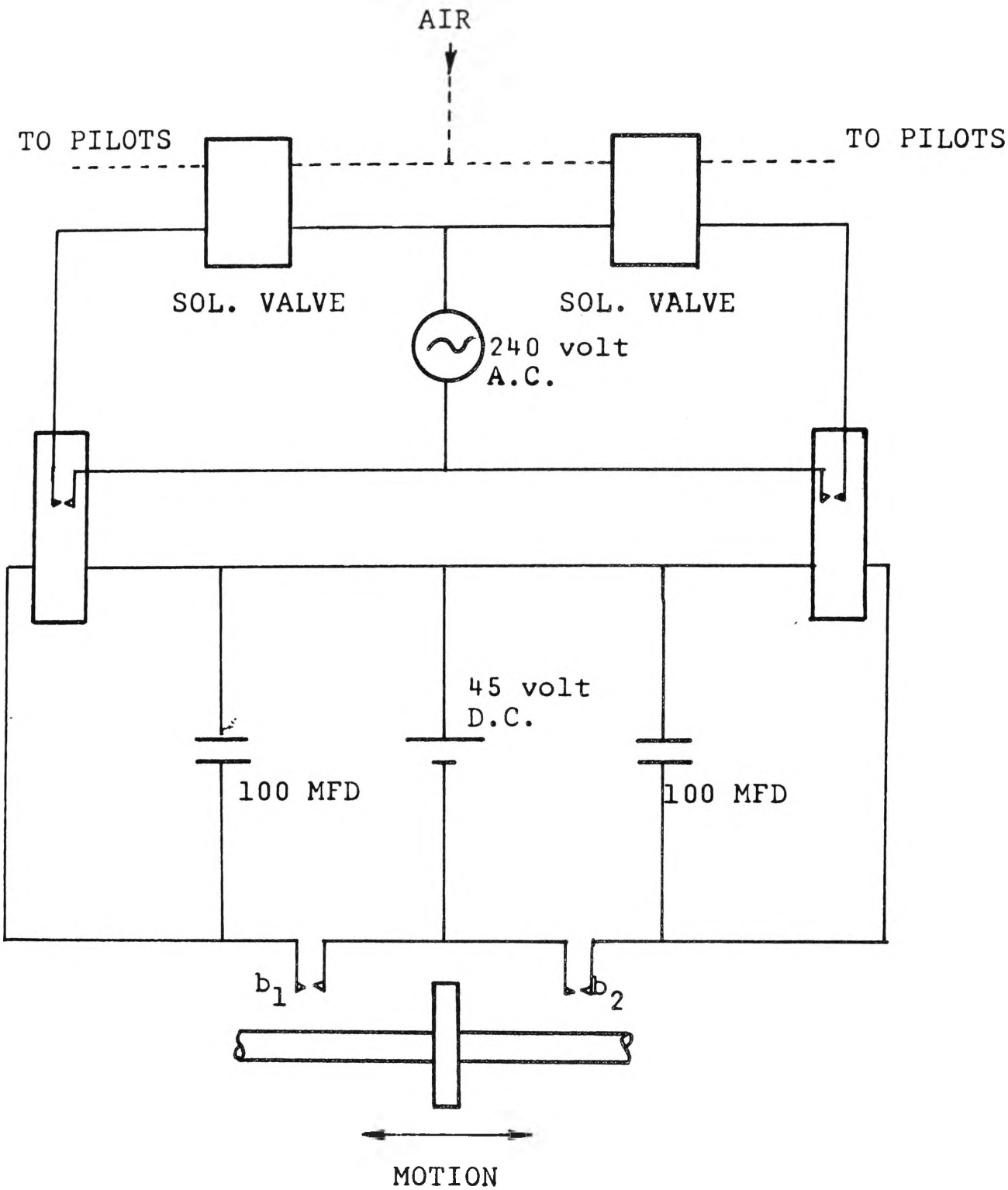


FIGURE. 3.1.7. Direction control circuit system

rigidly attached to the platform and are situated within the range of travel so that the counting of gamma photons begins after the motion is reversed and is at constant velocity.

(ℓ) Automatic Direction Control System

The reversal of motion of the velocity drive is caused by the change in the flow direction of air and oil simultaneously. Four-way directional valves which control the flow direction are operated automatically by a switching system (Figure 3.17) which consists of a relay circuit and two solenoid valves. Assume the motion of the shaft is initially towards the left. At the end of a stroke the microswitch $b_1$ is tripped and the circuit is triggered. A 45 volt battery charges the 100 MFD capacitor (function described in next paragraph) "instantly" and also energizes the relay on the left hand side of the circuit. The relay in turn closes the switch $S_1$, allowing the solenoid valve to be actuated by the 240 volt A.C. power supply. The solenoid valve then opens and allows air of about 20 p.s.i. from the air main to operate the pilots of the four-way directional valves and hence reverse the

flow direction. Consequently, the motion of the shaft is reversed leaving switch $b_1$ at its normally-open position.

Because of the difference in viscosity between air and oil the pilot of the air directional valve will be easier to operate than that of the oil directional valve. For this reason the reversal of the oil flow would be expected to lag behind and might cause vibrations if the solenoid valve has insufficient time to complete the operation. To prevent this happening the relay is energized by the charged capacitor even after the switch $b_1$ is opened, so that the solenoid valve can remain energized for 2 to 3 seconds longer, thus allowing the complete reversal of both directional valves.

Vibrations at the turn-around position can further be reduced by placing at the end a cushion block with a 0.5 cm thick hard rubber attached to act as a brake or damping for the shaft motion before the microswitch is tripped.

After the direction is reversed the shaft travels towards the other end where the microswitch $b_2$ will be closed and the same procedure repeated. Hence the two

TABLE 3.3.

| Time taken to travel a distance of 3 cm (s) | Velocity (mm/s) | Accuracy (%) |
|---|---|---|
| 1503.12 ± 12.12 | 0.02 ± 0.000 | ± 0.8 |
| 601.12 ± 4.90 | 0.05 ± 0.000 | ± 0.8 |
| 301.32 ± 2.40 | 0.1 ± 0.0008 | ± 0.8 |
| 150.59 ± 1.21 | 0.2 ± 0.002 | ± 0.8 |
| 100.08 ± 0.71 | 0.3 ± 0.002 | ± 0.7 |
| 75.10 ± 0.52 | 0.4 ± 0.003 | ± 0.7 |
| 60.01 ± 0.36 | 0.5 ± 0.003 | ± 0.6 |
| 50.05 ± 0.35 | 0.6 ± 0.004 | ± 0.7 |
| 42.86 ± 0.26 | 0.7 ± 0.004 | ± 0.6 |
| 37.49 ± 0.31 | 0.8 ± 0.006 | ± 0.8 |
| 33.32 ± 0.27 | 0.9 ± 0.007 | ± 0.8 |
| 30.01 ± 0.21 | 1.0 ± 0.007 | ± 0.7 |
| 27.27 ± 0.20 | 1.1 ± 0.008 | ± 0.7 |
| 25.05 ± 0.16 | 1.2 ± 0.006 | ± 0.5 |
| 23.07 ± 0.14 | 1.3 ± 0.006 | ± 0.6 |
| 21.43 ± 0.13 | 1.4 ± 0.007 | ± 0.6 |
| 20.02 ± 0.12 | 1.5 ± 0.009 | ± 0.6 |
| 18.75 ± 0.08 | 1.6 ± 0.008 | ± 0.5 |
| 17.65 ± 0.09 | 1.7 ± 0.008 | ± 0.5 |
| 16.67 ± 0.08 | 1.8 ± 0.010 | ± 0.5 |
| 15.79 ± 0.08 | 1.9 ± 0.010 | ± 0.5 |
| 15.01 ± 0.075 | 2.0 ± 0.010 | ± 0.5 |
| 14.28 ± 0.071 | 2.1 ± 0.010 | ± 0.5 |
| 13.63 ± 0.068 | 2.2 ± 0.011 | ± 0.5 |
| 13.04 ± 0.065 | 2.3 ± 0.011 | ± 0.5 |
| 12.50 ± 0.62 | 2.4 ± 0.012 | ± 0.5 |
| 12.00 ± 0.60 | 2.5 ± 0.012 | ± 0.5 |

TABLE 3.3. (Cont'd)

| Time taken to travel a distance of 3 cm (s) | Velocity (mm/s) | Accuracy (%) |
|---|---|---|
| 11.54 ± 0.055 | 2.6 ± 0.013 | ± 0.5 |
| 11.11 ± 0.045 | 2.7 ± 0.011 | ± 0.4 |
| 10.71 ± 0.043 | 2.8 ± 0.011 | ± 0.4 |
| 10.34 ± 0.042 | 2.9 ± 0.011 | ± 0.4 |
| 10.00 ± 0.046 | 3.0 ± 0.012 | ± 0.5 |
| 9.68 ± 0.040 | 3.1 ± 0.012 | ± 0.4 |
| 9.37 ± 0.038 | 3.2 ± 0.013 | ± 0.4 |
| 9.09 ± 0.035 | 3.3 ± 0.013 | ± 0.4 |
| 8.82 ± 0.036 | 3.4 ± 0.014 | ± 0.4 |
| 8.57 ± 0.034 | 3.5 ± 0.014 | ± 0.4 |
| 8.33 ± 0.034 | 3.6 ± 0.014 | ± 0.4 |
| 8.11 ± 0.033 | 3.7 ± 0.015 | ± 0.4 |
| 7.89 ± 0.031 | 3.8 ± 0.015 | ± 0.4 |
| 7.69 ± 0.030 | 3.9 ± 0.016 | ± 0.4 |
| 7.50 ± 0.030 | 4.0 ± 0.016 | ± 0.4 |
| 7.32 ± 0.030 | 4.1 ± 0.016 | ± 0.4 |
| 7.14 ± 0.029 | 4.2 ± 0.017 | ± 0.4 |
| 6.97 ± 0.028 | 4.3 ± 0.017 | ± 0.4 |
| 6.82 ± 0.027 | 4.4 ± 0.018 | ± 0.4 |
| 6.66 ± 0.024 | 4.5 ± 0.014 | ± 0.4 |
| 6.52 ± 0.022 | 4.6 ± 0.015 | ± 0.3 |
| 6.38 ± 0.020 | 4.7 ± 0.016 | ± 0.3 |
| 6.25 ± 0.019 | 4.8 ± 0.014 | ± 0.3 |
| 6.12 ± 0.018 | 4.9 ± 0.15 | ± 0.3 |
| 6.00 ± 0.020 | 5.0 ± 0.15 | ± 0.3 |

TABLE 3.4

Comparison of Performance of Drives

| Mössbauer Drive | Velocity Accuracy |
|---|---|
| M.E.S. Model B | ± 5% up to 1.0 mm/s |
| by N.S.E.C. (1965) | ± 1% 1.0 mm/s to 15 mm/s |
| Model MS-700 | ± 0.3% up to 10 mm/s |
| by Ranger Electronics | |
| Electromagnetic | ± 5% at $10^{-3}$ mm/s |
| Vali and Nybakken (1964) | ± 1% at 10 mm/s |
| Electromagnetic | ± 0.5% up to 10 mm/s |
| Lipkin et al (1964) | |
| Pendulum | ± 0.01 mm/s up to 10 mm/s |
| Flinn (1963) | |
| Pneumatic-hydraulic | ± 0.8% up to 1.5 mm/s |
| present thesis (1972) | ± 0.5% 1.6 mm/s to 4.5 mm/s |
| | ± 0.3% 4.6 mm/s to 6.0 mm/s |

N.S.E.C. - Nuclear Science and Engineering Corporation, Pittsburgh, U.S.A.

Ranger Electronics, Alva, Oklahoma, U.S.A.

microswitches together with the circuit produce an automatic reciprocating motion.

## (m) Measurement of the Velocity Accuracy and Calibration of the Velocity Settings

Before calibrating the accuracy of the spectrometer by using the absorption spectra of known absorbers (Section 3.4(d) ), an estimated accuracy of velocity was obtained. Assuming that the drive is moving at a constant speed, the velocity accuracy can be calculated from the time taken to travel a fixed distance (3.000 ± 0.001 cm). The results are shown in Table 3.3. The accuracy is calculated to be better than ± 0.8% for a velocity below 1.5 mm/s, better than ± 0.5% between 1.6 mm/s and 2.6 mm/s, and better than ± 0.4% between 2.7 mm/s and 6.0 mm/s. A comparison of performance with other types of drives is given in Table 3.4. This drive is comparable to some and considerably better than other commercially available constant velocity drives.

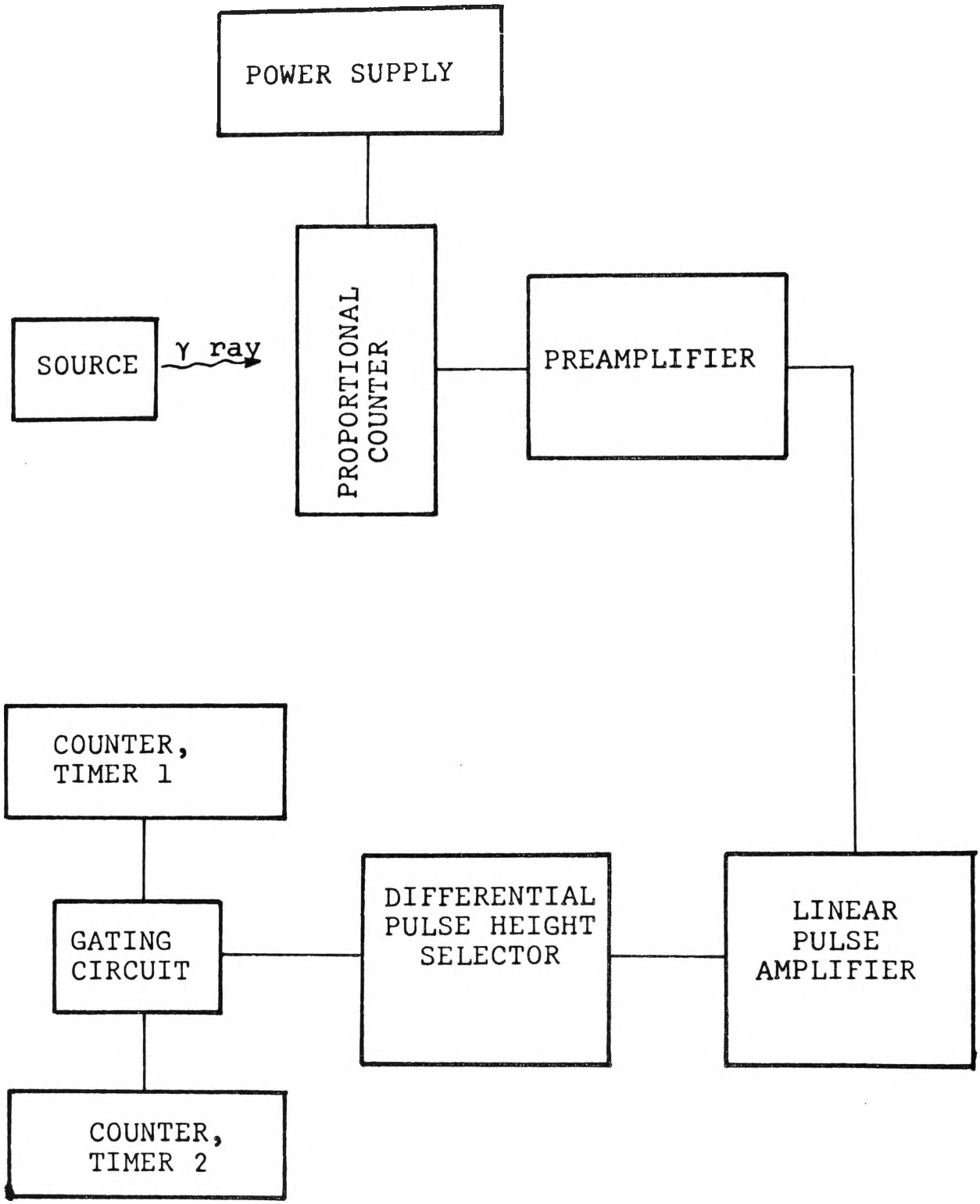


FIGURE 3.18 Detection system of the Mössbauer Spectrometer

## (3.3) The Detection System of the Constant Velocity Spectrometer

The gamma ray detection system shown in Figure 3.18 is composed of a proportional counter, a preamplifier, an amplifier, a pulse height selector, two sets of timer-counter units and a gating circuit. Since the reliability of the gamma-ray detection depends on the stability of the detection system, it is therefore important to have a stable main power supply. A 500 watts voltage stabilizer is used to supply the essential equipment such as the pulse amplifier, the pulse height selector and the high voltage d.c. power supply for the proportional counter. This equipment has a direct effect on the pulse height stability of the amplified gamma ray signals. The voltage stabilizer is capable of regulating the main voltage to within an accuracy of ± 0.25% for an input fluctuation of - 20% to + 10%.

The specially designed gating circuit for the control of the signal input to the timer-counter will be discussed in (a) of this section and the examination of the quality of the proportional counter and the performance of the detection system as a whole will be presented in (b)

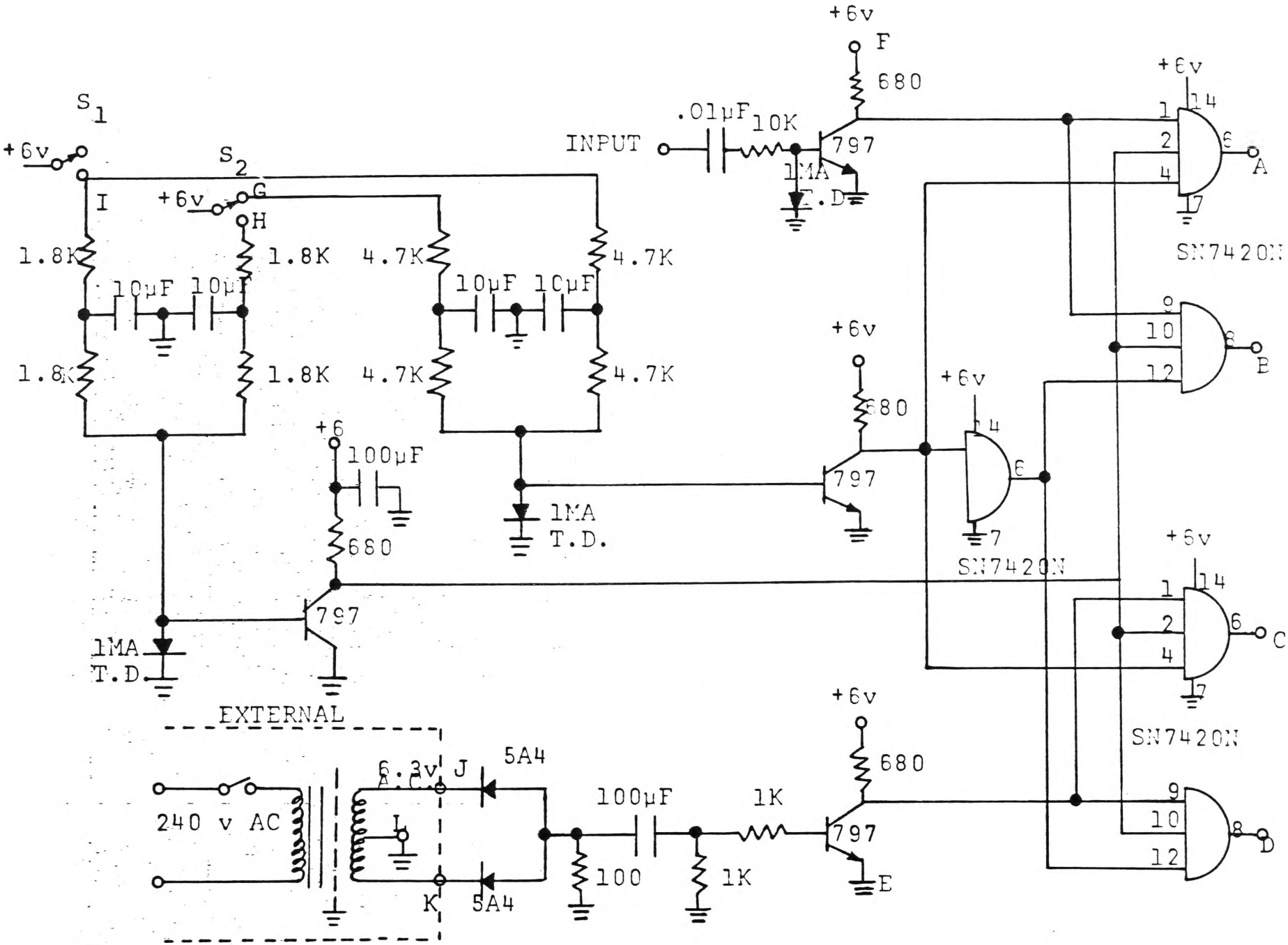


FIGURE 3.19 The Gating Circuit

and (c) respectively of this section.

(a) The Gating Circuit

The gating circuit shown in Figure 3.19 is used to control the time duration of the counting of gamma rays for both directions of motion automatically. Two scalers are connected to A and B and two timers are connected to C and D.

The amplified gamma ray signals are fed to the input of the gating circuit. The output signals of this circuit may be directed to either A or B, depending on which of the two microswitches, $S_1$ and $S_2$, is triggered. The mains frequency is used as a clock. The rectified signals of 100 pulses per second may be directed to either C or D, depending on which of the two microswitches, $S_1$ and $S_2$, is triggered.

Assume that the drive is initially moving to the left, before the end of the stroke microswitch $S_1$ is closed and the counting and timing are stopped instantly. $S_1$ remains closed during the period when the motion of the drive is reversed by a directional switch. It is then re-opened and the second set of scaler-timers start to record

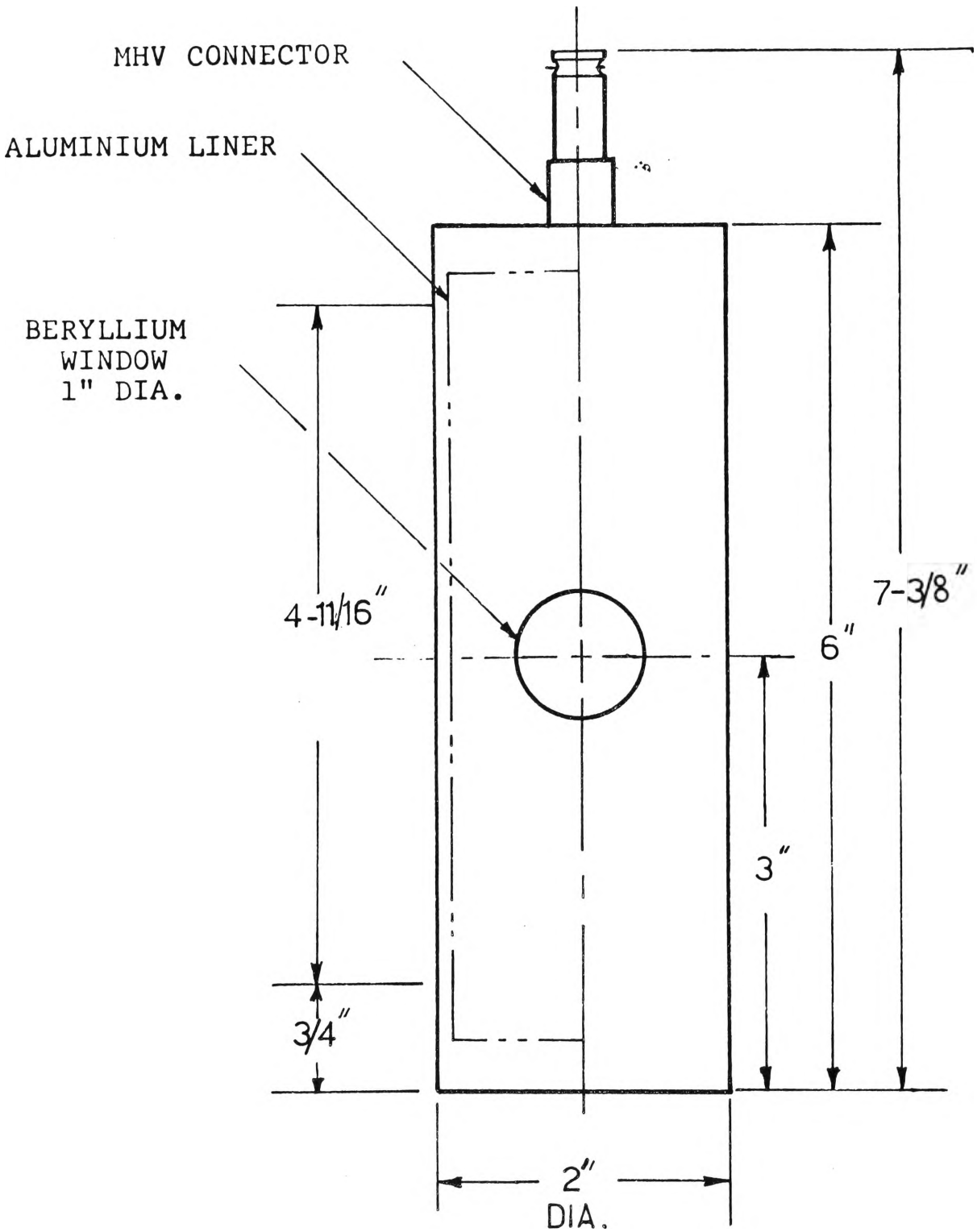


FIGURE 3.20 The proportional counter RSG-61-M1.

the counting rate for the opposite motion. The recording continues until the microswitch $S_2$ is closed. After the motion of the drive is reversed, $S_2$ is again reopened allowing the first set of scaler-timers to record. Two microswitches, in this way, enable two sets of scaler-timers to record alternately. The scalers and timers can be reset any time for new readings.

(b) The Resolving Power of the Proportional Counter

The detector chosen for use in the detection system is RSG-61-M1 proportional counter (Figure 3.20). It is a gas filled proportional counter designed for the detection of x-ray or gamma ray energies below 50 keV. Its outer shell is made of stainless steel and has an internal aluminium liner. It has a 1" diameter and 0.005" thick beryllium window. The detecting gas is krypton (97%), the quench gas is $CO_2$ (3%) and the gas pressure is one atmosphere. The beryllium window is brazed to the body and can withstand high temperature conditions. The photon transmission of beryllium is 99% for 14.4 keV and its fluorescence effect is very low. However, the stainless steel shell with aluminium liner gives 1.6 keV fluorescence, but this has negligible effect

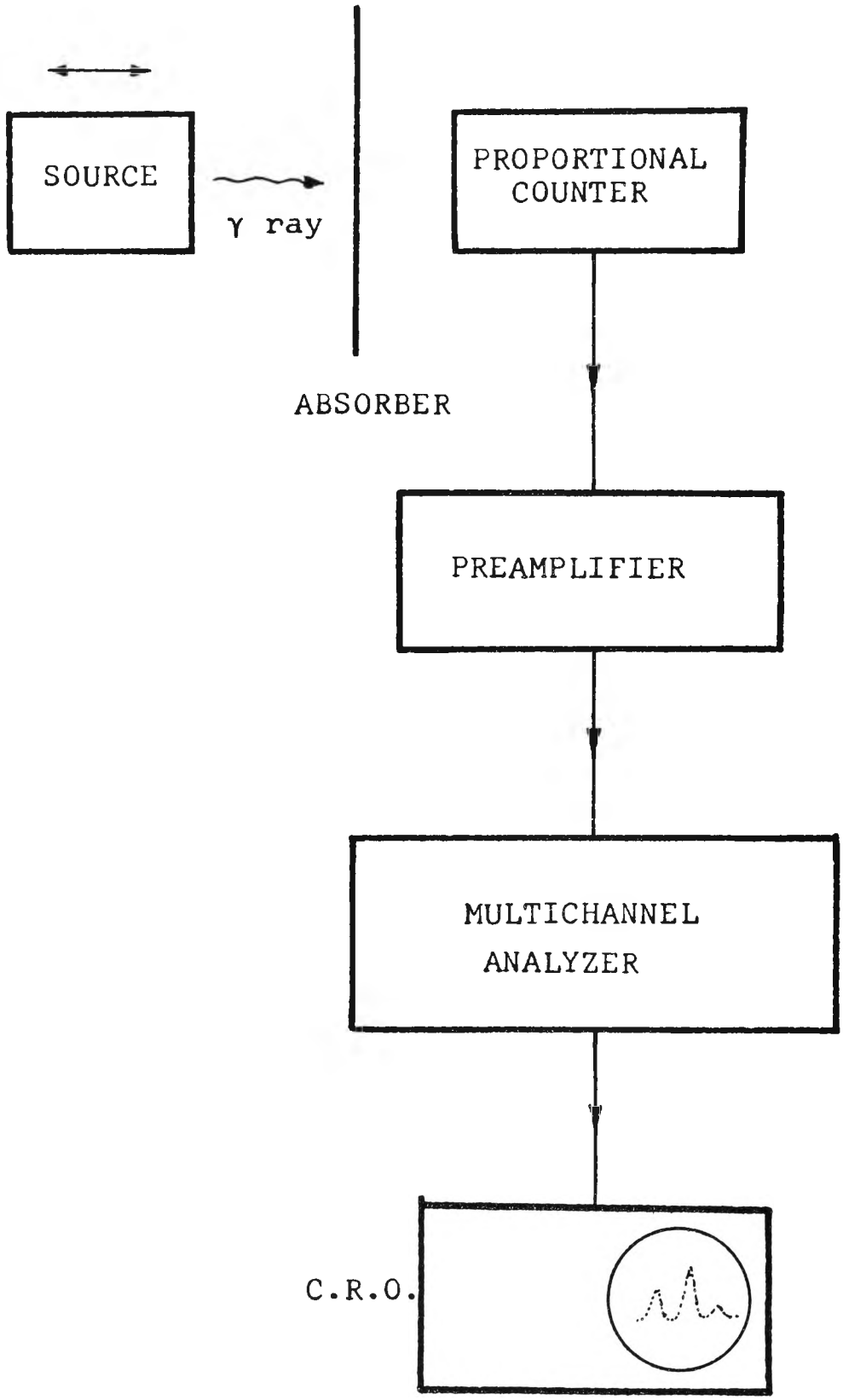


FIGURE 3.21. Equipment for scanning the energy spectrum of $Co^{57}$.

on counting efficiency. Krypton gas absorbs nearly 90% of all 14.4 keV gamma rays transmitted through the window and it gives very high signal-to-noise ratio at this energy. The $CO_2$ quench gas is used to improve pulse characteristics and to prevent the krypton gas from continuously discharging. The quench gas also permits operation at high voltage (in the range of 2000-2700 volts). The escaping peak of 14.4 keV (a secondary process generated by the incident photons exceeding the $K_{\alpha\beta}$ of krypton gas) does not interfere with the counting efficiency. The resolution (Equation 3.3) for 14.4 keV, specified by the manufacturer, is between 10% to 13%, measured at full width at half maximum of the energy-intensity curve.

$$\text{Resolution } (\%) = \frac{\text{Full width at half maximum (V)}}{\text{Pulse height (V)}} \times 100\% \qquad (3.3)$$

The resolving power can be measured by scanning the energy spectrum of the $^{57}Co$ source. Testing equipment was set up as shown in Figure 3.21. The source was placed at 15 cm from the proportional counter. The radiation signals detected by the proportional counter were amplified, then analyzed by the multichannel analyzer and finally

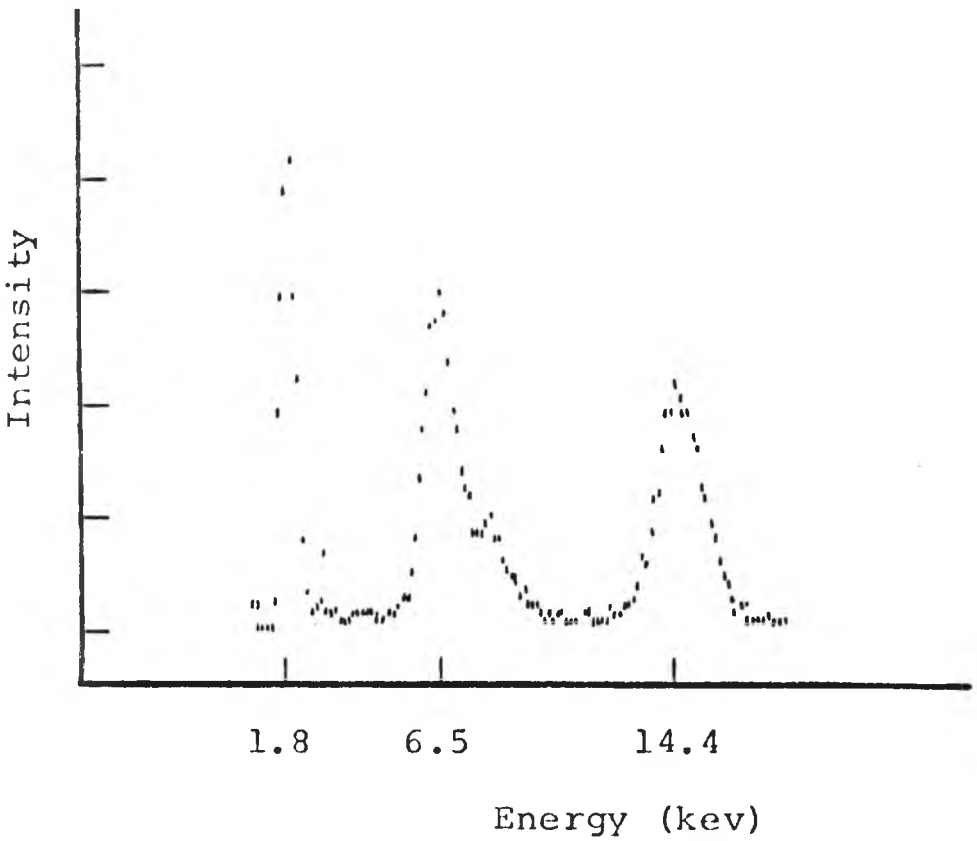


FIGURE 3.22. Energy Spectrum of $^{57}Co$

displayed on a cathode ray oscilloscope. A polaroid camera was used to photograph the energy spectrum, which represents the counting intensity as a function of signal pulse height or channel number.

Three energy peaks are shown on the spectrum (Figure 3.22), they are the 1.8 keV escaping peak of the 14.4 keV $\gamma_{M1}$ (occuring at Channel No. 9), the 6.5 keV $K_{\alpha\beta}$ (Channel No. 45) and the 14.4 keV (Channel No. 101) proportional counter is completely insensitive to the two higher energies, 122 keV and 136 keV and no peaks are recorded at high energy scanning (not included in Figure 3.22).

From direct measurement of the spectrum, the full width at half maximum values of the 6.5 keV and the 14.4 keV peaks are 9 channels and 12 channels respectively. Thus the resolutions of the 6.5 keV and the 14.4 keV energy peaks are 20% and 11.9% respectively.

The resolution for 14.4 keV is within the limit (10% to 13%) specified by the manufacturer. The energy peaks are very sharp and well separated and there is no indication of interference due to higher energies. This proportional counter is therefore considered to be satisfactory for the present investigation purpose.

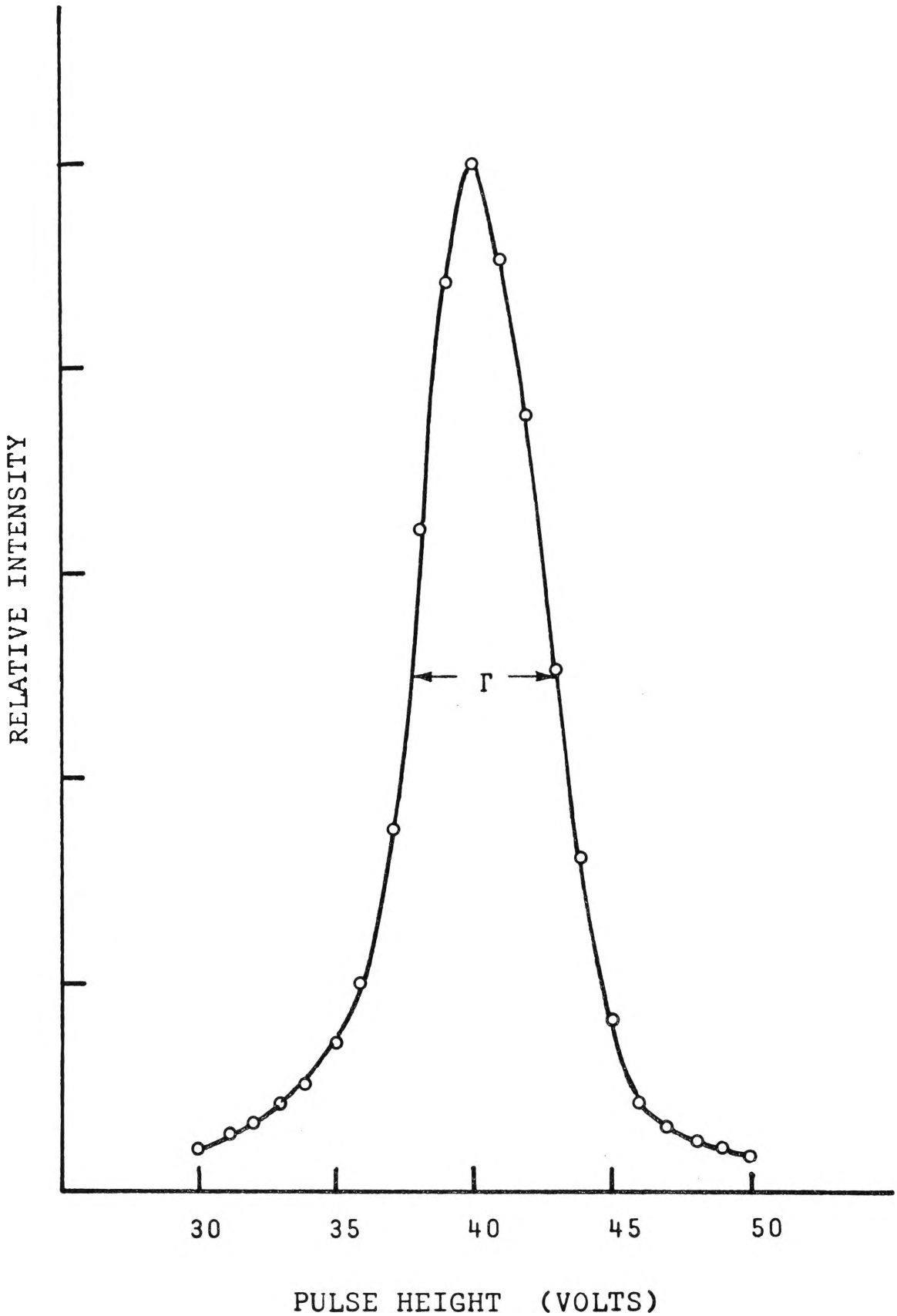


FIGURE 3.23. Energy scanning of the 14.4. kev gamma ray of $Fe^{57}$.

TABLE 3.5.

| Counts/ 600 sec. | Fluctuation | % Fluctuation |
|---|---|---|
| 76752 | +56 | +0.07 |
| 76716 | +20 | +0.03 |
| 76602 | -94 | -0.12 |
| 76814 | +118 | +0.15 |
| 76772 | +76 | +0.09 |
| 76703 | +7 | +0.01 |
| 76708 | +14 | +0.02 |
| 76545 | -151 | -0.2 |
| 76710 | +14 | +0.02 |
| 76639 | -57 | -0.07 |
| 76542 | -154 | -0.2 |
| 76637 | -59 | -0.07 |
| 76890 | +194 | +0.25 |
| 76722 | +26 | +0.03 |
| 76798 | +102 | +0.13 |
| 76550 | -146 | -0.2 |
| 76601 | -95 | -0.12 |
| 76724 | +28 | +0.04 |
| 76801 | +105 | +0.14 |
| 76693 | -3 | -0.005 |

Average = 76696

positive fluctuation average = +0.12%

negative average = -0.08%

positive maximum = +0.25%

negative maximum = -0.2%

(c) Stability of the Detection System

After measuring the resolving power of the proportional counter, the stability of the detection system as a whole was checked. The 14.4 keV $\gamma_{M1}$ of a stationary source was scanned by the single channel analyzer (Figure 3.18). The result, shown in Figure 3.23, represents the counting rate against the pulse height in volts with the maximum counting rate adjusted to occur at 40.0 ± 0.1 volts. The full width at half maximum is about 5.5 ± 0.1 volts.

After scanning the 14.4 keV energy distribution, the stability of the detection system was tested by the following procedures. The gatewidth of the pulse height selector was set at 6 volt between 37 and 43 volts, including the region of maximum intensity of the energy distribution curve. The gamma rays of pulse heights between 37 and 43 volts were accumulated for a time duration of 600 seconds and the reading recorded. The same procedure was repeated at thirty minute intervals for ten hours. The counting rates recorded are shown in Table 3.5.

The fluctuation is calculated to be ± 0.1% with a positive average of 0.12% and a negative average of 0.08%. These fluctuations may be due to the electronic drift and the counting statistics. The fluctuation of counting statistics is approximately equal to $\sqrt{N}$ where N is the total number of signals recorded, and in this case the fluctuation is about 0.09%. Hence the electronic drift can be regarded as negligible.

## (3.4) The Overall Performance of the Spectrometer

The preliminary tests of the drive and the detection system described in Sections 3.2 and 3.3 indicate that the equipment performs well individually. A more reliable test of the overall performance of the spectrometer requires obtaining well-resolved Mössbauer spectra of known absorbers. The linewidth, line position, absorption intensity, isomer shift, quadrupole splitting and magnetic hyperfine splitting of the known spectra can be studied in detail. If there were any intolerable vibration generated in the drive or high noise level existed in the detection system the Mössbauer spectrum would be broadened or more severely the resonance

(Statistical fluctuation: ± 0.5%)

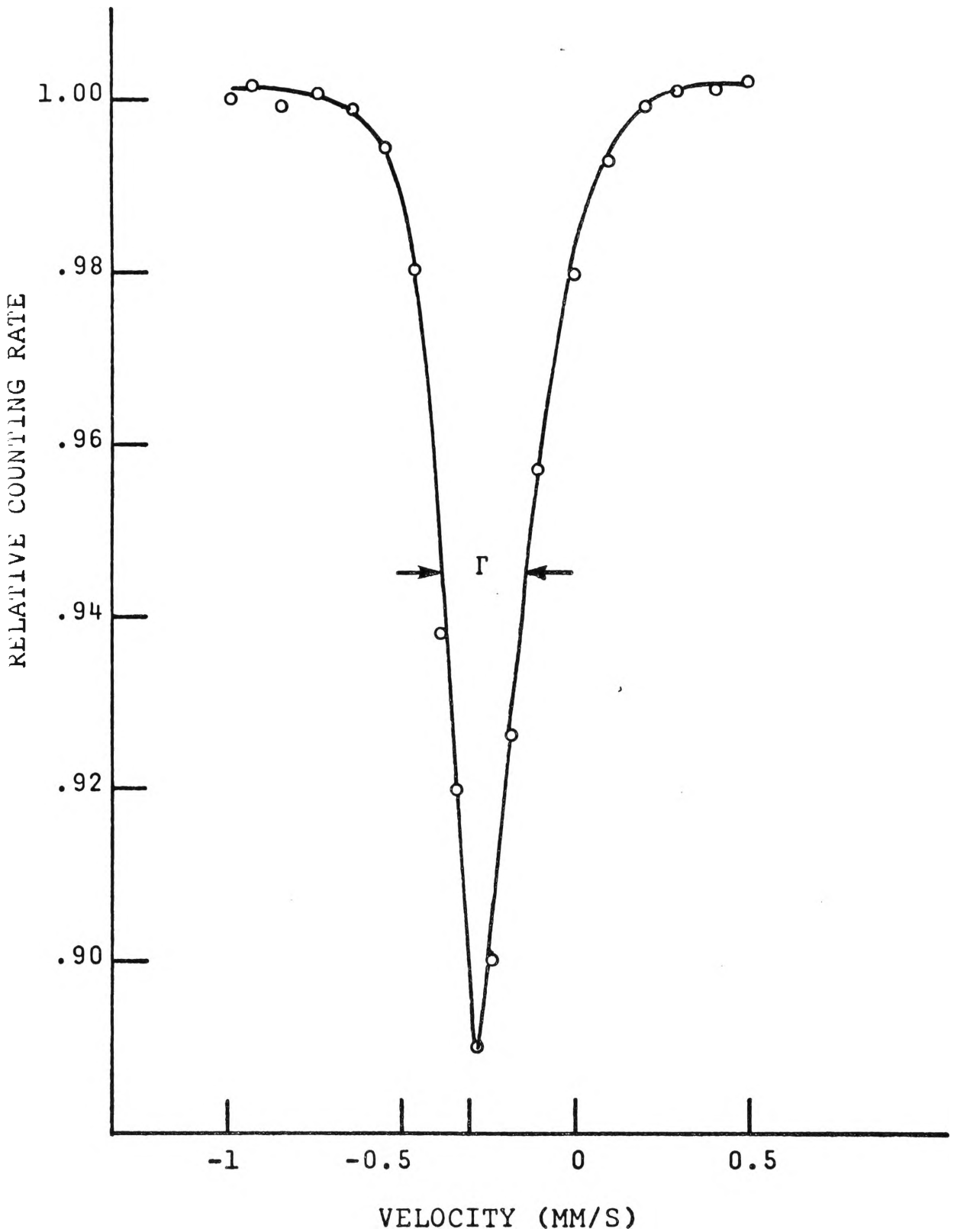


FIGURE 3.24. Mössbauer spectrum of $K_4Fe(CN)^6 . 3H_2O$.

absorption destroyed completely.

The absorbers used for the testing purpose in the following experiments are $K_4Fe(CN)_6.3H_2O$ and an iron foil containing more than 90 per cent of $^{57}Fe$ nuclei.

(a) The Mössbauer Spectra of $K_4Fe(CN)_6.3H_2O$

A single line source, $^{57}Co$ embedded in a copper host lattice, was mounted on the velocity drive, and a single line absorber, $K_4Fe(CN)_6.3H_2O$ of thickness of 0.1 mg $^{57}Fe$/cm was inserted in the absorber holder placed at 3 cm in front of the proportional counter (Figure 3.18). The counting rates with respect to Doppler velocities were recorded. The resultant absorption spectrum of this absorber is shown in Figure 3.24.

The absorption line is measured to have a line-width, $\Gamma$, of 0.26 ± 0.01 mm/s, which in terms of energy is

$$\Gamma = \frac{v}{c} \times E_r$$

$$= \frac{(0.26 \pm 0.01) \times 14.4 \times 10^3 \text{ eV}}{3 \times 10^8}$$

TABLE 3.6

Characteristic parameters of $K_4Fe(CN)_6.3H_2O$

| Source matrix | Linewidth (mm/s) | Isomer shift (mm/s) | Reference |
|---|---|---|---|
| Cu | 0.29 | -0.27 | Taylor et al(1964) |
| Pt | 0.28 | -0.39(-0.27)* | Valov et al (1965) |
| Pt | 0.27 | -0.39(-0.27)* | Kerler et al (1962) |
| S.S. | 0.38 | -0.34(-0.27)* | Kerler et al (1962) |
| Cu | 0.26±0.01 | -0.27±0.01 | Present result |

* Corrected value of isomer shift with respect to a $^{57}Co$ source embedded in a copper matrix.

$$= (1.25 \pm 0.05) \times 10^{-8} \text{ eV}$$

The maximum resonant absorption of 11 per cent is shown to occur at -0.27 ± 0.01 mm/s. This means that the isomer shift is -0.27 ± 0.01 mm/s or (1.30 ± 0.05) x $10^{8}$ eV.

The measured linewidth is about 33 per cent more than the theoretical value of 0.195 mm/s (9.34 x $10^{-9}$ eV). This is not unexpected since no experimental results obtained so far equal the natural linewidth. It is known that for a decay life time of the order $10^{-10}$ second or longer, extranuclear fields can widen the linewidth considerably. Since the life time of the 14.4 keV transition of $^{57}$Fe is 1.4 x $10^{-7}$ second (Section 2.4) line broadening is therefore inevitable.

The measured results shown in Table 3.6 are in good agreement with those measured by other workers. The narrow linewidth of 0.26 ± 0.01 mm/s is a good indication that the spectrometer is capable of producing good resolution spectrum of a sample.

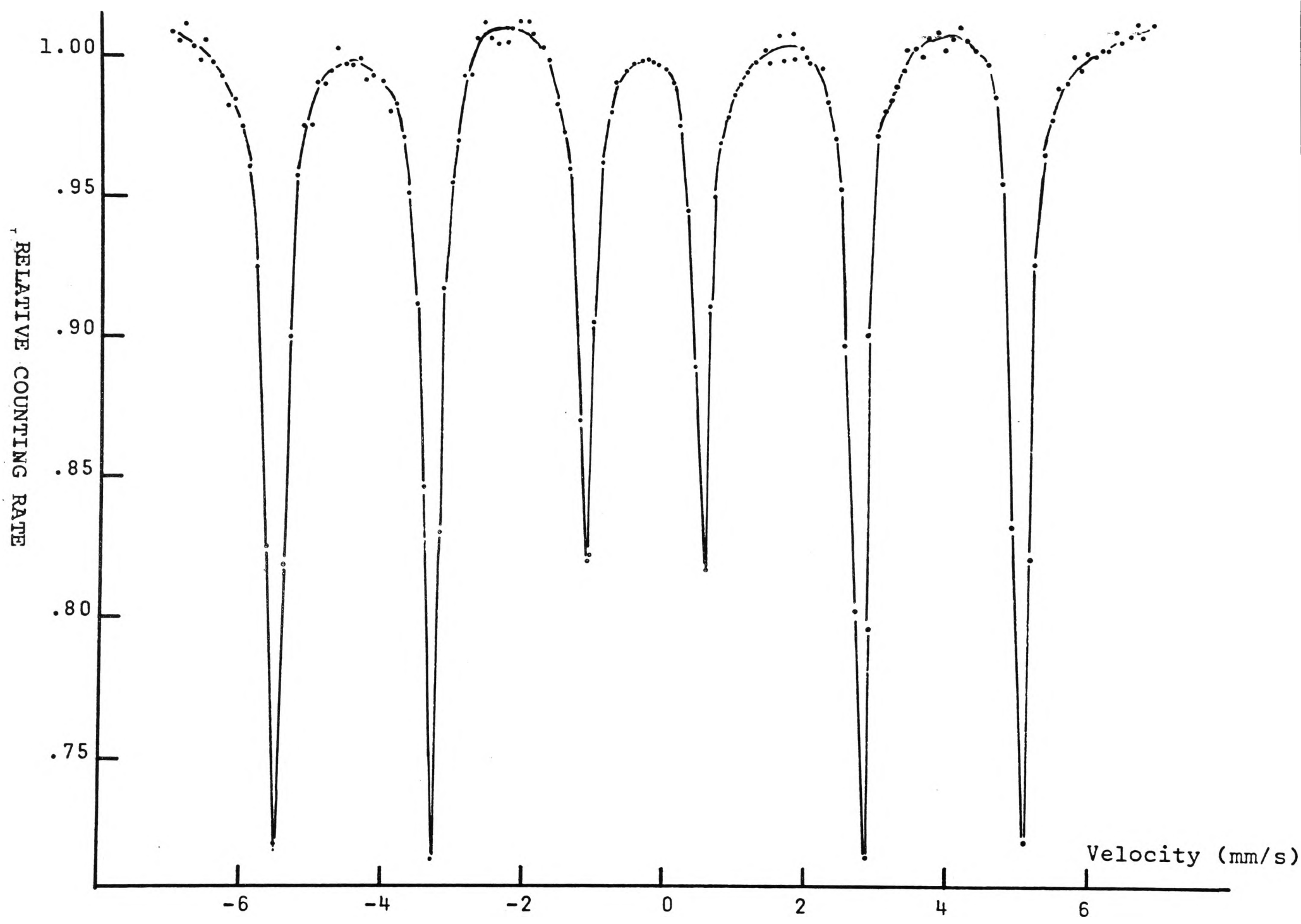


FIGURE 3.25. Mössbauer Spectrum of Iron

TABLE 3.7

Mössbauer data of iron (relative to a $^{57}Co$ source embedded in copper matrix).

| Absorption line | Position (mm/s) | Linewidth (mm/s) | Absorption Intensity (%) |
|---|---|---|---|
| $-\frac{1}{2} \rightarrow -\frac{3}{2}$ | -5.54 ± 0.01 | 0.25 ± 0.01 | 28 |
| $-\frac{1}{2} \rightarrow -\frac{1}{2}$ | -3.30 ± 0.01 | 0.25 ± 0.01 | 28.5 |
| $-\frac{1}{2} \rightarrow +\frac{1}{2}$ | -1.06 ± 0.01 | 0.23 ± 0.01 | 18 |
| $+\frac{1}{2} \rightarrow -\frac{1}{2}$ | +0.61 ± 0.01 | 0.23 ± 0.01 | 18 |
| $+\frac{1}{2} \rightarrow +\frac{1}{2}$ | +2.86 ± 0.01 | 0.25 ± 0.01 | 28.5 |
| $+\frac{1}{2} \rightarrow +\frac{3}{2}$ | +5.12 ± 0.01 | 0.25 ± 0.01 | 28 |

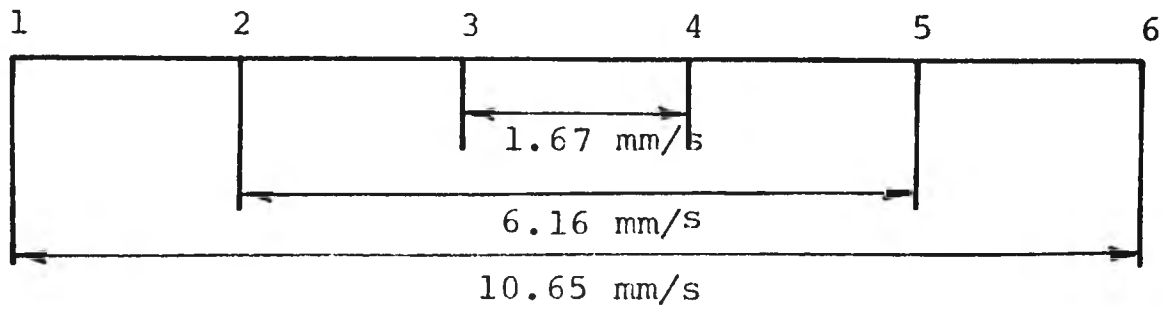


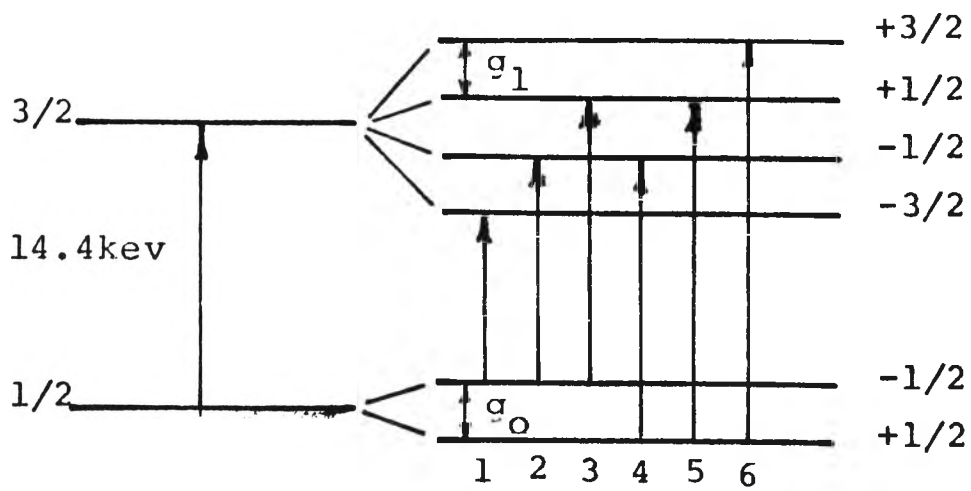


FIGURE 3.26 Magnetic hyperfine splitting of iron

TABLE 3.8

Characteristic parameters of magnetic hyperfine splitting of $^{57}Fe$

| $g_o$ (mm/s) | $g_1$ (mm/s) | $\mu_1/\mu_o$ | $\mu_1$ (n m) | H (kOe) | Reference |
|---|---|---|---|---|---|
| 3.96±0.10 | 2.23±0.03 | | -0.153±0.004 | 333±10 | Hanna et al (1960) |
| 3.924±0.008 | 2.244±0.005 | -1.715±0.004 | -0.1549±0.0013 | 330±3 | Preston et al (1962) |
| | | -1.715 | | | Kocher (1965) |
| 3.92±0.01 | 2.24±0.01 | -1.715±0.040 | -0.155±0.040 | 330±3 | Present results |

H the internal field at the nucleus.

$g_o$ the splitting in the ground state of $^{57}Fe$.

$g_1$ the splitting in the exited state of $^{57}Fe$.

$\mu_o$ the magnetic moment of the ground state.

$\mu_1$ the magnetic moment of the exited state.

TABLE 3.9

Characteristic parameters of iron foil absorption spectrum.

| Source matrix | Linewidth (mm/s) | Isomer Shift (mm/s) | Reference |
|---|---|---|---|
| Cu | 0.24 | -0.22 | Kocher(1965a) |
| Cu | | -0.23 | Nussbaum(1965) |
| Cu | | -0.23 | Steyert(1964) |
| Pt | 0.32 | -0.36 (-0.24)* | Zinn(1963) |
| Pt | 0.22 | -0.35 (-0.23)* | Kerler(1962) |
| S.S. | 0.39 | +0.08 (-0.23)* | Kerler(1962) |
| Cu | 0.23±0.01 | -0.225±0.01 | Present results |

* Corrected value of isomer shift with respect to a $^{57}Co$ source embedded in a copper matrix.

(b) Mössbauer Spectrum of Pure Iron

Similarly, the Mössbauer spectrum of an iron foil, enriched with 90 per cent of $^{57}Fe$, was also obtained. The spectrum (Figure 3.25) shows six absorption lines due to magnetic hyperfine splitting. A corresponding schematic diagram of the transition is shown in Figure 3.26. The values of line positions, linewidths and absorption percentages of these lines are given in Table 3.7. Comparisons of the measured and calculated results with those obtained by other workers are given in Tables 3.8 and 3.9.

The magnetic moment $\mu_1$ of the excited state can be calculated from the following relationship,

$$\frac{\mu_1}{\mu_0} = \frac{3g_1}{g_0}$$

where $\mu_0$ is the magnetic moment of the ground state,

$g_0$ is the energy gap of the ground state splitting,

$g_1$ is the energy gap of the excited state splitting.

Using the value of $\mu_0 = 0.0903 \pm 0.0007$ nm, calculated by Ludwig and Woodbury (1960), and the measured values from the spectrum ( Figure 3.25 ) :

$$g_0 = 3.92 \pm 0.01 \text{ mm/s}$$

$$g_1 = 2.24 \pm 0.01 \text{ mm/s}$$

the magnetic moment $\mu_1$ is found to be 0.155 ± 0.040 nm.

The internal magnetic field H of the nucleus can be calculated using Equation 1.40 (Chapter 1).

$$\Delta E = g\mu_n H = \frac{\mu H}{I} \qquad (1.40)$$

For a $^{57}Fe$ nucleus at ground state, the values of I, $\mu$ and $\Delta E$ are:

$$I = \frac{1}{2}$$

$$\mu = \mu_0 = 0.0903 \pm 0.0007 \text{ nm}$$

$$= 4.559 \pm 0.044 \times 10^{-25} \text{ erg/Oersted}$$

$$\Delta E = g_0 = 3.92 \pm 0.01 \text{ mm/s}$$

Hence the internal magnetic field H is found to be (330 ± 3) x $10^3$ Oersted.

The above results are in excellent agreement with those obtained by other workers. These experiments prove that the spectrometer built for the present investigations is reliable in providing an accurate and constant motion.

The Mössbauer spectra produced are well resolved enabling accurate measurements and calculations to be made.

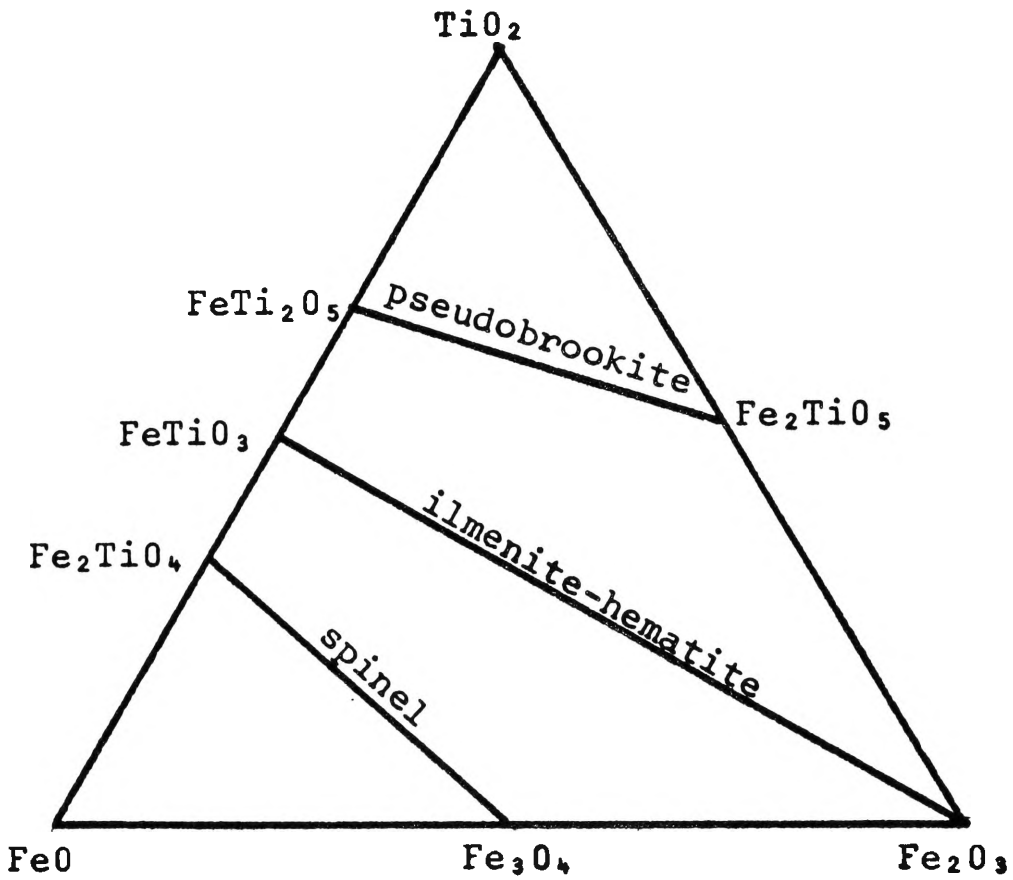


Fig. 4.1. The phase diagram of $FeO-Fe_2O_3-TiO_2$ ternary system.

# CHAPTER 4

## ILMENITE AND THE $FeO-TiO_2-Fe_2O_3$ TERNARY SYSTEM

The magnetic structure of the $FeO-TiO_2-Fe_2O_3$ ternary system (Figure 4.1) has long been studied by using magnetic measurements and neutron diffraction techniques. The discovery of the Mössbauer Effect provided an additional method for the investigation of the electronic and magnetic structure of this system.

There are three solid solution series in the ternary system,

(i) the pseudobrookite series ($FeTi_2O_5-Fe_2TiO_5$)

(ii) the ilmenite-hematite series ($FeTiO_3-\alpha Fe_2O_3$)

(iii) the spinel series ($Fe_2TiO_4-Fe_3O_4$)

The main interest of the present study concerns the investigation, by means of Mössbauer spectroscopy, of the magnetic properties of naturally occurring ilmenite (an ilmenite-hematite series mineral) and its oxidised forms. The ilmenite used was obtained from Swansea, New South Wales, Australia.

General information on natural ilmenite and pseudobrookite (which may be produced by the oxidation of natural

ilmenite) is given in this chapter. The Mössbauer spectra obtained for these minerals and their related compounds are presented in Chapter 5.

## (4.1) Natural Ilmenite

Ilmenite is a black metallic mineral and is a common rock-forming mineral in igneous and metamorphic rocks. Its hardness number is between 5.5 to 6, specific gravity 4.7 and melting point 1470$^{o}$C. It occurs naturally in veins, river placers and beach sands. Impurities such as hematite, magnetite, rutile and zircon are often associated with it. The natural mineral ilmenite is ferrimagnetic and this is considered (Akimoto 1954, Uyeda 1956) to show the existance of an ilmenite-hematite solid solution. The chemical composition per cent by weight of pure ilmenite ($FeTiO_3$) is iron 36.8, titanium 31.6 and oxygen 31.6, but the ratio of iron and titanium may vary considerably and magnesium or manganese may replace some of the iron in the lattice. It was found (Gibb et al, 1969) that natural ilmenites obtained from different regions of the world vary considerably in chemical composition, depending on the weathering process and parent rock.

Although the amounts of ferrimagnetic ilmenite-hematite series minerals in rocks are very small compared with those of spinel series minerals, they are important in rock magnetism because of their strong magnetic coupling and capability of causing a self-reversal of the thermo-remanent magnetization (Nagata, 1950, 1952, 1953; Nagata et al, 1952, a,b, 1953, a,b; Balsley and Buddington, 1958; Nagata and Shimizu, 1959).

In the ilmenite-hematite series both ilmenite ($FeTiO_3$) and hematite ($\alpha Fe_2O_3$) crystallize in the hexagonal system. The crystals are rhombohedral in structure. Natural ilmenite according to the ASTM index, has the following unit cell dimensions:

$$a_{rh} = 5.523A, \quad \alpha_{rh} = 54^{o}51^{1}$$

for a rhombohedral unit cell, and

$$a_h = 5.079A, \quad c_h = 14.135A$$

for a hexagonal one. Synthetic ilmenite has $a_{rh} = 5.538A$, $\alpha_{rh} = 54^{o}41^{1}$ (Akimoto 1957).

Hematite has cell dimensions

$$a_{rh} = 5.4271A, \quad \alpha_{rh} = 55^{o}15.8^{1}$$

for a rhombohedral unit cell, and

$$a_h = 5.0345A, \quad c_h = 13.749A$$

for a hexagonal one (Willis and Rooksby, 1952).

The structure of $\alpha Fe_2O_3$ consists of layers of Fe ions in the (111) planes with an oxygen layer between them. The structure of $FeTiO_3$ is achieved by replacing every other layer of Fe ions by a layer of Ti ions.

Posnjak and Barth (1934) found that ilmenite and hematite have different crystal symmetries, the former belongs to the space group $R\bar{3}$ and the latter to $R\bar{3}C$. Consequently, ilmenite-hematite solid solutions will have a range of crystal symmetries which are mixtures of $R\bar{3}$ and $R\bar{3}C$. (Ishikawa and Akimoto, 1958; Shirane et al, 1959).

Shull et al (1951) showed by neutron diffraction that at temperatures below $250^oK$ the spin orientations of Fe ions of $\alpha Fe_2O_3$ are parellel within a given (111) layer, but adjacent planes are coupled antiferromagnetically with spin direction parallel to the ternary axis of the crystal; and that above $250^oK$ the spin

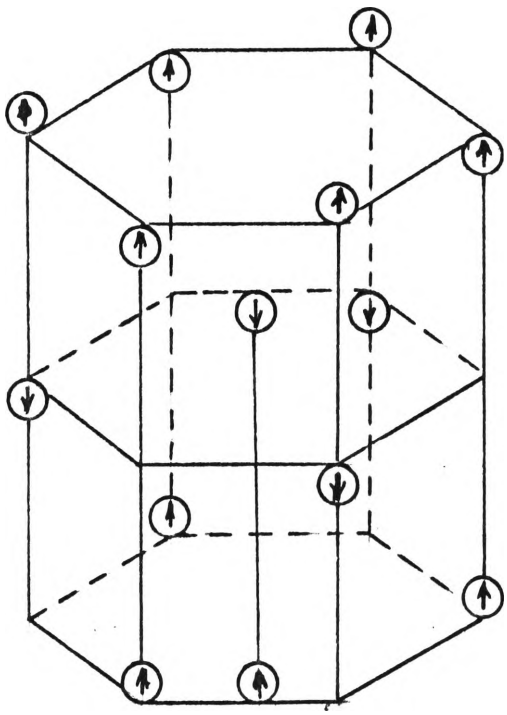

○ $Fe^{3+}$ ions

Magnetic structure for

$\alpha Fe_2O_3$

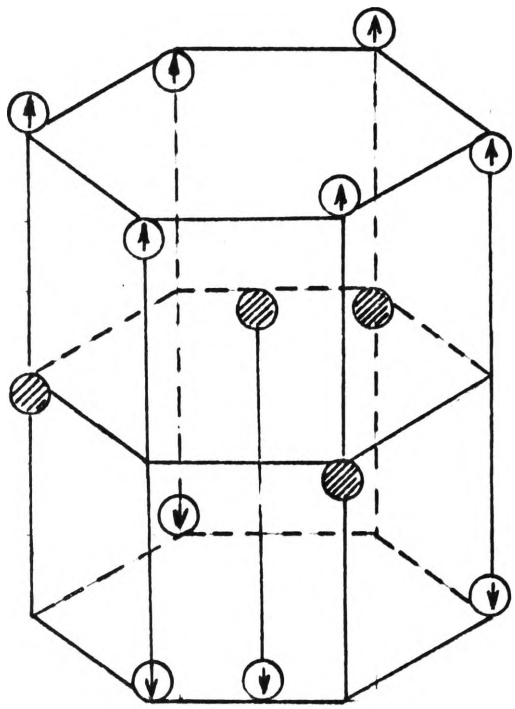

○ $Fe^{2+}$ ions

▨ $Ti^{4+}$ ions

Magnetic structure

for $FeTiO_3$

FIGURE 4.2

direction lies in the (111) plane and can turn freely in that plane. Bizette and Tsai (1956) showed by magnetic measurements that natural ilmenite is antiferromagnetic below its Néel temperature of 68°K and that the spin direction lies along the (111) axis. The magnetic structure of $FeTiO_3$ is different from that of the $\alpha Fe_2O_3$ as shown in Figure 4.2 and also illustrated schematically below.

$Fe_2O_3$ Fe↑-O-Fe↑-O-Fe↑

$FeTiO_3$ Fe↑-O-Ti-O-Fe ↓

The ilmenite-hematite series was long thought to be paramagnetic. However, the results of intensive investigations carried out by Nagata and Akimoto (1956), Ishikawa et al (1957) and Bozorth et al (1957) showed that, although pure $FetiO_3$ and $\alpha Fe_2O_3$ are both antiferromagnetic at low temperatures (below 55°K), the solid solutions $(1-x)FeTiO_3 - xFe_2O_3$ exhibit strong ferrimagnetic moments in the composition range of $0.1<x<0.6$. Solid solutions which show ferrimagnetic character at room temperature correspond to the composition range of $0.2\leqslant x\leqslant 0.5$. The result of x-ray analysis (Ishikawa and

Akimoto, 1958) and neutron diffraction analysis (Shirane et al 1959) show that the ferrimagnetism and the antiferromagnetism of this series correspond to the crystal symmetry of $R\bar{3}$ and $R\bar{3}C$ respecticely, the former equivalent to the ordered state and the latter the disordered state. It was also found that the magnetization changes linearly with temperature in the ferrimagnetic region. However, the nature of this ferrimagnetic phase is still not fully understood. It was reported (Shirane et al, 1959, Ruby et al, 1961) that the solid solution 0.88 $FeTiO_3$-0.12 $Fe_2O_3$ possesses a fairly large magnetic moment which is clearly observable by magnetic measurements, but there is no such indication when this is measured by neutron diffraction and Mössbauer spectroscopy at a temperature well below its Néel temperature of 170$^{o}$K. This anomaly was explained by assuming that the ferrimagnetic clusters were too small to produce a significant effect in the latter two measurements.

Shirane et al (1962) considered that the ferrimagnetic behaviour can be explained by the fact that the $Fe^{2+}$ and $Ti^{4+}$ in the solid solutions occupy alternate (111) layers, thus forming sublattices:

$$A: |x\ Fe^{3+},\ (1-x)\ Fe^{2+}|$$

$$\text{and}\quad B: |x\ Fe^{3+},\ (1-x)\ Ti^{4+}|$$

and when $Ti^{4+}$ ions are ordered on B layers, the difference between the moments on A and B layers respectively results in a ferrimagnetic moment.

## (4.2) Pseudobrookite Series

Curnow and Parry (1954) discovered that by oxidising natural ilmenite at a temperature between 600°C and 800°C, the susceptibility of their samples increased to more than ten times its original value. They explained this increase by a proposed change in $Fe^{3+}$: $Fe^{2+}$ ratio from 0.4:1 to 1.3:1. The curie point of this "magnetic ilmenite" is between 100°C and 200°C. However, heating the natural ilmenite at temperatures in excess of 800°C results in the conversion of most of the $Fe^{2+}$ to $Fe^{3+}$ and the product is weakly magnetic. Uyeda (1956) identified this final product as mainly pseudobrookite ($Fe_2TiO_5$) which has an orthorhombic crystal structure.

Pseudobrookite is a stable homogeneous phase in the intermediate stage of the $TiO_2$-$Fe_2O_3$ system (Figure 4.1). Synthetic samples can be prepared by heating a mixture of $Fe_2O_3$ and $TiO_2$ in appropriate proportions in air at 1200°C for several hours. A synthetic pseudobrookite solid solution series ($FeTi_2O_5$-$Fe_2TiO_5$) can be prepared by quenching from 1150°C. It was found (Chevallier and Mathieu, 1958) that this series is paramagnetic at temperatures higher than the liquid oxygen temperature. It was suggested (Gorter, 1957) that pseudobrookite becomes antiferromagnetic at a very low temperature. Muranaka et al (1971) concluded that both $Fe_2TiO_5$ and $FeTi_2O_5$ are paramagnetic at temperatures above 50°K and antiferromagnetic at lower temperatures.

The lattice parameters of $Fe_2TiO_5$, according to Akimoto et al (1957) are:

a = 9.767 A  b = 9.947 A  c = 3.717 A .

and those of $FeTi_2O_5$ are:

a = 9.798 A  b = 10.041 A  c = 3.741 A .

The volume of a unit cell of $Fe_2TiO_5$ and $FeTi_2O_5$ is 361.1 $A^3$ and 368.0 $A^3$ respectively and the magnetic susceptibility is 43 x $10^{-6}$ emu/gm and 53 x $10^{-6}$ emu/gm respectively. In $Fe_2TiO_5$, according to Wychoff (1951), $Fe^{3+}$ ions are situated in 8f sites and $Ti^{4+}$ ions in 4C sites, while in $FeTi_2O_5$ a half of 8f sites are occupied by $Ti^{4+}$ ions.

Uyeda (1956) suggested that the oxidation of natural ilmenite at temperatures below 850°C changes the sample into an ilmenite rich $FeTiO_3$ - $Fe_2O_3$ series, and that at temperatures higher than 850°C the pseudo-brookite series is produced.

Ramdohr (1926) and Frenzel (1956) suggested that the pseudobrookite series may co-exist naturally with ilmenite, especially in thermo-metamorphosed rocks. This hypothesis is supported by Avrahami and Golding (1969) who reported that there are indications of the presence of pseudobrookite in natural ilmenite when observed by Mössbauer spectroscopy (although there is no such indication from x-ray analysis). However, the present investigation of natural ilmenite samples by

TABLE 4.1

Magnetic structure of ilmenite-hematite series and pseudobrookite series.

| Compound | Néel Temp. ($^{O}$K) | Magnetic Structure at (300$^{O}$K) | Reference |
|---|---|---|---|
| $\alpha Fe_2O_3$ | 950 | Antiferro-magnetic | Kistner and Sunyar (1960) |
| $FeTiO_3$ | 55 | paramagnetic | Ishikawa (1957) |
| natural ilmenite | 68 | ferrimag-netic (paramagnetic) | Bizette et al (1956) Curnow and Parry (1954) Gibb et al (1969) |
| $Fe_2TiO_5$ | 50 | paramagnetic | Muranaka et al (1971) |
| $FeTi_2O_5$ | 50 | paramagnetic | Muranaka et al (1971) |
| 0.88 $FeTiO_3$- 0.12 $Fe_2O_3$ | 170 | paramagnetic | Ruby et al (1961) |
| 0.79 Fe Ti $O_3$- 0.21 $Fe_2O_3$ | 290 | paramagnetic | Shirane et al (1962b) |
| 0.67 Fe Ti $O_3$- 0.33 $Fe_2O_3$ | 370 | ferri-magnetic (paramagnetic) | Ruby et al (1961) |
| 0.5 Fe $TiO_3$- 0.5 $Fe_2O_3$ | 510 | antiferro-magnetic | Ruby et al (1961) |
| 0.3 $FeTiO_3$- 0.7 $Fe_2O_3$ | 670 | antiferro-magnetic | Ruby et al (1961) |

Mössbauer spectroscopy suggests the presence of a significant quantity of hematite in the solid solution of natural ilmenite. Its resonant absorption lines may be confused with those of pseudobrookite, particularly when its content in the sample is relatively low. More detailed discussions will be presented in Chapter 6.

A summary of the magnetic structure at 300$^{o}$K of the ilmenite-hematite series and pseudobrookite series is given in Table 4.1.

# CHAPTER 5

# MÖSSBAUER SPECTROSCOPY AND THE $FeO-TiO_2-Fe_2O_3$ TERNARY SYSTEM

## (5.1.) Information Obtainable from Mössbauer Spectra of Natural Ilmenite and its Oxidation Products

Mössbauer study of the synthetic ilmenite-hematite solid solutions (Ruby et al 1961, Shirane et al 1962 b) showed that the spectra are very sensitive to the variation of sample composition because of the difference in magnetic properties of the end members of the series. Similarly, measurement of the isomer shift, quadrupole splitting and magnetic hyperfine splitting from the Mössbauer spectrum of natural ilmenite or its oxidised products can reveal the ionic states and nuclear environments of Fe ions and magnetic properties of iron compounds in the sample. Each compound can be identified by its characteristic absorption lines. The intensities of absorption lines correspond to the relative amounts of iron compounds in a sample.

Shirane et al (1962 a) deduced from measurements on iron compounds that isomer shifts (with respect to $^{57}Co$ source embedded in a stainless steel matrix) can be

classified into two groups: (i) those corresponding to the $Fe^{3+}$ state with isomer shift ranging from 0.3 mm/s to 0.6 mm/s and (ii) those corresponding to the $Fe^{2+}$ state with isomer shift ranging from 1.2 mm/s to 1.5 mm/s. Walker et al (1961) calibrated the isomer shift from the calculated ion wave functions and identified the $Fe^{3+}$ electronic state as the $3d^5 4s^x$ state and the $Fe^{2+}$ electronic state as the $3d^6 4s^x$ state.

The hyperfine structure of the Mössbauer spectrum depends on the magnetic state of the sample. If the Fe ions are in the paramagnetic state and have an electronic relaxation time relatively shorter than the time of nuclear spin, the Mössbauer spectrum shows no magnetic hyperfine splitting but provides two observable parameters: (i) centre shift and (ii) quadrupole splitting. If the Fe ions are in the ferromagnetic, ferrimagnetic or antiferromagnetic state, or in the paramagnetic state with an electronic relaxation time large compared with the time of nuclear spin, then the magnetic hyperfine splitting can also be measured.

The chemical analysis of natural ilmenite samples (Curnow and Parry 1955, Uyeda 1956, Avrahami and Golding 1969 and Gibb et al 1969) reveals the relative amounts of

FeO, $TiO_2$ and $Fe_2O_3$ in a sample, but the amounts of various types of iron titanate compounds which are composed of these basic units, cannot be identified. For example, it could not be shown whether $Fe_2O_3$ and $TiO_2$ existed in free form individually or in the combined form of $Fe_2TiO_5$ (pseudobrookite). On the other hand, the x-ray analysis of natural ilmenite (Westcott 1966, Gibb et al 1969 and Avrahami 1969) identifies the content of the sample as mainly ilmenite with some non iron impurities and although there is a substantial amount of hematite, no x-ray lines of this compounds are observed. However, the content of iron compounds in a sample can be identified from the Mössbauer spectrum of this sample. But it is sometimes difficult to interprete an absorption spectrum when there is more than one compound present in a sample and when the absorption intensity is low and absorption lines may be overlapping each other. Compounds such as rutile and zircon, because there are no Fe ions in the compound, will not contribute any absorption lines to an absorption spectrum and therefore cannot be identified by Mössbauer Spectroscopy. These impurities are small in quantity and although they do not interfere drastically with the measurements generally, they may contribute some difficulties in spectrum interpretation when the absorption

intensity decreases and the content of by-product impurities increases at some stage of oxidation of a sample.

Mössbauer spectra of natural ilmenite have been studied by Gibb et al (1969) and Avrahami and Golding (1969) who concluded that the main compount in natural ilmenite is $FeTiO_3$ and that there exists at least one ferric compound which is difficult to identify because of its low absorption intensity.

Mössbauer studies of the artificially oxidised products of natural ilmenite have not been done previously and the present investigation is an attempt to clarify and supplement some of the findings obtained by using magnetic measurements (Curnow and Parry 1954, 1955 and Westcott 1966). The magnetic properties of natural ilmenite have been studied by these workers who found that the magnetic susceptibility increases with increasing oxidation temperature reaching a maximum value at a temperature between 700°C and 800°C, then decreases rapidly to zero at higher oxidation temperatures. Generally the magnetic strength of a specimen oxidised while in its natural state (with grain size approximately 200 $\mu$) is

higher than that of a specimen pre-crushed before oxidation (with grain size less than 50 μ). It was noted (Parry 1955, Westcott 1966) that oxidation at higher temperature increases the content of free rutile ($TiO_2$) and free hematite ($\alpha Fe_2O_3$) in the sample and that the $Fe^{3+}:Fe^{2+}$ ratio also increases. From the X-ray analysis of oxidised specimens, Curnow and Parry (1955) concluded that the final product when ilmenite is fully oxidised is $Fe_2O_3$. $TiO_2$ (pseudobrookite), while Westcott (1966) proposed the presence of an iron titanate $Fe_4(TiO_4)_3$ in the composition.

The specific aims of the present investigation are:

(i) to observe and analyze, if possible, the magnetic hyperfine splitting of the more strongly magnetic specimens which have been oxidised at temperatures between 700°C and 800°C;

(ii) to observe the transition of $FeTiO_3$ to $Fe_2TiO_5$ by oxidation at temperatures between 100°C and 1000°C;

(iii) to investigate the dependence of the oxidation process on particle grain size and the time duration of the oxidising reaction, and

(iv) to investigate the suggestion that pseudobrookite

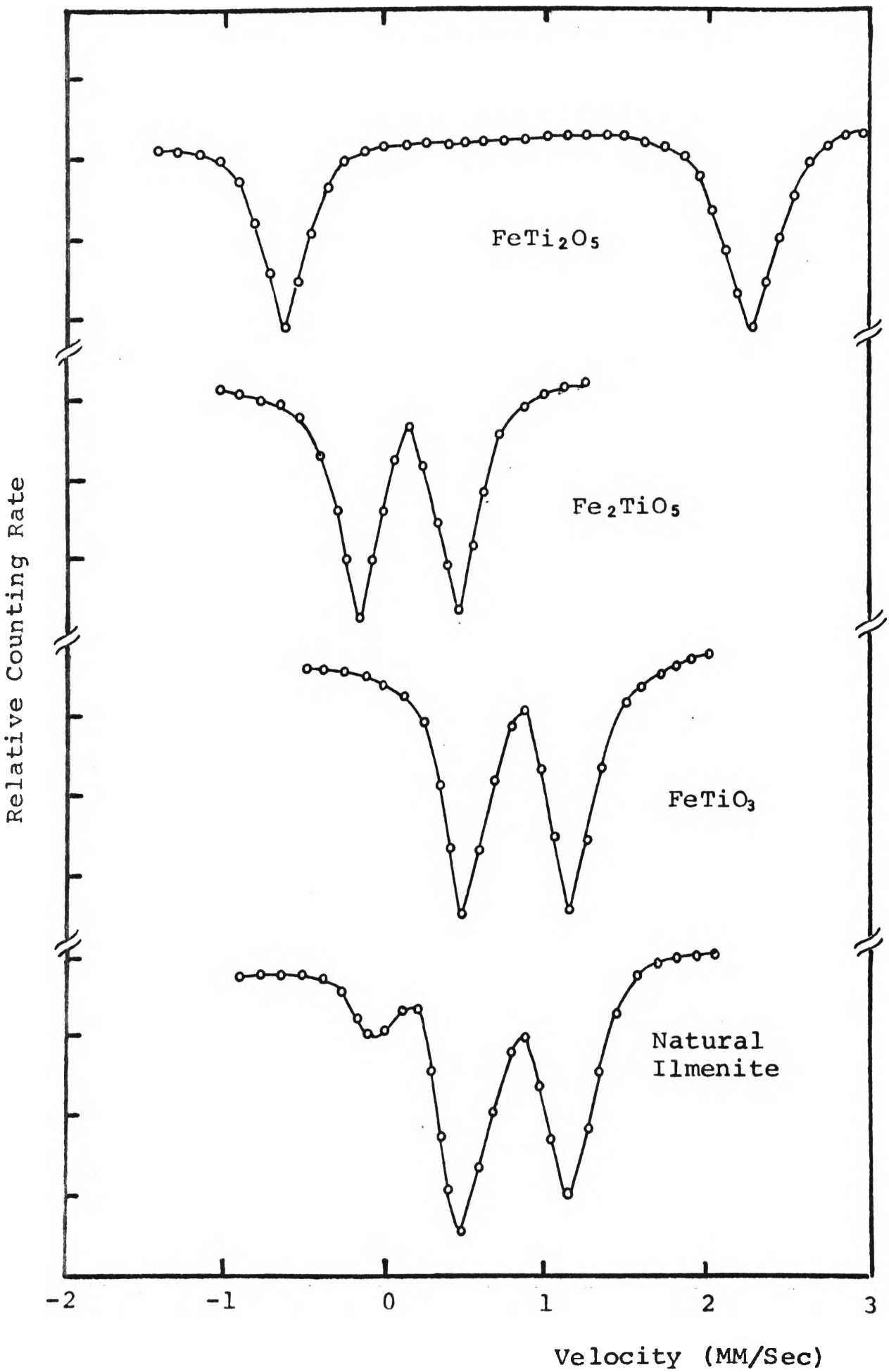


FIGURE 5.1. Mössbauer Spectra of some Iron Titanate Compounds

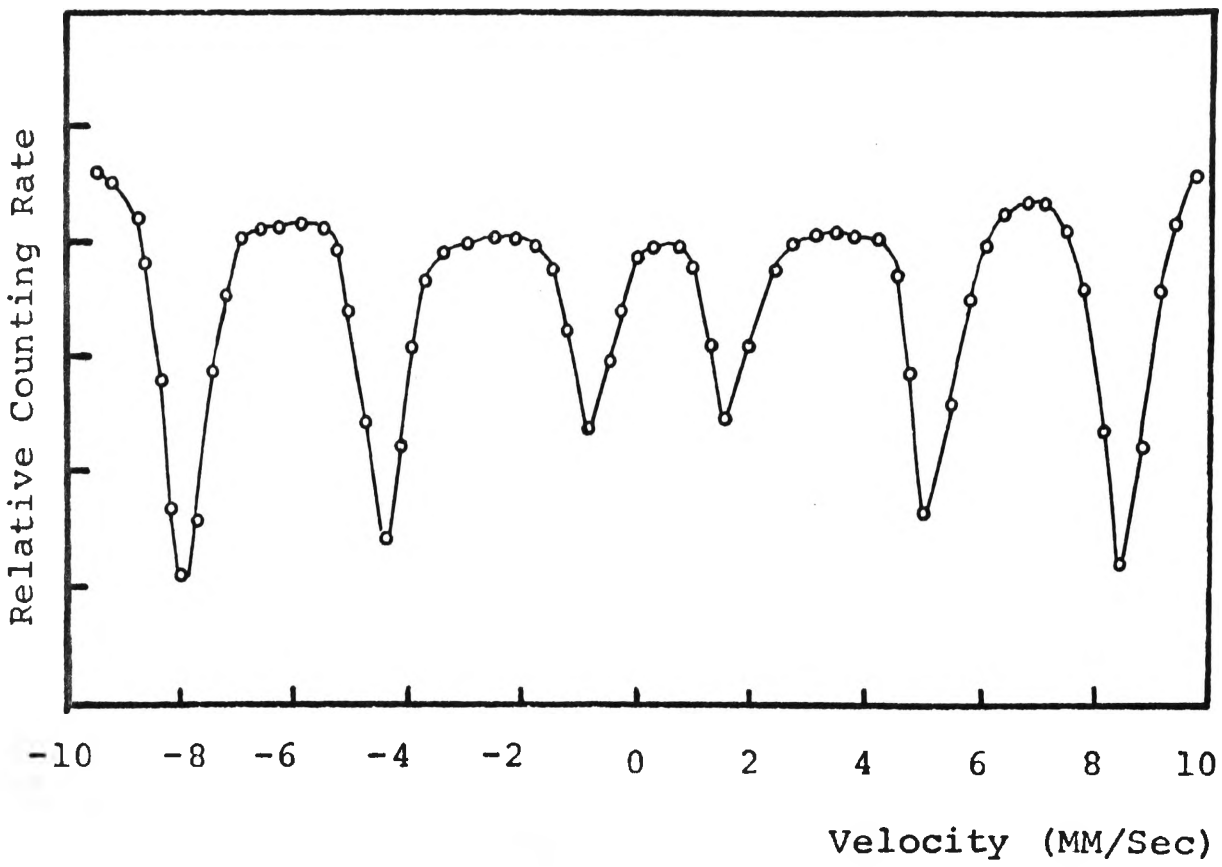


FIGURE 5.2. Mössbauer Spectrum of $\alpha Fe_2O_3$

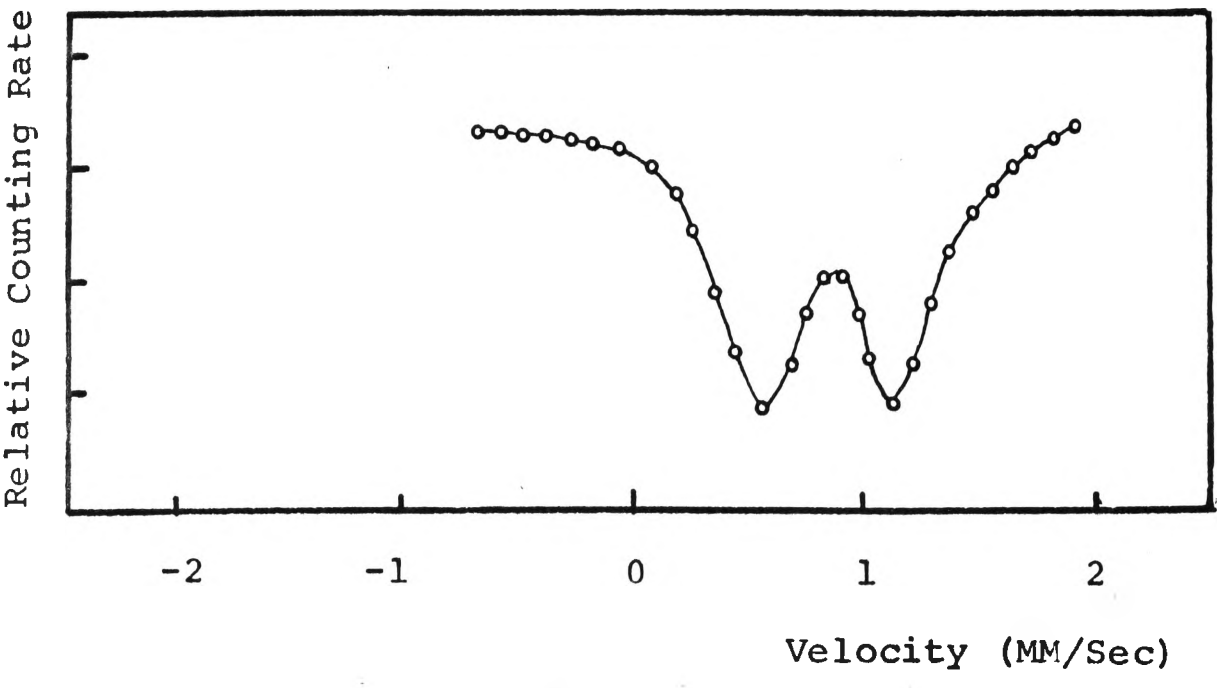


FIGURE 5.3. Mössbauer Spectrum of FeO

TABLE 5.1

Mössbauer measurements (at room temperature) of compounds in the $FeO$- $TiO_2$- $Fe_2O_3$ system

| Source Matrix | Absorber | Magnetic state at room temp. | Isomer shift (mm/s) | Ouadrupole splitting (mm/s) | Internal field (Oersted) | Reference |
|---|---|---|---|---|---|---|
| S.S | $\alpha Fe_2O_3$ | anti-ferro-magnetic | 0.47 (0.15)* | 0.12 | 515 | Kistner et al (1960) |
| S.S. | $\alpha Fe_2O_3$ | " | 0.47 (0.15)* | 0.20 | 520 | Shirane et al (1962a) |
| Cr | $\alpha Fe_2O_3$ | " | 0.51 | 0.20 | 517 | Cox et al (1963) |
| Cu | $\alpha Fe_2O_3$ | " | 0.12 | 0.10 | - | Eibschutz et al (1964) |
| - | $\alpha Fe_2O_3$ | " | 0.49 | 0.12 | 507 | Gol'Danskii et al (1965) |
| Pd | $\alpha Fe_2O_3$ | " | 0.32 (0.28)* | - | - | Avrahami and Golding (1969) |
| Pd | FeO | para-magnetic | 0.89±0.05 (0.85)* | 0.55/2 | - | Avrahami and Golding (1969) |
| S.S. | FeO | " | 1.15 | 0.30 | - | Shirane et al (1962a) |

TABLE 5.1 ( Cont'e )

| Source Matrix | Absorber | Magnetic state at room temp. | Isomer shift (mm/s) | Ouadrupole splitting (mm/s) | Internal field (Oersted) | Reference |
|---|---|---|---|---|---|---|
| S.S. | FeTiO | para-magnetic | 1.20 (0.88)* | 0.31 | - | Ruby et al (1961) |
| Pd | $FeTiO_3$ | " | 0.9 (0.86)* | 0.65/2 | - | Avrahami and Golding (1969) |
| S.S. | $FeTi_2O_5$ | " | 1.15 (0.83)* | 1.50 | - | Shirane et al (1962a) |
| S.S. | $Fe_2TiO_5$ | " | 0.48 (0.16)* | 0.35 | - | Shirane et al (1962a) |
| $Na_2[Fe(CN)_5NO].2H_2O$ | $Fe_2TiO_5$ | " | 0.53 (0.05)* | 0.37 | - | Gibb et al (1969) |
| Pd | $Fe_2TiO_5$ | " | 0.20 (0.16)* | 0.65/2 | - | Avrahami and Golding (1969) |
| - | natural ilmenite | " | 1.17 (0.85)* | 0.34 | - | Gol'Danskii (1965) |
| $Na[Fe(CN)_5NO].2H_2O$ | " | " | 1.35 (0.87)* | 0.35 | - | Gibb et al (1969) |

*Corrected value of isomer shift with respect to a $^{57}Co$ source embedded in a copper matrix.

may coexist with natural ilmenite.

## (5.2) Mössbauer Data and Spectra of Compounds of the Ilmenite-Hematite Series and Pseudobrookite Series

Mössbauer data at room temperature of compounds belonging to the ilmenite-hematite series and pseudo-brookite series are given in Table 5.1. Mössbauer spectra of these compounds, with respect to a $^{57}Co$ source embedded in a copper matrix, are shown in Figures 5.1 to 5.3, inclusive (references given in Table 5.1).

It is noted that there are some variations in the Mössbauer data of a given compound. This may be due to the difference in spectrometer sensitivity, difference in the quality of samples used or measurement errors. However, these data provide valuable information for identifying unknown compounds.

The spectra of some natural ilmenite samples show a small absorption line which is due to the presence of $Fe^{3+}$ ions in the sample (Gibb 1969, Avrahami and Golding 1969). The intensity of this line may change depending on the amount of $Fe^{3+}$ ions in the sample. Some

samples which have a composition close to the stoicheiometry $FeTiO_3$ do not show any $Fe^{3+}$ absorption line at all.

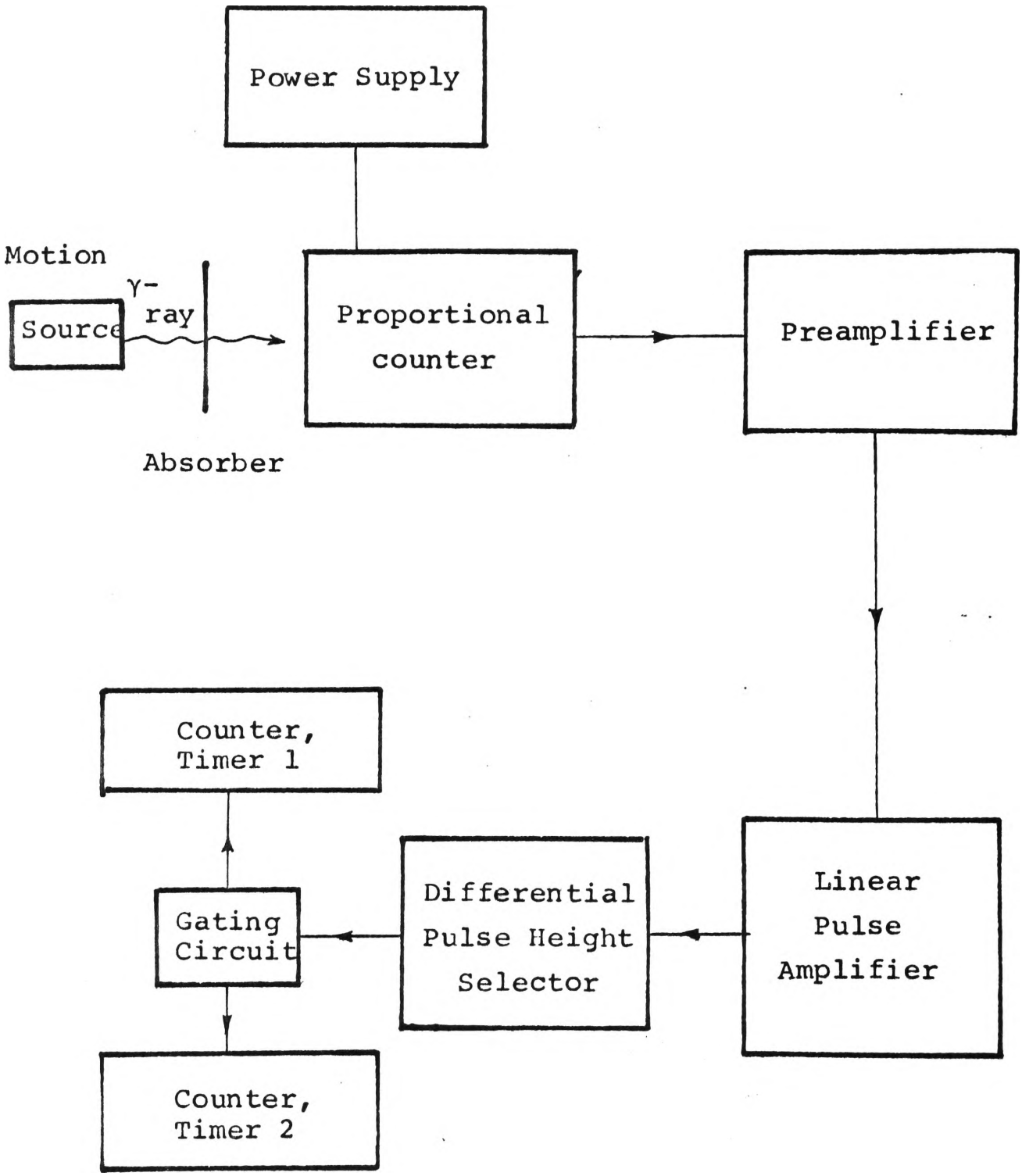


FIGURE 6.1. Detection system of the Mössbauer Spectrometer

# CHAPTER 6

# EXPERIMENTAL PROCEDURES AND RESULTS

## (6.1) The Preparation and Mounting of Specimens

The grain size of natural ilmenite is about 200 μ which is found experimentally too large for incorporation in satisfactory absorption specimens. Samples were therefore ground to a fine powder of less than 50 μ, which size gives a good absorption spectrum. This fine powder is then spread evenly over an area of 2.5 cm x 2.5 cm on a sticky cellulose tape. Two tapes, each with an ilmenite sample adhering, are then firmly pressed together, sandwiching the powder in between. Each sandwich specimen thus prepared contains 25.0 ± 0.5 mg sample powder which is equivalent to a thickness of 4 mg/cm$^2$. It was found by experiment that three of these sandwiches when overlaid give satisfactory Mössbauer spectra. Slightly thicker specimens may be used, but the effect of self absorption becomes serious if the specimen is made much thicker. (See Section 2.5, Chapter 2).

To ensure that the powder will not vibrate during the experiment, the specimen is inserted between

two thin perspex sheets and then screwed firmly onto the absorber holder which is held rigidly on the platform of the constant velocity drive. The specimen to be examined is placed between the detector and the source (a $^{57}Co$ source embedded in a copper matrix) at a distance of about 3 cm from the detector. The source is housed in the source holder which is mounted on the constant velocity drive. Its distance from the detector varies from 9 cm to 12 cm during the experiment, during which it moves with a constant velocity relative to the absorber.

Three series of experiments were conducted in the present investigation. In the first series, natural ilmenite samples from four different regions were examined. In the second series, the natural ilmenite sample was crushed to a fine powder of less than 50μ and then oxidised for one hour in an open-air quartz tube at a fixed temperature between 100°C and 1000°C. In the third series, the sample of natural grain size of about 200μ was first oxidised by the heat treatment described above and then, after it had cooled to room temperature, crushed to a fine powder of less than 50μ. Each sample was then prepared as an absorption specimen and its Mössbauer spectrum at room

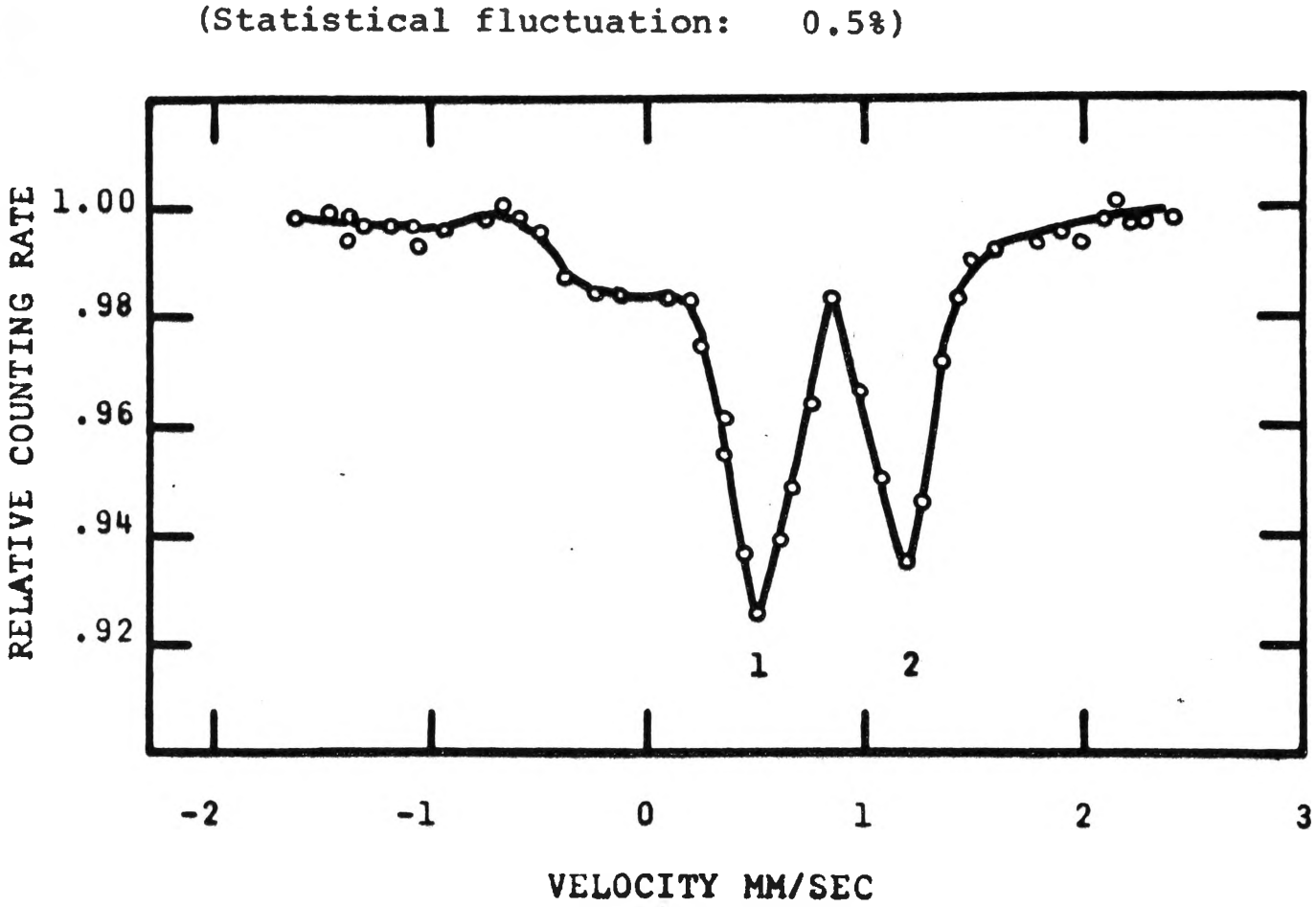


FIGURE 6.2. Mössbauer spectrum of natural Swansea Ilmenite

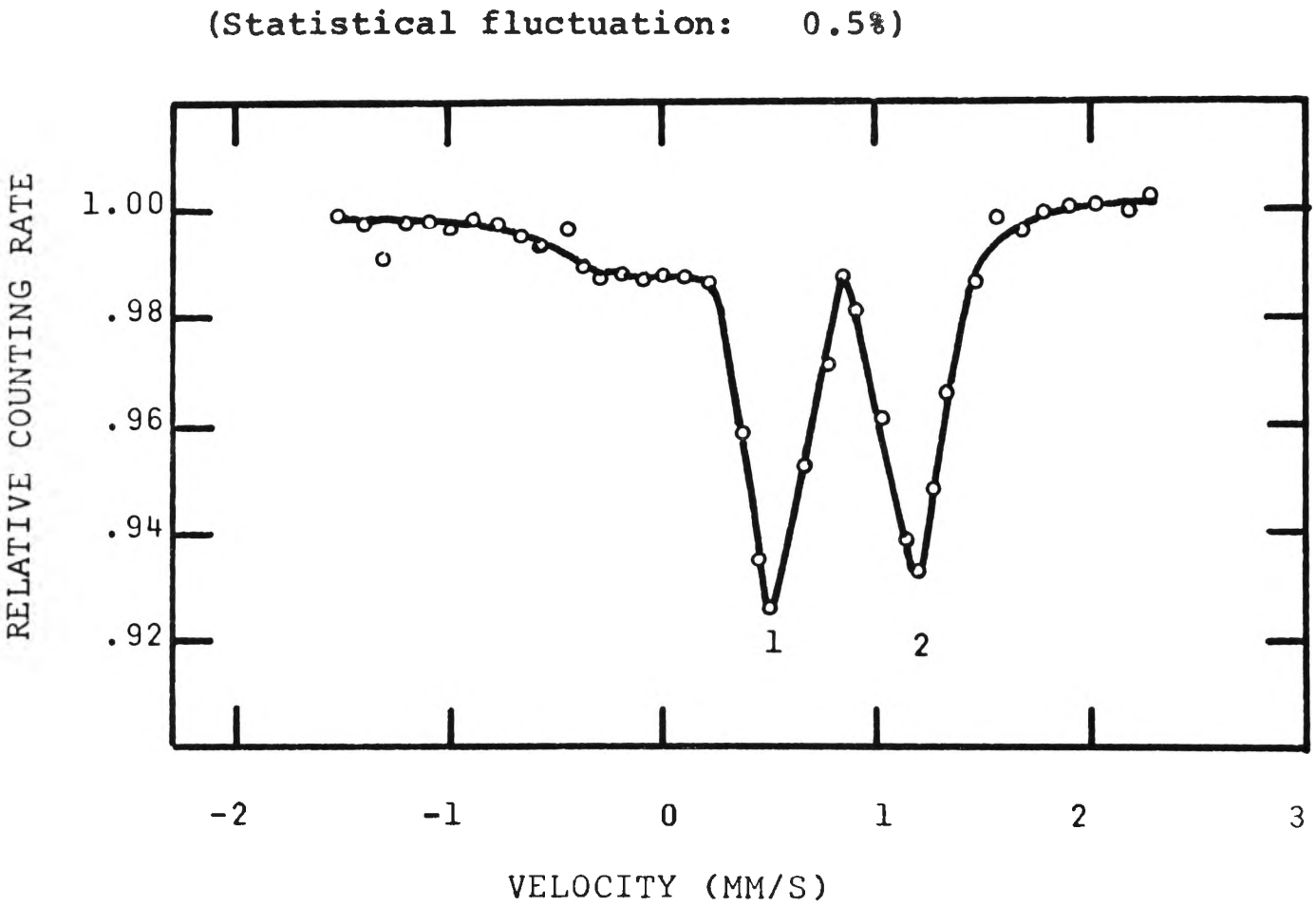


FIGURE 6.3. Mössbauer spectrum of natural Norwegian ilmenite

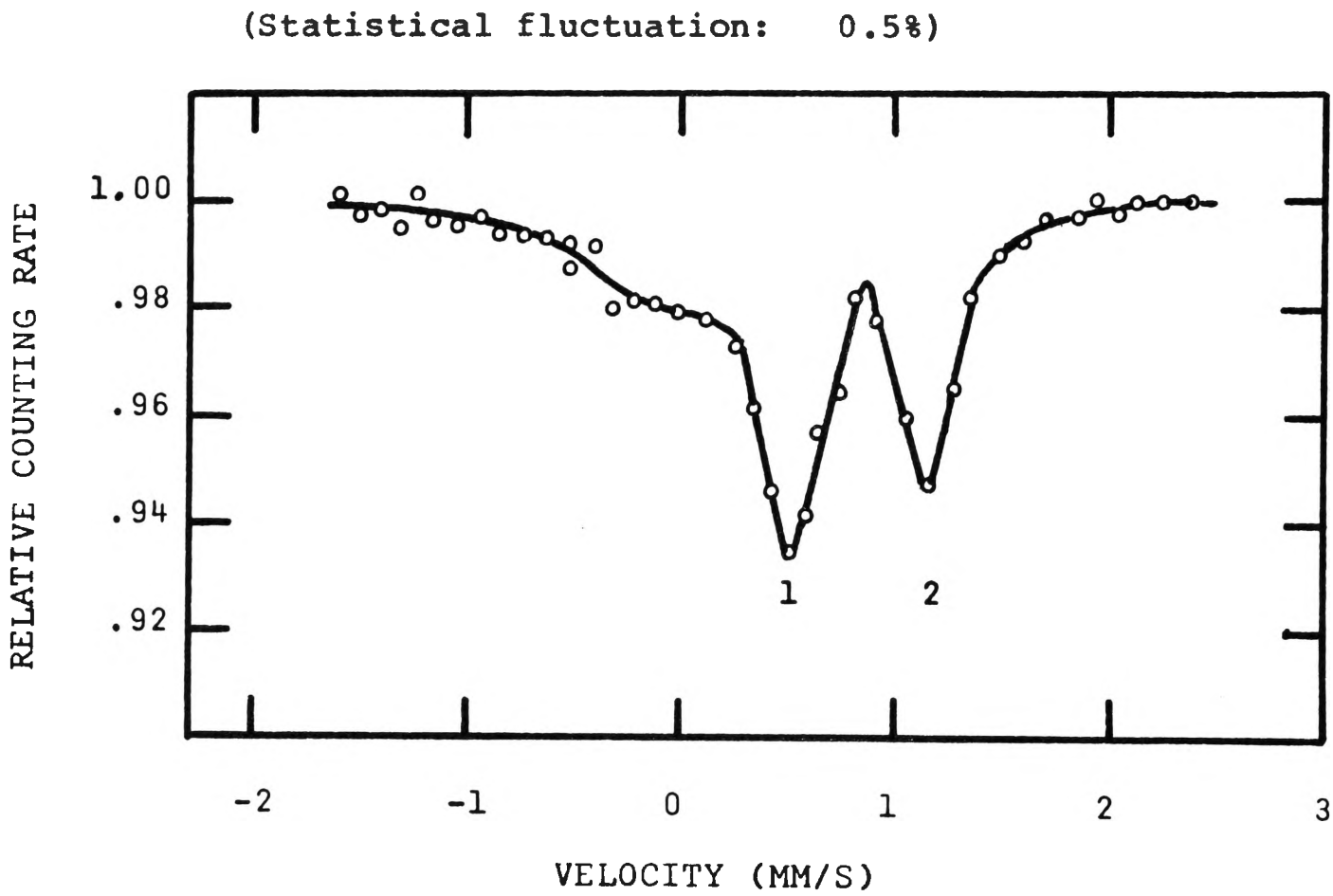


FIGURE 6.4. Mössbauer spectrum of natural Ceylon ilmenite

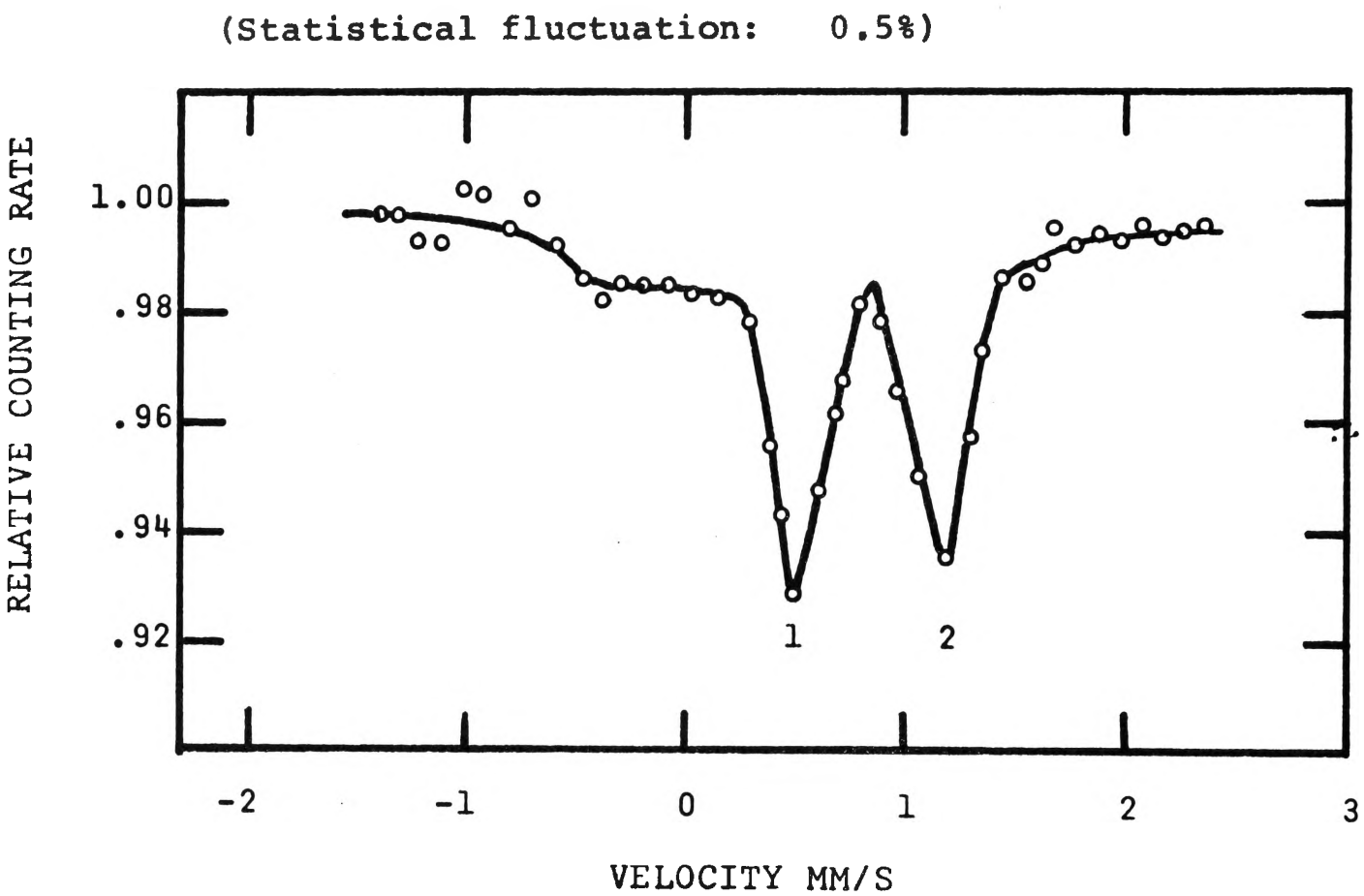


FIGURE 6.5. Mössbauer spectrum of natural Capel ilmenite

temperature obtained and analyzed. (The counting accumulation for each point on the spectrum is about 30,000).

## (6.2) Spectra of Ilmenite Samples from Different Regions

Natural ilmenite samples obtained from Swansea (N.S.W.), Capel (W.A.), Ceylon and Norway were examined in the first series of experiments. Mössbauer spectra of these samples, as shown in Figures 6.2 to 6.5, are found to be similar to each other, and indicate that they are mainly ilmenite in structure.

Since natural ilmenite is weakly ferrimagnetic at room temperature (Akimoto 1954, Curnow and Parry 1954, Uyeda 1956), it is expected to show ferrimagnetic hyperfine structure in its Mössbauer spectrum. But the spectra obtained in this experiment as well as those obtained by other workers (Gibb et al 1969, Avrahami and Golding 1969), show only quadrupole splitting which is an indication of paramagnetic character. Such behaviour is similar to that exhibited by the synthetic solid solution $(1-x)\ FeTiO_3 - xFe_2O_3$ when x is smaller than 0.22. Ishikawa (1962) proposed a superparamagnetic phase for solid solutions with $x < 0.22$. He suggested a lattice

TABLE 6.1

Chemical composition of natural ilmenites from Swansea and Capel

| Composition | Content (%) | |
|---|---|---|
| | Swansea | Capel |
| $TiO_2$ | 49.7% | 55% |
| FeO | 31.2% | 26.5% |
| $Fe_2O_3$ | 17.8% | 15.5% |
| $Fe^{3+}:Fe^{2+}$ | 0.51:1 | 0.52:1 |
| Total Fe:$TiO_2$ | 1:1·35 | 1:1.75 |

model in which $Fe^{3+}$ ions on the B layers are coupled antiferromagnetically with nine neighbouring Fe ions on adjacent A layers. The ferrimagnetic clusters in the solid solution are assumed to be small and surrounded by paramagnetic media and their size varies with respect to the content of hematite in the solid solution. Because of the small size of ferrimagnetic clusters, no long-range magnetic ordering can be observed. In the present investigation the content of hematite in the samples can be assumed to be less than 22 per cent (Table 6.1) and hence only spectra with paramagnetic character are produced.

The absorption spectrum shown in Figure 6.2 is that of a Swansea ilmenite sample. It shows two prominent absorption lines (labelled 1 and 2) at 0.5±.01mm/s and 1.2±0.01 mm/s respectively with an absorption depth of about 7 per cent. In addition there is a small absorption line adjacent to absorption line 1. The two prominent absorption lines have previously been determined by Ruby and Shirane (1961) as those of $Fe^{2+}$ in $FeTiO_3$. These two lines are the result of quadrupole splitting of a nuclear energy level of $Fe^{2+}$. The

splitting is caused by the interaction of the nuclear quadrupole moment with the gradient of the electric field produced by other charges in the lattice (Section 1.3). This means that the $Fe^{2+}$ nucleus of ilmenite is not spherical in shape. The excited state of $^{57}Fe$, with spin quantum number $I = {}^{3}/_{2}$, is split into two states with a magnetic quantum number $m_I = \pm {}^{3}/_{2}$. The energy gap between these energy levels due to quadrupole splitting can be measured directly from the absorption spectrum and is found to be

$$\Delta E_a = 0.7 \pm 0.01 \text{ mm/s}$$

$$= (3.36 \pm 0.05) \times 10^{-8} \text{ eV}$$

Hence the quadrupole splitting is given by

$$\varepsilon = \frac{\Delta E_a}{2}$$

$$= 0.35 \pm 0.01 \text{ mm/s}$$

$$= (1.68 \pm 0.05) \times 10^{-8} \text{ eV}$$

The centre shift can also be measured directly from the spectrum and is found to be

$$\delta = 0.85 \pm 0.01 \text{ mm/s}$$

$$= (4.08 \pm 0.05) \times 10^{-8} \text{ eV}$$

The centre shift is mainly caused by an isomer shift which is due to the differences in the S-electron densities at the nuclii of the source and absorber, (Section 1.3). The other factor which causes a centre shift is the second order Doppler effect resulting from the thermal motion of atoms. This factor is regarded as negligible for the source and absorber at the same temperature (in this case the room temperature). Thus the isomer shift is 0.85 ± 0.01 mm/s.

The linewidth of the 1.20 mm/s absorption line is 0.35 mm/s and that of the 0.5 mm/s absorption line is about 0.4 mm/s. The two absorption lines are of unequal depth with a ratio of approximately 1:0.8. The difference in linewidths and intensities may be due to the presence of $Fe^{3+}$ ions in the sample. Avrahami and Golding (1969) suggested that the $Fe^{3+}$ ions are those of pseudobrookite, which may coexist naturally with ilmenite, (although the x-ray diffraction spectrum of their sample did not indicate the presence of pseudobrookite). The absorption lines of pseudobrookite are found to have a quadrupole splitting of 0.35 mm/s and centre shift of

0.48 mm/s when referred to a stainless steel source (Shirane et al, 1962a). The absorption line positions of pseudobrookite will be at 0.13 mm/s and o.81 mm/s or at -0.18 mm/s and 0.50 mm/s when referred to the copper matrix source used in this experiment (Muir 1967 ). If there were a small amount of pseudobrookite present in the sample the linewidth of absorption 1 would be broadened, the intensity increased, and there would be a small absorption line situated at -0.18 mm/s position. However, it is not possible to determine these absorption line positions in the spectrum because of their low intensity. The small absorption line on the spectrum might, therefore, be due to another compound rather than pseudobrookite.

Gibb et al (1969) also encountered the same difficulty in the interpretation of Mössbauer spectra of natural ilmenite samples which contain a significant amount of $Fe^{3+}$ ions. The x-ray analysis of their samples did not indicate the presence of either $\alpha Fe_2O_3$ or $Fe_2TiO_5$ and there was an uncertainty as to the presence of $Fe_2O_3.3TiO_2$.

The chemical analysis of a Swansea and a Capel ilmenite provided by Kathleen Investment Pty. Ltd. (the suppliers) is given in Table 6.1.

Parry (1955) suggested that beach sand ilmenites contain approximately 8 per cent by weight of free rutile and 92 per cent ilmenite-hematite solid solution. The amount of hematite in Swansea and Capel samples is 17.8 per cent and 15.5 per cent respectively and the amount of free rutile is approximately 6 per cent and 13 per cent respectively (Westcott 1966). Assume that most of hematite molecules exist in solid solution, then the spectra obtained should show the characteristics of ilmenite-hematite solid solution. In fact these spectra (Figures 6.2 to 6.5) do bear some resemblance to the spectra of synthetic ilmenite-hematite solid solutions $(1-x)\ FeTiO_3 - x\ Fe_2O_3$ when $x \leqslant 0.21$ (Ruby et al 1961, Shirane et al 1962b). These synthetic samples exhibit only paramagnetic characteristics having two prominant ilmenite absorption lines and two hematite absorption lines due to quadrupole splitting. The isomer shift $\delta$ and quadrupole splitting $\varepsilon$ of hematite are 0.45 mm/s

and 0.2 mm/s respectively. The calculated line positions are situated at 0.25 mm/s and 0.65 mm/s with respect to the source used in this experiment. Thus it is highly probable that the small absorption line shown in the spectra of natural ilmenite might be due to hematite in the solid solution, but because of its low intensity it could be mistaken for the pseudobrookite absorption line as was suggested by Avrahami and Golding (1969).

The absence of the characteristic pattern of hematite in the X-ray analysis of a sample containing a significant amount of it may be explained by the same assumption that hematite exists mainly in solid solution rather than in free form and thus is situated in a different lattice environment and consequently the usual pattern is not observed. This assumption is strengthened by the fact that in Mössbauer spectra of synthetic samples containing up to 33 per cent of hematite (Ruby et al 1961, Shirane et al 1962b), no antiferromagnetic hyperfine structure of hematite is observable even though it is antiferromagnetic at room temperature.

TABLE 6.2

Absorption line intensities of ilmenites

| Absorption line | Absorption Depth (%) | | | |
|---|---|---|---|---|
| | Norwegian | Swansea | Capel | Ceylon |
| 1 | 7.8 | 7.5 | 7.5 | 7 |
| 2 | 7.5 | 7.0 | 7.8 | 6 |
| 3 | 1.5 | 2 | 2 | 2.5 |

The results of the series of experiments on oxidised samples presented in Sections 6.3 and 6.4 also support the assumption that hematite exists mainly in solid solution. More detailed discussion is given in Section 6.6.

Comparison of ilmenite absorption intensities in samples can indicate approximately the relative amount of $FeTiO_3$ in each sample. However, accurate determination of the $FeTiO_3$ percentage in a sample is not possible because of the low absorption intensity. Impurities such as rutile and zircon which contain no Fe ions cannot be detected by Mössbauer spectroscopy but their presence will reduce the intensity of absorption lines generally. In addition, absorption lines of $Fe^{3+}$ ions also affect the intensity of line 1 of $FeTiO_3$.

Direct comparison of the spectra shows that Norwegian ilmenite contains the most $FeTiO_3$ and the least number of $Fe^{3+}$ ions in the sample, followed by Swansea and Capel, with Ceylon ilmenite containing less $FeTiO_3$ but more $Fe^{3+}$ ions.

The following Sections, 6.3 and 6.4, are concerned with the description of the spectra of specimens

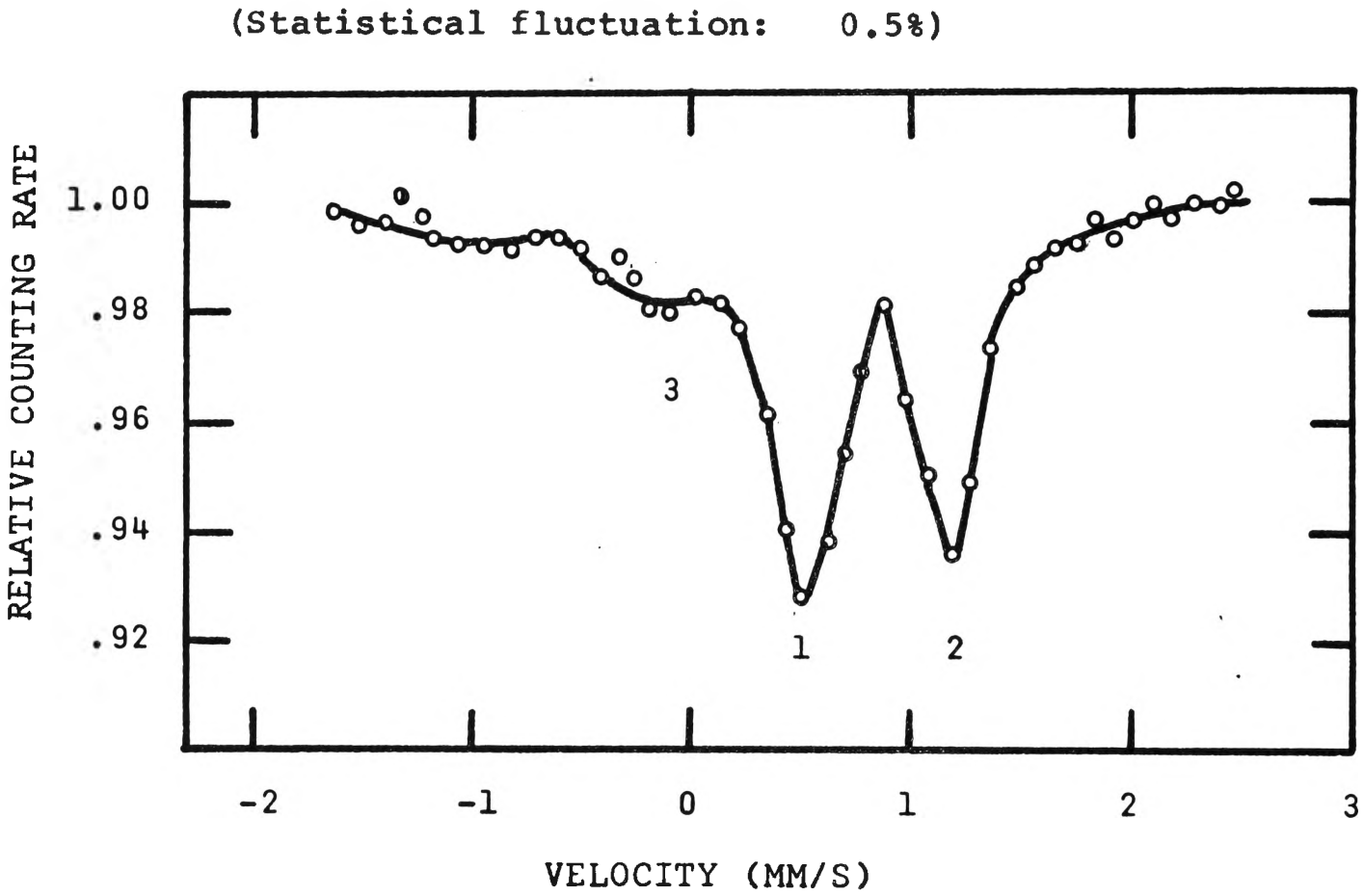


FIGURE 6.6. Mössbauer spectrum of a crushed ilmenite specimen which has been heated at 350°C for one hour.

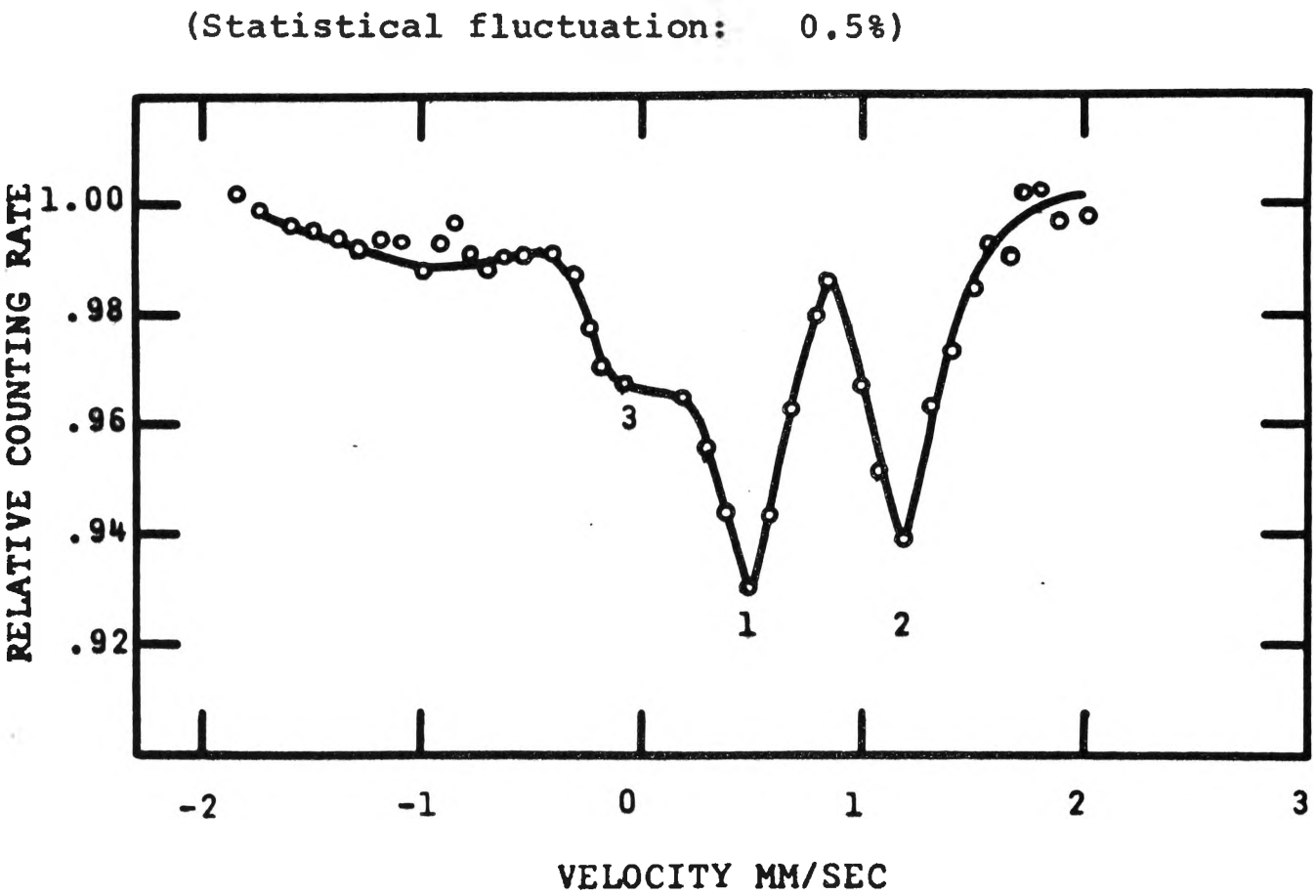


FIGURE 6.7. Mössbauer spectrum of a crushed ilmenite specimen which has been heated at 400°C for one hour.

oxidised under different conditions. Changes in absorption intensities with respect to temperature are given in Tables 6.3 and 6.4. Detailed discussions of results are given in Sections 6.5 to 6.9 inclusive.

## (6.3) Mössbauer Spectra of Specimens Pre-crushed before Oxidation

### (a) Ilmenite specimens heated at temperatures between 100°C and 350°C.

Absorption spectra of these specimens are similar to that of the unoxidised sample, with two prominent absorption lines, 1 and 2, of ilmenite and a small absorption line, 3, at -0.1 mm/s (see Figure 6.6). Evidently, heat treatment in this temperature range produces only a negligible effect and the specimens remain mainly ilmenite in content.

### (b) Ilmenite specimen heated at 400°C.

It can be seen from the absorption spectrum (Figure 6.7) that the low intensity absorption region at about -0.1 mm/s has increased in magnitude, indicating

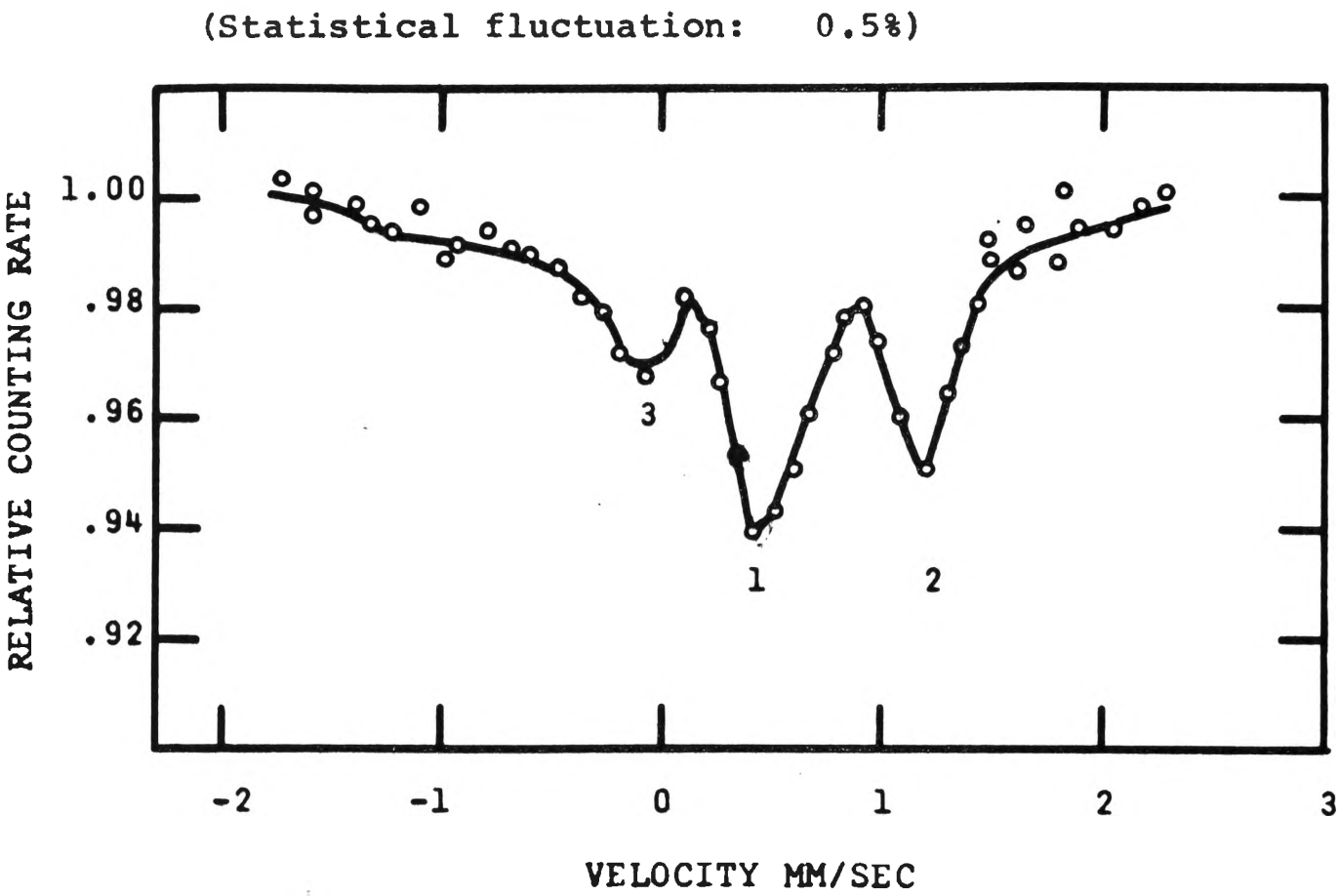


FIGURE 6.8. Mössbauer spectrum of a crushed ilmenite specimen which has been heated at 500°C for one hour.

an increase in absorption of $Fe^{3+}$ ions. This absorption peak is still not clearly defined, due to the overlapping by the absorption line 1. The counting fluctuation in the -1.0 mm/s region has increased slightly. This could be a possible indication of a very low intensity absorption of some other substance.

(c) Ilmenite specimen heated at 500°C.

In this spectrum the $Fe^{3+}$ absorption line (labelled 3) is better resolved although the absorption intensity appears to remain at 3 per cent. Because the influence of the absorption line 1 has decreased due to decrease in ilmenite content it can be deduced that the $Fe^{3+}$ content has increased slightly.

The counting fluctuation in the -1 mm/s and +1.5 mm/s regions is slightly increased compared to the previous spectrum. This may be regarded as an indication of an increase in free hematite content. The ilmenite absorption line 2 has shrunk to about 5 per cent but is still well defined. The absorption line 1 has decreased in intensity and is broadened due to the increase of $Fe^{3+}$ absorption.

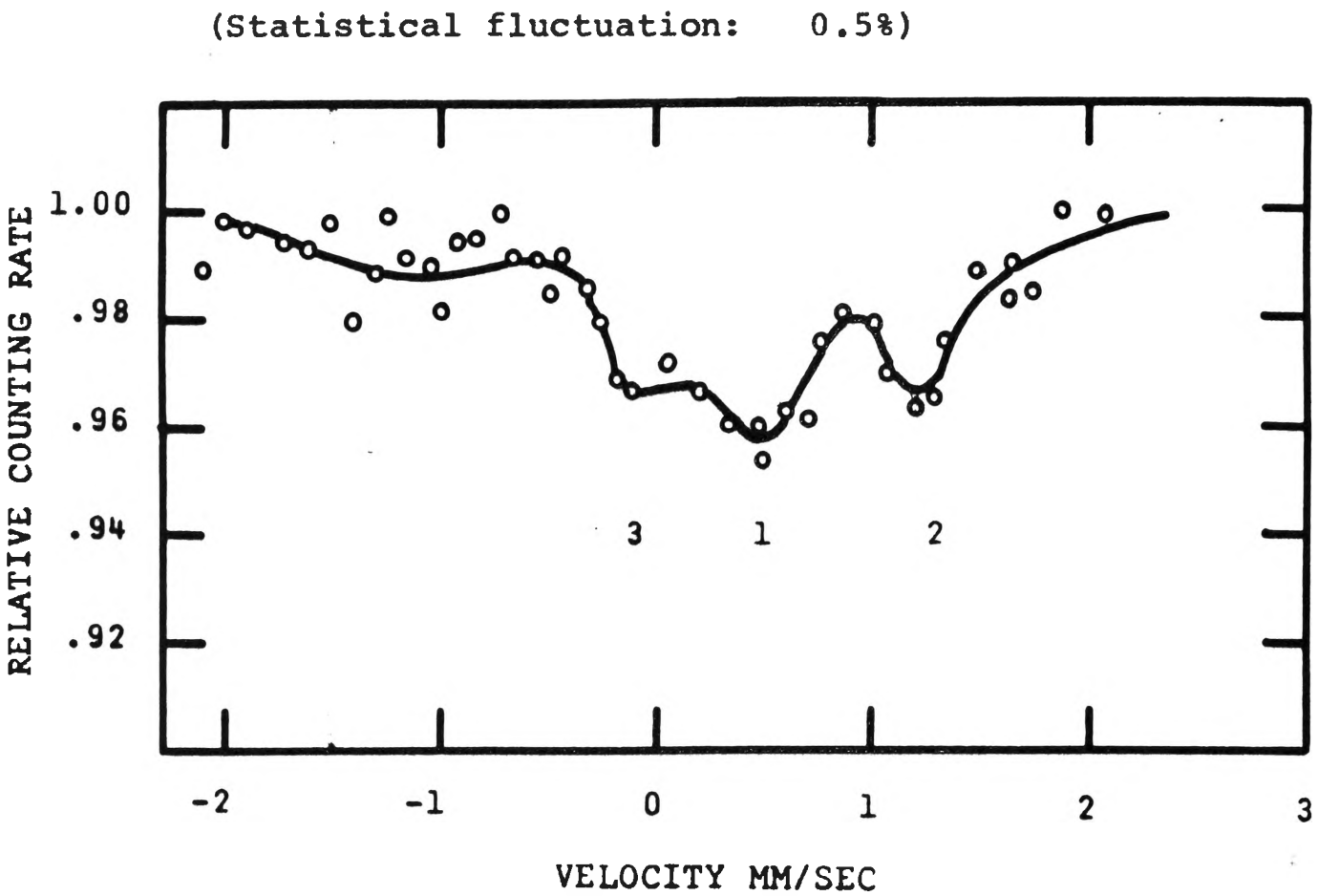


FIGURE 6.9. Mössbauer spectrum of a crushed ilmenite specimen which has been heated at 550°C for one hour.

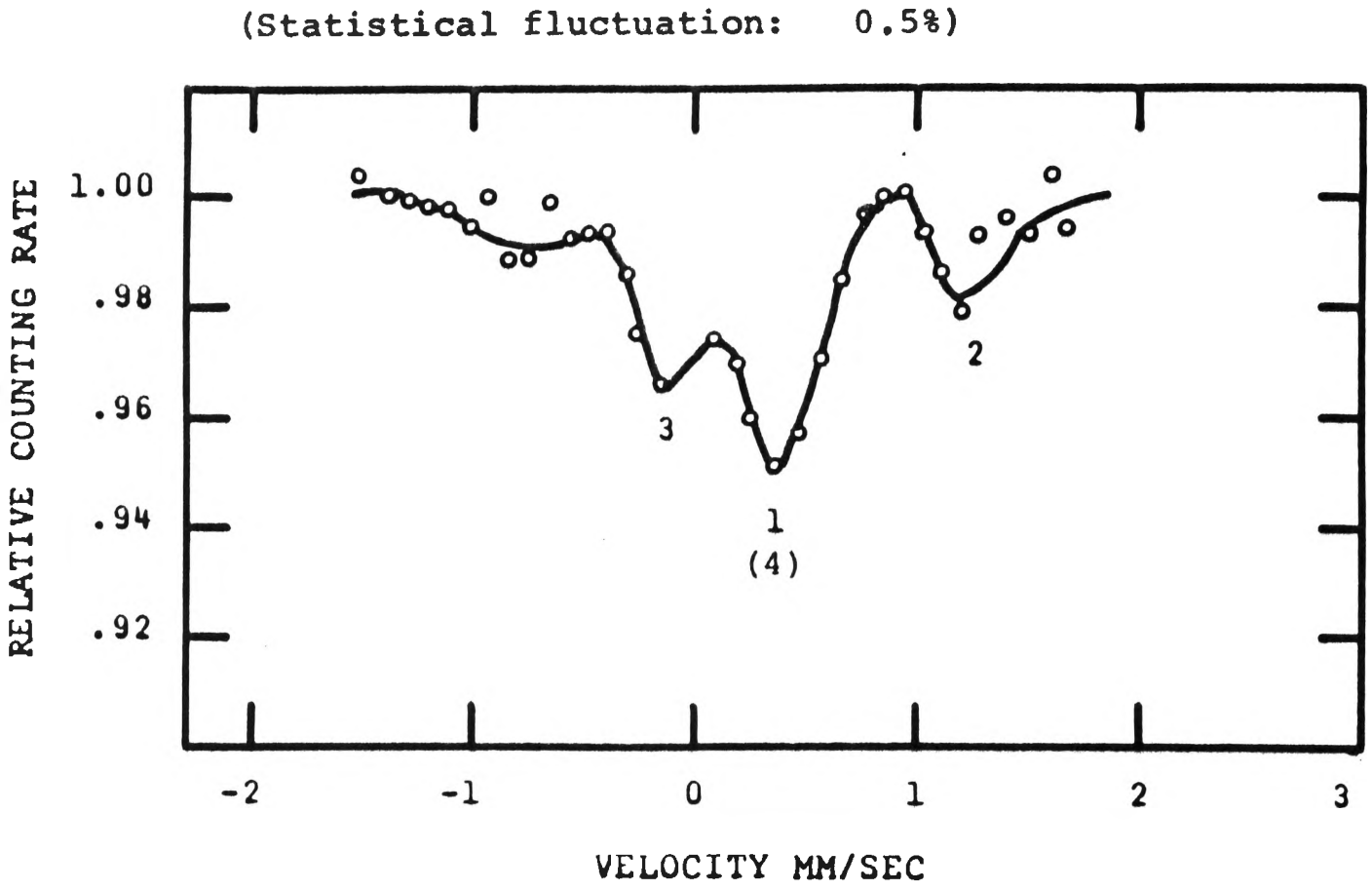


FIGURE 6.10. Mössbauer spectrum of a crushed ilmenite specimen which has been heated at 600°C for one hour.

(d) Ilmenite specimen heated at 550°C.

The absorption spectrum of this specimen (Figure 6.9) shows generally low intensity absorption lines. The ilmenite absorption line 2 has reduced further to about 4 per cent and absorption line 3 has increased to about 3.5 per cent. However, absorption line 1 is broadened and the intensity is lower than expected if it is a combination of ilmenite and pseudobrookite only. This may be an indication that some other absorption lines are also present in this region. The absorption at -1.0 mm/s has substantially increased, indicating the presence of free hematite. (A more detailed discussion is given in Section 6.6).

(e) Ilmenite specimen heated at 600°C.

The absorption spectrum (Figure 6.10) of this specimen is better resolved than the previous specimen. More ilmenite is oxidised at this temperature and the intensity of the absorption line 2 has reduced further to 2 per cent, absorption line 3 has increased to about 4 per cent and absorption line 1 to 5 per cent. The

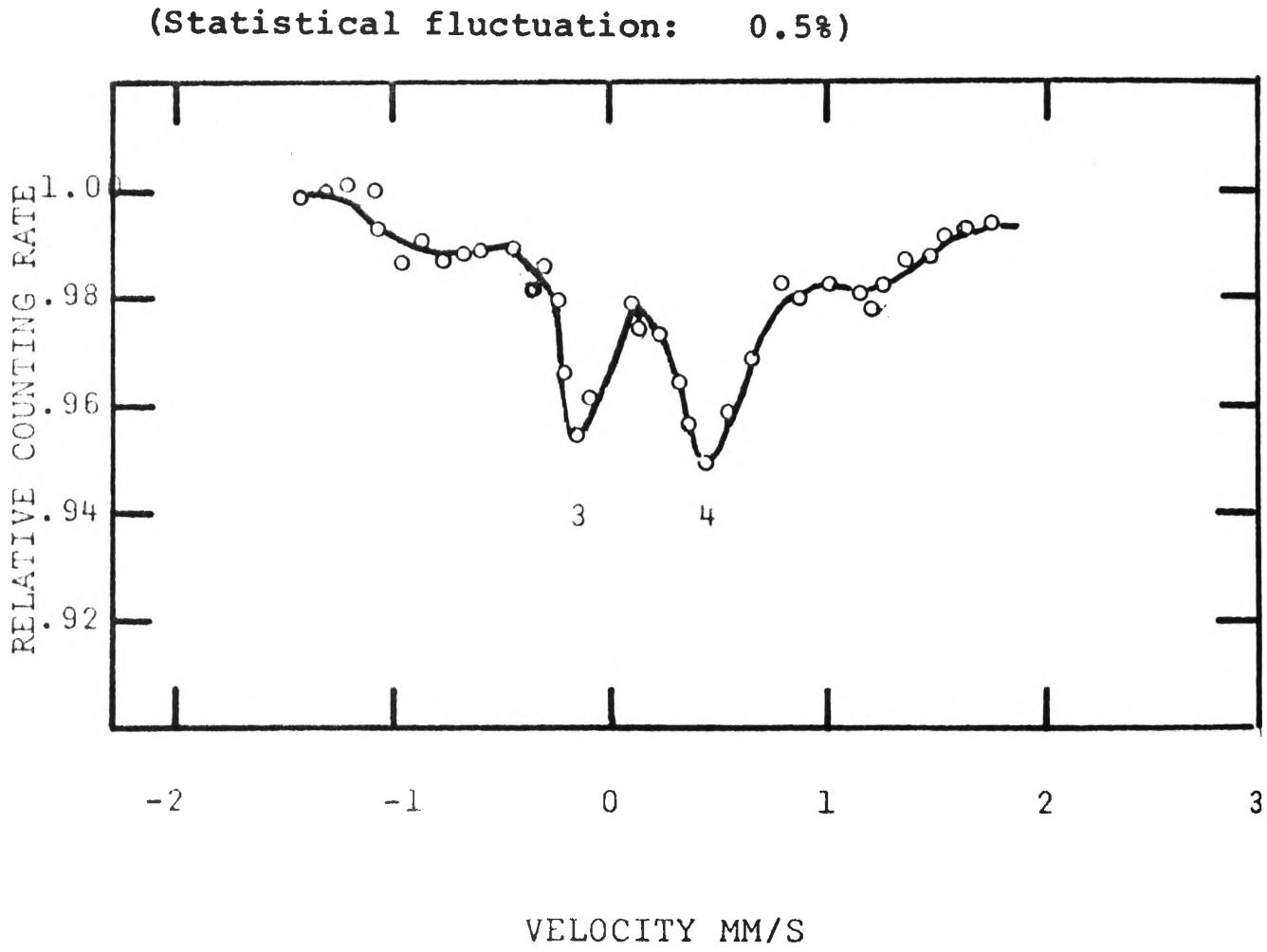


FIGURE 6.11. Mössbauer spectrum of a crushed ilmenite specimen which has been heated at 650°C for one hour.

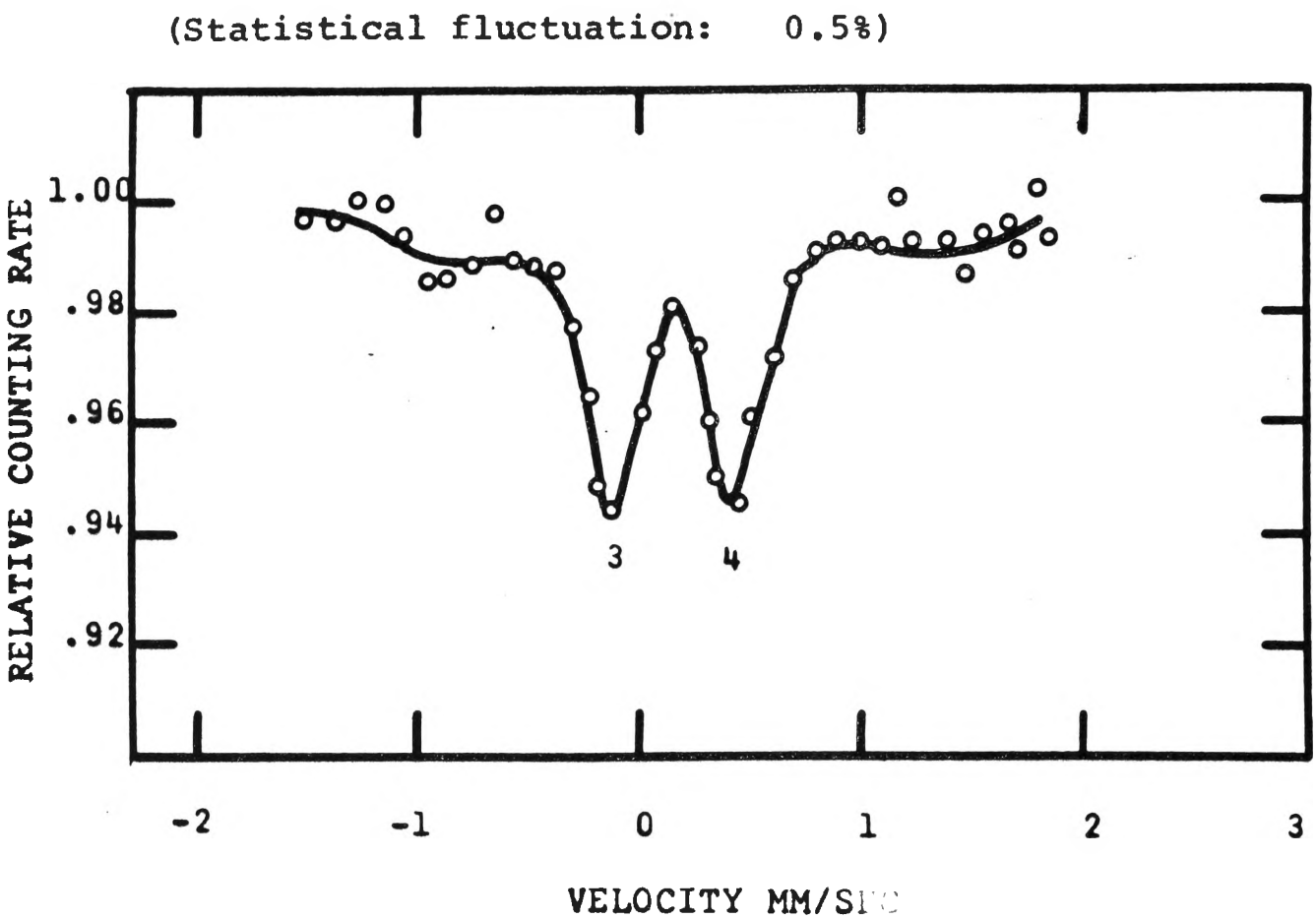


FIGURE 6.12. Mössbauer spectrum of a crushed ilmenite specimen which has been heated at 700°C for one hour.

absorption line 1 is renamed as absorption line 4, belongong mainly to pseudobrookite. The spectrum now shows predominantly pseudobrookite lines 3 and 4.

(f) Ilmenite specimen heated at 650°C.

Two well resolved absorption lines, 3 and 4, are shown in this spectrum (Figure 6.11), indicating that oxidation of ilmenite is approaching completion. The ilmenite absorption line 2 has now reduced to a small and unresolved line. The pseudobrookite line 3 has increased while there is no significant change in free hematite absorption at -1.0 mm/s.

(g) Ilmenite specimen heated at 700°C.

The ilmenite content in the specimen heated at this temperature seems to be nearly completely oxidised. Very little trace of ilmenite, if any, can be detected. The spectrum (Figure 6.12) shows two well resolved pseudobrookite absorption lines, 3 and 4, of equal intensity at the -0.15 mm/s and 0.43 mm/s positions respectively. Absorption line 1 is reclassified as absorption line 4 because there is very little trace of ilmenite

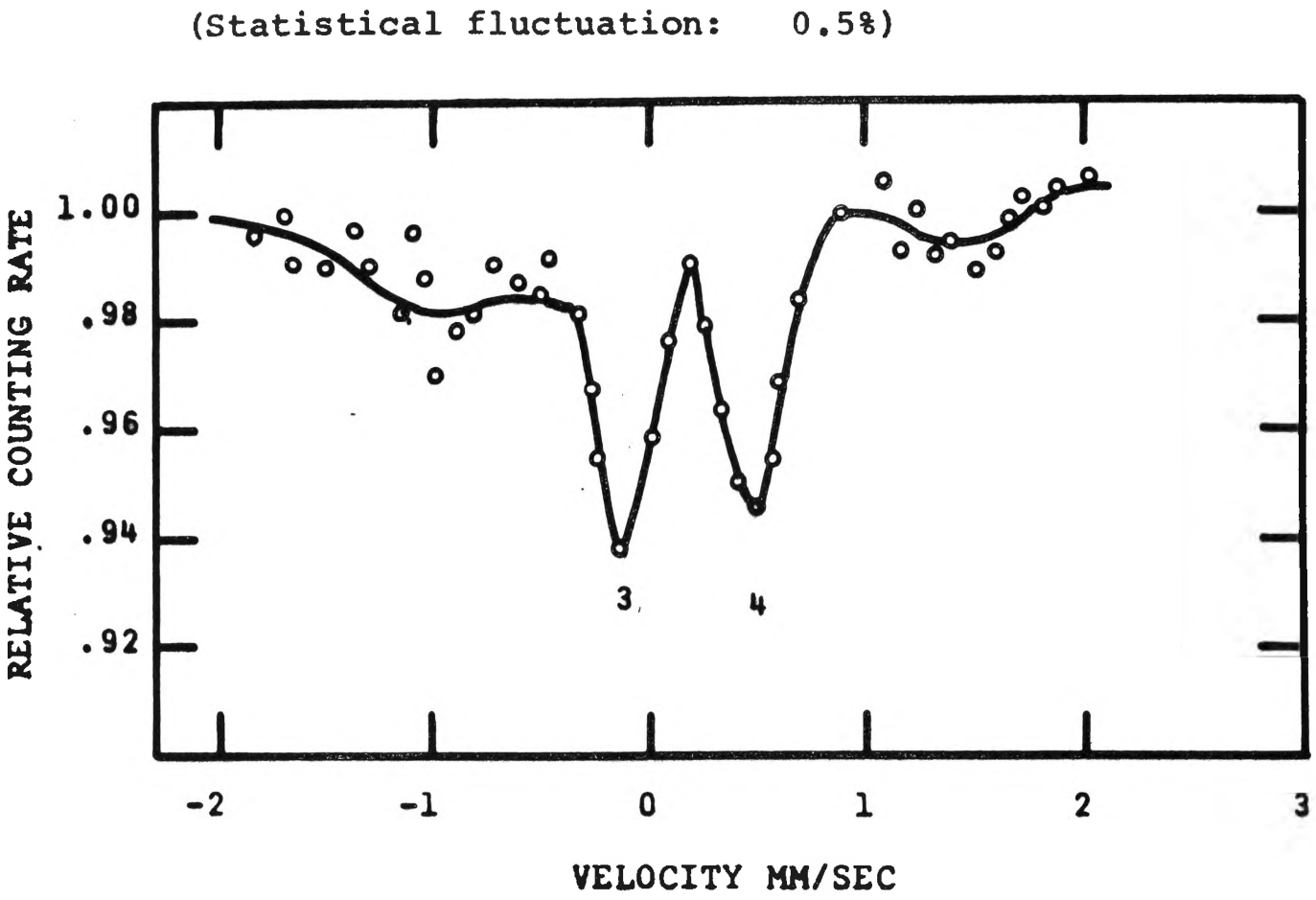


FIGURE 6.13. Mössbauer spectrum of a crushed ilmenite specimen which has been heated at 750°C for one hour.

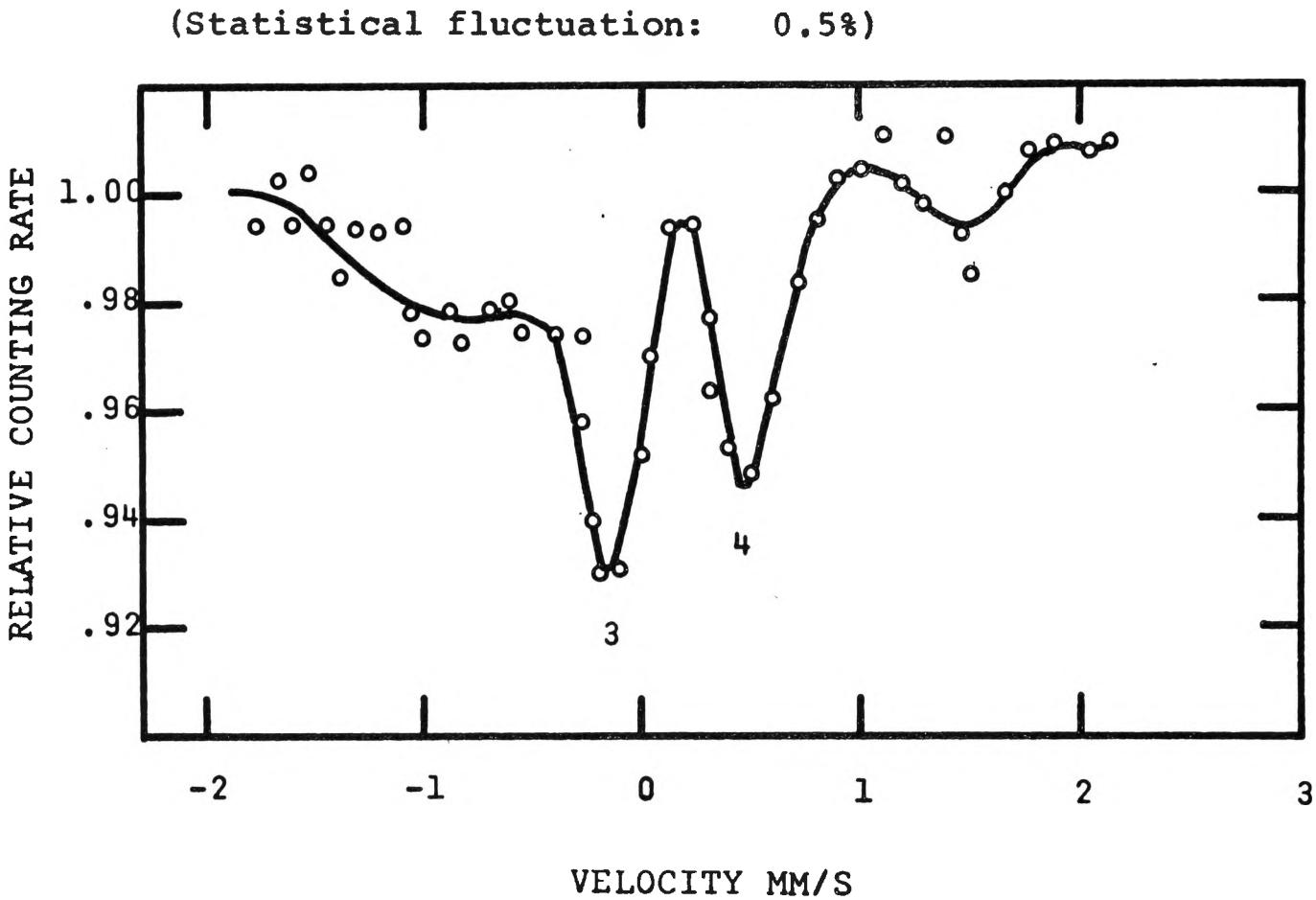


FIGURE 6.14. Mössbauer spectrum of a crushed ilmenite specimen which has been heated at 800°C for one hour.

and its position at 0.43 mm/s is significantly different from 0.5 mm/s position of absorption line 1. There is an indication of free hematite absorption at the 1.5 mm/s position.

(h) Ilmenite specimen heated at 750°C.

The spectrum (Figure 6.13) of this specimen shows two well resolved but unequal intensity lines of pseudo-brookite. Absorption line 3 is slightly higher in intensity than absorption line 4. This may be due to the influence of the free hematite absorption line at -1.0 mm/s. The hematite absorption in this spectrum is much higher than in the previous one. The absorption intensity is estimated to be about 2 per cent.

(i) Ilmenite specimen heated at 800°C.

The absorption intensity of free hematite has increased slightly to more than 2 per cent. The absorption intensity of line 3 has increased due to the influence of the broad absorption line at -1.0 mm/s.

(j) Ilmenite specimen heated at 850°C.

The absorption intensity of free hematite is

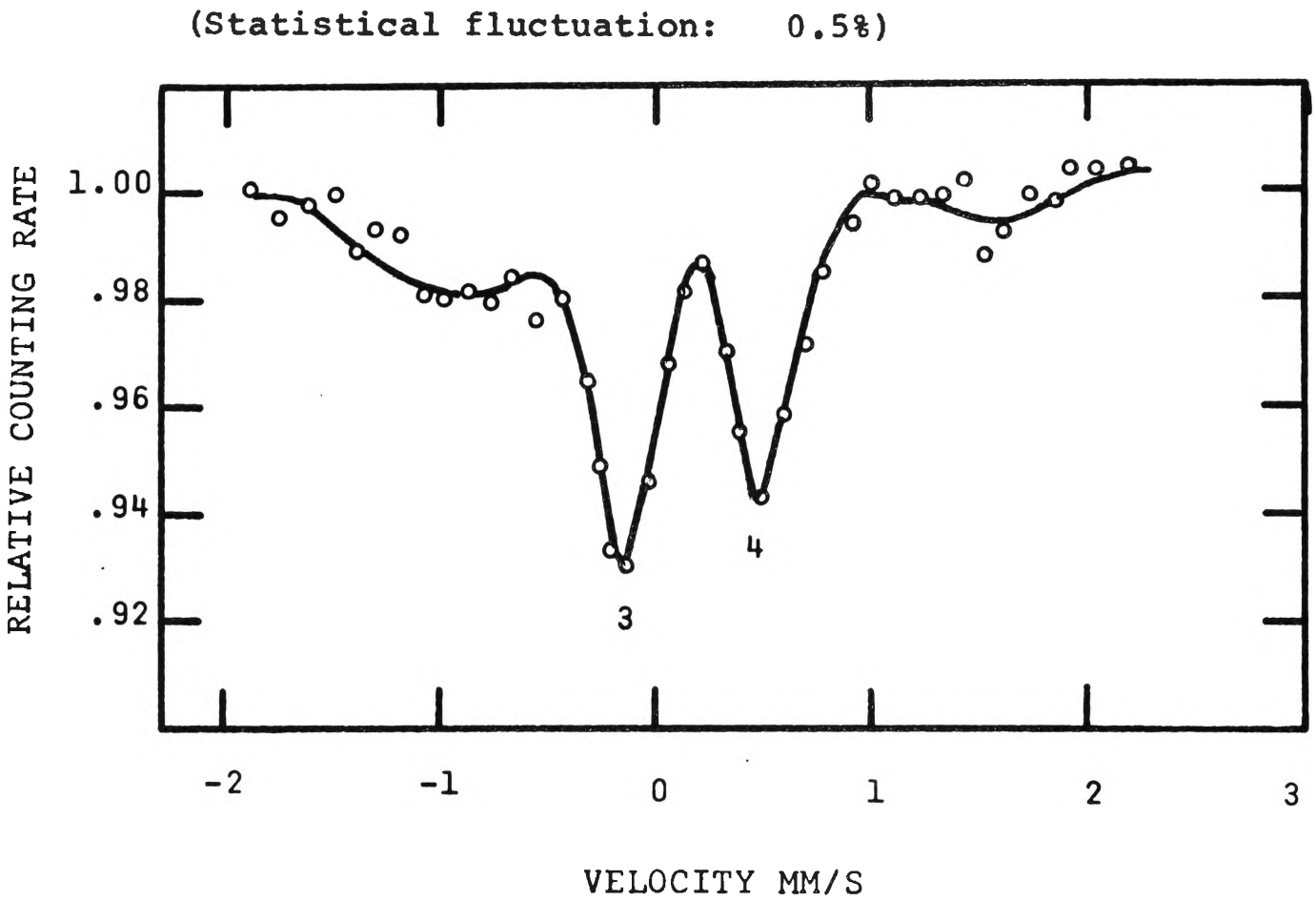


FIGURE 6.15. Mössbauer spectrum of a crushed ilmenite specimen which has been heated at 850°C for one hour.

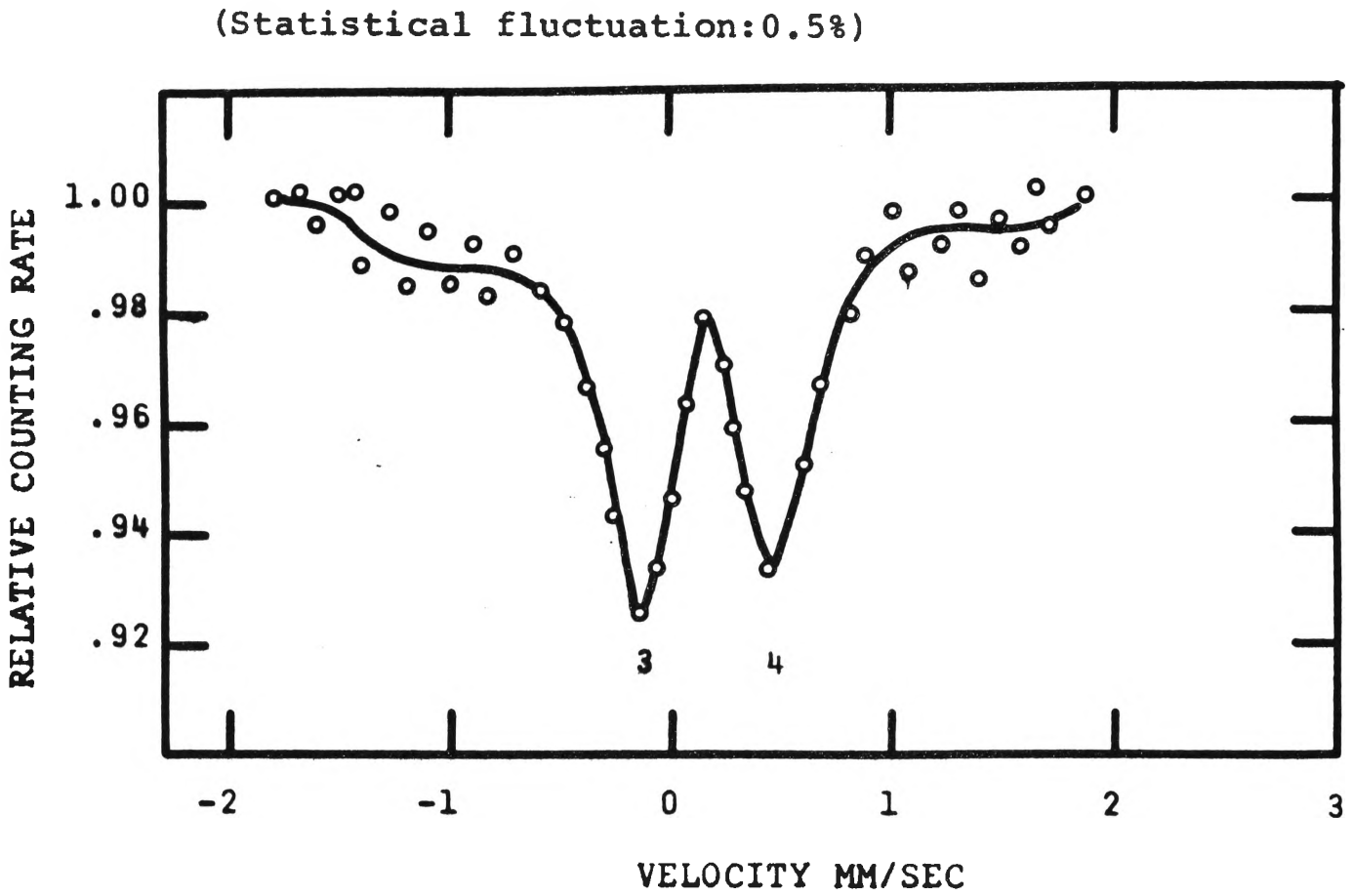


FIGURE 6.16. Mössbauer spectrum of a crushed ilmenite specimen which has been heated at 900°C for one hour.

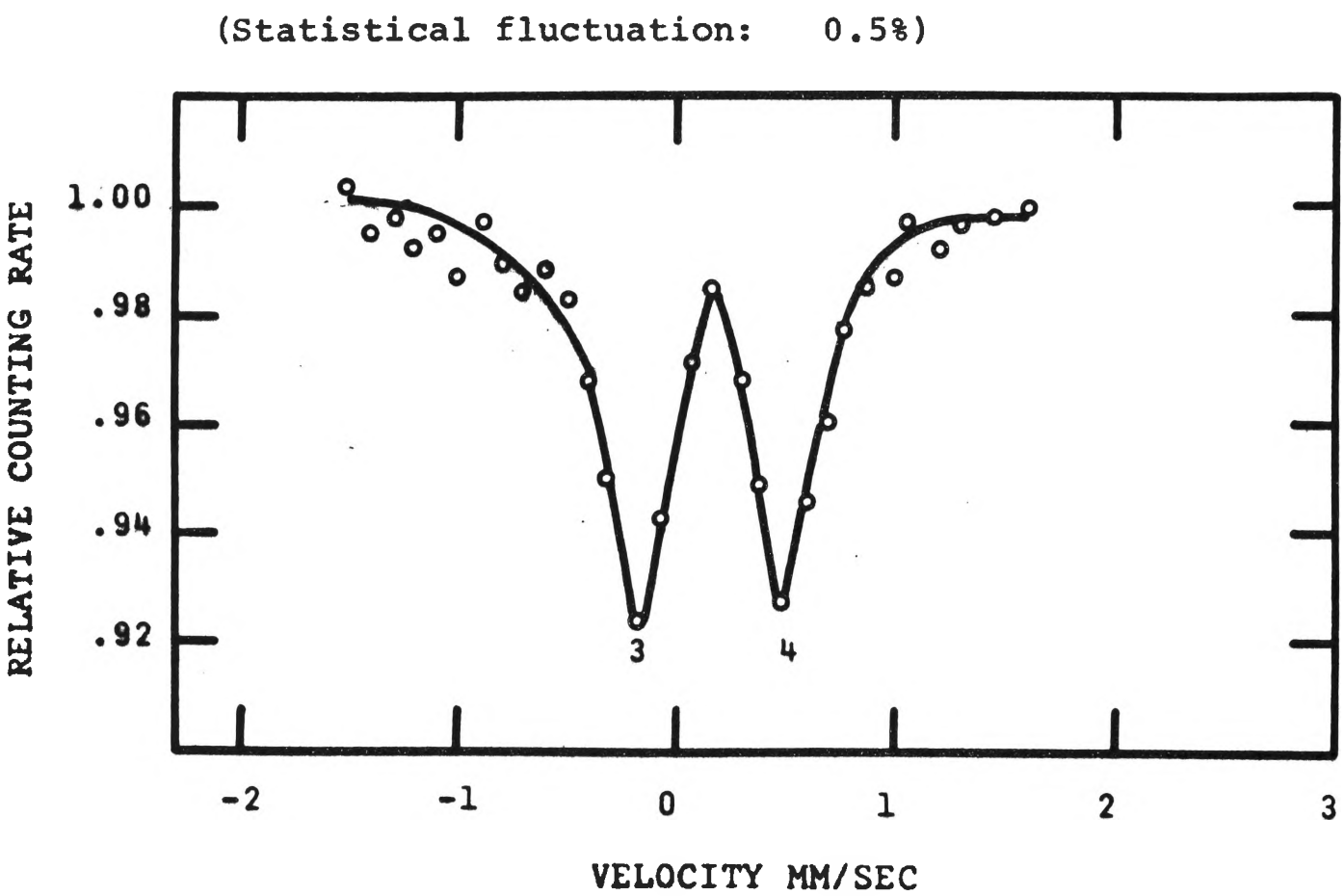


FIGURE 6.17. Mössbauer spectrum of a crushed ilmenite specimen which has been heated at 1000°C for one hour.

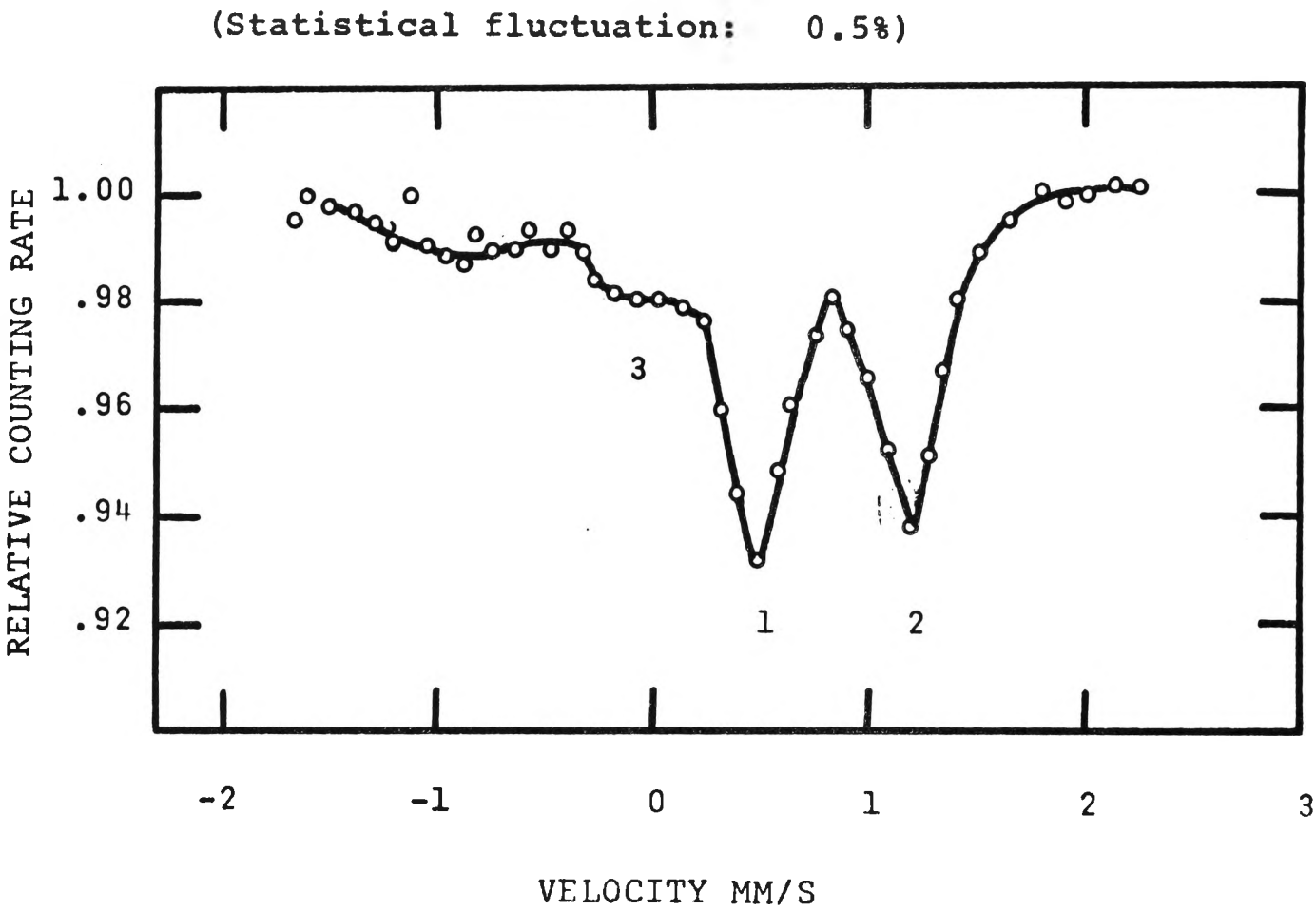


FIGURE 6.18. Mössbauer spectrum of an uncrushed ilmenite specimen which has been heated at 500°C for one hour.

shown to be reduced slightly, indicating that oxidation at this temperature produces less free hematite in the specimen. However, the absorption intensity of lines 3 and 4 has increased.

(k) and (l) Ilmenite specimens heated at 900°C and 1000°C.

Spectra of specimens heated at these temperatures are similar to each other. They show a further reduction of free hematite absorption intensity. The absorption intensity of lines 3 and 4 is about 8 per cent.

## (6.4) Mössbauer Spectra of Specimens Oxidised while of Natural Grain Size

(a) Ilmenite specimen heated at temperature between 100°C and 500°C.

Spectra of these specimens (Figure 6.18) are similar to the unoxidised sample with two well resolved absorption lines 1 and 2 of ilmenite. No noticeable increase in absorption line 3 has occurred. The specimen remains predominantly ilmenite in content.

(b) Ilmenite specimen heated at 550°C.

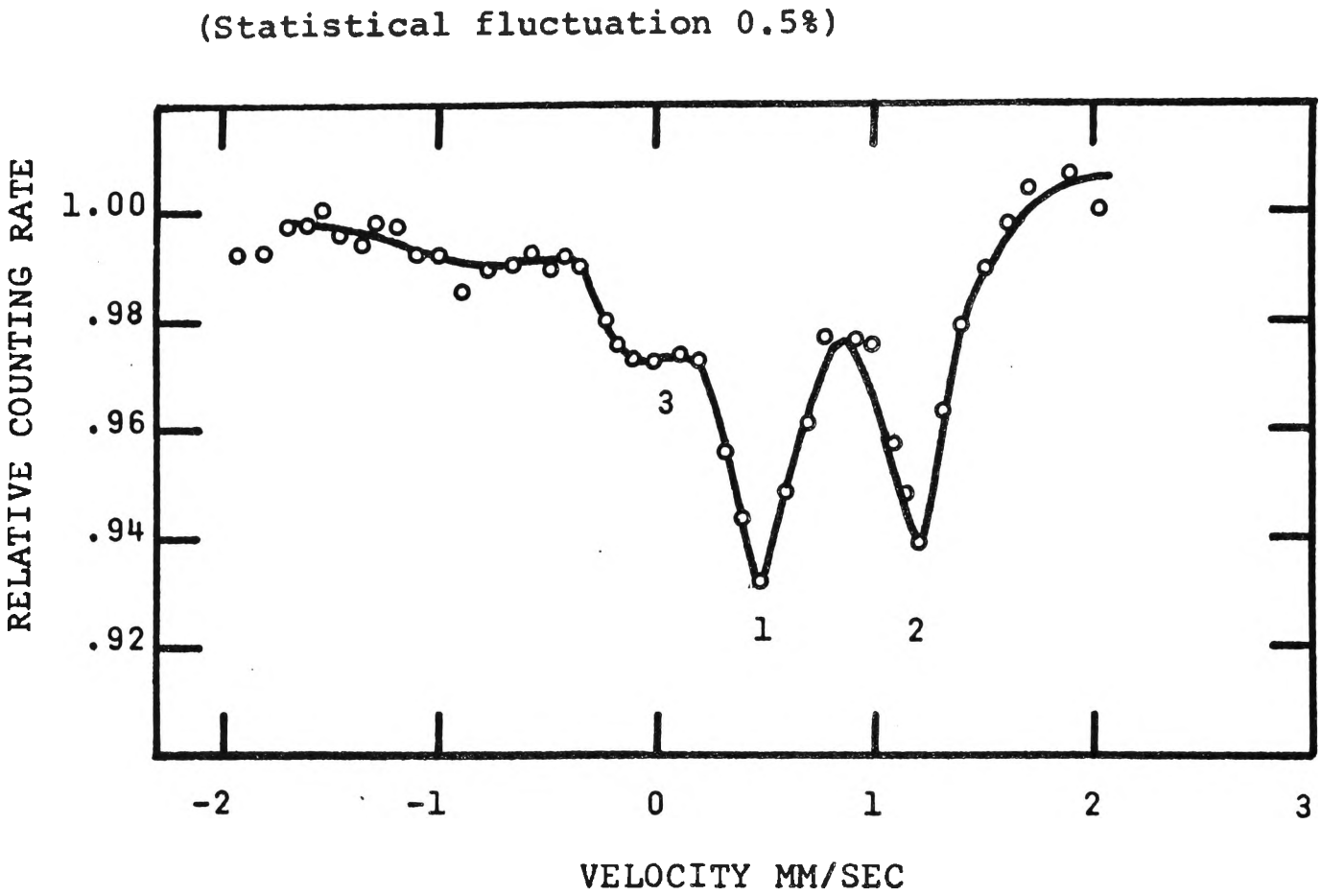


FIGURE 6.19. Mössbauer spectrum of an uncrushed ilmenite specimen which has been heated at 550°C for one hour.

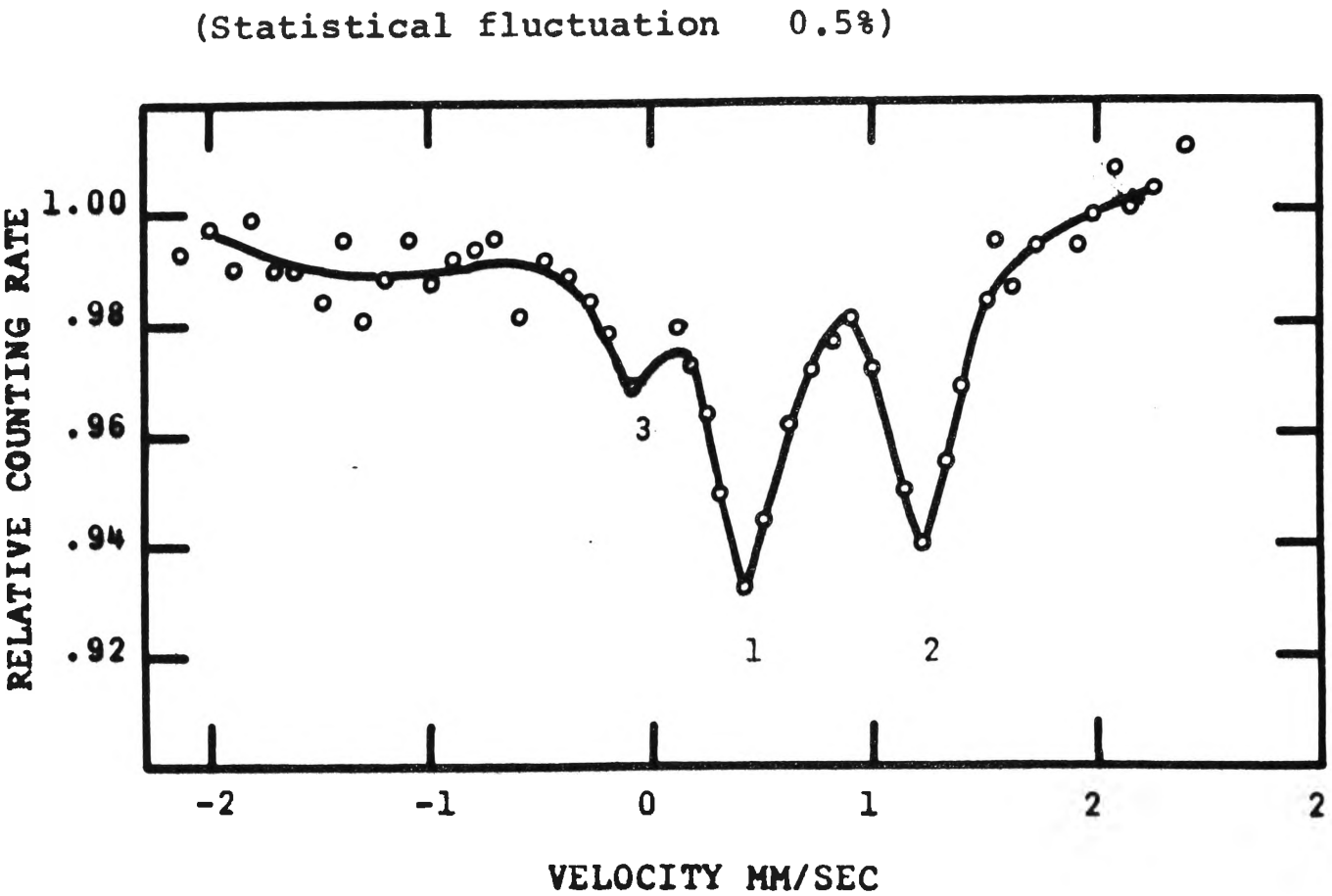


FIGURE 6.20. Mössbauer spectrum of an uncrushed ilmenite specimen which has been heated at 600°C for one hour.

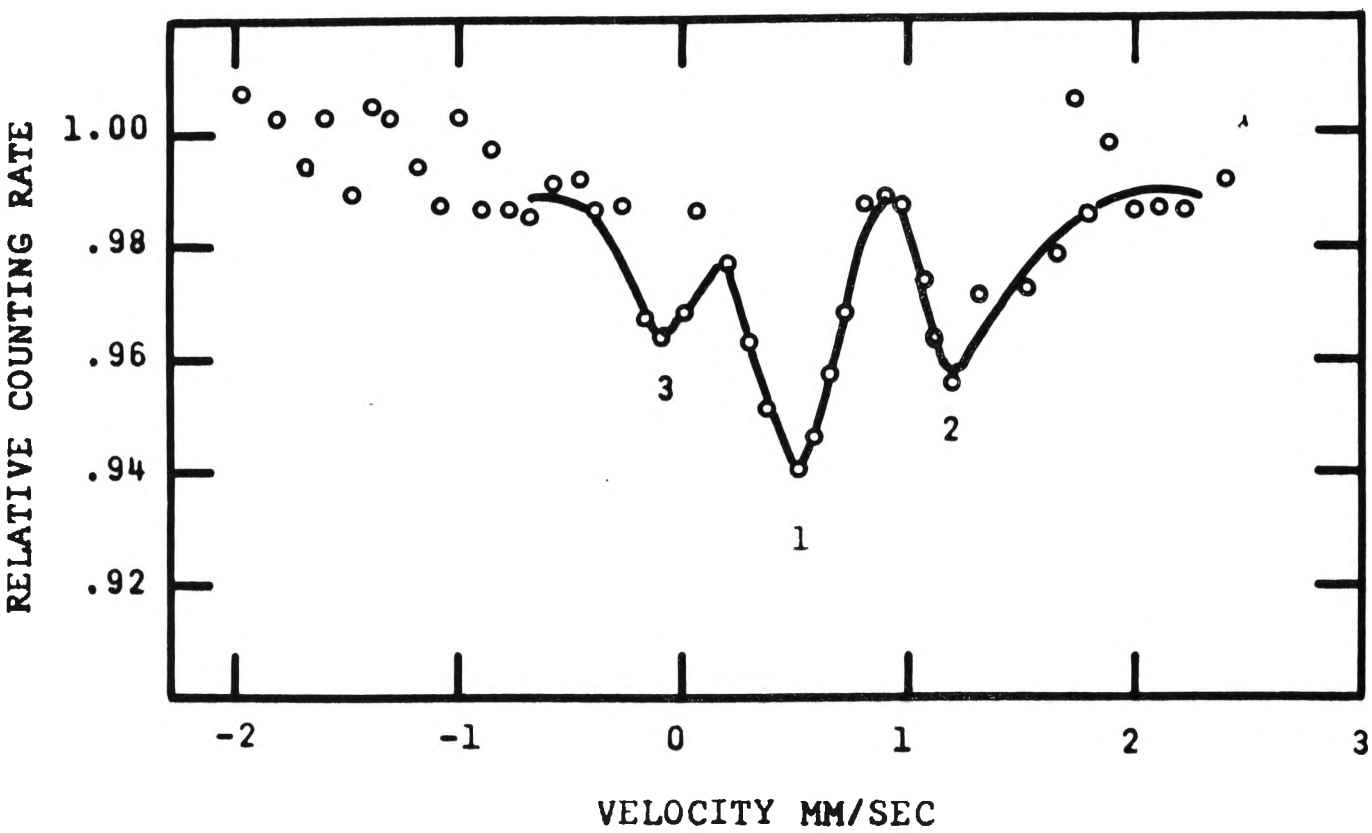


FIGURE 6.21. Mössbauer spectrum of an uncrushed ilmenite specimen which has been heated at 650°C for one hour.

The spectrum (Figure 6.19) of this specimen shows a slight increase in the intensity of absorption line 3. There is also an indication of free hematite absorption at -1.0 mm/s.

(c) Ilmenite specimen heated at 600°C.

The spectrum (Figure 6.20) of this specimen shows that it is still predominantly ilmenite in content, with two well resolved ilmenite absorption lines 1 and 2. Absorption line 3 has slightly increased to 3.5 per cent, indicating a small increase in $Fe^{3+}$ ions. A noticeable increase in the counting fluctuation in the -1.0 mm/s and 1.5 mm/s regions signifies an increase in free hematite content.

(d) Ilmenite specimen heated at 650°C.

Absorption lines 1 and 2 in this spectrum (Figure 6.21) are still resolved but are broadened and their intensities are 6 per cent and 4.5 per cent respectively.

Absorption line 3 has further increased to nearly 4 per cent in intensity. The fluctuations in the -1 mm/s and 1.5 mm/s regions have become larger.

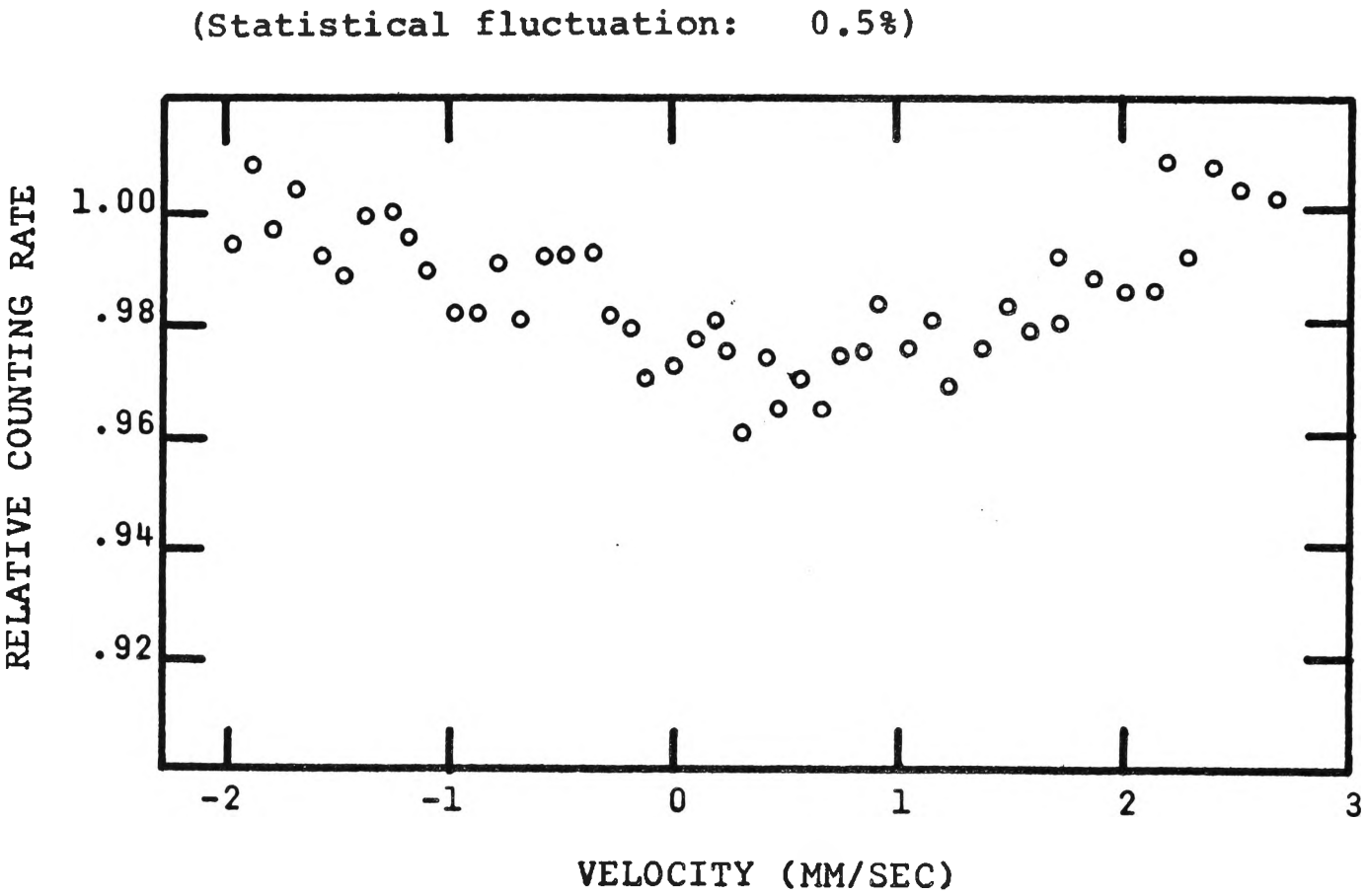


FIGURE 6.22. Mössbauer spectrum of an uncrushed ilmenite specimen which has been heated at 700°C for one hour.

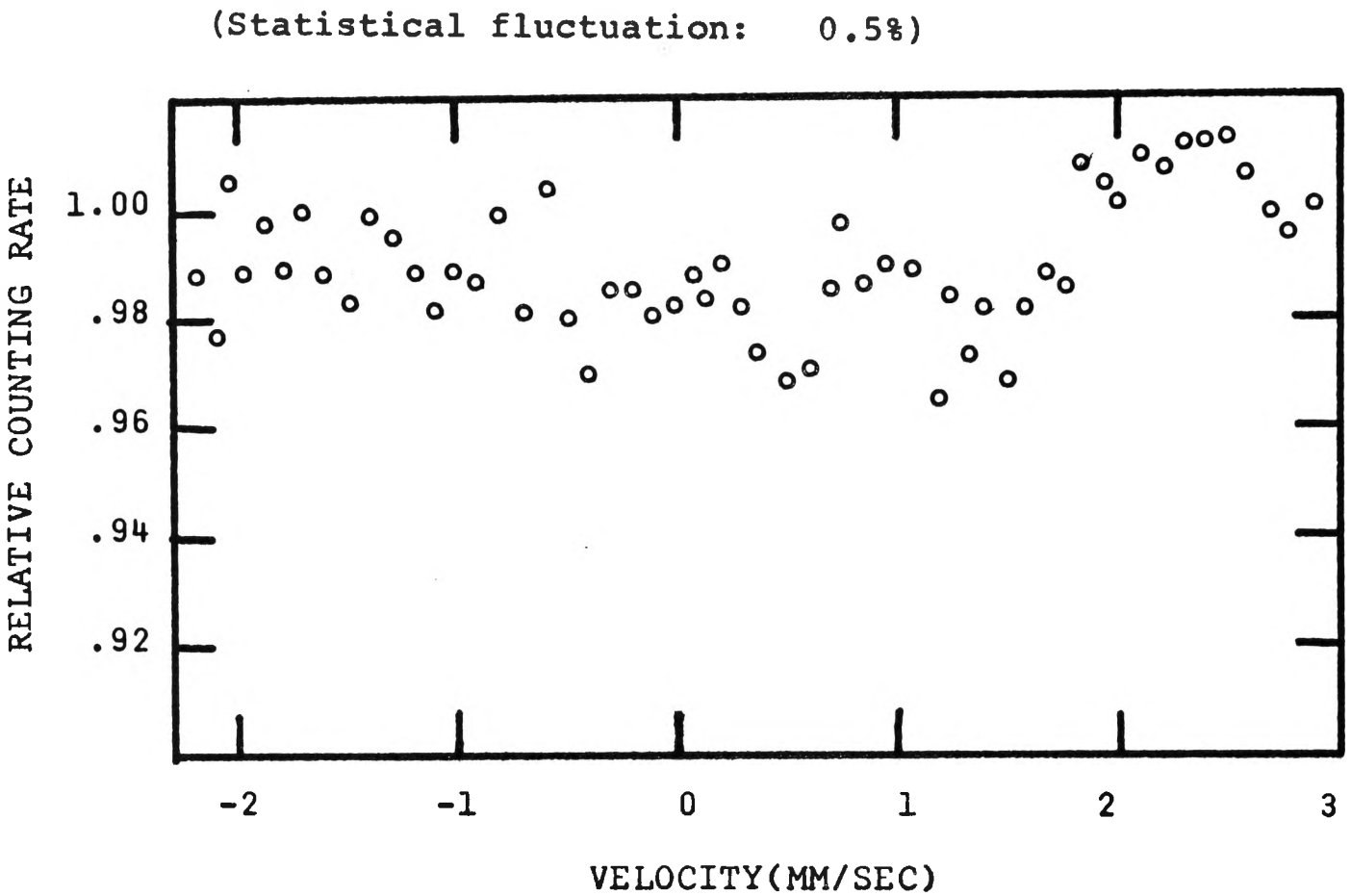


FIGURE 6.23. Mössbauer spectrum of an uncrushed ilmenite specimen which has been heated at 750°C for one hour.

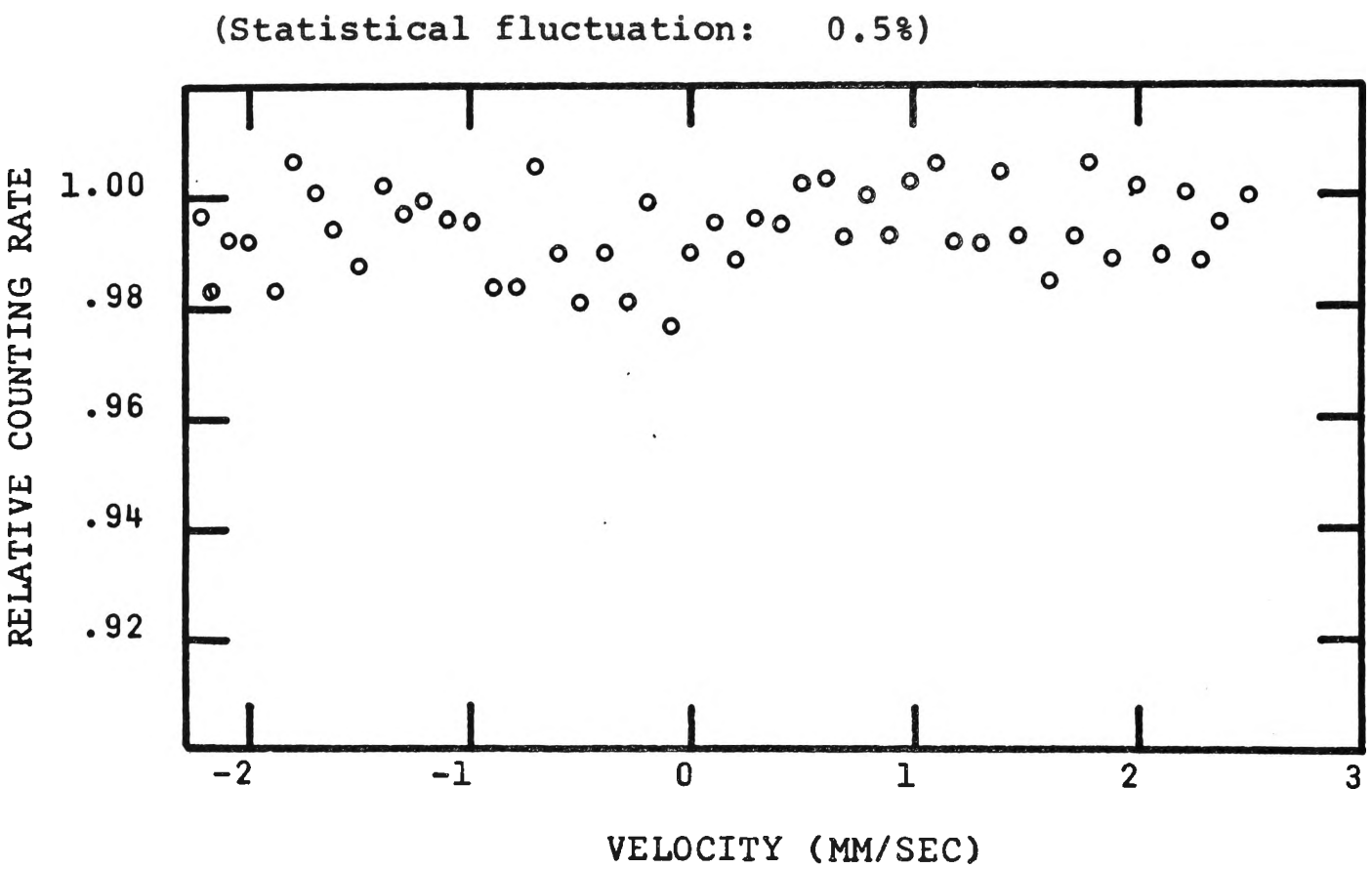


FIGURE 6.24. Mössbauer spectrum of an uncrushed ilmenite specimen which has been heated at 800°C for one hour.

(e) Ilmenite specimen heated at 700°C.

No resolved absorption lines are shown in this spectrum (Figure 6.22). A generally broadened absorption of low intensity is observed. The central region of the spectrum near the 0.5 mm/s position increases to about 4 per cent in intensity, indicating that ilmenite is still present in the specimen.

(f) Ilmenite specimen heated at 750°C.

The absorption spectrum (Figure 6.23) of this specimen shows a broadened absorption line similar to the previous specimen. The absorption intensity is about 3 per cent at the lowest point.

(g) Ilmenite specimen heated at 800°C.

The absorption spectrum (Figure 6.24) is similar to the previous one but the general absorption intensity has reduced to less than 3 per cent.

(h) Ilmenite specimen heated at 850°C.

A broadened absorption line similar to previous specimens is shown in this spectrum (Figure 6.25). However,

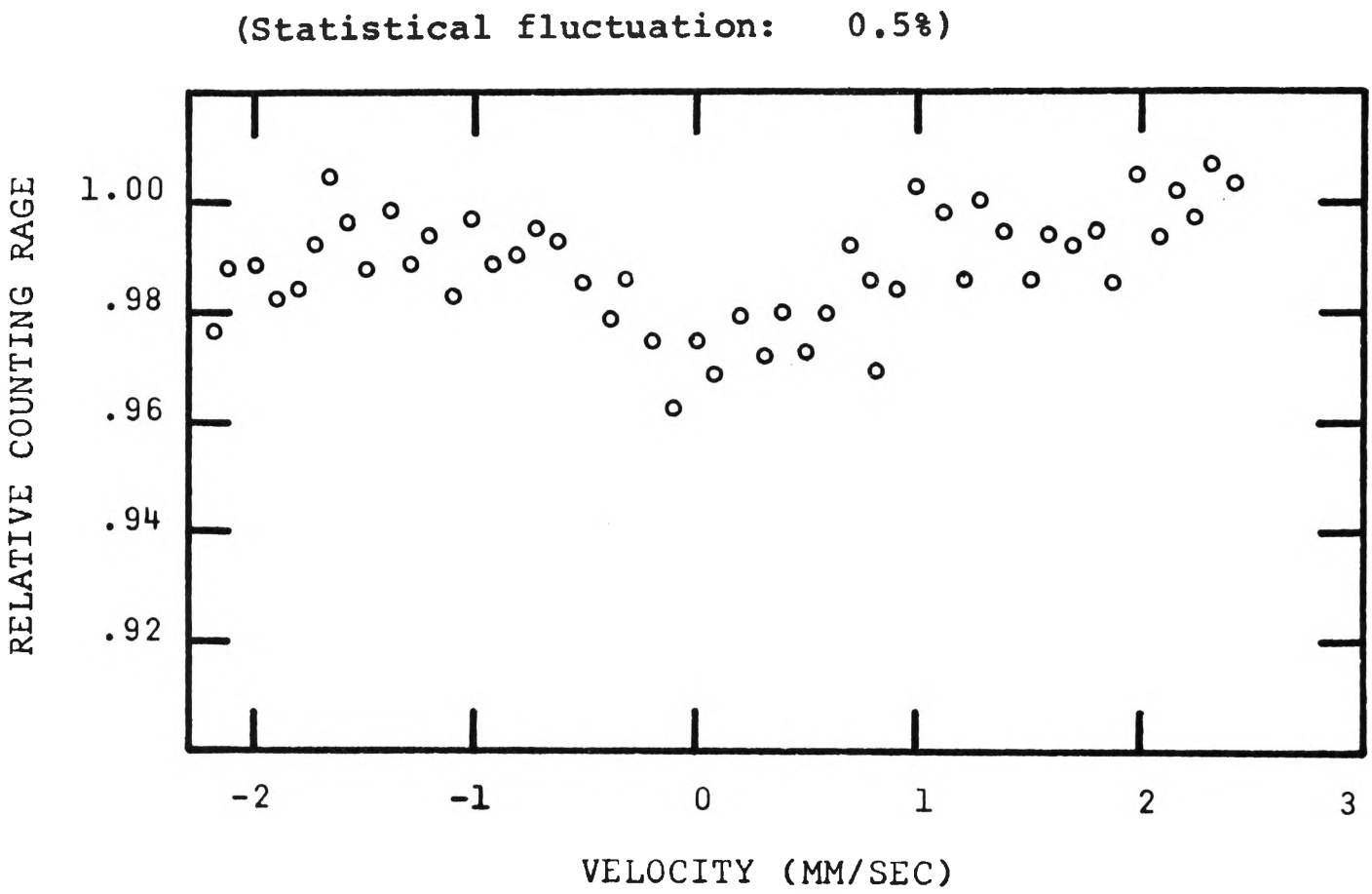


FIGURE 6.25. Mössbauer spectrum of an uncrushed ilmenite specimen which has been heated at 850°C for one hour.

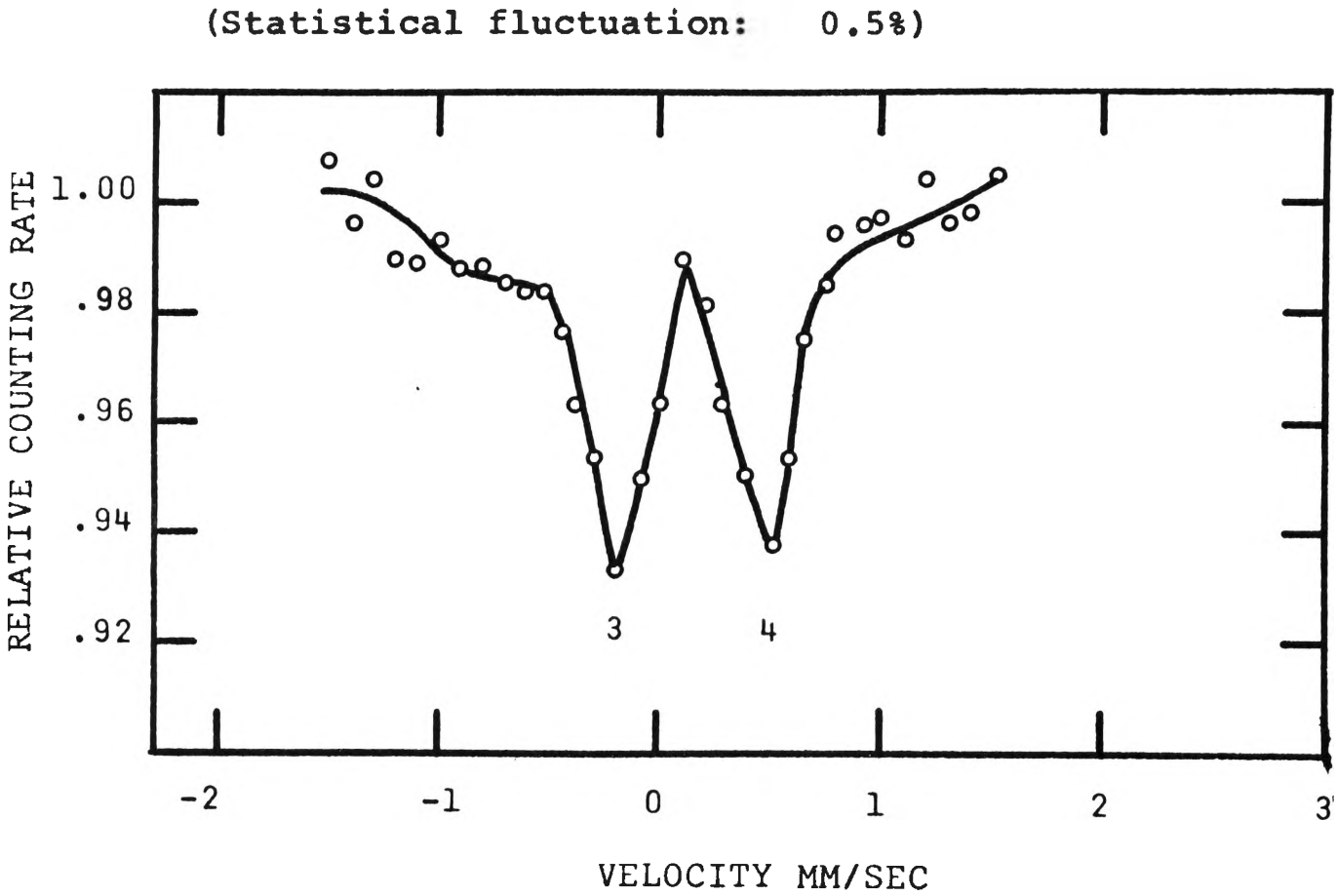


FIGURE 6.26. Mössbauer spectrum of an uncrushed ilmenite specimen which has been heated at 900°C for one hour.

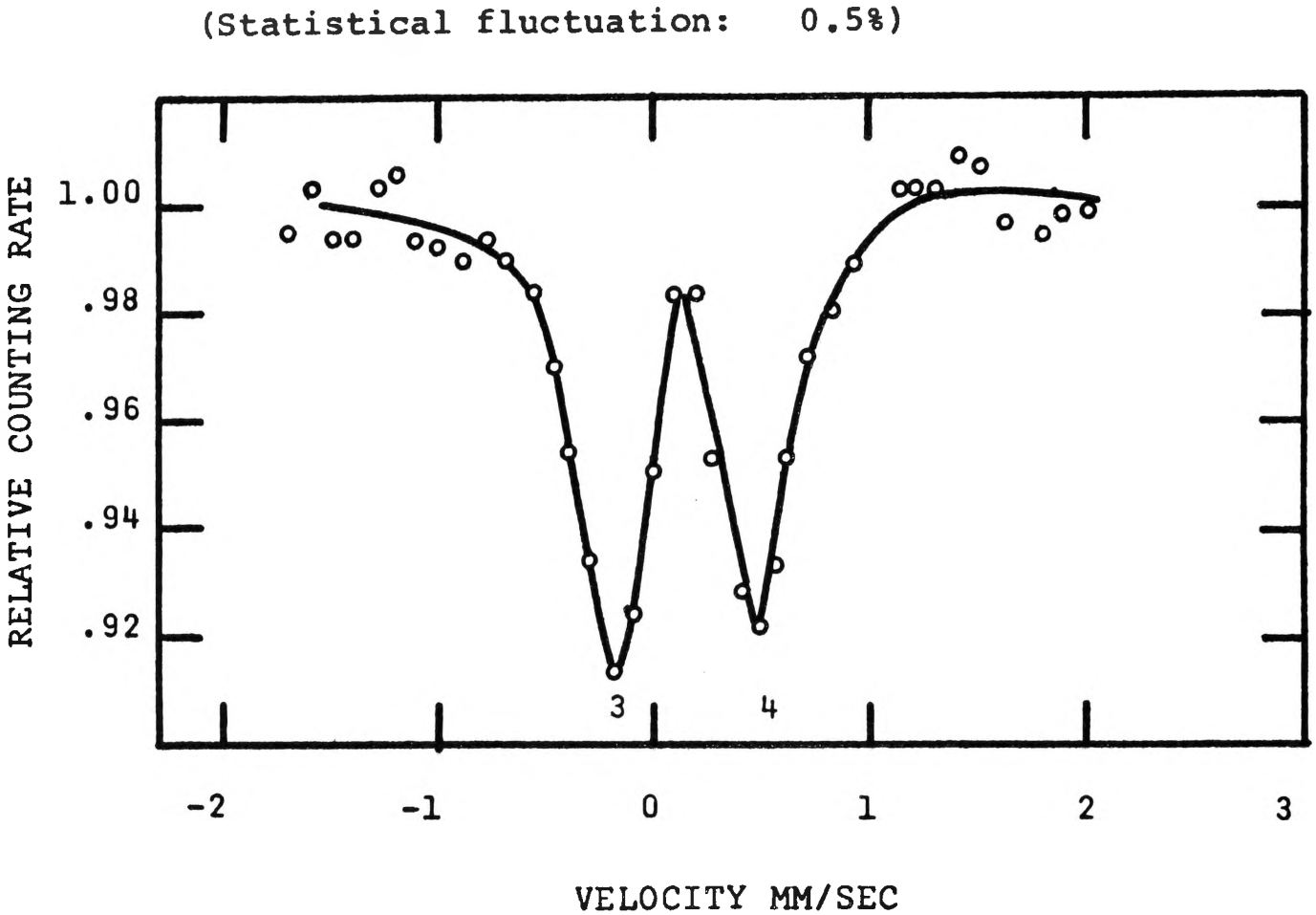


FIGURE 6.27. Mössbauer spectrum of an uncrushed ilmenite specimen which has been heated at 950°C for one hour.

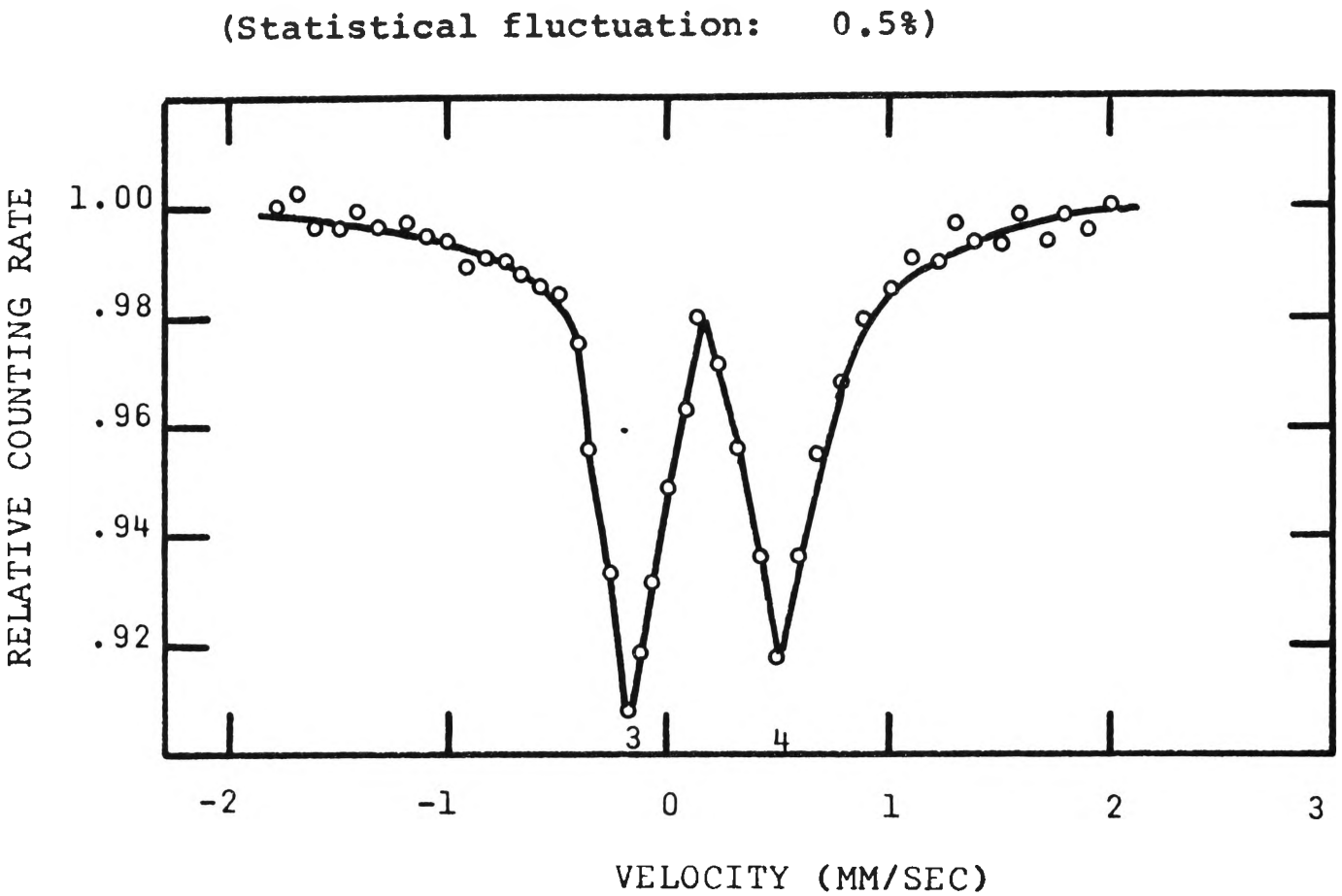


FIGURE 6.28. Mössbauer spectrum of an uncrushed ilmenite specimen which has been heated at 1000°C.

the most intense absorption region has shifted to between 0 mm/s and 5 mm/s. This may be an indication that pseudobrookite in the specimen has increased.

(i) Ilmenite specimen heated at 900°C.

The absorption spectrum (Figure 6.26) is markedly different to the broad unresolved spectra of specimens heated at temperatures between 700°C and 850°C. Two well resolved lines of pseudobrookite 3 and 4 have appeared at the -0.2 mm/s and 0.45 mm/s positions with an absorption intensity of about 7 per cent, linewidths of 0.4 mm/s and isomer shift of 0.13 mm/s. There is very little trace of ilmenite absorption, but free hematite absorption is indicated at -1.0 mm/s position.

(j) Ilmenite specimens heated at 950°C and 1000°C.

Absorption spectra of specimens (Figures 6.27 and 6.28) heated at 950°C and 1000°C are similar to each other. The absorption line intensities are more than 8 per cent. Absorption lines of free hematite at -1 mm/s and 1.5 mm/s are lower in intensity.

TABLE 6.3

Changes in intensities of absorption lines in the spectra of the second series with respect to heating temperature.

| Temperature | Absorption Depth (%) | | | |
|---|---|---|---|---|
| | line 1 | line 2 | line 3 | line 4 |
| 100-350 | 7 | 6.5 | 2 | |
| 400 | 7 | 6 | 3 | |
| 500 | 6 | 5 | 3 | |
| 550 | 4 | 3.5 | 3.5 | |
| 600 | 5 | 2 | 3.5 | |
| 650 | | 1.5 | 4.5 | 5 |
| 700 | | | 5.5 | 5.5 |
| 750 | | | 6.5 | 6 |
| 800 | | | 7 | 6 |
| 850 | | | 7 | 6 |
| 900 | | | 7.5 | 7 |
| 1000 | | | 7.5 | 7 |

Absorption line 1 is due to $Fe^{2+}$ ions ($FeTiO_3$) and $Fe^{3+}$ ions ($Fe_2TiO_5$ and $\alpha Fe_2O_3$).

Absorption line 2 is due to $Fe^{2+}$ ions ($FeTiO_3$)

Absorption line 3 is due to $Fe^{3+}$ ions ($Fe_2TiO_5$ and $\alpha Fe_2O_3$).

Absorption line 4 is mainly produced by $Fe^{3+}$ ions ($Fe_2TiO_5$).

TABLE 6.4

Changes in intensities of absorption lines the spectra of the third series with respect to the heating temperature.

| Temperature | Absorption Depth (%) | | | |
|---|---|---|---|---|
| | line 1 | line 2 | line 3 | line 4 |
| 100-500 | 7 | 6.2 | 2 | |
| 550 | 7 | 6 | 2.5 | |
| 600 | 7 | 6 | 3 | |
| 650 | 6 | 4.5 | 3.5 | |
| 700 | - | - | - | |
| 750 | - | - | - | |
| 800 | - | - | - | |
| 850 | - | - | - | |
| 900 | | | 7 | 6.5 |
| 950 | | | 8.5 | 8 |
| 1000 | | | 9 | 8.5 |

Absorption line 1 is due to $Fe^{2}$ ions ($FeTiO_3$) and $Fe^{3+}$ ions ($Fe_2TiO_5$ and $\alpha Fe_2O_3$).

Absorption line 2 is due to $Fe^{2+}$ ions ($FeTiO_3$)

Absorption line 3 is due to $Fe^{3+}$ ions ($Fe_2TiO_5$ and $\alpha Fe_2O_3$)

Absorption line 4 is due to $Fe^{3+}$ ions ($Fe_2TiO_5$).

## (6.5) The Effect of Sample Grain Size on the Oxidation of Natural Ilmenite

(a) In the case of the series of specimens which were crushed before oxidation, the degree of oxidation is clearly revealed by the absorption spectra of these specimens, as shown in Figures 6.5 to 6.17. It can be deduced from the spectra that heat treatment of specimens at temperatures below 400°C induces a negligible oxidation effect and the specimens remain relatively unchanged. This is in agreement with the results of Parry (1955) and Westcott (1966). Spectra of these specimens are similar to the spectrum of unoxidised natural ilmenite (Figure 6.2) which consists of two well resolved absorption lines (labelled 1 and 2) of $FeTiO_3$ in the paramagnetic state with an isomer shift, $\delta$, of 0.85±0.01 mm/s and quadrupole splitting, $\varepsilon$ of 0.35±0.01 mm/s. In addition, there is a small satellite (labelled 3) adjacent to the absorption line 1. It is one of the absorption lines of $Fe^{3+}$ ions. The absorption line 1 at 0.5 mm/s appears to be more intense than the absorption line 2 at 1.2 mm/s because of the overlapping of $Fe^{3+}$ and $Fe^{2+}$ absorption lines within this region. The linewidths of 1 and 2 are 0.4±0.01 mm/s and 0.35±0.01mm/s respectively

The effect of oxidation is obvious at heating temperatures above 400°C and below 750°C. Mössbauer spectra of these specimens (Figures 6.8 to 6.12) show that the absorption line 3 increases and the absorption line 2 reduces rapidly in intensity as the oxidation temperature increases. This means that the content of ilmenite decreases as the temperature increases. At oxidation temperatures between 550°C and 650°C the absorption spectra (Figures 6.9, 6.10 and 6.11) show that the absorption line 1 is broadened and has a lower intensity indicating that in this region of the spectrum there are adjacent absorption lines of comparable intensity overlapping each other. These lines are the ilmenite absorption line, the hematite absorption line and possibly the pseudobrookite absorption line, and lines of other iron titanate compounds. Because of low intensity no positive identification of these compounds is possible. The X-ray analysis (Parry 1955) of the specimen which has been heated at 650°C showed the presence of ilmenite and free hematite but no other iron titanate compounds were observed presumably because of the small quantities involved.

Specimens oxidised at temperatures between 750°C and 1000°C show no trace of ilmenite. Absorption spectra of these specimens (Figures 6.13 to 6.17) reveal two well resolved absorption lines (labelled 3 and 4) of pseudobrookite which has an isomer shift, $\delta$, of 0.12±0.01mm/s quadrupole splitting, $\varepsilon$, of 0.32±.01mm/s and linewidth, $\Gamma$, of 0.4±0.01mm/s. These results agree with the X-ray analysis of a fully oxidised sample by Curnow and Parry (1955) who concluded that the final product is $Fe_2O_3.TiO_2$ (pseudobrookite). The intensity of pseudobrookite absorption lines, as shown in Figures 6.16 and 6.17, continues to increase and is higher than those in Figure 6.15 where the conversion of ilmenite to pseudobrookite is shown to be completed. A more detailed dicusssion is given in Section 6.6.

(b) In the natural grain size series of specimens, no significant oxidation effect is observed in the spectra of specimens heated at temperatures between 100°C and 500°C, as shown in Figure 6.18. Above 500°C the oxidation effect begins to reveal itself (Figures 6.19, 6.20 and 6.21) and the content of ilmenite decreases while that of $Fe^{3+}$ ions increases. It was found

(Westcott 1966) that the content of free rutile in the specimen which has been oxidised at 650°C has significantly increased, indicating the oxidation of ilmenite.

Mössbauer spectra (Figures 6.22 to 6.25) of specimens oxidised at temperatures between 700°C and 850°C show only very broad and low intensity absorption. The expected ilmenite and pseudobrookite absorption lines have disappeared. This could be the result of overlapping of many absorption lines. A more detailed discussion is given in Section 6.9. Chemical analysis (Westcott 1966) of the specimen which has been oxidised at 700°C showed that there is 22.8 per cent of hematite and the $Fe^{3+}/Fe^{2+}$ ratio is 0.78 as compared to 17.9 per cent and 0.51 respectively in the unoxidised natural sample. Sharp absorption lines reappear again in the spectrum of a specimen heated at 900°C, as shown in Figure 6.26. No traces of ilmenite are shown in the spectrum which reveals only two well resolved absorption lines of pseudobrookite. Parry (1955) found that oxidation of sample at temperatures above 850°C resulted in the reduction by weight of FeO to 2 per cent from the

initial content of 31.2 per cent. Absorption spectra (Figures 6.27 and 6.28) of specimens heated at 950°C and 1000°C show that the intensity of pseudobrookite absorption lines continue to increase even after complete oxidation of ilmenite at 900°C. These spectra are similar to those shown in Figures 6.16 and 6.17 of the second series.

It can be concluded from these two series of experiments that the pre-crushed specimens, because of smaller grain size and therefore larger surface area to mass ratio, are oxidised to a greater extent than the uncrushed specimen at the same temperature.

The identification of the main product of a fully oxidised ilmenite sample as pseudobrookite agrees with the results obtained by Curnow and Parry (1955) and Uyeda (1956) but contradicts that of Westcott (1966) who proposed an iron titanate $Fe_4(TiO_4)_3$. No Mössbauer spectrum of this compound has been obtained but it is unlikely that it would be confused with that of pseudobrookite.

## (6.6) The Increase of Free Hematite and Free Rutile from the Oxidation of Natural Ilmenite

The absorption spectra of both series of specimens indicate a gradual increase of free hematite content as the oxidation temperature increases. Free hematite which is antiferromagnetic at room temperature has six absorption lines (Figure 5.2) and is different from hematite in the ilmenite-hematite solid solution which has only two absorption lines due to quadrupole splitting, (Shirane et al, 1962b). Two of the six absorption lines of free hematite are shown in the spectrum at about -1 mm/s and 1.6 mm/s positions (referred to the copper matrix source used in the present investigation). The absorption intensity of these lines is very low and could be mistaken for counting fluctuations. For crushed specimens oxidised at temperatures between 750°C and 850°C the free hematite content is at its maximum with an absorption depth approximately 2 per cent. A more accurate estimation of intensity cannot be given because of the counting fluctuations in this low intensity region. An attempt

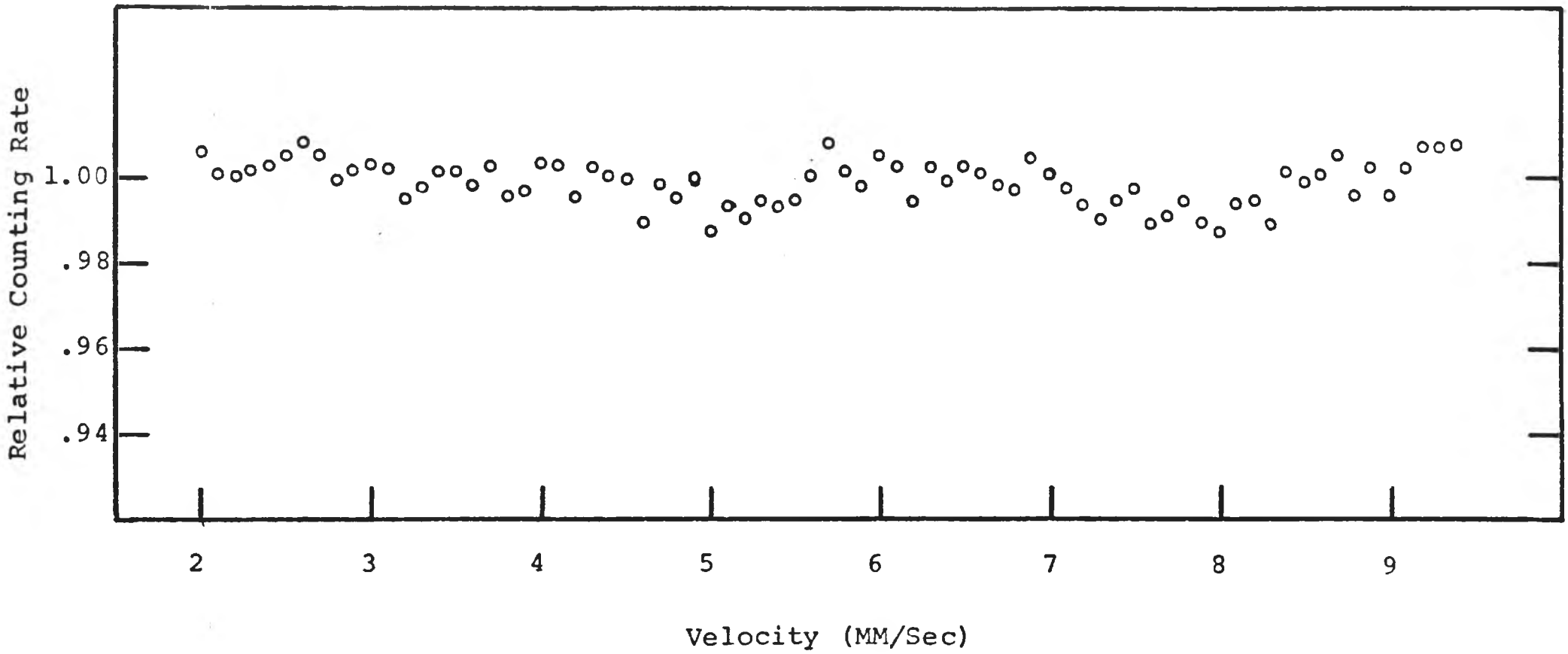


FIGURE 6.13a. Mössbauer Spectrum of a Crushed Ilmenite specimen which has been heated at 750°C for one hour.

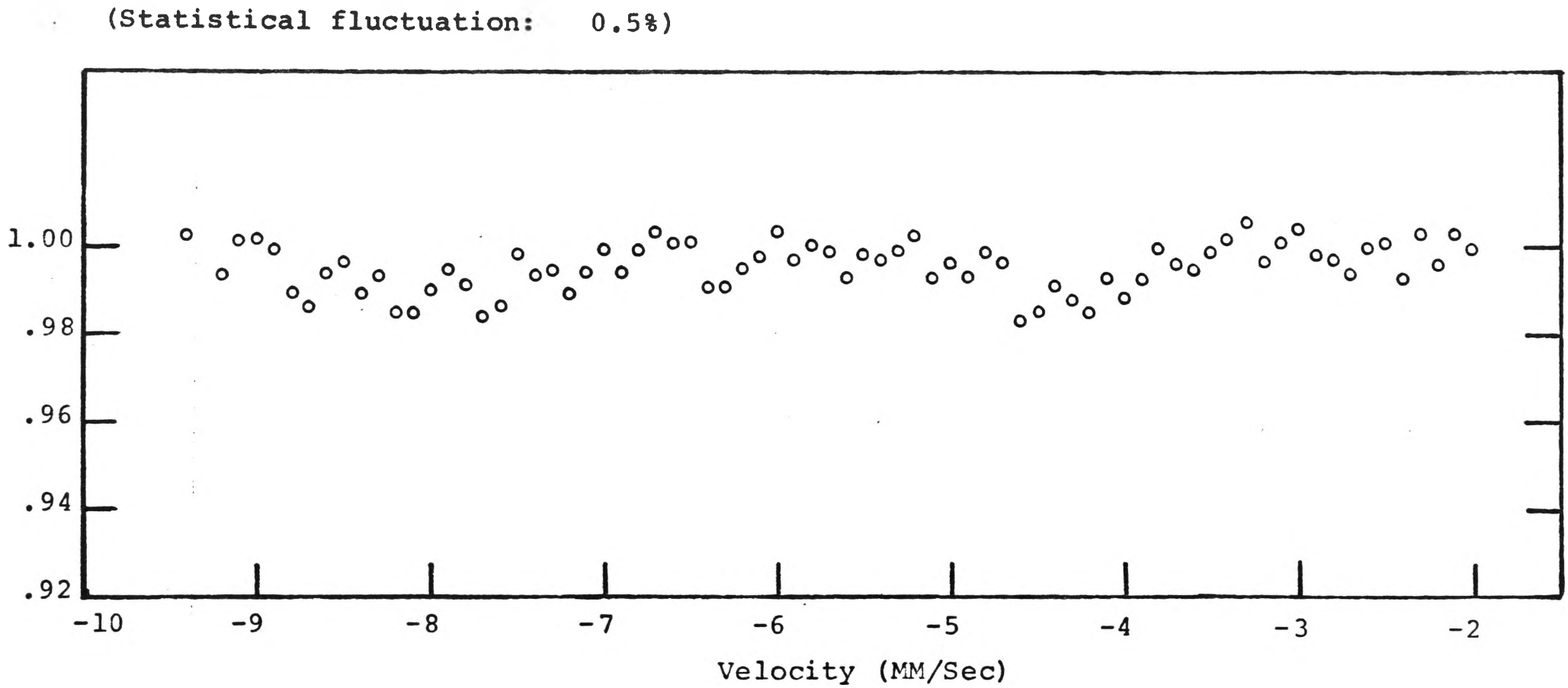


FIGURE 6.13b. Mössbauer Spectrum of a Crushed Ilmenite Specimen which has been heated at 750°C for one hour

was made to observe all six absorption lines of free hematite in the specimen, but because of the low intensity, only very broad absorption lines were detected approximately at -8 mm/s, -4.5 mm/s, 5 mm/s and 8 mm/s, which are approximately the positions of the four outer absorption lines of hematite (Kistner and Sunyar 1960).

The spectrum of the precrushed sample shown in Figure 6.13 shows that the ilmenite is completely converted to pseudobrookite at 750°C. Consequently, $\alpha Fe_2O_3$ in the solid solution is released. The chemical analysis of unoxidised natural ilmenite (Table 6.1) gives a $Fe:TiO_2$ ratio of 1:1.35. Since the final oxidised product, $Fe_2TiO_5$, has an Fe:Ti ratio of 2:1, it can be deduced that a substantial amount of free rutile ($TiO_2$) must also be released in the specimen. However, there is little tendency for $TiO_2$ and $\alpha Fe_2O_3$ to combine and form $Fe_2TiO_5$ at temperatures below 1000°C (Avrahami and Golding, 1969). Consequently, the absorption spectra show the increased presence of free hematite in the specimens. For specimens heated at temperatures in excess of 850°C, the amount of free hematite is noticeably reduced, indicating an increase in the tendency of rutile

and hematite to combine at these higher temperatures. Spectra shown in Figure 6.16 and 6.17 of the second series and figures 6.26 and 6.27 of the third series reveal a large increase in intensity of pseudobrookite absorption lines, a greater increase than that which would be produced by the oxidation of $FeTiO_3$ alone.

The increase of free hematite due to oxidation strengthens the hypothesis that the small absorption line in the spectrum of natural ilmenite (Figure 6.2) belongs to hematite of the solid solution rather than any other compound (Section 6.2).

If, as suggested by Avrahami and Golding (1969), this peak were caused by pseudobrookite which has two absorption lines, one of which is at the 0.45 mm/s position overlapping the ilmenite absorption line at 0.5 mm/s, then the oxidation which converts ilmenite to pseudobrookite should have little influence on the intensity of this overlapped line. However, the results (Figures 6.8 and 6.9) show that the intensity gradually decreases and broadens while at the same time free hematite increases, thus strongly suggesting that the small absorption peak is one of the absorption lines of hematite in an ilmenite-hematite solid solution.

## (6.7) Temperature Dependence of the Ilmenite-Pseudobrookite Conversion

The conversion of ilmenite to pseudobrookite by oxidation as a function of temperature can be estimated from the changes in intensity of their absorption lines. The area of an absorption line represents the relative number of $Fe^{2+}$ or $Fe^{3+}$ ions in a specimen. However, not all the ions of the same valency are from one compound. In an oxidised ilmenite specimen, the $Fe^{3+}$ ions could belong to pseudobrookite or hematite or some other ferric titanate compounds. Complications may arise when absorption lines overlap each other.

A second factor which affects the accuracy of estimation is the low intensity of absorption lines in the natural sample. Generally the absorption intensity does not exceed 8 per cent and it is therefore difficult to determine the area of an absorption line accurately. Mössbauer spectra of specimens heated at temperatures between 700°C and 850°C show only very low intensity absorption because of the overlapping of many absorption lines. Thus, direct estimation of the conversion becomes

impossible. It may be concluded that Mössbauer spectra, though indicating the degree of oxidation as a function of temperature, do not positively identify the oxidation products in the specimens which have been oxidised at temperatures below 700°C for the crushed sample series or below 900°C for the natural grain size series.

Besides the above mentioned difficulties, the accuracy of estimation may also be affected by non-uniformity of a specimen's thickness. Since the specimen is in powder form, the distribution of powder particles over an area of 2.5 cm x 2.5 cm may vary from specimen to specimen, even though each specimen has the same weight. However, this effect is considered to be negligible in the present experiments where thin specimens of thickness 12 mg/cm$^2$ are used and thus little self-absorption occurs.

It is noted that the conversion of ilmenite to pseudobrookite is not continuously observable by X-ray analysis. No pseudobrookite X-ray pattern was observed for samples of natural grain size oxidised at temperatures below 850°C (Parry 1955) or for pre-crushed samples at or below 700°C (Westcott 1966). Mössbauer results of the present

investigation agree with the former but contradict the latter. The Mössbauer spectrum of the pre-crushed specimen which has been oxidised at 700°C shows the definite presence of pseudobrookite, which indicates the oxidation is approaching completion.

Because of the limitations mentioned above, the ilmenite-pseudobrookite conversion graphs can only be regarded as approximate estimates.

(6.7) a. <u>The Ilmenite-Pseudobrookite Conversion Graph of the Crushed-Specimen Series</u>.

In the spectra of specimens oxidised at temperatures below 550°C, the absorption line 1 is mainly contributed by ilmenite with small amount of hematite and, presumably, pseudobrookite. The absorption line 3, as discussed in Section (6.6), includes hematite and pseudobrookite of comparable intensities. The absorption line 2 is that of ilmenite only. Hence the estimates of the relative amounts of ilmenite converted to pseudobrookite by oxidation depend on the reduction rate in intensity of the absorption line 2.

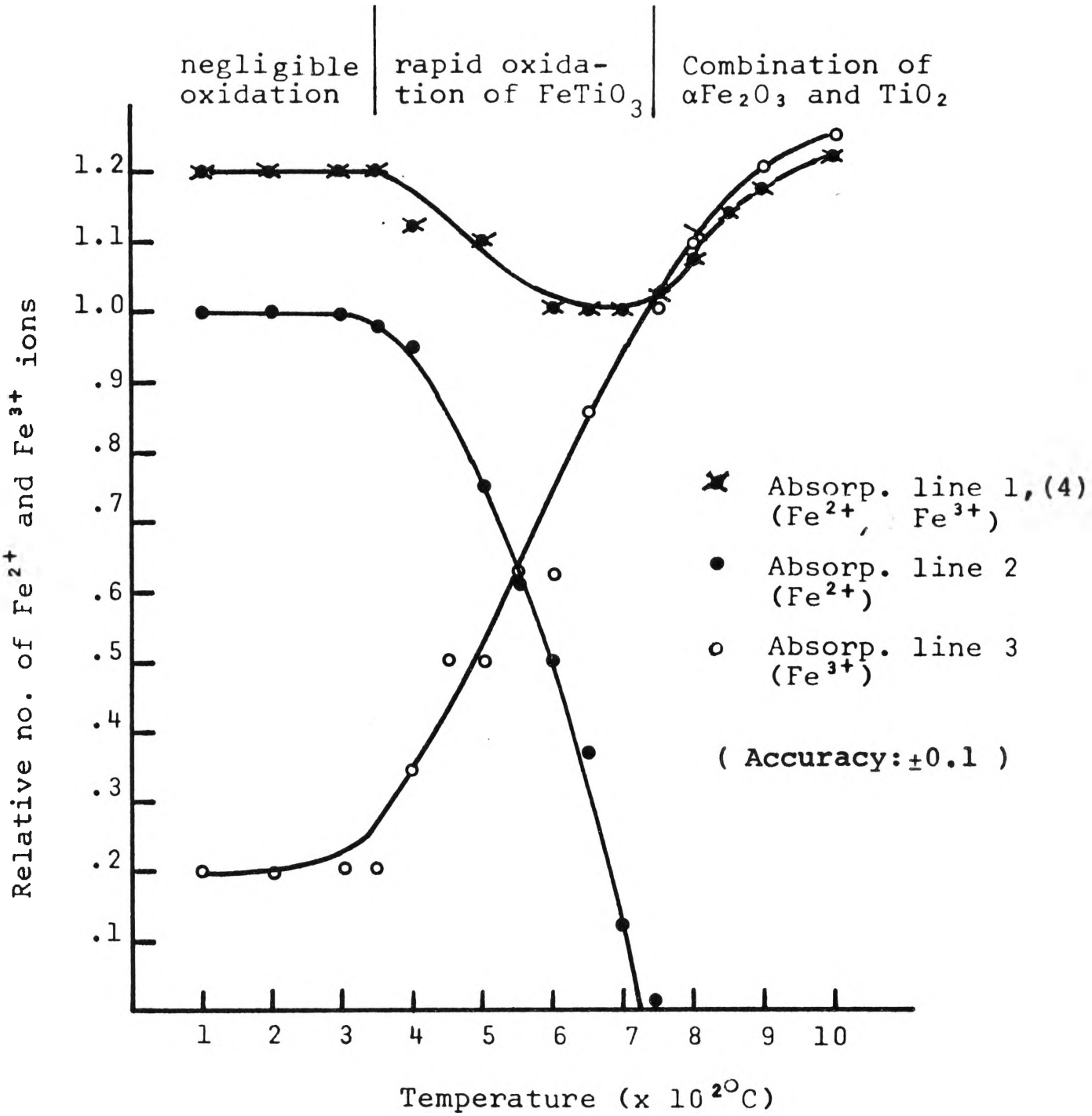


FIGURE 6.29. Ilmenite-pseudobrookite conversion graph of crushed specimen series

In the middle temperature range (600°C - 700°C), the absorption line 4 consists mainly of pseudobrookite with small amounts of hematite and ilmenite. The absorption line 3 includes pseudobrookite and a small amount of hematite. Within this temperature range the intensity of absorption line 2 rapidly reduces to a negligible value.

At temperatures higher than 700°C, absorption lines 3 and 4 are mainly due to pseudobrookite. Thus the increase in pseudobrookite content in the specimen can be estimated from the increase in the absorption intensity of these lines.

The conversion graph shown in Figure 6.29 consists of three curves, each representing the change in number of $Fe^{2+}$ or $Fe^{3+}$ ions (or both) as a function of temperature. Initially, the relative number of $Fe^{2+}$ ions in ilmenite, as deduced from the area of the absorption line 2 in the spectrum of the unoxidised sample (Figure 6.2) is normalized to unity. It decreases rapidly to zero as the oxidation temperature increases from 400°C to 750°C. At the same time the relative number of $Fe^{3+}$ ions

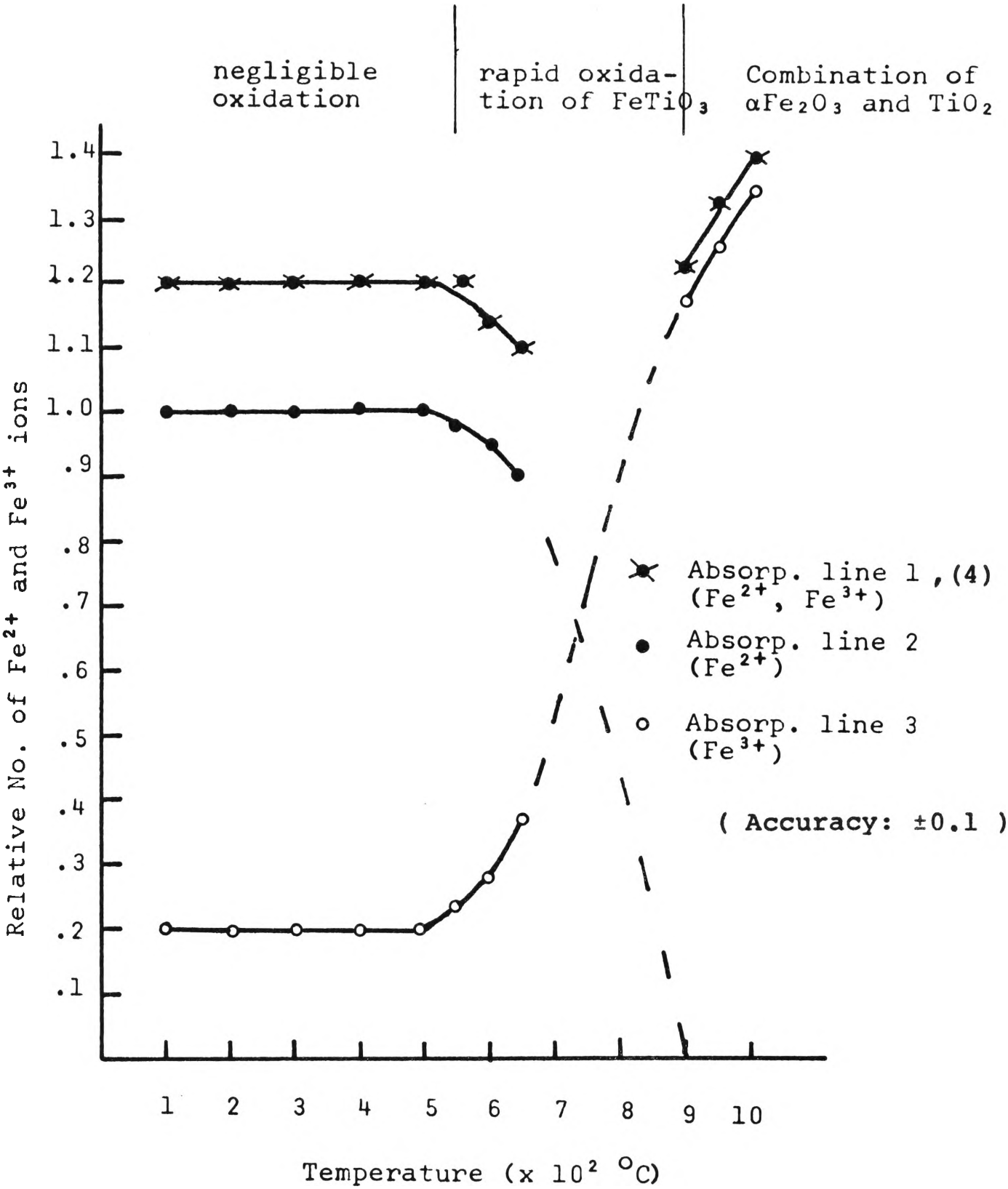


FIGURE 6.30. Ilmenite-pseudobrookite conversion graph of the natural grain size series.

(represented by the absorption line 3) increases rapidly. The absorption line 1 ($Fe^{3+}$ and $Fe^{2+}$ ions), however, decreases slowly because only the $Fe^{3+}$ ions are decreasing, due to the release of hematite from the solid solution, while the $Fe^{2+}$ ions (ilmenite) are converted to $Fe^{3+}$ ions (pseudobrookite). Above 750°C both absorption lines 3 and 4 of pseudobrookite increase to values higher than unity, indicating the formation of pseudobrookite from the combination of free hematite and free rutile in the specimen. (Section 6.6).

(6.7) b. <u>The Ilmenite-Pseudobrookite Conversion Graph of the Natural Grain Size Series</u>

It is not possible to construct a continuous ilmenite-pseudobrookite conversion graph from the spectra of this series because of the unresolved spectra of specimens oxidised at temperatures between 700°C and 850°C. However, assuming that the content of ilmenite continues to reduce rapidly by oxidation throughout this temperature range and is completely oxidised at about 900°C, a graph (Figure 6.30) for the absorption line can be extrapolated, similar to that shown in Figure 6.29. A continuous graph

TABLE 6.5

Oxidation stages of ilmenite with respect to temperature

| Oxidation Stage | Temperature Range | |
|---|---|---|
| | crushed sample series | natural grain size series |
| Negligible oxidation of ilmenite | below 400°C | below 550°C |
| Rapid oxidation of ilmenite | 450°C-700°C | 600°C-850°C |
| Combination of free $\alpha Fe_2O_3$ and $TiO_2$ | 750°C-1000°C | 900°C-1000°C |

TABLE 6.6.

Absorption line positions in spectra of the second series

| Temperature °C | Absorption line positions (mm/s) | | |
|---|---|---|---|
| | 1(4) | 2 | 3 |
| 350°C | 0.5 | 1.2 | - |
| 400°C | 0.5 | 1.2 | - |
| 500°C | 0.45 | 1.2 | -0.1 |
| 550°C | 0.45 | 1.2 | -0.1 |
| 600°C | 0.4 | 1.2 | -0.1 |
| 650°C | 0.4 | - | -0.1 |
| 700°C | 0.43 | - | -0.15 |
| 750°C | 0.45 | - | -0.15 |
| 800°C | 0.45 | - | -0.15 |
| 850°C | 0.45 | - | -0.2 |
| 900°C | 0.45 | - | -0.2 |
| 1000°C | 0.45 | - | -0.2 |

TABLE 6.7

Absorption line positions in spectra

of the third series

| Temperature °C | Absorption line position (mm/s) | | |
|---|---|---|---|
| | 1 (4) | 2 | 3 |
| 500° | 0.5 | 1.2 | - |
| 600° | 0.5 | 1.2 | -0.1 |
| 650° | 0.5 | 1.2 | -0.1 |
| 700° | - | - | - |
| 750° | - | - | - |
| 800° | - | - | - |
| 850° | - | - | - |
| 900° | 0.45 | - | -.2 |
| 950° | 0.45 | - | -0.2 |
| 1000° | 0.45 | - | -0.2 |

for absorption lines 1 and 3 cannot be deduced because the spectra of specimens heated at this temperature range show an unknown number of lines of low intensity. Generally the two conversion graphs (Figures 6.29 and 6.30) can be divided into three stages as listed in Table 6.5.

## (6.8) The Variation of Absorption Line Positions in the Spectra of Oxidised Specimens

Positions of absorption lines 1, 2, 3 and 4 in the spectra of oxidised specimens are observed and are listed in Table 6.6 and 6.7 for the two series of specimens. The slight shift in position of an absorption line is caused by the change in proportion of compounds represented by the absorption line. In the crushed-specimen series the position of absorption line 1 is gradually shifted to the left as temperature increases to 700$^{o}$C. This is because the content of ilmenite (absorption line at 0.5 mm/s and 1.2 mm/s) is decreasing, while that of pseudobrookite (0.45 mm/s and -0.2 mm/s) is increasing and that of hematite (-0.07 mm/s and 0.33 mm/s) is decreasing only slowly. At temperatures between 600$^{o}$C

and 650°C the content of ilmenite is very low and the absorption line position (0.4 mm/s) is between that of pseudobrookite and hematite. Above 750°C the absorption line 1 (or 4) is mainly pseudobrookite and therefore the position is at 0.45 mm/s. Absorption line 3, which is the combination of pseudobrookite and hematite, also gradually shifts to the left as pseudobrookite content increases and is at the -0.2 mm/s position at 900°C.

In the spectra of the natural grain size series a similar line shift is observed, except at temperatures between 700°C and 850°C where no sharp absorption lines are observed at all.

## (6.9) A Magnetic Anomaly in the Oxidation of Ilmenite Specimens at Temperatures between 700°C and 850°C

Absorption spectra (Figures 6.22 to 6.25) of specimens of natural grain size oxidised at temperatures between 700°C and 850°C show very broad and unresolved absorption of intensity less than 4 per cent. The expected ilmenite and pseudobrookite absorption lines

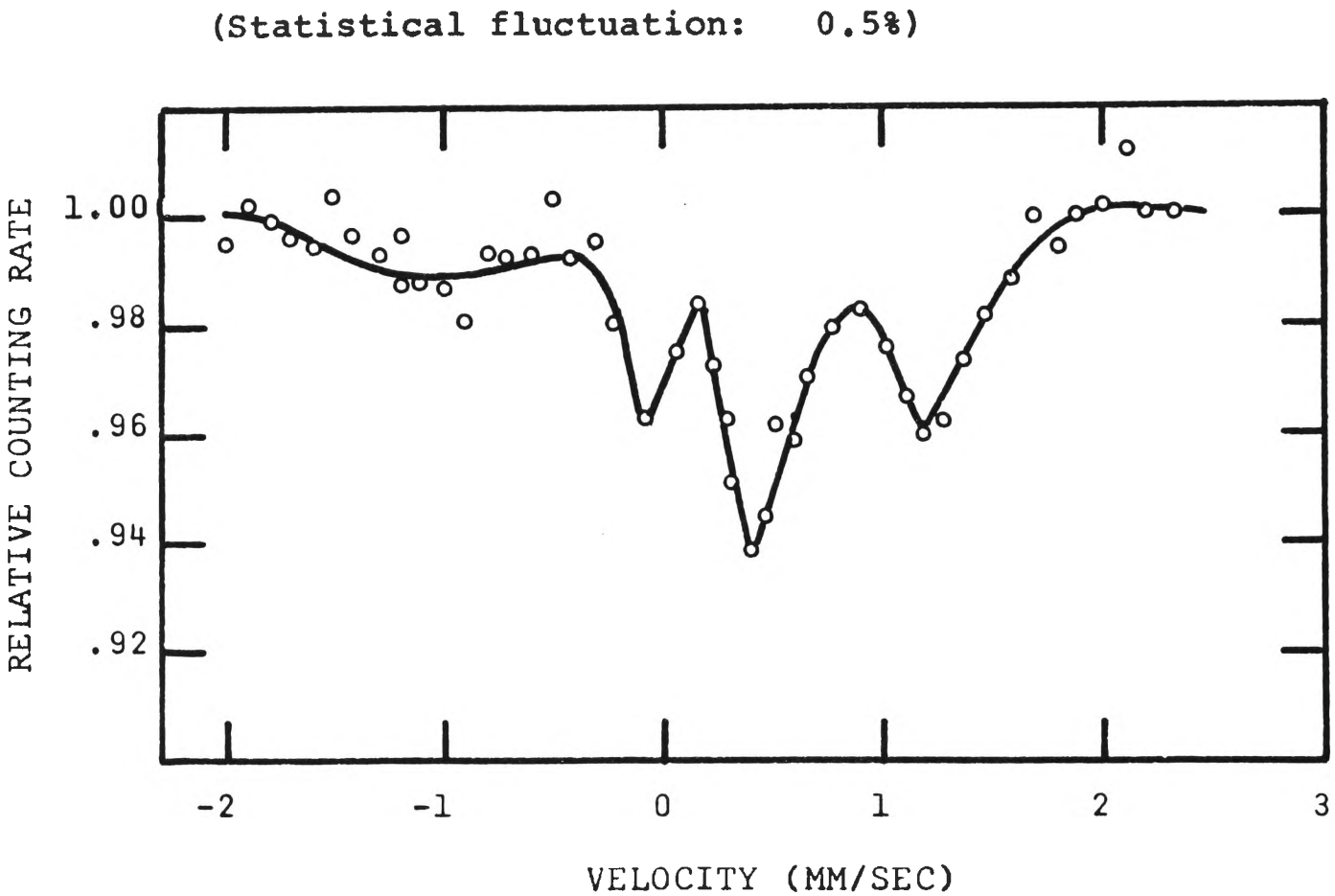


FIGURE 6.31. Mössbauer spectrum of magnetic grains extracted from the specimen which has been heated at 700°C for one hour.

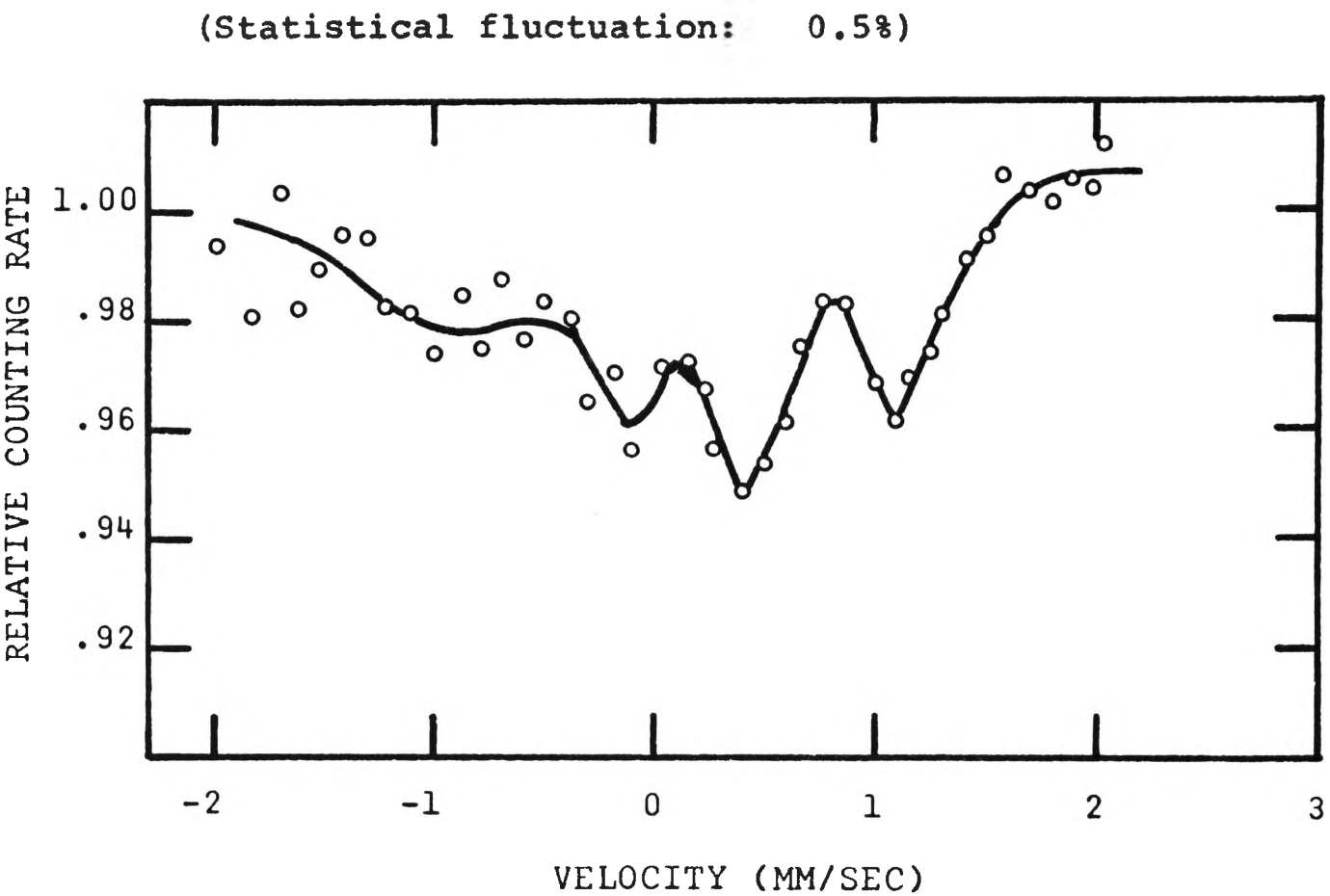


FIGURE 6.32. Mössbauer spectrum of magnetic grains extracted from the specimen which has been heated at 750°C fro one hour.

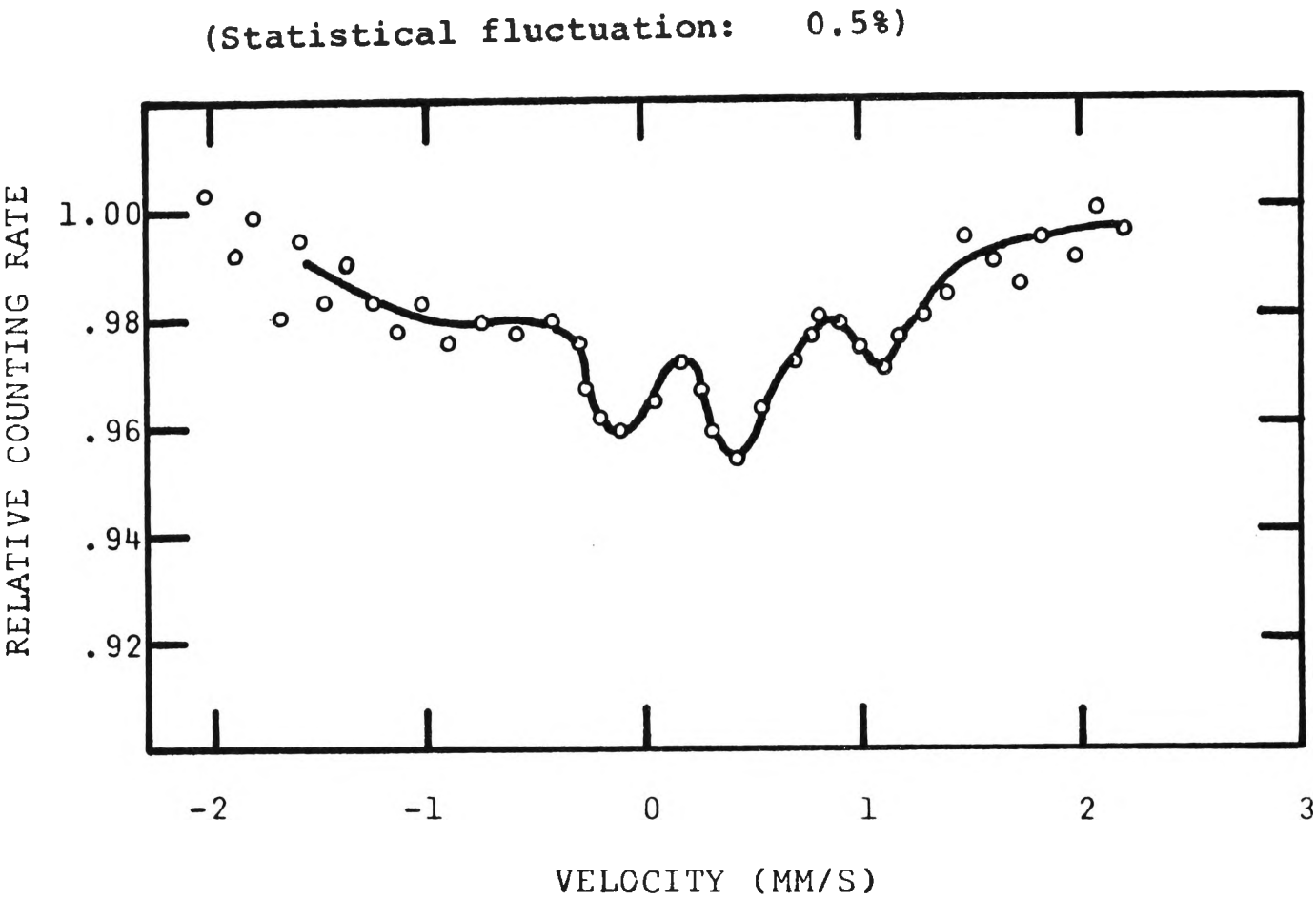


FIGURE. 6.33. Mössbauer spectrum of magnetic grains extracted from the specimen which has been heated at 800°C.

have disappeared. This could be the result of the overlapping of many absorption lines. It is known from magnetic measurements (Curnow and Parry, 1954) that natural ilmenite oxidised at a temperature between 600°C and 800°C becomes more magnetic. The Curie point of the "magnetic ilmenite" is between 100°C and 200°C. Hence one might suspect that the unresolved spectrum could be due to the influences of ferrimagnetic hyperfine splitting which would produce six absorption lines. In an attempt to observe more clearly the effect of magnetic hyperfine splitting, specimens containing more highly magnetic grains extracted by a hand magnet from the oxidised specimens were examined. However, the spectra of these specimens (Figures 6.31, 6.32 and 6.33) show no sign of magnetic hyperfine splitting. Instead they reveal absorption lines of ilmenite and pseudobrookite in the paramagnetic state. The results indicate that these more strongly magnetic specimens consist mainly of ilmenite rich ilmenite-hematite solid solutions and, perhaps, pseudobrookite produced by oxidation. It can be concluded that the magnetic field is not strong enough to affect the spectra.

It has been reported that a magnetic anomaly also occurs in a synthetic ilmenite-hematite solid solution which has no other impurities. Néel temperatures of (1-x) $FeTiO_3$-$xFe_2O_3$ where x = 0.21 and 0.33 are 290°K and 370°K respectively. Mössbauer spectra of these specimens were obtained by Ruby et al (1961) and Shirane et al (1962b). They revealed paramagnetic characteristics well below the respective Néel temperatures. These investigators, with the aid of neutron diffraction studies, were able to show that a considerable fraction of the magnetic spin is either uncoupled or tilted away from the magnetic axis. The magnetic structure of these solid solutions is inhomogeneous because of competing interactions which result from Ti ions which have become disordered within the lattice layers.

As mentioned in Section 6.2, Ishikawa (1961, 1962) proposed that the magnetic field is due to magnetic clusters in the solid solution. The size of magnetic clusters becomes small at lower concentrations of hematite and no long range magnetic ordering can be observed when the content of hematite in the solid solution is less than 22 per cent. This phase is called the superparamagnetic phase.

Ruby and Shirane (1961) suggested that the ferrimagnetic clusters are surrounded by paramagnetic Fe ions. The size of these clusters decreases with increasing temperature or increasing concentration of Ti ions.

In the present investigation, the increase of magnetic strength of specimens heated at temperatures between 700°C and 800°C may be due to the increase of hematite-ilmenite ratio in the solid solution to around 2:8 according to Bozorth et al (1957), or around 3:7 according to Ishikawa and Akimoto (1958), at which the maximum value of saturation moment is reached. However, the heat treatment also increases the paramagnetic $Fe^{3+}$ ions of pseudobrookite. Hence, the Mössbauer spectra reveal mainly $Fe^{2+}$ and $Fe^{3+}$ ions in paramagnetic state. The ferrimagnetic hyperfine splitting cannot be observed, presumably because of relatively less ferrimagnetic ions in the specimen and because the ferrimagnetic clusters are small.

The oxidation at this temperature range is very rapid, resulting in a change in crystal structure from

rhombohedral ($FeTiO_3$) to orthorombic ($Fe_2TiO_5$). Thus the specimen contains a mixture of both types of crystal structure. It was suggested by Akimoto et al (1957) that the pseudobrookite solid solution, $FeTi_2O_5$-$Fe_2TiO_5$, could be obtained by heating the natural ilmenite. Hence, there is a finite probability that pseudobrookite may be present in these specimens, or some $Fe^{2+}$ ions may exist in orthorombic cells. The quadrupole splitting of $Fe^{2+}$ ions, which depends on the electric field gradient, may vary considerably because of the change in nuclear environment of the $Fe^{2+}$ ions existing in different types of crystal structure or due to lattice imperfections. However, a large percentage of grains in the specimen is still in ilmenite-pseudobrookite form as shown in Figures 6.31 - 6.33. In addition, a fair amount of free hematite will also be present in the specimen due to the process of rapid oxidation (Section 6.6).

The most probable cause of spectrum broadening for natural grain sizes specimens heated at temperatures between 700°C and 850°C seems to be incomplete oxidation of the grains of the sample. The uncrushed natural grain

TABLE 6.8

Mössbauer data at room temperature

(Referred to $Co^{57}$ source in a copper host lattice)

| Compounds | Isomer Shift $\delta$ (mm/s) | Quadrupole Splitting $\varepsilon$ (mm/s) | References |
|---|---|---|---|
| $FeTiO_3$ | 0.85 | 0.35 | Present paper |
| $Fe_2TiO_5$ | 0.12 | 0.32 | Present paper |
| $FeTi_2O_5$ | 0.83 | 1.5 | (Shirane et al 1962) |
| $\alpha Fe_2O_3$ | 0.13 | 0.2 | (Shirane et al 1962) |

size is about 200μ which is much larger than the grain size of the crushed sample at about 50μ. There is thus a higher probability that ilmenite at the surface of the grains may be oxidised to pseudobrookite; while, in the interior of the grains, because of insufficient oxygen diffusion, the ilmenite may be converted to pseudobrookite series or some other titan-hematite compounds. Such compounds are suggested because of the high probability for the coexistance of compounds with rhombohedral and orthorombic structures (Nagata 1961). The resulting compounds in the specimens would then be:

(i) $FeTiO_3$ -$\alpha Fe_2O_3$ solid solution with four absorption lines;

(ii) Free $\alpha Fe_2O_3$ with six absorption lines;

(iii) $Fe_2TiO_5$ with two absorption lines;

(iv) $FeTi_2O_5$ with two absorption lines;

(v) Other titan-hematite compounds:

(vi) $TiO_2$ and other impurities.

Mössbauer data of these compounds are listed in Table 6.8.

TABLE 6.9

X-ray data of the specimen which has been oxidised at 700$^{o}$C for one hour.

| Complete Pattern d value (A) | ASTM Ilmenite Pattern d value (A) | Residual Pattern d value (A) |
|---|---|---|
| 3.73 | 3.73 | |
| 3.26 | | 3.26 |
| 2.74 | 2.74 | |
| 2.60 | 2.54 | |
| 2.23 | 2.23 | |
| 1.87 | 1.86 | |
| 1.78 | | 1.78 |
| 1.70 | 1.72 | |
| 1.63 | 1.63 | |
| 1.50 | 1.50 | |
| 1.47 | 1.47 | |
| 1.34 | 1.34 | |
| 1.27 | 1.27 | |

TABLE 6.10

X-ray data of the specimen which has been oxidised at 800°C for one hour.

| Complete Pattern d value (A) | ASTM $FeTiO_3$ d value (A) | ASTM $TiO_2$ d value (A) |
|---|---|---|
| 3.73 | 3.73 | |
| 3.26 | | 3.25 |
| 2.73 | 2.74 | |
| 2.56 | 2.54 | |
| 2.48 | | 2.49 |
| 2.23 | 2.23 | |
| 2.20 | | 2.19 |
| 2.07 | 1.87 | |
| 1.70 | 1.72 | |
| 1.69 | | 1.69 |
| 1.63 | 1.63 | |
| 1.61 | | 1.62 |
| 1.49 | 1.50 | 1.49 |
| 1.47 | 1.47 | |
| 1.36 | | 1.36 |
| 1.33 | 1.34 | |
| 1.28 | 1.27 | |

TABLE 6.11

X-ray data for the specimen which has been oxidised at 850°C for one hour.

| Complete Pattern d value (A) | ASTM Pseudobrookite d value (A) | ASTM Hematite d value (A) | ASTM Rutile d value (A) |
|---|---|---|---|
| | 4.90 | | |
| 3.67 | | 3.66 | |
| 3.46 | 3.48 | | |
| 3.25 | | | 3.25 |
| 2.71 | 2.74 | 2.69 | |
| 2.52 | | 2.51 | |
| 2.48 | 2.45 | | 2.48 |
| 2.28 | 2.22 | 2.28 | 2.30 |
| 2.20 | 2.20 | 2.2o | |
| 2.18 | | | 2.19 |
| 1.95 | 1.97 | | |
| 1.72 | | | |
| 1.70 | | 1.69 | 1.69 |
| 1.64 | 1.63 | 1.63 | 1.62 |
| 1.59 | | 1.60 | |
| 1.57 | | | |
| | | 1.45 | |
| 1.46 | 1.49 | 1.48 | 1.48 |
| 1.36 | 1.37 | 1.35 | 1.36 |
| 1.32 | | | |

TABLE 6.12

X-ray data for the specimen which has been oxidised at 950°C for one hour.

| Complete Pattern d value (A) | ASTM Pseudobrookite d value (A) | Residual Pattern d value (A) |
|---|---|---|
| 5.30 | | 5.03 |
| 4.89 | 4.90 | |
| 3.55 | | 3.55 |
| 3.47 | 3.48 | |
| 3.26 | | 3.26 |
| 2.75 | 2.75 | |
| 2.44 | 2.45 | |
| 2.41 | 2.40 | |
| 2.22 | 2.22 | |
| 2.20 | 2.20 | 2.19 |
| 1.97 | 1.97 | |
| 1.86 | 1.86 | |
| 1.75 | 1.74 | |
| 1.70 | | 1.70 |
| 1.66 | 1.66 | |
| 1.64 | 1.63 | |
| 1.54 | 1.54 | |

Since the weight of specimens used in the present investigation is fixed, the total content of $^{57}Fe$ in the specimen is, therefore, limited. An increase in the number of absorption lines due to more compounds being produced means a decrease in the absorption intensity of each line and thus results in a general broadening and a low intensity spectrum. X-ray diffraction powder photograph (Tables 6.9 - 6.11) of these specimens were obtained, and revealed large concentrations of ilmenite, smaller amounts of rutile ($TiO_2$) and hematite, and in the specimen which has been oxidised at 850°C, traces of pseudobrookite were also observable. No other compounds were observed, presumably because of a smaller molar percentage.

Photomicrographs of Swansea ilmenite which was heated in air at 850°C for one hour were examined (Westcott, 1966) and revealed that many of the grains had fused together and were duller than before heating. The grains were very mottled and showed good intergrowths of brownish hematite. The x-ray diffraction powder photograph indicated the definite presence of rutile, hematite, ilmenite and iron titanate.

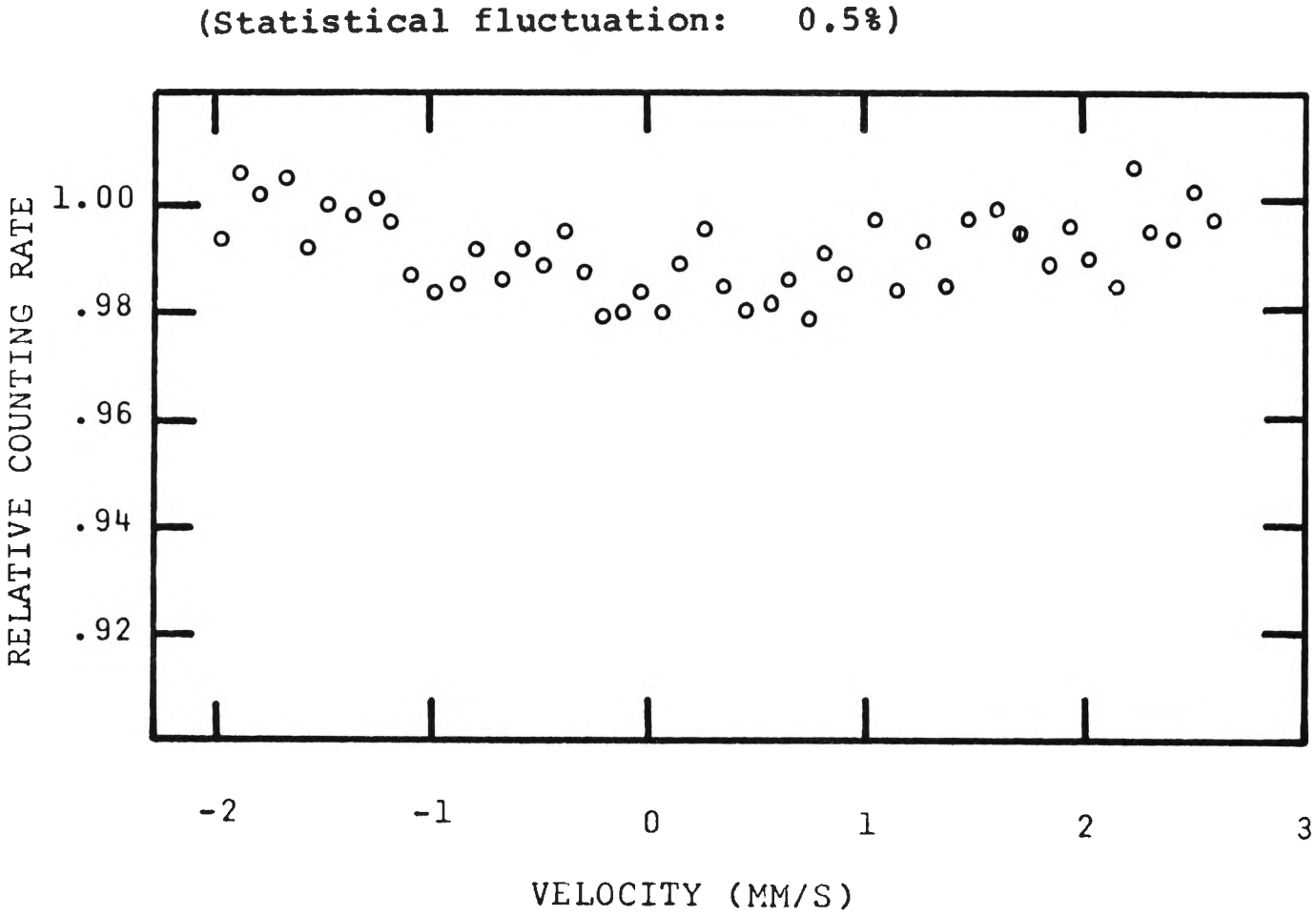


FIGURE 6.34. Mössbauer spectrum of the residual of the specimen which has been heated at 700°C for one hour.

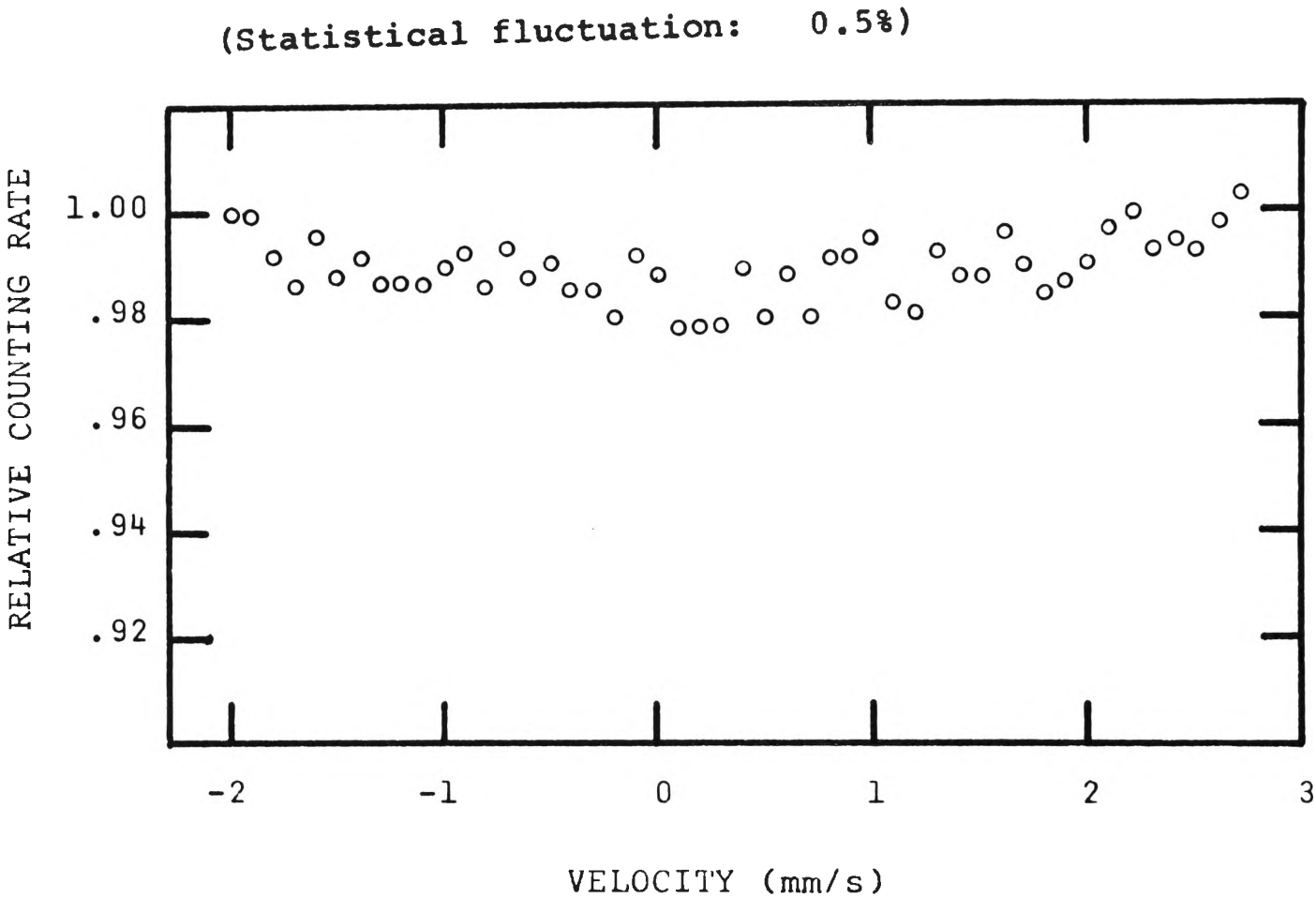


FIGURE 6.35. Mössbauer spectrum of the residual of the specimen which has been heated at 750°C for one hour

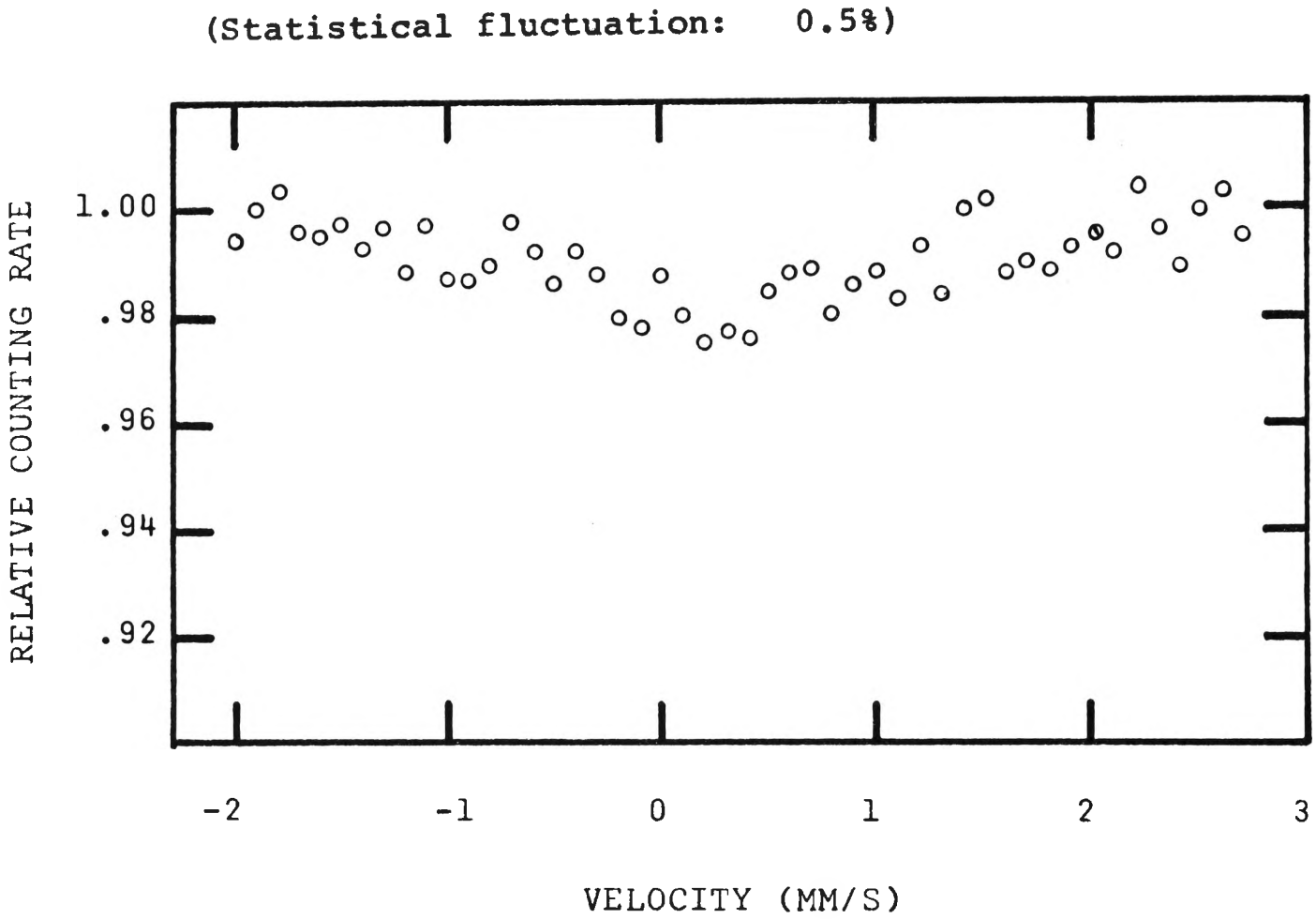


FIGURE 6.36. Mössbauer spectrum of the residual of the specimen which has been heated at 800°C for one hour.

After most of the magnetic grains have been removed from the specimens, the residuals become less magnetic. These residuals were also examined. Their spectra (Figures 6.34, 6.35 and 6.36) are broad and unresolved, similar to the spectra of the original specimens before the magnetic grains have been removed, but with lower intensity. The decrease in intensity is due to a decrease in Fe ions in the specimens and an increase in the proportional amount of rutile ($TiO_2$) and other impurities. As was discussed in Section 6.6, the oxidation of ilmenite to pseudobrookite will produce more free rutile. In the unoxidised Swansea ilmenite, according to Westcott (1966), the content of free rutile is about 6 per cent. After oxidation at 650$^{o}$C for an hour it increases to about 12 per cent. In the residuals considered above where magnetic grains have been removed from the specimens, the content of free rutile will be proportionately high. Thus the absorption of these spectra is expected to be low.

## (6.10) Time Dependence of Oxidation

In order to observe the time dependence of oxidation, specimens are heated at the same temperature but for

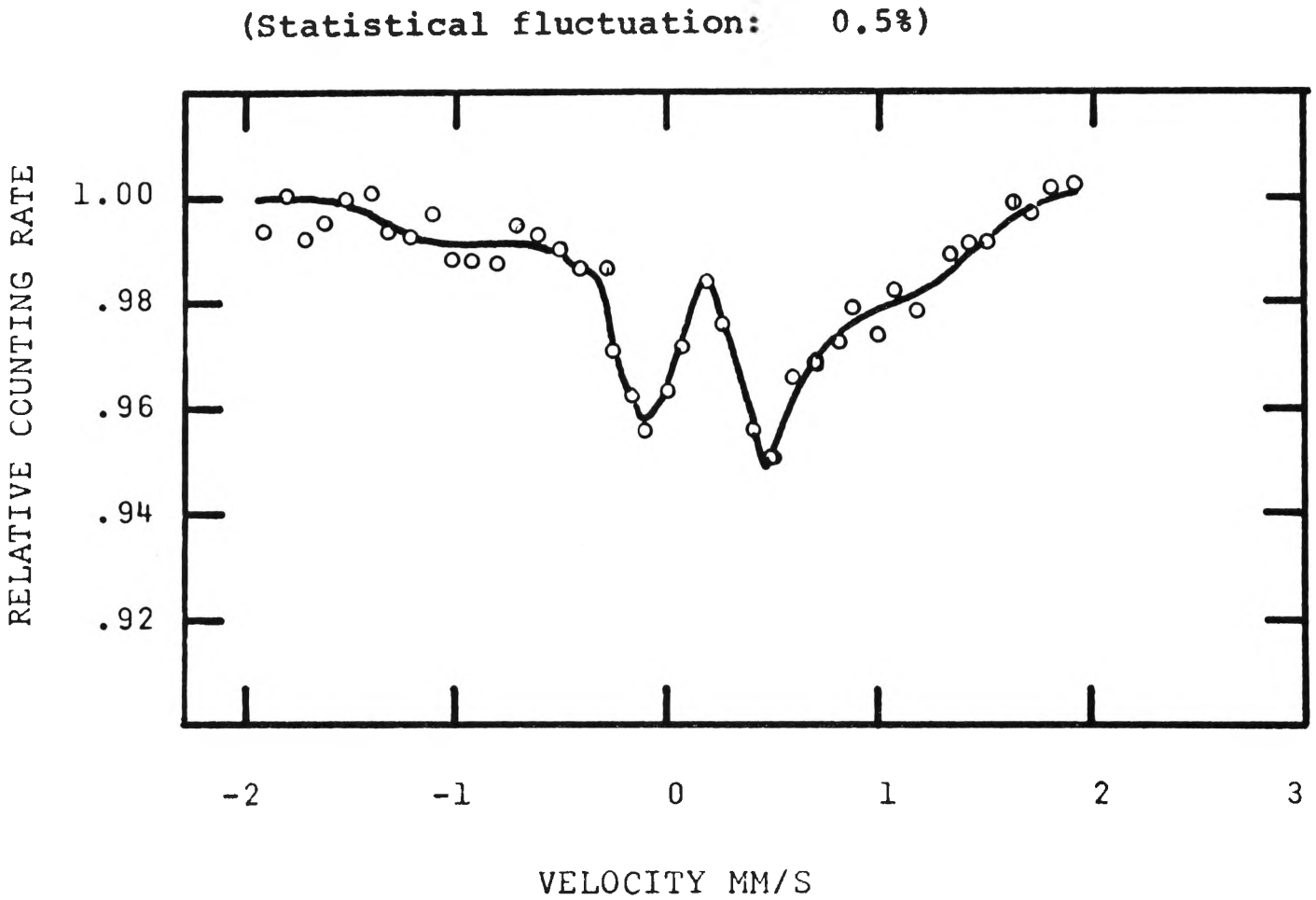


FIGURE 6.37. Mössbauer spectrum of the crushed specimen which has been heated at 550°C for four hours

different duration. The most suitable temperatures for this investigation are 550°C for the crushed specimens and 800°C for the specimens of natural grain size. These temperatures are about 100°C below the temperatures at which specimens will be well oxidised in an hour.

(a) Three crushed ilmenite specimens were prepared: the first one was heated at 550°C for one hour, the second one for four hours and the third one for three days. The absorption spectra (Figures 6.9, 6.37 and 6.38) of these specimens at room temperature clearly show three different stages of oxidation.

The first spectrum (Figure 6.9) shows that the specimen is mainly ilmenite in structure with absorption line 1 and 2 broadened due to overlapping of ilmenite, hematite and pseudobrookite absorption lines.

The second spectrum (Figure 6.37) shows two sharper and more resolved absorption lines 3 and 4 of pseudobrookite. The ilmenite line at 1.20 mm/s has nearly disappeared. The oxidation has converted most of the ilmenite in the sample to pseudobrookite. The absorption line 4 is slightly broader than the absorption line 3

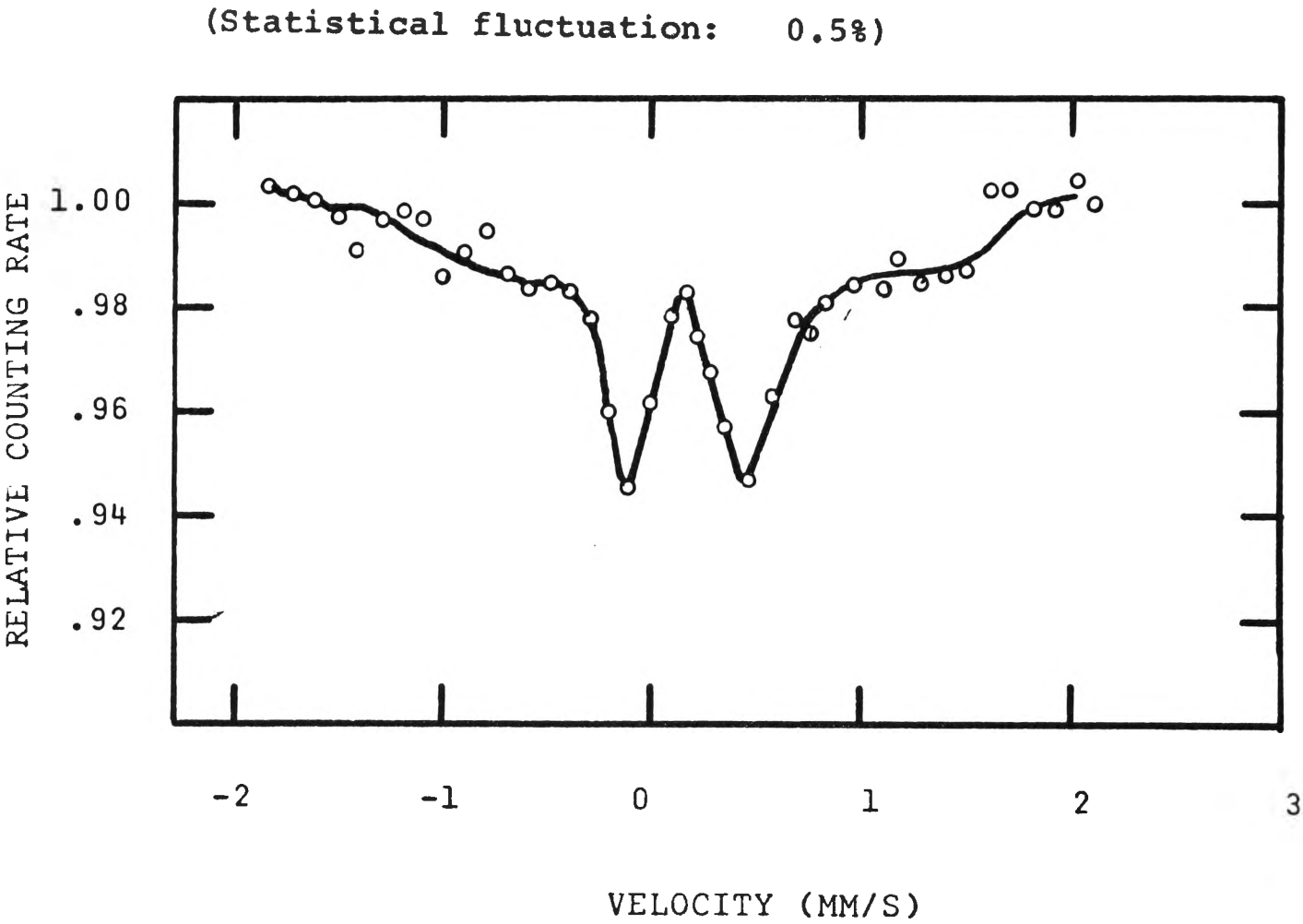


FIGURE. 6.38. Mössbauer spectrum of the crushed specimen which has been heated at 550°C for three days

indicating that a small amount of ilmenite-hematite solid solution still remains in the specimen.

The third spectrum (Figure 6.38) also shows two sharp lines of pseudobrookite. The resolution has improved slightly. There is very little trace of ilmenite. There is, however, an indication of free hematite absorption at about 1.5 mm/s and -1.0 mm/s. The oxidation of ilmenite at this stage can be regarded as completed. This absorption spectrum is equivalent to that of a specimen heated at 700°C. The presence of hematite absorption lines means that long time duration of oxidation at 550°C does not increase the probability of combination of free hematite and free rutile, though these combine readily at the higher temperature range, forming pseudobrookite (Section 6.6).

(b) Three specimens of natural grain size were prepared in the same way as for the crushed samples in (a) but at 800°C. Their absorption spectra also show three different stages of oxidation.

The spectrum (Figure 6.24) shows a broad and unresolved absorption of low intensity. This spectrum was

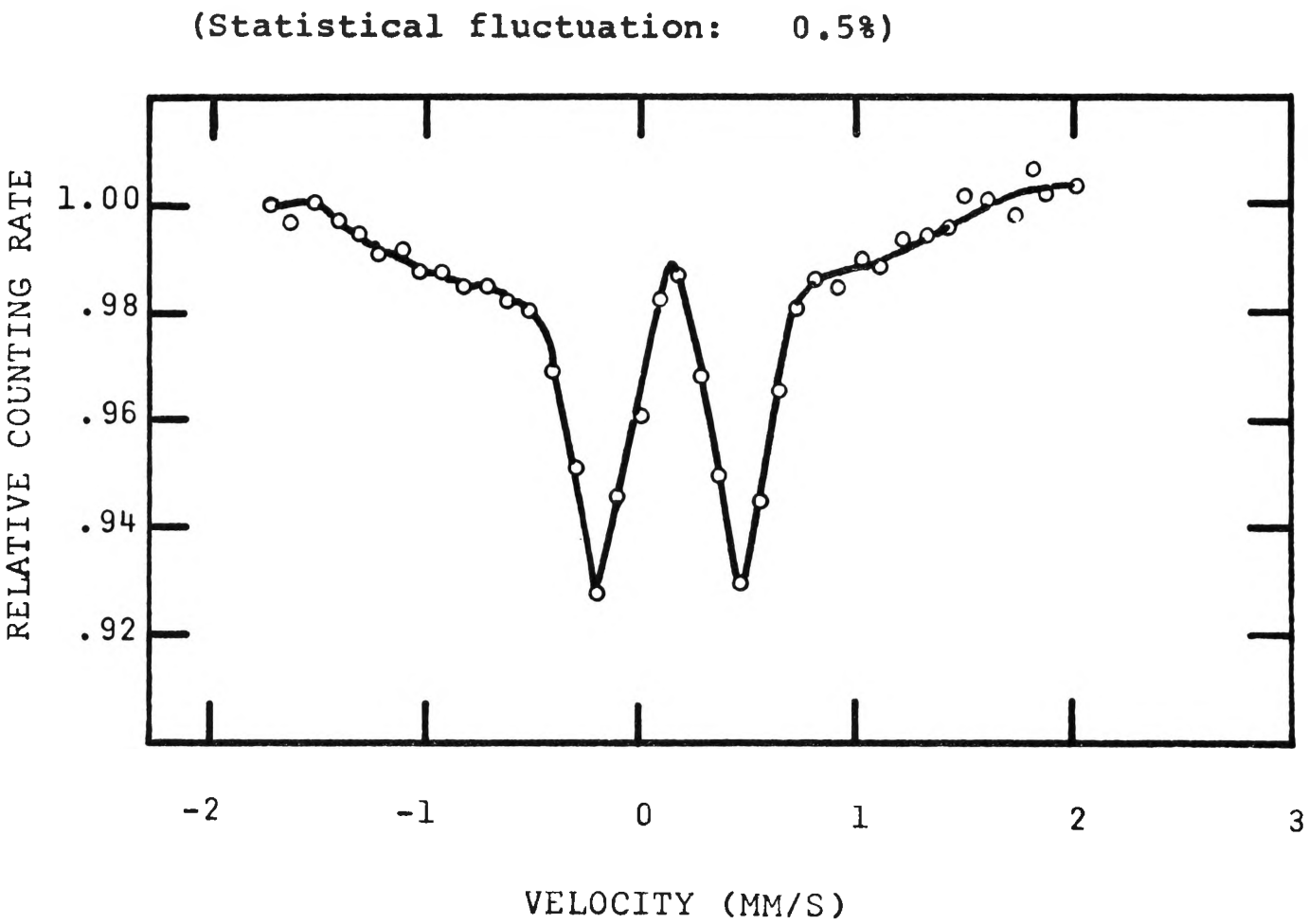


FIGURE 6.39. Mössbauer spectrum of the natural grain size specimen which has been heated at 800°C for four hours.

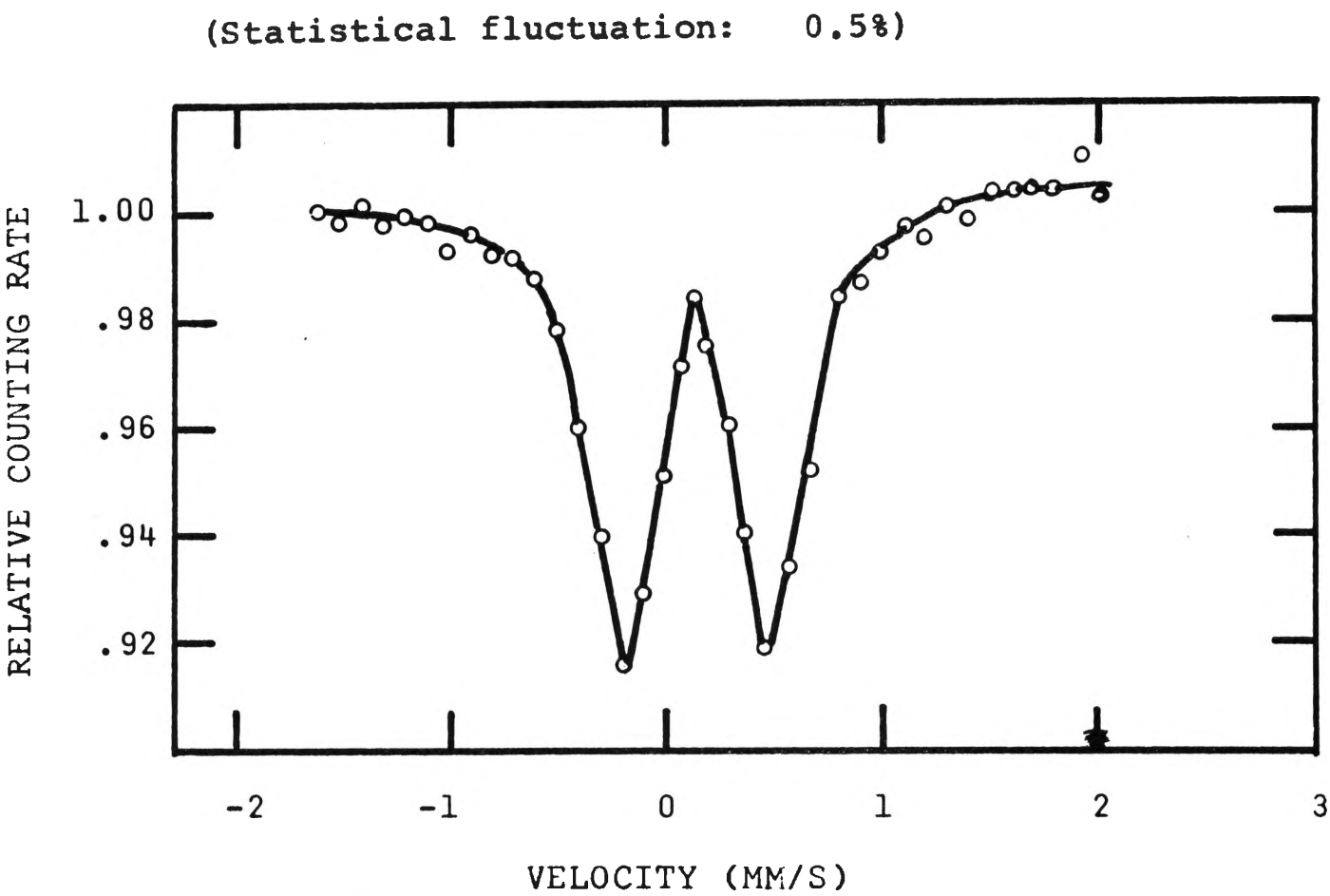


FIGURE 6.40. Mössbauer spectrum of the natural grain size specimen which has been heated at 800°C for three days.

explained previously as the overlapping of many absorption lines (Section 6.8).

The second spectrum (Figure 6.39) shows two sharp absorption lines 3 and 4 of pseudobrookite. There is very little trace of ilmenite.

The third spectrum (Figure 6.40) indicates that oxidation is close to completion. The intensity of absorption lines here is higher than that of the second spectrum. This means that more pseudobrookite is formed from the combination of free hematite and rutile.

(c) A specimen of natural grain size was heated at 500$^{o}$C for one day. The absorption spectrum of this specimen shows no obvious sign of oxidation and is similar to the spectrum of the natural sample.

The results in (a) and (b) indicate that in the temperature range within which ilmenite can be oxidised the time duration of oxidation has a significant influence on the degree of oxidation. However, the result in (c) shows that if the heating temperature is considerably lower than the critical oxidation temperature, about

500°C for the crushed specimen and 650°C for the natural grain size specimen, no improvement in oxidation can be achieved.

# CHAPTER 7

# CONCLUSIONS

## (7.1.) The Constant Velocity Spectrometer

The pneumatic-hydraulic constant velocity Spectrometer described in this thesis has proved to have a sufficiently good overall performance to elucidate the changes occurring in treated and untreated ilmenite samples as described below despite the presence of less than 0.7 per cent of $^{57}Fe$ nuclei.

## (7.2.) Natural Ilmenite Spectra

Natural ilmenite, though it is weakly ferrimagnetic as determined by magnetic measurements, shows only paramagnetic characteristics by Mössbauer spectroscopy. This implies that natural ilmenite samples contain some Fe ions in the paramagnetic state and some Fe ions in the ferrimagnetic state. However, the ferrimagnetic field is too weak to be detected by Mössbauer spectroscopy. The sample can be regarded as in a superparamagnetic phase. Mössbauer spectra of natural ilmenite samples obtained from Norway, Ceylon, Swansea (N.S.W.) and Capel (W.A.) reveal two well resolved absorption

lines of ilmenite and a small absorption line which is due to $Fe^{3+}$ ions in the sample. The inequality in intensity of the ilmenite absorption lines is the result of an overlapping of absorption lines due to $Fe^{2+}$ and $Fe^{3+}$ ions. The result of comparison of absorption intensities of these spectra suggests that Norwegian ilmenite has the highest content of $FeTiO_3$, followed by Swansea and Capel, with Ceylon ilmenite containing the least $FeTiO_3$.

## (7.3.) Oxidation of Ilmenite to Pseudobrookite

The results of Mössbauer Spectroscopy show that the degree of conversion (i.e. oxidation) of ilmenite to pseudobrookite is dependent on temperature. The content of pseudobrookite, as is indicated by its absorption intensity in the spectrum, increases with increasing temperature. The temperature ranges in which rapid oxidation occurs are between 400°C and 750°C for the crushed specimens and between 600°C and 900°C for the specimens of natural grain size. Above these temperatures no traces of ilmenite can be observed, indicating complete conversion.

## (7.4.) Effect of Particle Grain Size on Oxidation Process

Mössbauer spectra of the crushed specimens and the natural grain size specimens of ilmenite which have been heated in air at temperatures between 100°C and 1000°C for one hour reveal the effect of particle grain size on the oxidation of these specimens. The spectra of specimens of grain size less than 50 microns when crushed clearly show the degree of oxidation of ilmenite throughout the entire temperature range. However, the spectra of specimens of natural grain size of about 200 microns which have been heated at temperatures between 700°C and 850°C for one hour, show no resolved absorption lines. The general absorption intensity is less than four per cent. It has been proposed herein that this is mainly due to oxidation at these temperatures being incomplete because of insufficient oxygen diffusion inside the larger grains. The resultant compounds, existing in comparable proportions in the specimen, consist of ilmenite-hematite solid solutions, free hematite, pseudobrookite, free rutile and other titan-hematite. Because of the limited number of Fe ions in a specimen, the presence of all of these compounds with absorption lines at different positions results in lowering of line intensity

and broadening of the spectrum in general.

## (7.5.) Spectra of Extracted Magnetic Grains

Mössbauer spectra of specimens containing highly magnetic grains extracted from samples which have been heated at temperatures between 700°C and 800°C for one hour show no sign of magnetic hyperfine splitting. The spectra indicate persistant paramagnetic characteristics at room temperature which is well below the Néel temperatures of between 100°C and 200°C of these specimens. This behaviour is similar to some synthetic ilmenite-hematite solid solutions which also exhibit paramagnetic characteristics below their respective Néel temperatures. This seems to indicate that a considerable fraction of the magnetic spin is either uncoupled or tilted away from the magnetic axis. The magnetic structure of such solid solutions is inhomogeneous because of the competing interactions which result from Ti ions becoming disordered within the lattice layers. The magnetic clusters in the lattice are small and are surrounded by paramagnetic Fe ions. Hence the spectra reveal only paramagnetic characteristics.

## (7.6.) Free Hematite and Free Rutile

The content of free hematite in the specimen increases with increasing temperature of oxidation. This means that more hematite is released from the ilmenite-hematite solid solution as ilmenite is converted to pseudobrookite.

The content of free rutile in the specimen also increases with increasing temperature because the oxidation of ilmenite produces rutile. However, at temperatures above 900$^{o}$C, the proportion of free rutile and free hematite have both significantly decreased due to a higher probability of combination of rutile and hematite to form pseudobrookite at the higher temperatures. The intensity of the absorption line of pseudobrookite is considerably increased indicating an increase of pseudobrookite in the specimen. The release of hematite from the ilmenite-hematite solid solution is clearly indicated by the gradual decrease of $Fe^{3+}$ absorption in the absorbtion line 1 (due to a combination of $Fe^{2+}$ and $Fe^{3+}$ ions) and the increase in intensity of the free hematite absorption line at the -1 mm/s and 1.5 mm/s positions. However, if the $Fe^{3+}$ ions were those of pseudobrookite, then the oxidation of ilmenite to

pseudobrookite, which converts the $Fe^{2+}$ ions to $Fe^{3+}$ ion, should have little effect on the intensity of the absorption line 1. But the results show a considerable reduction in its intensity. It can be concluded, therefore, that the small $Fe^{3+}$ absorption lines in the spectrum of natural ilmenite are due to hematite in the solid solution rather than to any pseudobrookite as suggested by other workers.

(7.7.) Time Dependence of Oxidation

Mössbauer spectra of specimens heated at the same temperature but for different time durations indicate that, in the temperature range within which ilmenite can be oxidised effectively, the time duration of oxidation has a significant influence on the degree of oxidation. However, if the heating temperature is considerably lower than the critical oxidation temperature no significant oxidation can be observed however long the heating period.

(7.8.) Thus Mössbauer spectroscopy has enabled the revelation of the magnetic phase of natural ilmenite and its oxidation products. It makes possible the direct

observation of the oxidation effect on ilmenite samples and of the grain size, temperature and time duration dependence of oxidation. It has positively identified the final oxidation product as mainly pseudobrookite. Finally, the strong suggestion that the small absorption line belongs to hematite of the solid solution has opened a way for clarifying the controversy regarding this absorption line.

# APPENDIX I

## COMPONENTS OF THE VELOCITY DRIVE

1. One air compressor unit, Model 60, speed 650 r.p.m. tank size 2' diameter x 6' long, pressure range 100-125 p.s.i.g., made by Pulford and Son Pty. Ltd., Sydney.

2. One shut off valve, type AC243B, for main air supply control.

3. One compressed air preparation unit, Hannifin 3/8" unit, consists of
   air line filter Model No. F-1037
   regulator, Moden No. R-2037
   lubricator, Model No. LN-1037
   adaptors are used for connection of 5/16" copper tubes.

4. One precision air regulator, S.M.C. Shoketsu Model No. 2302-202, maximum supply pressure 100 p.s.i.g., secondary pressure range 0.14 ∿ 60 p.s.i.g., port size B.S.P. 1/4" for air cylinder pressure control.

5. One precision air regulator, S.M.C. Shoketsu Model No. 2302-002, maximum supply pressure 100 p.s.i.g., secondary pressure range 0.14 ∿ 30 p.s.i.g., port size B.S.P. 1/4" for operational pressure control.

6. One air pressure gauge, Hannifin 2" dial, centre-back-mounted, part No. 2156, range 0-160 p.s.i.g., for indication of main air supply pressure.

7. Two air pressure gauges: Hannifin 2" dial centre-back-mounted, range 0-60 p.s.i.g., for indication of operational pressure.
8. Two four-way directional valves, Jeffries-Parker-Hannifin Model No. V2/74, double pressure pilot operated, 1 1/8" diameter pilots, minimum operation pressure 10 p.s.i.g. for control of air and oil flow direction.
9. Two three-way solenoid directional valves, Model T200-25-D2F, actuated by 240V A.C., made by Jeffries-Parker-Hannifin Pty. Ltd., for operating the four-way directional valves.
10. One 6" diameter bore, double acting air cylinder, Model JAC 307-1, rod diameter 1", made by Jeffries-Parker-Hannifin Pty. Ltd.
11. One 3" diameter bore, double acting hydraulic cylinder, Model HD25C, made by Jeffries-Parker-Hannifin Pty. Ltd.
12. Copper pipe lines of 5/16" inside diameter for directing air and oil flow.
13. Eighteen shut off valves which can stand pressure up to 1000 p.s.i.g. for control of oil flow in capillary tubes.
14. One pair of rigid couplings for coupling the air cylinder and oil cylinder.
15. One copper oil reservoir of tank size 7" x 7" x 8" with lid.
16. Tube fittings.

    Type Z373-3 ripplied connectors
    Type Z169 adaptors
    Type Z164-DS adaptors
    Type Y975 tee

Type Z18 nuts
Type Z404 sleeves

17. Rubber tubes of 5/16" inside diameter for directing air flow.
18. Plastic tubes of 5/16" inside diameter for directing oil flow.
19. Copper capillary tubes of various inside diameters for controlling flow rate of oil.
20. One temperature control unit, Haake Model R21 with temperature limit of -30 to 150°C for controlling viscosity of oil.
21. One stainless steel water bath of size 10" x 17" x 24".

# APPENDIX 2

## ELECTRONIC EQUIPMENT FOR MÖSSBAUER SPECTROMETERS

1. High Voltage Power Supply, Model 230A, made by B.W.D. Electronic Pty. Ltd., Australia.

2. Scintillation detector, Model X P1010 photomultiplier mounted with NaI (Tℓ) crystal, made by Amperex Electronic Corporation.

3. Proportional counter, model RSG-61-M1, gas absorption - 97% Kr and 3% $CO_2$, pressure 76 cm of Hg, made by Reuter Stokes Electronic Components Inc., Cleveland, Ohio, U.S.A.

4. Preamplifier, type No. NE 5202A, made by Nuclear Enterprises Ltd., England.

5. Non-overloading linear pulse amplifier, type NE 5202, made by Nuclear Enterprises Ltd., England.

6. Differential pulse height selector, type NE 5103, made by Nuclear Enterprises Ltd., England.

7. Gating control unit, special design, see Chapter 3.

8. Two electronic counters, Model PW 4032, made by Philips Electronics.

9. Two timer counters, Model TC 11, made by Advance electronics Ltd., England.

10. Electronic A.C. voltage stabilizer, Model SS500, made by Stabilac Pty. Ltd., Sydney.

## REFERENCES

ADLER, A.D. and HANE, M (1966) - Amer. J. Phys. 34, 189.

AKIMOTO, S. (1954) - J. Geomag. Geoelect. 6, 1.

AKIMOTO, S. (1955) - Jap. J. Geophys. 1, 1.

AKIMOTO, S. (1957) - Thesis, Univ. of Tokyo.

AKIMOTO, S., NAGATA, T. and KATSURA, T. (1957) - Nature, 179, 37.

AVRAHAMI, M. and GOLDING, R.M. (1969) - N.Z. Jnl. Sci., 12, 594.

BALSLEY, J.R. and BUDDINGTON, A.F. (1958) - Econ. Geol. 53, 777.

BIZETTE, H. and TSAI, B. (1956) - Compt. rend. 242, 2124.

BLACKBURN, J.F., REETHOF, G. and SHEARER, J.L. (1960) - "Fluid Power Control", Technology Press of M.I.T. and John Wiley & Sons, Inc., New York and London.

BOYLE, A.J.F. and HALL, H.E. (1962) - Rep. Progr. Phys., 25, 441.

BOZORTH, R.M., WALSH, D.E. and WILLIAMS, A.J. (1957) - Phys. Rev., 108, 157.

CHEVALLIER, R. and MATHIEU, S. (1958) - Bull. Soc. Chim. France, 5, 726.

COX, D.E., SHIRANE, G., FLINN, P.A., RUBY, S.L. and TAKEI, W.J. (1963) - Phys. Rev. 132, 1547.

CRAIG, P.P., NAGLE, D.E. and COCHRAN, D.R.F. (1960) - Phys. Rev. Letters, 4, 561.

CURNOW, C.E. and PARRY, L.G. (1954) - Nature, 174, 1101.

CURNOW, C.E. and PARRY, L.G. (1955) - J. and Proc. Roy. Soc. N.S.W., 89, 64.

DANIELS, J.M. and ROSENCWAIG, A. (1969) - J. Phys. Chem. Solids, 30, 1561.

EIBSCHUTZ, M., GORODETSKY, G., SHTRRIKMAN, S. and TREVES, D. (1964) - J. Appl. Phys. 33, 1071.

FLINN, P.A. (1963) - Rev. Sci. Instrum., 34, 1422.

FRAUENFELDER, H. (1963) - "The Mössbauer Effect", W.A. Benjamin Inc.

FRENZEL, G. (1956) - Heidelb. Beitr. Min. Petrogr., 5, 165.

GIBB, T.C., GREENWOOD, N.N. and TWIST, W. (1969) - J. Inorg. Nuclear Chem., (G.B.) 31, 947-954.

GOLDANSKII, V.I., EGIZAROV, B.G., ZAPOROZHETS, V.M., OSTANEVICH, YU.M., and CHUPROVA, I.D. (1965) - Prikl. Geofiz. Vses. Nauchn.-issled. Inst. Geofiz. Metodov Razvedki No. 44, 202.

GORTER, E.W. (1957) - Advanc. Phys., 6, 288.

GRUVERMAN, I.J. (1965) - "Mössbauer Effect Methodology" Vol. 1. Plenum Press, New York.

HANNA, S.C., HEBERLE, J., LITTLEJOHN, C., PERLOW, G.J., PRESTON, R.S. and VINCENT, D.H. (1960) - Phys. Rev. Letters, 4, 177.

HEITLER, W. (1949) - "Quantum Theory of Radiation". Clarendon Press, Oxford.

ISHIKAWA, Y. (1957) - J. Phys. Soc. Japan, 12, 1083.

ISHIKAWA, Y. (1958) - J. Phys. Soc. Japan, 13, 828.

ISHIKAWA, Y. (1961) - Proc. Int. Conf. on Magnetism and Crystallography, Kyoto, Sept.

ISHIKAWA, Y. (1962) - J. Phys. Soc. Japan, 17, Suppl. B-1, 239.

ISHIKAWA, Y. and AKIMOTO, S. (1957) - J. Phys. Soc. Japan, 12, 1083.

ISHIKAWA, Y. and AMIMOTO, S. (1958) - J. Phys. Soc. Japan, 13, 1298.

KANKELEIT, E. (1964) - Rev. Sci. Instrum, 35, 194.

KERLER, W. and NEUWIRTH, W. (1962) - Z. Physik, 167, 176.

KISTNER, O.C. and SUNYAR, A.W. (1960) - Phys. Rev. Letters, 4, 412.

KOCHER, C.W. (1965a)- Phys. Letters, 14, 287.

KOCHER, C.W. (1965b)- Rev. Sci. Instrum. 36, 1018.

KUHN, W. (1929) - Phil. Mag., 8, 625.

LAMB, W.E. (1939) - Phys. Rev., 55, 190.

LUDWIG, G.W. and WOODBURY, H.H. (1960)- Phys. Rev. 117,1286.

LIPKIN, H.J. (1960) - Ann. Phys. 9, 332.

LIPKIN, J., SCHECHTER, B., SHTRIKMAN, S. and TREVES, D. (1964) - Rev. Sci. Instrum., 35, 1336.

MÖSSBAUER, R.L. (1958) - Z. Physik, 151, 124.

MÖSSBAUER, R.L. (1959) - Z. Naturforsch, 14a, 211.

MUIR, A.H. (1967) -"Mössbauer Effect Data Index, 1958-1965".

MURANAKA, S. SHINJO , T., BANDO, Y. and TAKADA, T. (1971) - J. Phys. Soc. Japan, 30, 890.

NAGATA, T. (1950) - Nature, 165, 245.

NAGATA, T. (1952) - Nature 169, 704.

NAGATA, T. (1953) - Nature, 172, 850.

NAGATA, T. (1961) - "Rock Magnetism", Maruzen Co. Ltd., Tokyo, 1961.

NAGATA, T. and AKIMOTO, S. (1956) - Geofiz. pura e appl., 34, 36.

NAGATA, T., AKIMOTO, S. and UYEDA, S. (1951) - Proc. Japan Acad., 27, 643.

NAGATA, T., AKIMOTO, S., and UYEDA, S. (1952a) - Proc. Japan Acad., 28, 277.

NAGATA, T., UYEDA, S., and AKIMOTO, S. (1952b) - J. Geomag. Geoelect., 4, 22.

NAGATA, T., AKIMOTO, S., and UYEDA, S. (1953a) - Nature, 172, 630.

NAGATA, T., AKIMOTO, S. and UYEDA, S. (1953b) - J. Geomag. Geoelect., 5, 168.

NAGATA, T. and SHIMIZU, Y. (1959) - Nature, 184, 1472.

NAGATA, T., UYEDA, S., AKIMOTO, S. and KAWAI, N. (1952) - J. Geomag. Geoelect., 4, 102.

NUSSBAUM, R.H. and HOUSLEY, R.M. (1965) - Nuclear Phys. 68, 145.

PARRY, L.G. (1955) - M. Sc. Thesis, University of New South Wales.

POSNJAK, E. and BARTH, T.F.W. (1934) - Zeits, Krist., 88, 271.

POUND, R.V. and REBKA, G.A. (1960a)- Phys. Rev. Letters, 4, 240.

POUND, R.V. and REBKA, G.A. (1960b)- Phys. Rev. Letters, 4, 337.

PRESTON, R.S., HANNA, S.S. and HEBERLE, J. (1962) - Phys. Rev., 128, 2207.

RUEGG, F.C., SPIJKERMAN, J.J. and DEVOE, J.R. (1965) - Rev. Sci. Instrum., 36, 356.

RAMDOHR, P. (1926) - N. Jb. Min. Geol., 54, 320.

ROSSITER, M.J. and CLARKE, P.T. (1965) - Nature, 207, 402.

RUBY, S.L. and SHIRANE, G. (1961) - Phys. Rev., 123, 1239.

SHIRLEY, D.A., KAPLAN, M., AXEL, P. (1961) - Phys. Rev., 123, 816.

SHIRANE, G., PICKERT, S.J., NATHANS, R., and ISHIKAWA, Y. (1959) - J. Phys. Chem. Solid, 10, 35.

SHIRANE, G., COX, D.E. and RUBY, S.L. (1962a) - Phys. Rev., 125, 4, 1158.

SHIRANE, G., COX, D.E., TAKEI, W.J. and RUBY, S.L. (1962b) - J. Phys. Soc. Japan, 17, 10, 1598.

SHULL, C.G., STRAUSER, W.A. and WOLLAN, E.O. (1951), Phys. Rev., 83, 333.

STEYERT, W.A. and TAYLOR (1964) - Phys. Rev., 134, A716.

TAYLOR, R.D., KITCHENS, T.A., NAGLE, D.E., STEYERT, W.A. and MILLETT, W.E. (1964) - Solid State Commun.2, 209.

UYEDA, S. (1956) - J. Geomag, Geoelect., 8, 39.

UYEDA, S. (1957) - J. Geomag. Geoelect. Kyoto, 9, 61.

UYEDA, S. (1958) - Jap. J. Geophys. 2, 1.

VALOV, P.M., SOKOLOVA, V.K., VILENSKII, A.G. and VAINSHTEIN,E.E. (1965) - Inst. Exptl. Tech. (USSR) 1965, 1186.

VISSCHER, J.M. (1960) - Ann. Phys., 9, 194.

WALKER, L.R., WERTHEIM, G.K. and JACARINO, V. (1961) - Phys. Rev. Letters, 6, 98.

WEISSKOPF, V. (1931) - Ann. Physik, 9, 23.

WEISSKOPF, V. and WIGNER, E. (1930) - Z. Physik, 63, 54.
- Z. Physik, 65, 18.

VALI, V. and NYBAKKEN, T.W. (1964) - Rev. Sci. Instrum., 35, 1085.

WERTHEIM, G.K. (1961) - J. Appl. Phys. Suppl. 32, 110S.

WERTHEIM, G.K. (1964) - "Mössbauer Effect: Principles and Applications" Academic Press, New York and London.

WESTCOTT, M.T. (1966) - M.Sc. Thesis, Uni. of N.S.W.,

WILLIS, B.T.M. and BOOKSBY, H.P. (1952) - Proc. Phys. Soc. B., 65, 950.

WOOD, R.W. (1934) - "Physical Optics" Macmillan, New York, 3rd Edition.

WYCKOFF, R.W.G. (1951) - "Crystal Structures" Interscience, Publishers Inc., New York, Vol. 4.

ZINN, W., KALVIUS, M., KANKELEIT, E., KIENLE, P. and WIEDEMANN, W. (1963) - J. Phys. Chem. Solid 24, 993.